Immunometabolic and Functional Profiling of Monocytes in Neuroinflammation

Claire L. Wishart

A thesis submitted in fulfillment of the requirements of Doctor of Philosophy

School of Medical Sciences, Faculty of Medicine and Health
Infection, Immunity, and Inflammation Research Theme,
University of Sydney, 2024

Supervisor
Professor Nicholas J.C. King

Co-Supervisors
Professor Laurence Macia
Professor Markus Hofer

Authorship attribution statement

Chapter 1 (Introduction) contains material published from the following articles:
1. Spiteri, A.G.*, Wishart, C.L.*, Pamphlett, R., Locatelli, G. & King, N.J.C., Microglia and monocytes in inflammatory CNS disease: integrating phenotype and function. *Acta Neuropathologica* (2021).
*This article was co-authored with Dr Alanna G. Spiteri. Sections from this article were only included in Chapter I if they were originally written and drafted by myself. These sections were further edited when incorporating them into this thesis. * denotes equal contribution.*

Chapter 2 (Materials & Methods) contains material published from the following articles:
1. Wishart, C.L.*, Spiteri, A.G.*, Locatelli, G. & King, N.J.C, Wishart, C.L., Spiteri, A.G., Locatelli, G. & King, N.J.C, Integrating transcriptomic datasets across neurological disease identifies unique myeloid subpopulations driving disease-specific signatures. *Glia* 71, 4 (2023). ** denotes equal contribution. This work was co-authored with Dr Alanna G. Spiteri. As per the Thesis and Examination of Higher Degrees by Research Procedures 2020 (most recently amended April 2024), Part 6, Section 29, Clause 3, I acknowledge that the Materials and Methods from this paper, which were included in Chapter 2 of this thesis, are also included in Chapter 2 (Materials and Methods) of Dr Alanna Spiteri's PhD thesis (2023).*
2. Wishart C.L., Spiteri A.G., Tan, J., Macia, L., & King, N.J.C., Deep Metabolic Profiling of Immune Cells by Spectral Flow Cytometry—A Comprehensive Validation Approach. *Available at SSRN 4896833* (2024) (pre-print).
3. Wishart, C.L., Spiteri A.G., Tan, J., Macia, L., & King, N.J.C., Therapeutic glycolysis blockade preferentially targets pathogenic monocytes and attenuates CNS inflammation in flavivirus encephalitis. *Research Square* (2024) (preprint).

Chapter 3 (Results Chapter I) of this thesis is published as:
Wishart, C.L.*, Spiteri, A.G.*, Locatelli, G. & King, N.J.C., Integrating transcriptomic datasets across neurological disease identifies unique myeloid subpopulations driving disease-specific signatures. *Glia* 71, 4 (2023).
** denotes equal contribution. This work was co-authored with Dr Alanna G. Spiteri. We both were involved in experimental design, data curation and analysis, and manuscript writing and editing. As per the Thesis and Examination of Higher Degrees by Research Procedures 2020 (most recently amended April 2024), Part 6, Section 29, Clause 3, I acknowledge that this Results Chapter was also included in Dr Alanna Spiteri's PhD thesis (2023) as Chapter 6.*

Chapter 4 (Results chapter II) of this thesis is formatted into a manuscript.
Wishart, C.L. & King, N.J.C. Metabolism drives MC heterogeneity in the diseased CNS microenvironment.
I curated and analysed the data and wrote the drafts of the experiments. Original single-cell RNA-sequencing Rhapsody data was acquired with the assistance of Alanna G. Spiteri.

Chapter 5 (Results Chapter III) of this thesis is published as*:*
Wishart C.L., Spiteri A.G., Tan, J., Macia, L., & King, N.J.C., Deep Metabolic Profiling of Immune Cells by Spectral Flow Cytometry—A Comprehensive Validation Approach. *Available at SSRN 4896833* (2024) (pre-print).
I designed all experiments, analysed the data, wrote the drafts of the manuscript. All experiments were performed by me. Assistance for the HIF1α validation experiment was provided by Dr. Jian Tan. Kate Pilkington and Dr Alanna G. Spiteri provided assistance with autofluorescence analysis. Manuscript editing was performed by Dr Alanna Spiteri, Dr Jian Tan, and Professor Nicholas J.C. King. Metabolic inhibitors used for these experiments were provided by Professor Laurence Macia.

Chapter 6 (Results chapter IV) of this thesis is formatted into a manuscript:
Wishart, C.L., Spiteri A.G., Tan, J., Macia, L., & King, N.J.C., Therapeutic glycolysis blockade preferentially targets pathogenic monocytes and attenuates CNS inflammation in flavivirus encephalitis. *Research Square* (2024) (preprint).
I designed the experiments, analysed the data, and wrote the drafts of the manuscripts. I performed all experiments, alongside assistance from Dr Alanna Spiteri and Jemma Taitz with culls and qPCR with Camille Potier. The single-cell RNA sequencing Rhapsody data acquisition was performed in collaboration with Dr Alanna G. Spiteri, who was responsible for designing the sorting strategy and barcoding strategy.

Attestment of authorship attribution statement

In addition to the statements above, in cases where I am not the corresponding author of a published item, permission to include the published material has been granted by the corresponding author.

Nicholas J.C. King

Signature:

August 31st, 2024

As supervisor for the candidature upon which this thesis is based, I can confirm that the authorship attribution statements above are correct.

Nicholas J.C. King

Signature:

August 31st, 2024

Statement of originality

I certify that the intellectual content of this thesis is the product of my own work and that all the assistance received in preparing this thesis and sources has been acknowledged.

Claire L. Wishart

Signature:

August 31st, 2024

Acknowledgements

First and foremost, I would like to thank my supervisor, Professor Nick King. Nick, I can't express my gratitude enough for your guidance, mentorship, and expertise over these last few years. Your passion for science is infectious, evident from our very first meeting before I started my honours, where I listened as a slightly confused 20-year-old to you talk about laminar flow in blood vessels and its influence on immune cell trafficking. It's been a pleasure to sit down and discuss science, ideas, and your grandkids for hours. You've served as my role model in science, demonstrating the importance of scientific ethics and integrity, especially in times when they seemed scarce. I really can't thank you enough for trusting me and giving me the space to learn, experiment, and find myself as a researcher throughout this PhD. In your own words: with your help, I believe this PhD is my own Hadrian's wall – it's what has made me.

I would also like to thank my co-supervisors, Professor Laurence Macia and Associate Professor Markus Hofer. Laurence, thank you for your expertise in metabolism and immunology, and for always encouraging me to see the bigger picture, make endless dot point summaries and think about the impact of my work and my future. Markus, thank you for the conversations we had about my career and future, and always offering the time to help me achieve those career goals.

I must give thanks to my lab members and other colleagues who have helped with this PhD. From my own lab, I would like to thank Dr Zheng Ling and Dr Alanna Spiteri. Zheng, thank you for your help with culls, expertise in cell culture and virological methods, and taking the time to find the best protocol whenever I asked for your help. A massive thank you must be given to Alanna. Alanna, thank you for being my scientific mentor from day one. I've learned so much from you, including the importance of systematic and careful work, and how to thoughtfully approach experiments and research. You're one of the biggest go getters I've ever met, and I have complete faith that you will make big waves in whichever field you find yourself. It's been such a pleasure to work with you collaboratively, and I really can't thank you enough for the endless help with experiments, manuscript writing, editing, and for always being there to listen to my rants throughout my PhD.

From the Nutritional Immunometabolism Lab, I would like to thank Dr Jian Tan, Dr Duan Ni, Jemma Taitz, and Camille Potier-Villette for their help with experiments. I would like to give

extra thanks to Jian for his help with metabolic experiments and expertise in metabolism, an area that was a bit daunting for me but that was helped a lot with your insight and experience.

I would like to thank the Sydney Cytometry Team, especially Dr Thomas Ashhurst, for their expertise and guidance throughout the years. I would also like to thank Professor Alex Sharland and Mou Paul for their help with Rhapsody data and their incredibly generous offer to share costs with us for these experiments.

I cannot go without thanking the friends I've made along the way. Jemma and Camille, thank you both for the all the support and endless laughs throughout my PhD. I need to give special thanks to Jemma, without whom I don't think I could have completed this PhD alone. You've been such a support and rock throughout these last few years and I feel so incredibly lucky to have met you in this chaotic and often distressing experience that is a PhD. You've always been my ear to rant to, someone I laugh the hardest with, and commiserate with. You've grown into such an amazing researcher and I'm so proud of the person you are.

I would like to thank my family members who have supported me throughout this experience. Mom and Owen, thank you so much for your support throughout my PhD, you've helped more than you could possibly know. Julie, thank you for all your support and chats throughout the years, and helping me remember that perfectionism isn't always the best option. Tayler, you introduced me into the world of science and a PhD and showed me the ropes from day one. I won't forget you helping me discuss experiments for my very first honours interview. Laine and the (former) blip, Luke, I can't thank you enough for listening to my rants practically every Friday night for the last few years, trips to the beach, and breakfasts. Luke, special thanks to you for the endless interest in my PhD and your weirdly fast ability to grasp immunology concepts that made me question my own intelligence. To my other half, Laine, I don't really have the words or room left in these acknowledgments to express how much gratitude I have to have you in my life – you know what it is. You've been a huge support throughout my PhD – thank you for always being there and making sure I never faced the most challenging times alone.

Finally, I need to thank my partner, Quinn. I know you didn't want a big acknowledgement, so I'll keep it short and sweet. This PhD would not have been possible without you. Your support, love, and presence have meant everything to me.

Posters and Presentations

Posters

Wishart, C.L., Spiteri, A.G., & King, N.J.C. Connecting single-cell myeloid transcriptomes across CNS disease. 2022. Oz Single Cell, Gold Coast, QLD Australia.

List of conference presentations

Wishart, C.L., Spiteri, A.G., Tan, J., Macia, L., King, N.J.C. Monocyte metabolic profiling in CNS disease uncovers glycolysis as a therapeutic target to reduce inflammatory pathology. 2023. Australian and New Zealand Society for Immunology, Auckland, New Zealand.

Wishart, C.L., Spiteri, A.G., Tan, J., Macia, L., King, N.J.C. Single-cell immunometabolic profiling by spectral flow cytometry. 2022. Cytek Asia Pacific user group meeting. Melbourne, VIC, Australia. *Invited speaker*.

Wishart, C.L., Spiteri, A.G., & King, N.J.C. Connecting single-cell myeloid transcriptomes across CNS disease. 2022. Oz Single Cell, Gold Coast, QLD Australia.

Wishart, C.L., Spiteri, A.G., & King, N.J.C. Connecting myeloid transcriptomes across neuroinflammatory disease. 2021. Australasian Cytometry Society. Virtual conference.

List of seminar presentations

Wishart, C.L., Spiteri, A.G., Tan, J., Macia, L., King, N.J.C. Targeting glycolysis reduces monocyte-mediated neuroinflammatory disease. 2024. Centre for Infection and Immunity Seminars, Sydney, NSW, Australia.

Wishart, C.L., Spiteri, A.G., Tan, J., Macia, L., King, N.J.C. Monocyte metabolic profiling in CNS disease uncovers glycolysis as a therapeutic target to reduce inflammatory pathology. 2023. Infection, Immunity and Inflammation Research theme seminar series, Sydney, NSW, Australia.

Wishart, C.L., Spiteri, A.G., Tan, J., Macia, L., King, N.J.C. Monocyte metabolic profiling in CNS disease uncovers glycolysis as a therapeutic target to reduce inflammatory pathology. 2023. Infection, Immunity and Inflammation Research theme seminar series, Sydney, NSW, Australia.

Wishart, C.L., **Spiteri, A.G.**, Locatelli, G. & King, N.J.C. Connecting Transcriptomes Across Neuroinflammatory Disease Reveals Conserved and Unique Microglial and Monocyte Response Programs. 2022. Neuroimmunology Australian Webinar Series, Virtual Meeting.

Wishart, C.L., **Spiteri, A.G.**, Locatelli, G. & King, N.J.C. Connecting Transcriptomes Across Neuroinflammatory Disease Reveals Conserved and Unique Microglial and Monocyte Response Programs. 2022. Biology domain seminar series, Sydney, NSW, Australia.

Wishart, C.L., Spiteri, A.G., Locatelli, G. & King, N.J.C. Connecting Transcriptomes Across Neuroinflammatory Disease Reveals Conserved and Unique Microglial and Monocyte Response Programs. 2021. Infection, Immunity and Inflammation Research theme seminar series, Sydney, NSW, Australia.

List of publications

Research Publications

Wishart, C.L., Spiteri, A.G., Tan, J., Macia, L., King, N.J.C.. Deep metabolic profiling of immune cells by spectral flow cytometry – a comprehensive validation approach. Available at SSRN 4896833 (2024) (pre-print).

Wishart, C.L., Spiteri, A.G., Tan, J., Macia, L., King, N.J.C.. Therapeutic glycolysis blockade preferentially targets pathogenic monocytes and attenuates CNS inflammation in flavivirus encephalitis. *Research Square* (2024) (preprint).

Reyes, J.G.A., Ni, D., Santner-Nanan, B., Pinget, G.V., Kraftova, L., Ashhurtst, T.M., Marsh-Wakefield, F., **Wishart, C.L.**, Tan, J., Hsu, P., King, N.J.C., Macia, L., Nanan, R.. A unique human cord blood $CD8^{+}CD45RA^{+}CD27^{+}CD161^{+}$ T-cell subset identified by flow cytometric data analysis using Seurat. *Immunology* (2024).

Spiteri, A.G., **Wishart, C.L**., Pinget, G.V., Purohit, S.K., Macia, L., King, N.J.C., Niewold, P., NK cell profiling in West Nile virus encephalitis reveals potential metabolic basis for functional inhibition. *Immunology and Cell Biology* (2024).

Spiteri, A.G., Pilkington, K.R., **Wishart, C.L.**, Macia, L., King, N.J.C.. High-dimensional methods of single-cell microglial profiling to enhance understanding of neuropathological disease. *Current Protocols* (2024).

Spiteri, A.G., **Wishart, C.L**., Ni, D., Viengkhou, B., Macia, L., Hofer, M.J., King, N.J.C.. Temporal tracking of microglia and monocyte single-cell transcriptomics in lethal flavivirus infection. *Acta Neuropathologica Communications* (2023).

Wishart, C.L.*, Spiteri, A.G.*, Locatelli, G. & King, N.J.C., Integrating transcriptomic datasets across neurological disease identifies unique myeloid subpopulations driving disease-specific signatures. *Glia* (2023).

Ni, D., Tan, J., Robert, R., Taitz, J., Ge, A., Potier-Villette, C., Reyes, J.G.A., Spiteri, A.G., **Wishart, C.L.**, Mackay, C., Piccio, L., King, N.J.C., Macia, L.. GPR109A expressed on

medullary thymic epithelial cells affects Treg development. *European Journal of Immunology* (2023).

Spiteri, A.G., Terry, R.L., **Wishart, C.L**., Ashhurst T.M., Campbell, I.L, Hofer, M.J. & King, N.J.C. High-parameter cytometry unmasks microglial cell spatio-temporal response kinetics in severe neuroinflammatory disease. *J Neuroinflammation* 18, 166 (2021).

Reviews

Spiteri, A.G.*, **Wishart, C.L**.*, Pamphlett, R., Locatelli, G. & King, N.J.C. Microglia and monocytes in inflammatory CNS disease: integrating phenotype and function. *Acta Neuropathologica* (2021).

Abstract

Monocyte-derived cells (MCs) play crucial roles in central nervous system (CNS) diseases, acting to both enhance and dampen immune-mediated pathology. However, the relationship between their functional and metabolic profiles in various CNS pathologies is not well understood. Traditional paradigms, such as the M1/M2 macrophage polarization paradigm, fail to capture the observed *in vivo* heterogeneity. Through transcriptomic integration and meta-analysis of murine models of various neuropathologies, we identified significant transcriptional, metabolic, and functional diversity within CNS MCs. Disease-specific myeloid responses were reflected in core subpopulations that expanded in different disease contexts and were driven by specific metabolic processes, highlighting a complex function-associated metabolic model rather than the simplistic M1/M2 paradigm.

The M1/M2 paradigm, established by bulk metabolic approaches, does not effectively connect phenotype and function. Cytometric approaches, such as spectral and conventional flow cytometry, enable simultaneous investigation of metabolic and functional phenotypes at the single-cell level. In this study, we thus developed and validated a spectral flow cytometry-based metabolic panel that investigates eight metabolic pathways simultaneously. This robust tool is essential for better understanding the metabolic underpinnings of myeloid responses in disease.

In the context of West Nile virus encephalitis, a model of severe neuroinflammation, single-cell RNA-sequencing and metabolic flow analysis revealed that brain MCs follow a trajectory from the bone marrow through distinct metabolic profiles before differentiating into pro-inflammatory HIF1-α^+ and iNOS$^+$ M1-like populations, as well as glycolytically more quiescent antigen-presenting cells. Inhibiting glycolysis with 2-deoxy-D-glucose reduced neuroinflammation and disease signs without increasing viral load, primarily by reducing iNOS$^+$ MC differentiation and cellular migration.

Together, this thesis highlights the complexity of myeloid cell functions and metabolism in CNS diseases, providing new therapeutic targets for severe or uncontrolled inflammation.

List of Acronyms and Abbreviations

Acronym	Full Form
2DG	2-deoxy-D-glucose
2-NBDG	2-(N-(7-Nitrobenz-2-oxa-1,3-diazol-4-yl)Amino)-2-Deoxyglucose
5xFAD	5 familial AD mutations
ACAC	Acetyl–coenzyme A carboxylase
AA	Amino acid
AD	Alzheimer's disease
AF	Autofluorescence
ALS	Amyotrophic lateral sclerosis
APCs	Antigen-presenting cells
ATP	Adenosine triphosphate
BBB	Blood-brain barrier
BHK	Baby Hamster Kidney
BM	Bone marrow
BODIPY	4,4-difluoro-4-bora-3a,4a-diaza-s-indacene
BrdU	Bromodeoxyuridine
BSA	Bovine serum albumin
CCL2	C-C Motif Chemokine Ligand 2
CCL5	Chemokine C-C motif ligand 5
CCR2	C-C chemokine receptor type 2
CCR5	C-C chemokine receptor type 5
cDCs	Conventional DC
CFSE	Carboxyfluorescein succinimidyl ester
CM T cells	Central memory T cells
CNS	Central nervous system
CPT1α	Carnitine Palmitoyltransferase 1 alpha
CPT1A	Carnitine palmitoyltransferase 1A
CSF-1R	Colony-stimulating factor-1 receptor
CSF-1	Colony-stimulating factor 1 signaling
CX3CR1	CX3C motif chemokine receptor 1
CXCL12	C-X-C motif chemokine 12
C-XCR4	C-X-C chemokine receptor type 4
DAM	'Disease-associated microglia'
DAF-FM diacetate	4-Amino-5-Methylamino-2',7'-Difluorofluorescein diacetate
dLN	Draining lymph nodes
DC	Dendritic cells
DEGs	Differentially expressed genes
DMSO	Dimethyl sulfoxide

Acronym	Full Form
DMEM	Dulbecco's Modified Eagles Medium
DMOG	Dimethyloxalylglycine
dMC	MCs from disease conditions
dMg	Microglia from disease conditions
dpi	Days post-infection
EAE	Experimental Autoimmune Encephalomyelitis
ETC	Electron transport chain
FADH2	Flavin adenine dinucleotide
FA	Fatty acid
FAO	Fatty acid oxidation
FAS	Fatty acid synthesis
FCS	Foetal calf serum
Fcrls	Fc receptor-like S
FCCP	Carbonyl cyanide 4-(trifluoromethoxy)phenylhydrazone
FC	Fold change
FIZZ1	Found in inflammatory zone 1
FMO	Fluorescence minus one
GAPDH	Glyceraldehyde 3-phosphate dehydrogenase
GEO	Gene Expression Omnibus
GM-CSF	Granulocyte-macrophage colony-stimulating factor
GMPs	Granulocyte-monocyte progenitors
GO	Gene ontology
GSEA	Gene set enrichment analysis
HEPES	4-(2-Hydroxyethyl)piperazine-1-ethanesulfonic acid
HEXB	Hexosaminidase B
HIF-1α	Hypoxia-inducible factor 1 alpha
hMg	Microglia from homeostatic conditions
HSC	Hematopoietic stem cells
IDH	Isocitrate dehydrogenase
IDH1	Isocitrate dehydrogenase 1
IDO	Indoleamine-2,3-dioxygenase
IFN	Interferon
IL-<number>	Interleukin-<number>
IL4I1	Interleukin-4-induced one
KL	Kullback-Leibler
LAT1	L-type amino acid transporter 1
LDHA	Lactate dehydrogenase A
LN AA	Large neutral amino acid
LPS	Lipopolysaccharide
LXR	Liver X Receptor

Acronym	Full Form
M-CSFR	Macrophage colony-stimulating factor receptor
MCs	Monocyte-derived cells
MDP	Monocyte-DC precursors
MDMs	Monocyte-derived macrophages
MGnD	'Microglial neurodegenerative'
MHC	Major histocompatibility complex
MHC-I	Class I MHC
MHC-II	Class II MHC
MMPs	Multipotent progenitors
MS	Multiple sclerosis
NADH	Nicotinamide adenine dinucleotide
NADPH	Nicotinamide adenine dinucleotide phosphate
NF-κB	Nuclear factor kappa-light-chain enhancer of activated B cells
NK	Natural killer
NO	Nitric oxide
NOX	NADPH oxidases
NLRP3	NLR family pyrin domain containing 3
NS	Non-structural protein
OXPHOS	Oxidative phosphorylation
P2RY12	Purinergic receptor P2Y12
PAMPs	Pathogen-associated molecular patterns
PCA	Principal component analysis
PCs	Principal components
PBS	Phosphate-buffered saline
PFKB4	6-phosphofructo-2-kinase/fructose-2,6-biphosphatase 4
PFU	Plaque-forming units
PPARα	Peroxisome Proliferator-Activated Receptor Alpha
PPARγ	Peroxisome proliferator-activated receptor gamma
PPP	Pentose-phosphate pathway
PRRs	Pattern recognition receptors
PT	Photothrombosis
pDCs	Plasmacytoid DC
RNA	Ribonucleic acid
RIG1	Retinoic acid-inducible gene 1
ROS	Reactive oxygen species
SALL1	Spalt like transcription factor 1
SARS Cov-2	Severe acute respiratory syndrome-related coronavirus 2
scMEP	Single-cell metabolic regulome profiling
scRNA-seq	Single-cell RNA sequencing
SCENITH	Single cell energetic metabolism by profiling translation inhibition

Acronym	Full Form
SD	Standard deviation
Siglech	Sialic acid-binding immunoglobulin-type lectin H
SOCS1	Suppressor of cytokine signallig 1
SSC-A	Side scatter-area
TBI	Traumatic brain injury
TCA cycle	The tricarboxylic acid cycle
TcR	T cell Receptor
TGF-β	Transforming growth factor beta
TLR	Toll-like receptors
TMEM119	Transmembrane protein 119
TMEV	Theiler's Murine Encephalomyelitis Virus
TOFA	5-(Tetradecyloxy)-2-furoic acid
TNF	Tumor necrosis factor
TRAIL	TNF-related apoptosis-inducing ligand
TREM2	Triggering receptor expressed on myeloid cells 2
TPM	Transcripts per million mapped reads
UMAP	Uniform manifold approximation and projection
VEGFA	Vascular Endothelial Growth Factor A
VLA-4	Very late antigen-4
WNV	West Nile virus
WNVE	West Nile virus encephalitis

Table of Contents

List of Tables

List of Figures

List of Supplementary Figures

Chapter 1: Introduction

1.1 Immunometabolism: an emerging field

1.1.1 Overview

Immunology is a relatively new field that encompasses the responses to infections, cancer, transplantation, sterile tissue injury and a myriad of other disease constellations. Our increasing understanding of the immune system has significantly improved human life; for instance, vaccination alone has extended human lifespan by approximately 30 years (Rappuoli et al., 2014). Given the vast scope of the immune system, numerous branches of understanding have emerged to explore its different components. Understanding these various facets is critically important for elucidating the mechanisms of various diseases.

One of the key facets of understanding the immune system is the role of metabolism, a field known as *immunometabolism*. Immunometabolism explores how metabolic processes within cells influence immune responses. These metabolic processes comprise a complex set of chemical reactions that ultimately dictate how immune cells produce and use energy. These processes are arranged into various metabolic pathways, which subserve homeostasis, proliferation, cell division, maintenance of structural integrity and fluidity, and adaptation to changes in the surrounding microenvironment. Every immune cell possesses a unique metabolic profile that is integral to its function, determining how it responds to and interacts with other cells and pathogens.

In general, metabolism can be broadly categorized into anabolic and catabolic processes. Anabolic processes, such as fatty acid synthesis, protein synthesis, and nueclotide synthesis, use energy to synthesize molecules, whereas catabolism breaks down complex molecules to release energy. Catabolic metabolic processes include glycolysis, oxidative phosphorylation (OXPHOS), fatty acid oxidation, and different aspects of amino acid metabolism. This complex web of interactions is facilitated by sets of nutrient transporters, rate-limiting enzymes, signaling molecules, and metabolites. Adenosine triphosphate (ATP), the universal energy currency of cells, is either stored or transferred during these metabolic reactions. This provides energy required for differentiation, proliferation, and function of immune cells; thus metabolic processes play a decisive role in immune cell responses. For example, a metabolic shift towards glycolysis commonly occurs with immune cell activation, permitting both the rapid generation of energy and the biosynthetic precursors necessary to fulfill effector

functions. In addition to metabolic programming, nutrient availability and diet influences the immune system, as substrate availability can skew immune cells towards specific metabolic processes and consequently, specific immune functions. Metabolic reprogramming depends on the close relationship between cellular metabolism, immune function, and substrate (e.g., glucose, amino acids, and fatty acids) availability, which is essential for the flexibility of the immune system and its ability to generate a specialized response against infections and other diseases.

The emerging field of immunometabolism holds immense promise across various experimental settings, offering insights that could significantly improve our approach to understanding diseases and thus developing treatments. Despite significant advancements in the field over the last 10 years, much remains unknown about these interactions and how they are altered during immune responses. Understanding these metabolic mechanisms and their dynamics is essential for advancing our knowledge of the immune system and understanding disease processes.

1.1.2 Overview of the immune system

The mammalian immune response is a highly evolved, complex system employed by the body principally to protect against invasive pathogens, cancer and autoimmune disease by identifying indicative cellular abnormalities, and depending on the manner of recognition, initiating a specific process from an armoury of possible mechanisms to destroy or suppress such cells. It is broadly categorized into innate and adaptive arms, which cooperate in this defence. Metabolism plays a crucial role in this system, as different immune cells require specific metabolic pathways to carry out their relevant functions effectively.

The *innate immune response* is the initial line of defence to infection. It reacts rapidly, but, consistent with its evolutionary origins in short-lived creatures, does not provide lasting protection and is often deemed ‘non-specific’, as future encounters with the same pathogen results in this same generic response, unchanged in speed or intensity. Essential components of the innate immune system consist of physical barriers, such as the skin and mucous membranes, cellular defences, including macrophages, neutrophils, dendritic cells (DC), natural killer (NK) cells and innate lymphoid cells, as well as different soluble protein systems like the complement system, chemokines and cytokines found in blood and other body fluids. Cells of the innate immune system use pattern recognition receptors (PRRs) to detect pathogen-associated molecular patterns (PAMPs) expressed by the pathogen. On recognition of these frequently repetitive patterns, innate cells act to eradicate the pathogen by phagocytosis, and/or

degranulation and exocytosis of various toxic and inflammatory mediators that chemically destroy the pathogen or inhibit its replication, as well as recruiting additional immune cells to the infection site via secreted chemokines and cytokines, and activating them via the same or other locally-produced soluble factors. Depending on the route of inoculation, dose of pathogen and the immune status of the individual, this first-line response may successfully eradicate the pathogen.

Mobilization of the *adaptive immune response* occurs in response to a pathogen that has overcome the initial innate response. While this response is slower, it generates an attack exquisitely specific to the pathogen and once the pathogen is successfully eradicated, leaves a quorum of memory cells that generally grant lasting specific immunity that is reactivated in an accelerated manner on future encounter with the same pathogen and with much greater intensity. The adaptive immune response is comprised of lymphocytes, specifically, B cells and T cells. B cells produce specific antibodies that can either destroy pathogens or abnormal cells, *e.g.,* in collaboration with the complement system, or mark them for destruction by other cells. The two main types of T cells, $CD4^+$ helper T cells, which produce cytokines to aid other immune cells, and $CD8^+$ cytotoxic T cells, which can directly kill infected and cancerous cells, are both specific for the relevant cellular abnormality and this specificity defines the memory response to a future encounter.

The innate and adaptive arms of the immune system work co-operatively to eradicate an infection. Upon successful invasion by a pathogen, the innate immune system promptly initiates a response to contain the spread of the infection. DCs and macrophages, having usually first phagocytosed the pathogen, function as antigen-presenting cells (APCs) by presenting digested peptide fragments of the pathogen (*i.e.,* antigen) on their surfaces for recognition by T cells. This event mainly takes place in lymphoid tissues, such as the spleen or lymph nodes, and is essential for triggering the adaptive immune response.

When activated, T cells proliferate and differentiate into multiple subtypes with distinct functions. Some T cells assist B cells in generating high-affinity antibodies that recognise the pathogen, whereas others differentiate into cytotoxic T cells that eliminate infected cells. After the pathogen is eliminated, most effector T cells undergo apoptosis, but a small proportion differentiate into memory T cells, which remain poised to mount a stronger and more efficient response upon re-infection.

The immune response is carefully controlled to prevent excessive reactions that may cause tissue damage or an insufficient reaction that may result in chronic infection or tumor development. The innate immune system may generate an overactive inflammatory response that leads to direct tissue damage, whereas the adaptive immune response may generate a response that attacks the body's own cells, leading to autoimmune disease, often with both systems working in synergy. Current immunotherapic approaches target these imbalances in inflammatory diseases, infections, and cancer.

1.1.3 Adaptive immune cells

1.1.3.1 T cells

T cells are a key group of adaptive immune cells with crucial roles in the immune response to infection. They are derived from hematopoietic stem cells (HSC) in the bone marrow (BM) and subsequently develop in the thymus through a selection process that ensures self-tolerance and the capacity, via their T cell Receptor (TcR), to identify foreign peptide antigens presented in the context of major histocompatibility complex (MHC) molecules. The TcR is generated by random re-arrangement of its genes and is unique to each successfully selected T cell, with clones that recognise ‘self’ peptides too avidly, usually deleted.

The metabolic needs of T cells change dynamically throughout their lifecycle and in response to activation. During the quiescent state, naïve T cells primarily rely on OXPHOS and fatty acid oxidation to meet their energy demands (Wang et al., 2011). These efficient processes allow T cells to conserve resources while circulating in the bloodstream and lymphatic system, awaiting activation.

$CD4^+$ T cells, or helper T cells, play a crucial role in orchestrating the immune response by assisting other cells. Their TcR recognise ‘non-self’ antigenic peptides in the context of Class II MHC (MHC-II) molecules, usually on antigen-presenting cells such as DCs, macrophages, and B cells, which express it. Upon activation, $CD4^+$ T cells undergo metabolic reprogramming, shifting from OXPHOS to glycolysis (Michalek et al., 2011), supporting their proliferation, differentiation, and cytokine production. These effector functions are additionally supported by fatty acid synthesis and amino acid metabolic pathways (Berod et al., 2014). For instance, arginine metabolism regulates the expression of components of the TCR (Rodriguez et al., 2002), whereas glutamine metabolism promotes T cell proliferation (Wang et al., 2011). $CD4^+$ T cells can develop into numerous subtypes, such as type 1, 2 and 17 T helper cells, or regulatory T cells, each performing functions that include activating

macrophages, defending against extracellular pathogens, and modulating immune responses (Zhu and Paul, 2008). This differentiation process is tightly regulated and is skewed by the different metabolic pathways employed (Berod et al., 2014, Nakaya et al., 2014, Shi et al., 2011).

$CD8^+$ T cells, also known as cytotoxic T cells, are the immune system's main protection against intracellular invaders, such as viruses and some bacteria, as well as cancer cells (Zhang and Bevan, 2011). These cells also identify 'non-self' antigenic peptides via their TcR, but in the context of Class I MHC (MHC-I) molecules which are found on virtually all nucleated cells in the body, in contrast to the more restricted expression of MHC-II. Upon activation, $CD8^+$ T lymphocytes also undergo a metabolic switch to glycolysis (Gubser et al., 2013), which supports their rapid proliferation and acquisition of cytolytic functions. This metabolic reprogramming facilitates $CD8^+$ T cell-induced apoptosis or cell death by cytolytic mechanisms, thereby directly eliminating infected or cancerous cells.

$CD4^+$ and $CD8^+$ T cells undergo particular differentiation stages in response to antigen presentation (Kaech et al., 2002). Naïve T cells develop in the thymus, but are not usually exposed there to their cognate antigen in the context of infection. Once they leave the thymus, they circulate as naïve T cells from the blood stream into the lymphatic system and back again, until they are detained in a lymphoid organ by an environment responding to local infection, where they may be activated by their cognate antigen, usually presented by a DC. Following activation, naïve T cells differentiate into effector T cells, proliferate and are released back into the circulation to home to the site of infection where they help to control it according to their functional specialization (Kaech et al., 2002). Local environmental factors and cytokines encountered during activation impact the differentiation pathway of these effector cells, which exit the lymph nodes via the blood vessels to areas of inflammation using chemokine gradients and adhesion molecules. After a pathogen is eradicated, most effector T cells undergo apoptotic cell death during a contraction phase, while a minority remain as memory T cells, which undergo accelerated reactivation to a more intense response upon pathogen re-encounter (Kaech et al., 2002). Memory T cells, which can include central memory T cells circulating in the lymph nodes, effector memory T cells monitoring peripheral tissues, and resident memory T cells at the site of resolved infection, have a distinct metabolic profile. Similar to naïve T cells, memory T cells primarily use OXPHOS (O'Sullivan et al., 2014) and fatty acid oxidation (van der Windt et al., 2012, Van Der Windt et al., 2013), which are energy efficient processes

that enable their long-term survival and ability to respond more rapidly upon re-exposure to the antigen.

1.1.3.2 B cells

B cells, also known as B lymphocytes, are crucial components of the adaptive immune system, mainly recognized for their capacity to produce antibody. B cells also co-ordinate with other immune cells by presenting antigens and producing cytokines. Derived from HSCs in the BM (Pieper et al., 2013), they differentiate into pro-B cells, which, similar to T cells, undergo genetic rearrangement to generate a distinct B cell receptor on each B cell (Hardy et al., 1991). Like T cells, the developmental process ensures that B cells are tolerant of 'self' and capable of binding to specific antigens.

The metabolic requirements of B cells evolve through their development and activation stages, employing various metabolic pathways. In their resting state, B cells primarily rely on OXPHOS to meet their energy needs. This efficient metabolic process supports their maintenance and surveillance functions as they migrate to the spleen and undergo differentiation into either follicular or marginal zone B cells (Pieper et al., 2013). Follicular B cells move through the blood and lymphoid tissues, whereas marginal zone B cells are located in the spleen to protect against infections (Pieper et al., 2013).

B cell activation is initiated by antigen binding, which triggers their rapid differentiation and expansion in specialized areas called germinal centers located in lymph nodes or the spleen (Phan et al., 2009). Upon activation by antigen binding, B cells undergo significant metabolic reprogramming. This activation triggers a marked increase in amino acid and glucose uptake to support their rapid differentiation and proliferation. Whereas in T cells, increased glucose uptake is linked to aerobic glycolysis, in B cells glucose is directed towards the the pentose phosphate pathway (PPP) (Waters et al., 2018). This leads to the production of biosynthetic intermediates essential for new ribosome generation, and consequently, antibody production (Waters et al., 2018). Furthermore, the synthesis of fatty acids and sterols promotes B cell proliferation following their activation (Dufort et al., 2014). In the process of somatic hypermutation, B cells undergo affinity maturation to further enhance the affinity of their B cell receptors for antigens, as well as change the type of antibodies they generate with the assistance of T helper cell cytokines. This process, known as class switch recombination, requires substantial energy and biosynthetic inputs, resulting in the creation of plasma cells

that produce high affinity antibodies, as well as memory B cells, ensuring long-lasting immunity (LeBien and Tedder, 2008).

1.1.4 Innate immune cells

1.1.4.1 NK cells

NK cells are essential to the innate immune system because they may identify and kill virus-infected or cancer cells without antigen sensitization. NK cells arise from a lymphoid progenitor in common with T cells and B cells in the BM (Abel et al., 2018). During their maturation, NK cells acquire surface receptors that allow them to distinguish healthy cells from those stressed or changed by infection or malignancy. These receptors include killer immunoglobulin-like receptors, which bind with MHC class I molecules on prospective target cells, while natural cytotoxicity receptors identify stress-induced ligands (Lanier, 2005). In healthy cells, normal MHC-I molecules suppress NK cell activation, but many virus-infected or tumor cells downregulate MHC-I (Lanier, 2005, Vivier et al., 2011, Liao et al., 1991). This results in NK cell activation, which increases both OXPHOS and glycolysis (Donnelly et al., 2014). These metabolic pathways are essential for the production of cytotoxic granules with perforin and granzymes, enabling NK cells to kill the infected target cells (Lanier, 2005). Indeed, strategies that reduce metabolic rates of these pathways in mouse NK cells reduces cytokine-induced proliferation and impairs NK cell cytoxicity against a range of cell lines *in vitro* (Assmann et al., 2017, Mah et al., 2017). Furthermore, NK cells produce cytokines such as interferon (IFN)- γ to boost the antibacterial and anticancer activities of other immune cells and interact with DC, macrophages, and T cells to regulate the immune system (Wolf et al., 2023). Production of IFN-γ and NK cell degranulation is impaired by inhibiting amino acid uptake via amino acid transporters such as CD98 (Jensen et al., 2017), emphasizing the importance of this pathway in regulating the interactions of NK cells with other immune cells.

1.1.4.2 Granulocytes

Granulocytes, which include neutrophils, eosinophils, and basophils, are essential components of the innate immune system. They are characterized by their granule-laden cytoplasm.

Neutrophils are the most abundant granulocyte in the bloodstream. Neutrophils are generally the first responders to bacterial infection and their bactericidal activity is facilitated by granules containing antimicrobial peptides and enzymes. They have a limited life span (Pillay et al., 2010), and are typically among the first to react to inflammatory triggers, playing a vital role

in the acute inflammatory response. This rapid response is supported by their reliance on glycolysis for quick bursts of energy, even under low-oxygen conditions commonly found in infected and inflamed tissues (Morrison et al., 2023). Additionally, neutrophils use the PPP to generate nicotinamide adenine dinucleotide phosphate (NADPH) (Azevedo et al., 2015), which is essential for producing reactive oxygen species (ROS) that help kill pathogens. Neutrophil development initiates with HSCs in the BM, which develop into multipotent progenitors (MMPs). MMPs subsequently generate granulocyte-monocyte progenitors (GMPs) (Evrard et al., 2018). GMPs advance through proliferative phases including myeloblasts, promyelocytes, and myelocytes, then transition to non-proliferative stages such as metamyelocytes and banded cells before developing into neutrophils that circulate in the bloodstream.

Eosinophils are recognized for their roles in combating multicellular parasites (Fabre et al., 2009, Gebreselassie et al., 2012) and their contribution to the development of allergic diseases, such as asthma (Wardlaw et al., 2000). Eosinophils exacerbate tissue inflammation and damage during allergic reactions by releasing cytotoxic granule proteins, cytokines, and chemokines, which also regulate the immune system (Rosenberg et al., 2013). *Basophils* are the least abundant granulocyte and are particularly important in allergic reactions and parasitic infections. Their defense against pathogens is mediated by the release of histamine, heparin, and other mediators from their granules, which promote inflammation and recruit other immune cells to the site of infection or injury. Although the metabolism of eosinophils and basophils are not well described, some studies suggest that these cells are glycolytic and rely on certain metabolic regulators, such as hypoxia-inducible factor 1 alpha (HIF1α), to sustain glycolysis and their homeostatic activities (Sumbayev et al., 2009).

1.1.4.3 Dendritic cells

DCs are professional antigen-presenting cells that connect the innate and adaptive immune systems. These cells are classified into two principal types: conventional DC (cDCs) and plasmacytoid DC (pDCs). cDCs are effective at processing and presenting antigens to T cells, resulting in T cell-mediated immunological responses (Cabeza-Cabrerizo et al., 2021, Yin et al., 2021). In contrast, pDCs contribute significantly to antiviral immunity by producing large amounts of type I interferons (IFN) in response to viral infection (Colonna et al., 2004). HSCs in the BM develop into common myeloid progenitors, which then differentiate into DC progenitors via a finely controlled process mediated by particular transcription factors and cytokines (Anderson III et al., 2021), primarily through FLT3 ligand/FLT3 axis with additional

support from other cytokines such as colony-stimulating factor 1 signalling (CSF-1) (MacDonald et al., 2005, Karsunky et al., 2003). These progenitors mature into either cDCs or pDCs before migrating out of the BM (Schlitzer et al., 2015) to remain in peripheral tissues or circulate in the blood stream. In the human bloodstream, DCs have been characterized as five distinct subsets, which are distinct from monocyte-derived DC (MacDonald et al., 2002), although an increasing level of resolution in phenotyping has lead to the identification of significantly increased heterogeneity among certain DC subtypes (Collin and Bigley, 2018).

In their resting state, DCs primarily engage catabolic metabolism, such as OXPHOS, which is powered by fatty acid oxidation and glutaminolysis, to breakdown resources for energy production and cellular maintenance. Activated DCs undero anabolic metabolism, which promotes biosynthesis and cell growth. This metabolic shift includes a switch from glycolysis and channeling glycolytic intermediates into the PPP (O'Neill and Pearce, 2016, Krawczyk et al., 2010). Furthermore, the tricarboxylic acid (TCA) cycle is reconfigured, resulting in the accumulation of intermediates that regulate numerous immunological processes and aid in fatty acid synthesis (O'Neill and Pearce, 2016, Krawczyk et al., 2010). These metabolic changes are essential for DC function in antigen processing, presentation, and cytokine production.

1.1.4.4 Monocytes

Monocytes are myeloid lineage hematopoietic cells that are part of the mononuclear phagocyte system (Guilliams et al., 2014, Van Furth et al., 1972). They arise from the definitive HSC in adulthood and develop from monocyte-DC precursors (MDP) and GMP through a number of consecutive differentiation stages in the BM (Hettinger et al., 2013, Yáñez et al., 2017). The developmental fate of these monocytes is determined by transcription factors such as PU.1, interferon regulatory facor 8, Kruppel-like factor 4, and GATA binding factor 2 (Alder et al., 2008, McKercher et al., 1996, Kurotaki et al., 2013, Feinberg et al., 2007), while their development, survival, and proliferation are controlled by the growth factor receptor, CD115 (also referred to as colony-stimulating factor-1 receptor, CSF-1R, or macrophage colony-stimulating factor receptor, M-CSFR), along with its ligands, macrophage colony-stimulating factor and interleukin (IL)-34 (Mossadegh-Keller et al., 2013, Dai et al., 2002). However, it has been demonstrated that CSF-1 signalling is not required for monocyte production, but is specifically required for monocytes that are committed to differentiate into a tissue-resident macrophage and thus replenish the tissue resident pool (MacDonald et al., 2010). After being produced in BM, monocytes are released into the bloodstream. During inflammation, CSF-1 is

increased to accelerate monocyte production (i.e., myelopoiesis) in order to meet the increased demand for myeloid cells (Roth et al., 1997). While it is unclear whether myelopoiesis is mediated by specific metabolic pathways, hyperglycemia significantly enhances myelopoeisis (Zhu et al., 2022), suggesting that increased glucose availability may fuel the increased glycolytic demand of this process.

Circulating monocyte subsets have different phenotypes, sizes, transcriptional patterns, and migratory abilities. Monocyte subsets are defined by their CD14 and CD16 expression levels in humans (Passlick et al., 1989) and in mice by the surface markers Ly6C, CX3C motif chemokine receptor 1 (CX3CR1), C-C chemokine receptor type 2 (CCR2), L-selectin, and CD43 (Geissmann et al., 2003). Human monocytes are 80-90% $CD14^{+}CD16^{-}$ classical monocytes. Intermediate monocytes ($CD14^{+}CD16^{+}$) and non-classical monocytes ($CD14^{lo}CD16^{+}$) make up the remaining 10–20% (Passlick et al., 1989). In mice, "classical" monocytes express $Ly6C^{hi}$, $CX3CR1^{int}$, $CCR2^{+}$, L-$selectin^{+}$ and $CD43^{lo}$ markers, and are also known as "inflammatory monocytes," while "non-classical" or “patrolling” monocytes express $Ly6C^{lo}$, $CX3CR1^{hi}$, $CCR2^{lo}$, L-$selectin^{-}$, and $CD43^{+}$ (Geissmann et al., 2003, Palframan et al., 2001, Jakubzick et al., 2013). These cells are often characterized as $CX3CR1^{hi}$ based on reporter mice, although antibody staining reveals lower surface protein levels compared to reporter expression, making CX3CR1 unreliable for discriminating monocyte subsets by antibody staining (Meghraoui-Kheddar et al., 2020). A transcriptional analysis demonstrated a link between $Ly6C^{hi}$ monocytes in mice and 'classical' $CD14^{+}CD16^{-}$ monocytes in humans, and $Ly6C^{lo}$ monocytes and 'non-classical' $CD14^{lo}CD16^{+}$ monocytes (Ingersoll et al., 2010).

Presently, monocytes are viewed as a distinct cell type with multiple functions. $Ly6C^{hi}$ monocytes can migrate to tissues and retain their phenotype (Jakubzick et al., 2013), but they can also differentiate into tissue-resident macrophages (Yona et al., 2013) or $Ly6C^{lo}$ monocytes (Yona et al., 2013, Mildner et al., 2017). During inflammation, monocytes develop into macrophages and DCs, which fulfill different functions from resident cells. Based on their monocytic lineage, these unique cell types are called "monocyte-derived macrophages" and "monocyte-derived DCs", often known as monocyte-derived cells (MCs) (Guilliams et al., 2014). It is unclear whether monocytes themselves have distinct metabolic profiles prior to their differentiation into effector MCs. However, they undergo significant immunometabolic reprogramming during differentiation. For instance, monocyte differentiation into DC involves a switch from glycolysis to OXPHOS, increased glutaminolysis, and reduced dependence on

fatty acid oxidation (Adamik et al., 2022). This distinct metabolic reprogramming during monocyte differentiation opens avenues for intervention when effector MCs cause significant damage. For instance, targeting fatty acid oxidation was shown to impair monocyte differentiation into macrophages following cardiac transplant, which prolonged survival after heart transplant (Zhu et al., 2022).

1.1.4.5 Macrophages

Macrophages are a diverse group of myeloid cells that are essential for maintaining homeostasis and protecting the body in different tissues. They are recognized for their capacity to phagocytose pathogens and apoptotic cells, present antigens, and release various cytokines and growth factors that regulate inflammation and tissue healing.

Macrophages can develop from either embryonic yolk sac progenitors or BM-derived monocytes (Ginhoux et al., 2016). Erythro-myeloid progenitors originating from the yolk sac around embryonic day 7.5 migrate to developing tissues and mature into tissue-resident macrophages (Mass et al., 2016, Gomez Perdiguero et al., 2015). These cells are implanted into tissues before birth and can continue to exist through self-renewal for the entire lifespan of the organism (Ginhoux et al., 2016). They include, but are not limited to, microglia in the central nervous system (CNS), Langerhans cells in the skin, Kupffer cells in the liver, and alveolar macrophages in the lungs. Recently, it has been demonstrated that tissue-resident macrophages have specialized metabolic profiles depending on their tissue of residence, which is influenced by their functional identity and tissue-specific nutritional landscape (Heieis et al., 2023). For instance, T cell membrane protein 4^{+} efferocytic macrophages in the intenstine express high levels of markers related to fatty acid synthesis, which may support membrane expansion required for the phagocytosis of apoptotic cells (Heieis et al., 2023). On the other hand, Kupffer cells in the liver are exposed to a lipid-rich environment, and thus showed a higher reliance on fatty acid oxidation over glucose metabolism for cell maintenance and survival (Heieis et al., 2023).

In addition to embryonically-derived macrophages, monocytes originating from the BM, which travel in the circulation, are able to enter tissues and differentiate into certain tissue-resident macrophages, based on signals from the surrounding environment (Yona et al., 2013). Monocyte-derived macrophages can substitute for tissue-resident populations in specific inflammatory situations (Ajami et al., 2011, Leuschner et al., 2012) or during regular turnover in certain tissues (Yona et al., 2013). Once inside tissues, monocytes can differentiate into

macrophages that perform roles akin to their embryonic counterparts, but are influenced by the specific stimuli of their surroundings, such as inflammation and infection, and retain distinct transcriptomic signatures, including in the liver (Beattie et al., 2016). The metabolic platicity of these monocytes may play a crucial role in their ability to replace tissue-resident macrophages. For instance, during influenza infection in the lung, BM-derived monocytes replenished over half of the foetally-derived resident macrophage pool (Li et al., 2022a). This was attributed to their higher glycolytic capacity and metabolic plasticity, allowing them to survive and outcompete resident macrophages in the dynamic metabolic environment of inflammation (Li et al., 2022a).

1.2 Interplay between cellular metabolism and MC function

1.2.1 The dual facets of macrophage activation

Macrophages are adaptable cells that can rapidly be polarized, choosing one functional state over a notionally opposite state. This transition is brought about by a variety of microenvironmental triggers, including cytokines, pathogens, apoptotic cells, and other signaling molecules, resulting in a distinct functional phenotype. Macrophages are often divided into two polarization states based on gene expression, surface markers, cytokine production, and metabolic characteristics: pro-inflammatory M1 macrophages and anti-inflammatory M2 macrophages (Murray et al., 2014, Xue et al., 2014, Rodríguez-Prados et al., 2010) (Table 1.1).

Table 1.1. Molecular and metabolic signatures of macrophage polarization in mice.

Macrophage Subtype	Marker Expression	Biological Functions	Signalling Molecules & Cytokines	Metabolic Pathways & Metabolites
M1	CD80, CD86, MHC-II, iNOS	Pro-inflammatory cytokine production, NO release, pathogen killing, antigen presentation	IL-1β, TNF, IFN-γ, IL-6, IL-12, IL-23, NO, ROS	Glycolysis, oxidative PPP, Fatty acid synthesis, citrate, succinate, itaconate
M2	Arginase 1, found in inflammatory zone 1 (FIZZ1), suppressor of cytokine signalling 1 (SOCS1), CD206, CD36	Anti-inflammatory response, wound healing, tissue remodelling	TGF-β, IL-10, IL-4, IL-13, IL-8, IL-1 receptor a, Vascular Endothelial Growth Factor A (VEGFA), IL-33	OXPHOS, TCA cycle, Fatty acid oxidation, Glutamine synthesis, Glutaminolysis, Amino acid uptake, Kynurenine, Polyamine

M1 macrophages, which are regarded as pro-inflammatory, are activated by pro-inflammatory microbial components such as lipopolysaccharide (LPS), ligands for toll-like receptors (TLR), or cytokines generated by T helper type 1 cells, such as tumor necrosis factor (TNF) and IFN-γ (Nathan et al., 1983). M1 macrophages have the ability to eliminate infections and present antigens to T cells, which initiate adaptive immune responses. In order to eradicate pathogens and induce inflammation, they may also produce large amounts of inflammatory molecules, IL-1β, TNF, nitric oxide (NO), and ROS (Murray et al., 2014). Co-stimulatory (e.g., CD80, CD86) and antigen presenting molecules (*e.g.,* MHC-II) and transcription factors, including nuclear factor kappa-light-chain enhancer of activated B cells (NF- κ B) and HIF-1α are among the surface markers and transcription factors used to identify M1 macrophages. M1 macrophages swiftly switch to aerobic glycolysis for the production of ATP and increase glucose uptake in response to TLR-activating pathogen-derived danger signals, such as LPS, and cytokines, such as IFN-γ (Rodríguez-Prados et al., 2010, Freemerman et al., 2014, Palsson-McDermott et al., 2015). When activated, M1 macrophages shift towards glycolysis to meet the increased energy demands of rapid cytokine production and microbial killing (Van den Bossche et al., 2017, Viola et al., 2019). This metabolic shift supports the generation of ROS and NO, which are essential for their antimicrobial activities.

M2 macrophages, often referred to as regulatory or anti-inflammatory macrophages, are activated by cytokines such as IL-13 or IL-4, produced by innate and adaptive immune cells such Th2 lymphocytes, mast cells, and basophils (Mills et al., 2000, Stein et al., 1992, Corraliza et al., 1995). The anti-inflammatory properties of M2 macrophages reduce inflammation and promote tissue repair. These cells are characterized by various phagocytic markers (*e.g.,* CD206 and CD36) and the production of anti-inflammatory and pro-repair molecules, such as transforming growth factor β (TGF-β) (Viola et al., 2019). M2 macrophages with elevated arginase activity produce collagen and polyamines, which help with tissue remodeling and wound healing. Metabolically, alternatively-activated macrophages are more reliant on on fatty acid oxidation and glutaminolysis to fuel increased OXPHOS (Viola et al., 2019, Huang et al., 2014, Wang et al., 2018).

1.2.2 Challenges surrounding the M1/M2 conceptual framework

The M1/M2 framework for categorizing MC activation, dividing these cells into two distinct phenotypes, classically activated (M1) and alternatively-activated (M2) macrophages, is widely considered oversimplified (Van den Bossche et al., 2017). The functional and metabolic

features of polarized macrophages have largely been characterized under *in vitro* conditions following stimulation with specific cytokines or microbial antigens. Outside of *in vitro* conditions, MCs exhibit a broad spectrum of activation states that reflect their highly plastic and dynamic nature, responding to a multitude of environmental cues and capable of switching between metabolic processes (Stienstra et al., 2017). Moreover, the activation of macrophages is context-dependent, varying significantly with different tissue environments and stimuli (Lachmandas et al., 2016, Heieis et al., 2023, Xue et al., 2014). Even in controlled *in vitro* conditions, macrophages exposed to defined stimuli adopt a spectrum of activation states, comprising at least nine distinct programs regulated by specific transcriptional factors (Xu et al., 2014). Thus, the M1/M2 model does not adequately represent this variability, nor does it account for the reversibility of macrophage phenotypes, a feature that is particularly important in understanding their roles in disease.

The intricate relationship between macrophage metabolism and function extends beyond the traditional M1/M2 paradigm. For example, while antigen presentation and the production of inflammatory mediators are both considered M1-like functions, they require different biosynthetic intermediates and consequently different metabolic profiles. Consequently, the scientific community is thus moving towards a more refined understanding of MC activation that acknowledges the complex metabolic reprogramming that underlies distinct functions (Table 1.2), rather than viewing MC activation as a simply binary M1 or M2 polarization state.

1.2.2.1 OXPHOS: the tricarboxylic acid cycle and electron transport chain

OXPHOS is a crucial metabolic process that occurs within the mitochondria. Known for its energy-producing efficiency, OXPHOS is usually linked with the extended lifespan of specific cells such as tissue resident macrophages, as well as general homeostatic functions. This process comprises a complex series of reactions in the electron transport chain (ETC) and the TCA cycle (Figure 1.1, Figure 1.2). The latter fuels the ETC with energy-dense molecules such as nicotinamide adenine dinucleotide (NADH) and flavin adenine dinucleotide ($FADH_2$), which are then oxidized, resulting in ATP production.

The TCA cycle undergoes significant modifications based on bioenergetic needs. For example, M2-like macrophages, known for maintaining homeostasis and tissue repair, exhibit a functional and complete TCA cycle. This is crucial for fulfilling the ATP requirements due to the high levels of glycosylation of lectin and mannose receptors, which are essential for M2

macrophage function (Jha et al., 2015). The relationship between glycolysis and the TCA cycle in M1-like macrophages shows distinct temporal phases. Initially, the activation triggers an upregulation of both glycolysis and the TCA cycle, with enhanced TCA cycle flux supporting chromatin remodelling needed for the inflammatory response (Lauterbach et al., 2019). As inflammation progresses, NO accumulation leads to acotinase inhibition, creating breaks in the TCA cycle (Palmieri et al., 2020). These disruptions result in the accumulation and mitochondrial export of key metabolic regulators including citrate, succinate, and itaconate, which then execute their regulatory roles on various metabolic pathways (Figure 1.1).

Citrate plays a critical role in modulating cellular metabolism, and thus is important in sustaining the macrophage inflammatory response. It is produced in the TCA cycle either through derivatives of glycolytic pyruvate or from the catabolism of fatty acids. Transport of citrate into the cytosol is induced in response to LPS, TNF, or IFN-γ stimulation (Infantino et al., 2014) and its cytosolic accumulation promotes the production of ROS, NO, and prostaglandin E2 (Infantino et al., 2014). Cytosolic citrate can inhibit glycolysis (Yalcin et al., 2009), and stimulate lipid synthesis and gluconeogenesis (Martin and Vagelos, 1962). During glucose deprivation, increased citrate efflux into the cytosol is necessary for NADPH production, which is catalysed by cytosolic $NADP^+$-dependent IDH (IDH1) (Palmieri et al., 2015).

Succinate is an intermediate of the TCA cycle produced from succinyl-CoA. Succinate increases HIF1α stability under normoxic conditions (Figure 1.1) by blocking prolyl hydroxylase, which otherwise constantly ubiquitinylates HIF1α for proteasomal degradation in the presence of oxygen (Tannahill et al., 2013). Furthermore, during inflammation, succinate is released by inflammatory macrophages and can accumulate in the extracellular milieu (Rubic et al., 2008), as observed in ischemic tissue (Chouchani et al., 2014) and CNS inflammation (Peruzzotti-Jametti et al., 2018).

Itaconate is produced in the TCA cycle (Figure 1.1) in M1-like macrophages via the upregulation of the enzyme aconitate decarboxylase 1 (Michelucci et al., 2013). Itaconate has anti-bacterial properties, and may play a role in immunomodulation, suppression of inflammation, and immune tolerance (Lampropoulou et al., 2016). Itaconate inhibits succinate dehydrogenase, leading to the accumulation of succinate in LPS-activated macrophages, which is associated with reduced mitochondrial respiration, increased ROS production, proinflammatory cytokine release, and inflammasome activation (Lampropoulou et al., 2016).

While OXPHOS is needed for phagocytosis, cytokine production relies on the upregulation of both OXPHOS and glycolysis following TLR2 stimulation (Lachmandas et al., 2016). Inhibiting the ETC with rotenone significantly reduces the phagocytic capacity of TLR2-stimulated monocytes, whereas untreated or LPS (TLR4)-stimulated monocytes were unaffected. Inhibiting glycolysis also did not affect the phagocytic capacity of stimulated monocytes, suggesting that OXPHOS, but not glycolysis, is an important determinant of the phagocytic capacity of human monocytes.

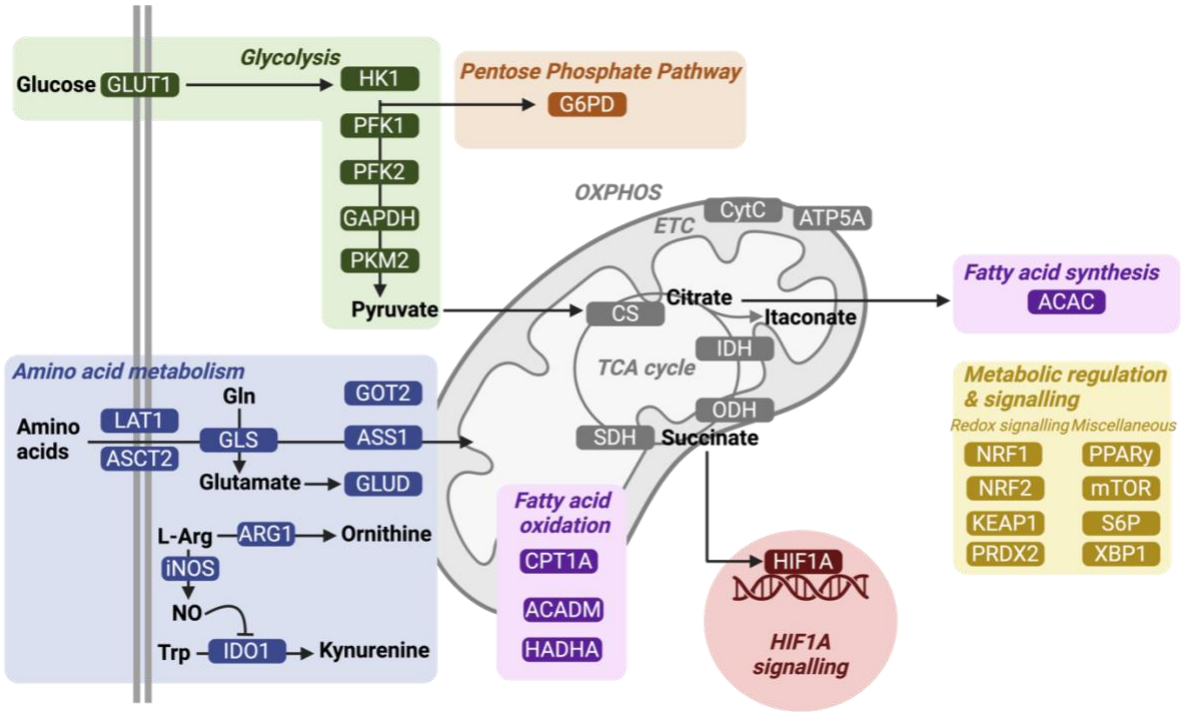

Figure 1.1 Overview of key metabolic pathways in MCs.

Figure is adapted from Artyomov and Van den Bossche 2020.

Table 1.2. Metabolic regulation of various myeloid functions.

Biological Function	Associated Immune Response	Metabolic Processes	Refs.
Type I Interferon Response	Anti-viral immunity	↑ Glycolysis ↑↓ HIF1α signalling ↓ OXPHOS, ETC ↑ Hexosamine biosynthesis pathway-associated O-linked b-N-acetylglucosamine signalling ↓ Cholesterol biosynthesis ↓ Serine metabolism Itaconate boosts IFN response	(Xiao et al., 2020, Peng et al., 2021, Shen et al., 2021, Jiang et al., 2016, Bajwa et al., 2016, Li et al., 2018b, Swain et al., 2020)
Inflammatory Response (cytokine production, inflammasome activation, NO production)	Inflammatory response, pathogen clearance, tissue damage	↑ Glycolysis ↑ HIF1α signalling ↑ Fatty acid synthesis ↑ OXPHOS Succinate oxidation ↑ Citrate accumulation for FAS Engagement of aspartate-arginosuccinate shunt to regulate NO production Succinate accumulation	(Yeudall et al., 2022, Mills et al., 2016, Infantino et al., 2011, Wen et al., 2011, Van den Bossche et al., 2017, Jha et al., 2015, Lachmandas et al., 2016, Tannahill et al., 2013, Zasłona and O'Neill, 2020)
ROS Production	Microbicidal activity, regulation of inflammatory response	↑ Oxidative PPP ↑ FAO ↑ FA metabolism OXPHOS (reverse electron flow)	(Hall et al., 2013, Wen et al., 2011, Mills et al., 2016, Mullarky and Cantley, 2015)
Antigen Presentation	Pathogen clearance, T cell mediated immunity	↑ Glycolysis ↑ Fatty acid synthesis ↓ OXPHOS, ETC	(Lee et al., 2018, Everts et al., 2014, Ibrahim et al., 2012)
Phagocytosis	Pathogen clearance, tissue repair	↑ FA and cholesterol synthesis ↑ Glycolysis ↑ OXPHOS	(Everts et al., 2014, Lachmandas et al., 2016, Lee et al., 2018, Pavlou et al., 2017)
Efferocytosis	Clearance of apoptotic debris, tissue repair	↑ OXPHOS ↑ Glycolysis ↑ PPP flux depending on oxygen availability ↑ Arginine and ornithine catabolism ↑ Kynurenine pathway ↑ Fatty acid oxidation ↑ Sterol pathway activity	(Yurdagul et al., 2020, Ravishankar et al., 2012, Ravishankar et al., 2015, Park et al., 2011, Zhang et al., 2019c, Morioka et al., 2018, Wang et al., 2023, He et al., 2022, Noelia et al., 2009, Tsai et al., 2022)
Production of anti-inflammatory or pro-resolving mediators	Tissue repair, immune suppression, resolution of inflammation	↑ Glutamine metabolism ↑ Lipid synthesis (pro-resolving mediators) ↑ OXPHOS ↑ Mitochondrial uncoupling ↑ Itaconate ↓ Glycolysis	(Varga et al., 2016, Giannakis et al., 2019, Faas et al., 2021)
Myeloid cell migration	Infiltration into inflamed tissues	↑ Glycolysis ↑ HIF1-α signalling	(Semba et al., 2016, Kaushik et al., 2019)

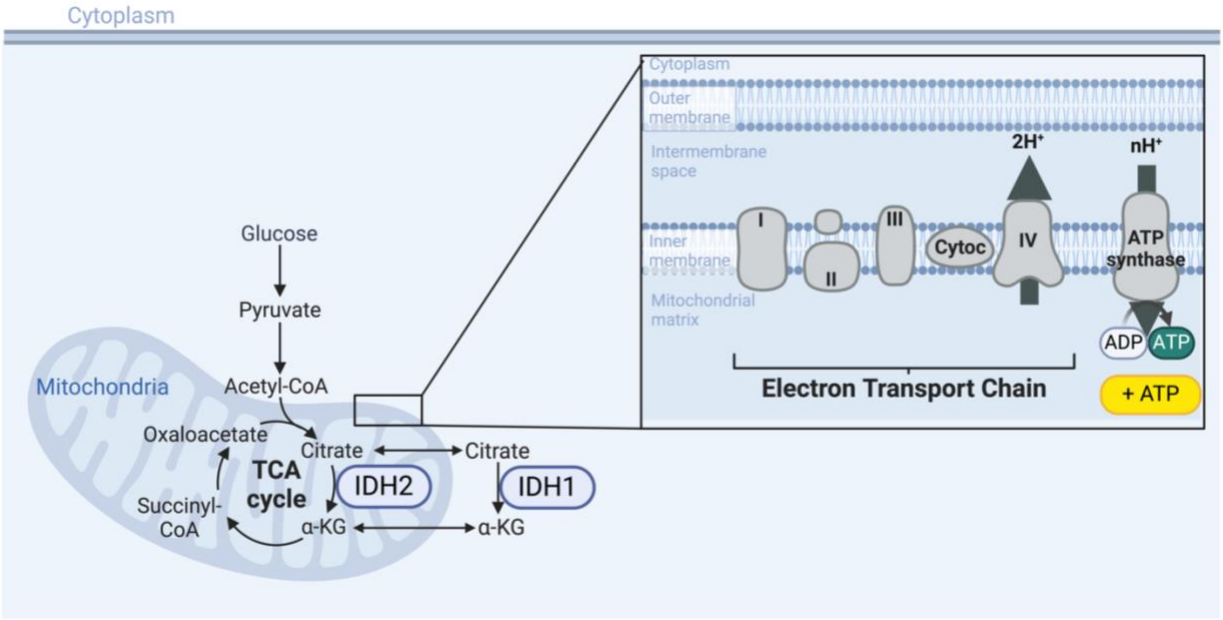

Figure 1.2 Overview of the main metabolic processes involved in OXPHOS.

1.2.2.2 Glycolysis and the PPP

Enhanced glycolysis enables immune cells to generate sufficient ATP and biosynthetic intermediates for specific effector functions. Increased glycolysis is thus well recognized as a marker of metabolic change in most immune cells undergoing rapid activation, such as in response to stimulation of antigen receptors, stimulation of PRRs, and cytokine receptors (O'Neill et al., 2016).

Glycolysis begins with the uptake of extracellular glucose from the environment, which is then metabolised within the cytosol (Figure 1.1 and 1.3). Through this process, glucose is transformed into pyruvate, generating two ATP molecules for each glucose unit. Glycolysis is relatively inefficient in ATP production; however, it is pivotal for the metabolic adaptation of cells as it offers metabolic intermediates for the production of ribose, amino acids, and fatty acids. It also fuels the PPP (Figure 1.3), enabling the creation of NADPH and ribose-5-phosphate.

Glycolysis serves as a central metabolic regulator of inflammatory macrophage function, including phagocytosis, antigen presentation, ROS production, the anti-viral response, and the release of pro-inflammatory cytokines (Viola et al., 2019) (Table 1.2). Glycolytic intermediates are precursors for the synthesis of nucleotides and amino acids, necessary for the production and secretion of cytokines. Thus, enhanced glycolysis in M1 macrophages supports their ability to produce and secrete large amounts of pro-inflammatory cytokines.

In macrophages, the switch to glycolysis involves the initiation of various transcription factors and signalling molecules. In response to TLR4 stimulation, histone deacetylase 7 regulates the glycolytic enzyme pyruvate kinase M 2 to link glycolysis and inflammatory responses in macrophages (Gupta et al., 2020). In addition, the transcription factor HIF1α plays a pivotal role in the transition to glycolysis under both oxygen-poor (hypoxic) and oxygen-rich (normoxic) conditions (Wang et al., 2017). Notably, HIF1α is a cardinal metabolic and functional orchestrator in macrophages, regulating the gene expression associated with all glycolytic enzymes (Taylor and Scholz, 2022), transporters, and inflammatory mediators (Wang et al., 2017, Viola et al., 2019, Rius et al., 2008).

The PPP, which takes place in the cytosol alongside glycolysis, has two distinct phases (Figure 1.3). The first, or oxidative phase, utilizes the energy derived from the transformation of glucose-6-phosphate into ribulose-5-phosphate to reduce $NADP^+$ to NADPH. Numerous

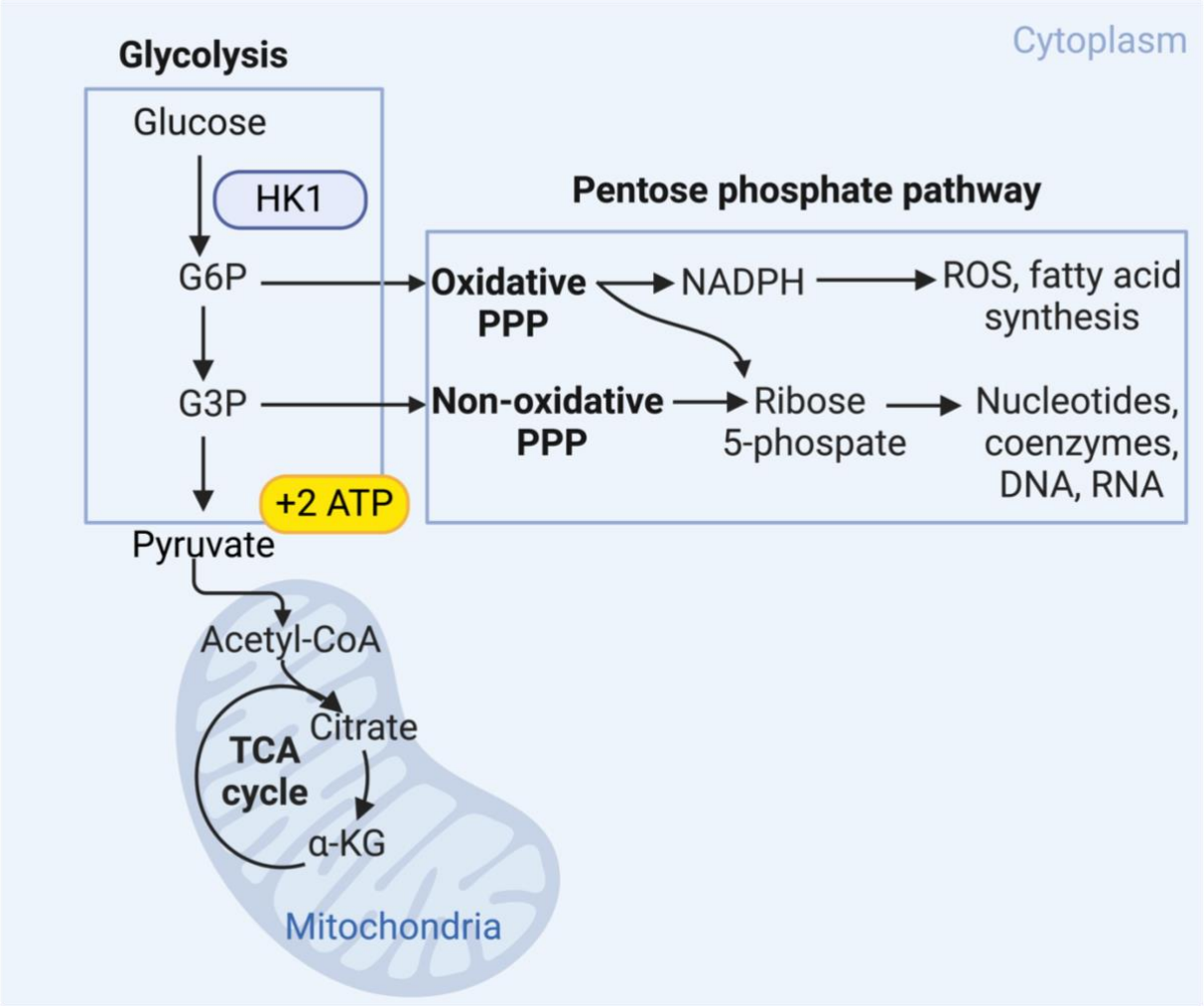

Figure 1.3 Overview of the main metabolic processes involved in glycolysis and the PPP.

enzymes use NADPH, including NADPH oxidase and iNOS, which use NADPH to produce ROS and NO, respectively. These are vital in eliminating pathogens and contribute significantly to macrophage responses. Elevated NADPH levels also aid in shielding against oxidative stress and providing the reducing capacity necessary to produce the antioxidant, glutathione. The second phase of the PPP, the non-oxidative phase, redirects glycolysis intermediates towards the creation of ribose-5-phosphate. This is an essential precursor for nucleotides and amino acids that are necessary for cell growth and proliferation.

1.2.2.3 Hypoxia-inducible factor is a regulator of metabolism and migration

Hypoxia is a common feature of inflammation (Taylor and Colgan, 2017). In order to respond appropriately to inflammation, MCs metabolically adapt to reduced oxygen concentrations, a process that it mediated by the transcription factor HIF1α. To reduce oxygen consumption by mitochondria, HIF1α regulates various aspects of cellular metabolism, including the the utilization of glucose, fatty acids, and glutamine (Taylor and Scholz, 2022, Papandreou et al., 2006). This is accompanied by an increase in glycolytic activity (Kim et al., 2006), the production of fatty acids or lipogenesis (Metallo et al., 2012, Wise et al., 2011), and the breakdown of glutamine through glutaminolysis (Corbet et al., 2014, Yoo et al., 2020). In addition to its effect on metabolism, HIF1α also regulates MC function. It accomplishes this by regulating gene expression associated with glycolytic enzymes and transporters, as well as regulating the production of inflammatory mediators and inflammatory signalling (Wang et al., 2017, Viola et al., 2019, Rius et al., 2008).

A critical mechanism by which HIF1α influences monocyte function is by its effect on myeloid cell migration. Hypoxia accelerates macrophage migration, an effect that is diminished with the deletion of HIF1α on myeloid cells (Semba et al., 2016). This effect is mediated by the relationship between HIF1α and glycolysis: HIF1α-induced pyruvate dehydrogenase kinase isozyme 1 induces glycolytic reprogramming by redirecting pyruvate conversion into lactate (Semba et al., 2016), a process that actively changes glucose metabolism from glucose oxidation to glycolysis (Semba et al., 2016). This in turn supports cytoskeletal actin remodelling that occurs during cellular migration.

1.2.2.4 Lipid metabolism

1.2.2.4.1 Fatty acid synthesis

Fatty acid synthesis is an anabolic process that results in the production of new fatty acids. These fatty acids play a vital role in macrophage biology by serving as essential components of membrane phospholipids, acting as signalling molecule that regulate transcription factors (e.g., PPARγ), and the production of inflammatory mediators, such as prostaglandins, prostacyclins, thromboxanes, leukotrienes, lipoxins, resolvins, protectins, and marensins, which exhibit immunoregulatory effects on immune cells, including macrophages (Rosa Neto et al., 2021). Lipid droplets produced by mammalian cells in response to inflammatory challenge, such as LPS, can also mediate innate immune via a suite of immunity-related proteins that are expressed on lipid droplets derived from infected cells (Bosch et al., 2020).

Fatty acids can be synthesized *de novo* through core metabolic processes such as the TCA cycle, glycolysis, and glutaminolysis (Almeida and Everts, 2021). Alternatively, they can be hydrolyzed from intracellular lipid stores or obtained directly from the extracellular space. The enzyme acetyl–coenzyme A carboxylase (ACAC) plays a central role in lipid metabolism by converting acetyl-CoA to malonyl-CoA, which is crucial for *de novo* fatty acid synthesis (Figure 1.4).

Cellular membranes and organelles, which are comprised of essential fatty acids such as phospholipids, fluctuate in shape in response to changes in cell morphology, activation, and function. Increased fatty acid synthesis contributes to the structural integrity of cellular membranes, enhancing membrane fluidity (Schumann, 2016). This enables cytoskeleton remodelling, local membrane reorganization, and facilitates macrophage functions like phagocytosis, pseudopodia extension for engulfing bacteria and debris (Schumann, 2016), migration across endothelial barriers, and cell adhesion (Wei et al., 2016). Additionally, *de novo* fatty acid synthesis in myeloid cells supports the expansion of endoplasmic reticulum and Golgi apparatus, aiding in the synthesis, transport, and secretion of proteins during the inflammatory response (Everts et al., 2014).

In addition to the physical impact on membrane composition, *de novo* fatty acid synthesis is also a key player in the inflammatory response. Genetic inhibition of fatty acid synthesis reduces NO production and pro-inflammatory signalling in macrophages upon TLR stimulation (Infantino et al., 2013). Moreover, ACAC, a rate-limiting enzyme in fatty acid

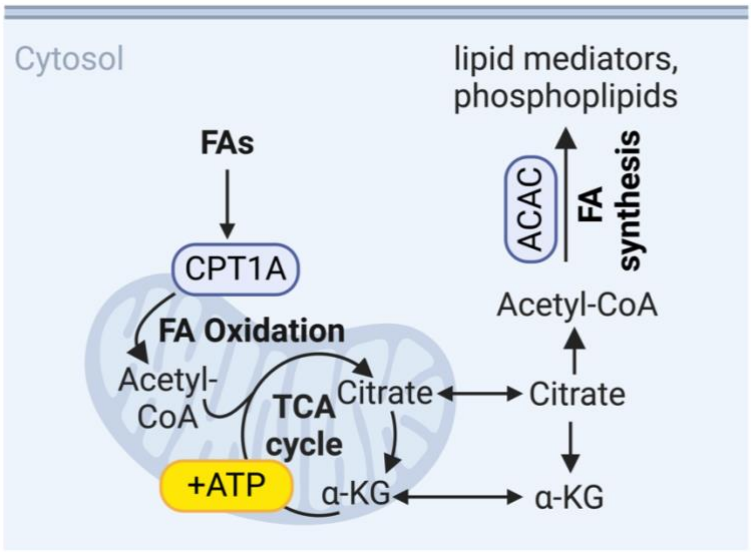

Figure 1.4 Overview of the main metabolic processes involved in fatty acid synthesis and fatty acid oxidation.

synthesis, is necessary for the LPS-induced switch to glycolysis for the production of inflammatory cytokines, but is dispensable for IL-4 induced reprogramming of M2 macrophages (Yeudall et al., 2022). This demonstrates that fatty acid synthesis is a regulator of the sustained production of proinflammatory cytokines in TLR-activated macrophages. In this complex interplay, however, different TLR ligands also have distinct effects on fatty acid synthesis and the lipidome of macrophages (Hsieh et al., 2020). Stimulation of MyD88-dependent TLRs (such as TLR1/2, TLR7, or TLR9) increases the synthesis of saturated fatty acids and monounsaturated fatty acids, while TLR3 stimulation diminishes the production of both these types of fatty acids (Hsieh et al., 2020). The varied production of different fatty acids seems to be dependent on the specific PRR, with PRRs that induce a strong type I response potentially opposing the effects of TLR3 stimulation (Hsieh et al., 2020). Similarly, accumulation of the cholesterol precursor, 7-dehydrocholesterol, was shown to act as a signalling lipid that enhanced the type I IFN response through interferon regulatory factor 3 phosphorylation (Xiao et al., 2020). This led to enhanced anti-viral immunity for a number of viruses, including vesicular stomatitis virus and Zika virus (Xiao et al., 2020). Therefore, the rearrangement of lipid composition in a PRR- or cytokine-specific manner is likely a fundamental process for effectively regulating and coordinating pathogen-specific inflammatory responses in macrophages.

1.2.2.4.2 Fatty acid oxidation

Fatty acid oxidation, also known as β-oxidation, is a catabolic process by which fatty acids are broken down to generate energy within cells. This catabolic process primarily occurs in the mitochondria (Figure 1.4), but it can also occur in peroxisomes for very long-chain fatty acids. The carnitine shuttle system is the initial mechanism by which long-chain fatty acids enter the mitochondria during fatty acid oxidation, wherein fatty acids in the form of acetyl-CoA undergo a series of enzymatic reactions following entry into the TCA cycle. This acetyl-CoA produces ATP, NADH, and $FADH_2$, three essential molecules that are needed in the ETC to produce a substantial amount of ATP. Fatty acid oxidation is an essential metabolic route that enables the cells to use fats as a substitute energy source, particularly in environments with limited glucose availability. As mentioned above, macrophages skew their catabolic metabolism in accordance with nutrient availability; Kupffer macrophages in the liver are in a lipid-rich environment and are therefore more reliant on the breakdown of fatty acids over glucose as a primary energy source (Heieis et al., 2023).

Increased uptake of fatty acids from the extracellular environment generally promotes an anti-inflammatory response in macrophages. Once inside the cell, free fatty acids are shuttled into mitochondria by Carnitine Palmitoyltransferase 1 alpha (CPT1α) and undergo β-oxidation (Figure 1.4). This process produces substrates via the TCA cycle that fuel OXPHOS, acting as signalling molecules for the synthesis of other macromolecules (Almeida and Everts, 2021). Although fatty acid oxidation is often associated with an anti-inflammatory macrophage response (Van den Bossche et al., 2017), under certain conditions, fatty acid oxidation may also contribute to specific pro-inflammatory properties of macrophages, such as NLR family pyrin domain containing 3 (NLRP3) inflammasome activation and IL-1β synthesis (Moon et al., 2016).

1.2.2.5 Amino acid metabolism

Amino acids in macrophages have considerable functional and regulatory roles. Immune cell activation increases the demand for amino acids, leading to the upregulation of amino acid transporters such as the L-type amino acid transporter 1 (LAT1, CD98) (Figure 1.1). Many amino acids are critical for energy generation, and their catabolism contributes to metabolic pathways, notably the TCA cycle. Moreover, amino acids are integral to the synthesis of crucial inflammatory mediators such as cytokines. In myeloid cells, the uptake of amino acids such as tryptophan, arginine and glutamine, and the availability of their metabolites, are key drivers of cellular identity, inducing differentiation, functional polarization, and interaction with other immune cells.

Arginine is a crucial amino acid in various metabolic processes including the urea cycle and protein synthesis, and as a precursor to compounds such as NO and citrulline (Figure 1.1). Arginine metabolism via enzymes such as arginase and iNOS regulate macrophage activation: The expression of *Nos2* (iNOS) by pro-inflammatory macrophages leads to the conversion of arginine into cytotoxic NO and citrulline, hence enhancing the antibacterial properties of macrophages (MacMicking et al., 1997) (Figure 1.5). Nevertheless, excessive generation of NO can lead to hyperinflammation and excessive tissue destruction, as observed in conditions such as influenza and West Nile virus (WNV) encephalitis (Perrone et al., 2013, Xu et al., 2020, Getts et al., 2012). In contrast, M2 macrophages express arginase 1, which results in the synthesis of ornithine and urea (Figure 1.1 and Figure 1.5). This process promotes cellular proliferation and tissue regeneration, but it may also impede crucial T cell activities (Kieler et al., 2021, Kelly and O'neill, 2015).

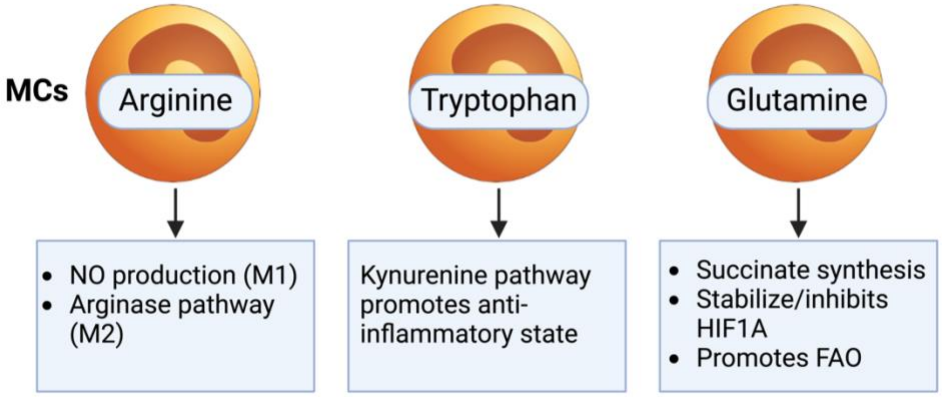

Figure 1.5 Overview of effector functions in MCs associated with arginine, tryptophan, and glutamine metabolism.

Tryptophan, an essential amino acid, is a precursor for NAD+ synthesis, playing a crucial role in glycolysis, the TCA cycle, and OXPHOS *inter alia*. It is mainly degraded through the kynurenine pathway, facilitated by the enzyme indoleamine-2,3-dioxygenase (IDO), which converts tryptophan into kynurenine and other molecules (Fallarino et al., 2012) (Figure 1.1). IDO expression generally increases during inflammation (Kwidzinski and Bechmann, 2007) and can induce an M2-like, anti-inflammatory macrophage phenotype (Figure 1.5), while decreased IDO expression promotes a pro-inflammatory state (Wang et al., 2014). This effect may be mediated by the inverse relationship between IDO and the inflammatory meditator NO, with NO downregulating IDO expression (Thomas and Stocker, 1999, Thomas et al., 1994) (Figure 1.1), and both being induced by IFN-γ, suggesting their relationship is influenced by local structural cellular responses and the temporal flux of responding immigrant immune cells.

Glutamine also serves multiple roles, contributing to nucleotide synthesis, NADPH and energy production, among several other biosynthetic pathways involved in cellular proliferation and functions (Figure 1.1). Interestingly, glutamine usage by these cells is flexible, accommodating both M1 and M2-like macrophage phenotypes, depending on the metabolic demands of the cell. M1 macrophages, which are generally pro-inflammatory, primarily utilize glutamine for succinate synthesis (Figure 1.5). This is facilitated by a disruption in the TCA cycle and stabilizes HIF1α through the gamma-aminobutyric acid shunt (Tannahill et al., 2013) (Figure 1.5). Furthermore, recent findings indicate that glutamine can fuel lactate production and fatty acid oxidation in a glucose-independent manner, even in the absence of a disrupted TCA cycle (Liu et al., 2023). This metabolic flexibility seemingly encourages epigenetic reprogramming toward a pro-inflammatory macrophage phenotype. On the other hand, anti-inflammatory M2 macrophages exploit glutamine metabolism at various stages to adapt to their specific needs. Firstly, the α-ketoglutarate derived from glutaminolysis (glutamine derived from glutamate) serves as fuel for OXPHOS and fatty acid oxidation in M2 macrophages (Figure 1.5) (Liu et al., 2017b). Secondly, glutamine metabolism contributes to the promotion of M2-specific gene expression through epigenetic reprogramming (Liu et al., 2017b). Lastly, it helps inhibit the expression of HIF1-α (Figure 1.5), thus diverging from the pattern observed in M1 macrophages.

1.3 The central nervous system during homeostasis and disease

The CNS, comprising the brain and spinal cord, is critically important in orchestrating the body's functions. Under homeostatic conditions it is a tightly-regulated immunological environment primarily controlled by the blood-brain barrier (BBB). This mechanical barrier, comprised of endothelial cells and other support cells in the brain, restrict the entry of immune cells and other substances. These cells, in conjunction with other resident cells of the brain such as microglia and astrocytes, have a crucial role in preserving neuronal health and synaptogenesis and responding to various housekeeping requirements, such as clearing debris of cellular turnover.

Under disease conditions, however, this equilibrium is disrupted. CNS disease can alter the permeability of the BBB, allowing leakage of large protein molecules, as well as the infiltration of peripheral immune cells. This phenomenon carries the potential of inducing inflammation, which although required for pathogen defence, carries a substantial risk of injuring neurons, which have limited capacity for regeneration. Notably, neurodegenerative diseases, such as Alzheimer's disease, are distinguished by persistent inflammation and the buildup of detrimental inflammatory mediators, whereas more acute conditions such as stroke and viral encephalitis elicit a rapid, but often overexuberant, immune response.

1.3.1 Resident cells

Resident cells of the CNS include cells of nominally immune origin, such as microglia, in addition to other more clearly structural cells, such as astrocytes, oligodendrocytes, neurons, and endothelial cells. Nevertheless, each of these cell types play important roles both in maintaining homeostasis in the CNS and in interacting with the immune system during disease.

Microglia are the primary immune cells of the CNS. They are the tissue-resident macrophages of the brain parenchyma, derived from foetal yolk-sac, seeded during embryogenesis (Ginhoux et al., 2010). The resident microglia population of the CNS is maintained by self-renewal with minimal contribution from peripheral monocytes (Réu et al., 2017, Füger et al., 2017, Ajami et al., 2007, Tay et al., 2017). Under homeostatic conditions, microglia play a number of vital roles, including immune surveillance, synaptic maintenance, regulation of neurogenesis, and the secretion of neurotrophic factors (Spiteri et al., 2020). Following CNS injury, they are also important in scar formation via the generation of a glial scar with other non-immune cells such

as astrocytes (Werner et al., 2020). Under homeostatic conditions, microglia are identified by their low expression of CD45 and high expression of CX3CR1 (Getts et al., 2008, Greter et al., 2015). However, during inflammation, microglia upregulate CD45 and are joined by a large number of phenotypically similar MCs (Spiteri et al., 2020). Thus, a substantial amount of research has aimed to identify microglia-specific markers that are not shared by other infiltrating populations. These have included purinergic receptor P2Y12 (P2RY12), hexosaminidase B (HEXB), spalt like transcription factor 1 (SALL1), and transmembrane protein 119 (TMEM119), among others (Spiteri et al., 2020). It should be noted, however, that some of these 'microglia-specific' markers are downregulated by microglia during inflammation or upregulated by infiltrating MCs, thus limiting their utility in various inflammatory disorders (Spiteri et al., 2020).

In addition to microglia, other tissue-resident macrophages have been identified at the interfaces of the CNS and peripheral compartments. These are generally referred to as border-associated macrophages, which are found in regions such as the meninges, perivascular spaces, and the choroid plexus (Goldmann et al., 2016). These cells play a crucial role in immune surveillance and maintaining homeostasis. They are also involved in regulating the entry of immune cells into the CNS, thus acting as gatekeepers at the BBB and other CNS borders (Liu et al., 2016, Lim et al., 2018, He et al., 2016). Unlike microglia, some border-associated macrophages are partially replenished by peripheral monocytes under homeostatic conditions and do not rely entirely on self-renewal for population maintenance (Goldmann et al., 2016). They are generally identified by expression of specific markers, such as CD206 and CD169 (Goldmann et al., 2016, Jordão et al., 2019).

Astrocytes are supportive cells of non-immune origin that play an important role both in homeostatic and immune functions in the CNS. These cells are generally best-known for their structural support role, providing a scaffold for neurons and aiding in guiding neuronal migration during development (Lee et al., 2022). They also provide structural support to the BBB by forming tight junctions between endothelial cells, thereby regulating the entry of immune cells and other substances into the CNS (Abbott et al., 2006, Alvarez et al., 2013). In addition to their supportive roles, astrocytes perform various maintenance functions, such as nutrient transport, regulating ion balance, neurotransmitter recycling, and regulating synaptic function and plasticity (Volterra and Meldolesi, 2005). In response to injury or disease,

astrocytes adopt a ‘reactive’ phenotype, changing their morphology and function to modulate the immune response, modulate synaptic activity, and aid in tissue repair (Escartin et al., 2021).

Oligodendrocytes are specialized glial cells that are responsible for myelinating neurons. Myelin is a fatty layer that serves as electrical insultation, facilitating rapid transmission of nerve impulses. In various diseases, such as multiple sclerosis (MS) and CNS injury, oligodendrocyte loss is an important contributor to impaired nerve conduction and various neurological deficits (Kuhn et al., 2019). Loss of oligodendrocytes can also contribute to neurodegeneration, as these cells provide neuronal support and protection that shield axons from physical and chemical injury (Kuhn et al., 2019). Conversely, regeneration of mature oligodendrocytes from oligodendrocyte progenitor cells facilitates remyelination and regeneration in the damaged CNS (Kuhn et al., 2019).

Neurons themselves, while primarily responsible for transmitting information, can also influence the immune response. These cells can release neurotransmitters and other signaling molecules that alter the activity of microglia and astrocytes, thereby influencing the inflammatory environment (Szepesi et al., 2018). Neurons can also produce chemotactic molecules that recruit peripheral immune cells to the site of injury or infection (Getts et al., 2008). They express very low levels if any MHC molecules normally, even during early infection, which presumably has temporal protective implications for NK and T cell recognition and interactions (Spiteri et al., 2024).

1.4 Monocytes in neurological diseases: function, phenotypes, and metabolic profiles

Inflammation of the CNS is a pathological feature of various neurological disorders that is often associated with neurodegeneration and a progressive decline in neurological function. While a variety of immune cells contribute to this process, the role of monocytes is particularly notable due to their significant potential to exacerbate damage. Monocytes play a pivotal role in the pathogenesis of disease across different contexts, including sterile tissue injury, autoimmune-induced inflammation, and viral infection of the brain. Although these conditions have different causes and involve various cell types, mitigating uncontrolled inflammation—largely driven by inflammatory monocytes—is a shared goal of numerous treatment approaches aimed at diminishing the progression of these diseases.

Monocytes exhibit a degree of functional overlap across different disease states; however, they also develop unique and disease-specific phenotypes, transcriptional signatures, metabolic patterns, and functions. Technological advances, particularly in single-cell profiling, have significantly improved our understanding of monocyte heterogeneity in disease. These approaches allow for detailed characterization of monocytes at the individual cell level, both transcriptionally and phenotypically. Such precise measurements have significantly refined our grasp of the wide array of monocyte profiles associated with disease and their various functions, offering promising insights for more targeted therapeutic strategies that may differentially target protective and pathogenic monocyte subsets in disease to modulate these functions.

1.4.1 Sterile injury

Sterile injury in the CNS most commonly occurs as a result of stroke or mechanical/percussive damage, with the former likely to complicate the latter. *Stroke* is broadly classified into two types: hemorrhagic and ischemic. The latter is accountable for around 10% of global mortality and represents 5% of the total number of years lived with disability (Naghavi et al., 2017). Hemorrhagic stroke occurs from blood vessel rupture, leading to bleading within or around the brain. This is often caused by high blood pressure, aneurysm or vessel malformations. Strokes mostly result from ischemia (Katan and Luft, 2018), which results from occlusion of the arteries caused by atherosclerosis, arterial plaque rupture, embolism from the heart, or diseases in smaller blood vessels generally linked to high blood pressure (Vos et al., 2017, Katan and Luft, 2018). Ischemic stroke presents with diverse clinical signs and symptoms, which are influenced by factors such as the severity and duration of ischemia, the specific brain region affected, as well as the patient's age, gender, and the existence of other comorbidities (Sommer, 2017). Rodent models can replicate certain consequences of ischemic brain injury, but generally fall short of accurately reflecting the complex pathophysiological mechanisms and comorbidities that contribute to spontaneous stroke in humans (Macrae, 2011).

Spinal cord injury (SCI) is an incapacitating condition that arises from acute trauma to the spinal cord. This results in permanent deficits in motor, sensory, and autonomic functions distal to the location of the lesion. Immunologically, SCI is characterized by an initial mechanical injury, followed by a subsequent inflammatory response that can result in secondary tissue damage, exacerbating the original damage and associated functional deficits (Anjum et al., 2020, Alizadeh et al., 2019). Disability from SCI therefore varies, depending on the degree of

initial injury and the extent of secondary damage. A contusion or compression injury model is frequently used in rodents to study SCI, which closely mimics the human condition by inducing similar pathophysiological changes in the spinal cord (Cheriyan et al., 2014).

Traumatic brain injury (TBI) similarly results from external mechanical force to cause disruption of normal brain function. This can include cognitive, physical and psychosocial deficits (Maas et al., 2008). The neuroinflammatory response following injury is a decisive factor in the pathogenesis of TBI, and, as for SCI, can lead to secondary brain damage (Davis, 2000). To replicate the clinical manifestations of TBI, animal models such as the controlled cortical impact model have been developed (Xiong et al., 2013). This model enables investigation of the involvement of immune cells in the inflammatory cascade following injury (Xiong et al., 2013). However, accurate replication of the human condition is limited, primarily due to disparities in the physiological responses to injury and the heterogeneity of clinical presentation between the two species (Xiong et al., 2013).

1.4.1.1 Monocytes in sterile injury

The immune response to CNS injury is significantly influenced by the infiltration of peripheral immune cells. In particular, monocytes play a critical role in determining the course of disease. Monocytes exhibit dualistic functions in the processes of tissue recovery and damage. On one hand, they aid in the removal of debris and facilitate tissue healing. On the other hand, they can also adopt a pro-inflammatory phenotype, which poses a lethal threat to the integrity of the surviving tissue, especially adjacent to the primary damage (Yong et al., 2019). The various roles of monocytes in CNS injury, in addition to their phenotype (RNA and protein) are detailed in Table 1.3.

After injury, monocytes release inflammatory mediators, such as TNF and IL-1β, which exacerbate damage and further impair function, especially in hemorrhagic stroke (Ritzel et al., 2015, Dimitrijevic et al., 2007, Kronenberg et al., 2018, Hammond et al., 2014). Indeed, in ischemic stroke, TBI, and SCI, CCR2-deficient mice show a reduction in inflammation and secondary damage when monocytes are depleted (Dimitrijevic et al., 2007, Kronenberg et al., 2018, Somebang et al., 2021, Zhang et al., 2021). However, the presence of pro-inflammatory monocytes facilitates immune processes essential for healing, notwithstanding their involvement in secondary damage (Yong et al., 2019) and their depletion increases the likelihood of hemorrhagic transformation following stroke. This emphasizes the essential role of these cells in tissue repair and highlights their functional duality (Gliem et al., 2012).

Pro-inflammatory monocytes enhance microglial activation, which is essential for the generation of glial scars and which in turn play a crucial role in wound containment (Rohl et al., 2007). The role of inflammatory monocytes in promoting microglial proliferation and subsequent repair has been demonstrated in experimental ischemic stroke models. After the initial inflammatory reactions, monocytes are trapped by the glial scar, a process aided by C-X-C chemokine receptor type 4 (CXCR4)-C-X-C motif chemokine 12 (CXCL12) signaling, reducing additional damage (Werner et al., 2020). Furthermore, a recent study identified stroke-associated myeloid cells following ischemic injury, which comprised a mixed population of microglia and peripheral myeloid cells (Beuker et al., 2022). These cells showed signs of enhanced lipid metabolism and phagocytosis, suggesting that this population was required for clearance of lipid-rich debris, such as oligodendrocytes, following ischemic injury

Table 1.3. Functions and phenotypes of monocytes in sterile injury

RNA	***Cxcr4*-GFP^{+}CD45^{hi}CD11b^{+}Ly6C^{hi} MCs** ↑ *Siglech Cx3cr1* and *C1q* ('microglia-specific' genes) ↑ *Cybb* and the Src kinase *Fgr* (super-oxide-generating) ↑ *Tlr8*, *Ifi202*, *Clec7a*, *Clec4d* and *Oas2* (pattern recognition molecules) ↑ *C3*, *Cfb* and *Cfp* (complement system components) ↑ *H2-Aa*, *H2-Ab1* and *CD74* (antigen processing and presentation via MHC-II) ↑ *Irf7*, *Ifi200b*, *Ifi202*, *Ifitm2*, *Ifitm3*, *Oas2*, *Oasl2*, *Rsad2*, *Trim25* and *Tlr8* (interferon-related genes) ↑ *Ccr1*, *Ccr2*, *Cxcr4*, *Plxna1*, *Plxnc1*, *Plxnd1*, *Adgre5*, *Gpr35*, *Gpr65* and *Gpr132* (cell surface receptors) ↑ *Thbs1*, *Emp1*, *Ifi207* and *Dab* (Other genes) (Photothrombotic stroke model , RNA-seq, (Werner et al., 2020)
Protein	**CD45^{hi}CD11b^{+}Ly6C^{+}Ly6G^{-} monocytes** (tMCAO, flow cytometry, (Ritzel et al., 2015)
	***Cxcr4*-GFP^{+}CD45^{hi}CD11b^{+}Ly6C^{hi} Ly6C^{hi} monocytes/MCs** (PT and tMCAO, flow cytometry, (Werner et al., 2020)
	CD45^{hi}CD11b^{+}Ly6C^{lo}CX3CR1^{int} MCs ↑ CX3CR1, CD206 and Dectin-1 ↓ Ly6C (middle cerebral artery occlusion stroke model, flow cytometry, (Wattananit et al., 2016)
Neuro-protective roles	• Ly6C^{hi} monocyte infiltration correlated with the expression of anti-inflammatory genes *TFG-β, CD163* and *Ym1* and are required for long-term functional recovery from stroke (Wattananit et al., 2016). • Depletion of Ly6C^{hi}CCR2^{+} monocytes worsened functional outcomes and increased infarct volume 24 hours post-stroke (Chu et al., 2015). • Ly6C^{hi} monocyte infiltration prevents hemorrhagic infarct transformation and correlates with tissue expression of *collagen-4*, *TGF-β1* and *thrombospondin-1* genes, implicating a role for BBB maintenance following ischemic injury (Gliem et al., 2012).
Neuro-toxic roles	• Ly6C^{hi} monocyte infiltration exacerbates infarct volume at 24 hours and five days post-stroke (Dimitrijevic et al., 2007, Kronenberg et al., 2018), and contributes to early motor deficits in the first three days post-intracerebral hemorrhage (Hammond et al., 2014).

after stroke, which was shown to be mediated by triggering receptor expressed on myeloid cells 2 (TREM2) (Kurisu et al., 2019). Together, this work demonstrates that monocytes are involved in the repair phase following stroke, either through promoting microglial activation to help in forming a glial scar, or by clearing cellular debris.

The paradoxical functions of monocytes following injury can likely be ascribed to their ability to differentiate into distinct populations that may either contribute to secondary damage or aid in tissue repair. In mechanical spinal cord injury models, various monocyte subsets infiltrate into the CNS via distinct routes. 'Protective' monocytes enter through the choroid plexus, while potentially damaging monocytes enter through the spinal cord leptomeninges, relying on the CCL2 chemotactic pathway (Shechter et al., 2013). The differential recruitment and subsequent function inside the CNS may pre-ordained by Ly6C expression of the immigrant monocytes (Terry et al., 2015).

1.4.1.2 Metabolic profiles of monocytes in sterile injury *in vivo*

Monocytes play a crucial role in controlling neuroinflammation and promoting tissue healing following injury by mechanisms such as phagocytosing apoptotic cells and debris (Van Broeckhoven et al., 2021). Post-SCI there is a marked build-up of myelin debris, which hinders the regeneration of neural tissue (Sheng et al., 2021). Monocytes can contribute to remyelination and neural regeneration, however, excessive phagocytosis of myelin debris by these cells can disrupt intracellular lipid homeostasis, leading to the development of pro-inflammatory, foamy macrophages (Kopper and Gensel, 2018, Ryan et al., 2022, Bogie et al., 2020) (Figure 1.6). These macrophages have reduced functionality and maintain chronic M1-like characteristics, which worsens the accumulation of myelin debris and hinders regeneration (Gensel and Zhang, 2015).

Transcriptional analyses show that macrophages infiltrating the site of SCI initially take on a pro-inflammatory and migratory phenotype in the acute stage of injury (Zhu et al., 2017). As the injury persists, these cells transition to a lipid metabolic phenotype. This transition is influenced by nuclear receptors that sense lipids, such as Liver X Receptor/Retinoid X Receptor and Peroxisome Proliferator-Activated Receptor Alpha, which regulate the synthesis and breakdown of fatty acids (Zhu et al., 2017). Macrophages display a foam cell-like phenotype 7 days after the damage. Significantly, the genetic deletion of CD36, a receptor that

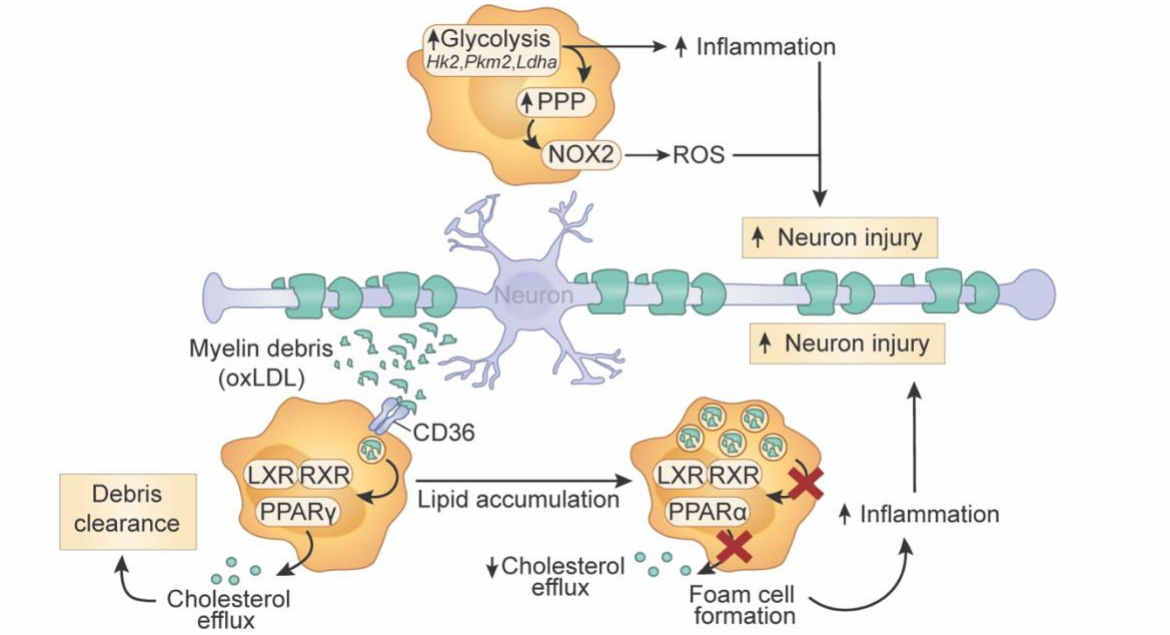

Figure 1.6 Monocyte metabolic profiles in sterile injury in vivo.

Pro-inflammatory MCs exhibit a glycolytic metabolic profile that generates ROS via the PPP, exacerbating inflammation and neuron injury. In addition, MCs expressing CD36 facilitate the phagocytosis of myelin debris, promoting a 'lipid metabolism' phenotype regulated by nuclear receptors such as Liver X Receptor (LXR)/Retinoid X Receptor (RXR) and Peroxisome Proliferator-Activated Receptor Alpha (PPARα). This phenotype initially aids in regeneration but excessive phagocytosis leads to foam cell formation due to impaired cholesterol recycling, which hinders tissue regeneration and heightens inflammatory responses, increasing neuron damage.

binds to oxidized lipids, is associated with a significant decrease in the build-up of lipid droplets within macrophages (Zhu et al., 2017). These findings suggest that the formation of foam cell macrophages hinders their ability to clear myelin debris, likely because the route responsible for recycling cholesterol becomes overloaded. As a result, this contributes to ongoing inflammation and limits the ability to regenerate tissue after SCI (Van Broeckhoven et al., 2021).

Myelin breakdown after ischemic stroke generates several different types of lipids, including polyunsaturated fatty acids, free cholesterol, cholesterol esters, and phospholipids (Becktel et al., 2022, Chung et al., 2018), which undergo various processes in parallel. Stroke-induced infarcts promote both enzymatic and non-enzymatic lipid peroxidation, leading to increased oxidation of lipoprotein particles (Zeiger et al., 2009). Scavenger receptors, such as CD36, identify lipids that have undergone oxidation (Stewart et al., 2010). In addition, after stroke, myeloid cells in the brain upregulate cholesterol metabolism pathways, which are necessary for removing damaged myelin from the ischemic brain (Beuker et al., 2022). Studies have shown that microglia and monocytes recruited after a stroke have an increased phagocytic ability, particularly evident in the expression of CD36 (Beuker et al., 2022). These findings further support the important role of myeloid cells in removing lipid debris after a stroke.

Research on the metabolic profiles of MCs following CNS injury is limited. Thus, insights into the metabolic processes facilitating cellular debris clearance has in part been derived from the established metabolic pathways identified in controlled *in vitro* settings or from analogous processes observed in peripheral organs following injury. Efferocytosis is known to rely on aerobic glycolysis during engulfment of apoptotic cells, as indicated by increased glucose uptake and enhanced lactate release (Morioka et al., 2018), which may support the upregulation of receptors recognizing apoptotic cells (Schilperoort et al., 2023), or the energy-intensive demands of cytoskeleton rearrangement during phagocytosis (Morioka et al., 2018). Cytoskeletal rearrangement may also be supported by arginine and ornithine derived from apoptotic cells, which are metabolized into the polyamine putrescine pathway in macrophages via arginase 1 and ornithine decarboxylase during efferocytosis (Yurdagul et al., 2020). Moreover, fatty acids derived from apoptotic cells can trigger a metabolic cascade post-efferocytosis, leading to anti-inflammatory signaling via the activation of the IL-10 transcription factor, pre-B cell leukemia transcription factor-1 (Zhang et al., 2019c). This research also noted an increase in lipid metabolites associated with fatty acid oxidation, along

with the enhanced expression of genes related to mitochondrial electron transport and OXPHOS. Furthermore, glutamine catabolism through a non-canonical transaminase pathway has been shown to fuel mitochondrial OXPHOS and ATP production to potentiate efferocytosis, while enabling the synthesis of the antioxidant, glutathione, to prevent oxidative stress from phagocytosis of apoptotic cells (Merlin et al., 2021). Finally, efferocytosis stimulates the kynurenine pathway (Ravishankar et al., 2012), enhances fatty acid oxidation (Zhang et al., 2019c), and activates the sterol pathway (Noelia et al., 2009). However, this metabolic signature may depend on the type of apoptotic cells, as the phagocytosis of neoplastic cells by macrophages in a lung tumour model revealed a specific gene expression signature linked to OXPHOS, glycolysis, and gluconeogenesis, in addition to ribosomal gene expression (Gonzalez et al., 2023). As described above, it is therefore likely that efferocytosis of certain cells following CNS injury, such as apoptotic neurons or oligodendrocytes, induce distinct metabolic programs. Together, these studies demonstrate that efferocytosis relies on various metabolic processes, including aerobic glycolysis, arginine and ornithine metabolism, fatty acid oxidation, and glutamine catabolism, which collectively support the engulfment of apoptotic cells and subsequent cellular functions.

In addition to their phagocytic functions in CNS injury, MCs may exacerbate inflammatory damage via the production of ROS , which can permanently damage neurons, contributing to secondary injury. To generate ROS, MCs channel glycolytic intermediates toward the oxidative arm of the PPP, facilitating ROS production via NADPH and NADPH oxidases (NOX) (Viola et al., 2019). Anti-inflammatory macrophages, on the other hand, use the non-oxidative branch of the PPP, which provides redox equilibrium to support cellular antioxidants such as glutathione (Blagih and Jones, 2012). Post SCI and TBI, there is an increase in macrophage-specific NOX activity (NOX2) in macrophages and microglia at the site of injury (Cooney et al., 2013, Cooney et al., 2014). Increased NOX activity is associated with increased ROS output from macrophages and microglia and NOX inhibition has been shown to improve SCI and TBI outcomes (Zhang et al., 2016, Zhang et al., 2019a, Zhang et al., 2012). Indeed, NOX2 deficiency notably increases anti-inflammatory macrophage/microglial activation after TBI (Barrett et al., 2017). These findings highlight the significance of redox-associated metabolic processes and antioxidant mechanisms in orchestrating the inflammatory response following CNS injury, suggesting that modulating these pathways may present viable strategies for reducing oxidative stress and promoting recovery following injury.

Finally, in the early stage of ischemia, $CD11b^+$ cells in the damaged CNS of mice with a permanent middle cerebral artery occlusion express genes related to both glycolysis and OXPHOS. Genes related to glycolysis, such as lactate dehydrogenase A and pyruvate kinase M2, remain expressed for a prolonged period after an injury (Lauro et al., 2019). Moreover, inhibition of hexokinase 2, a rate-limiting glycolytic enzyme, reduced microglial activation, providing neuroprotection *in vivo* (Li et al., 2018c), emphasizing the link between the metabolic change to glycolysis in brain myeloid cells and their pro-inflammatory profile following ischemic injury.

1.4.2 Demyelinating disease

MS is a recognized chronic inflammatory demyelinating disorder in the CNS, presumptively of autoimmune origin. A hallmark of this disease is a recrudescent or continuous neuroinflammation that results in progressive degeneration of neurons and oligodendrocytes, leading to increasing physical and cognitive impairments with time (van Wageningen et al., 2019, Voet et al., 2019). The disease presents in various forms, including isolated clinical cases, gradually progressive disease, or in a relapsing-remitting pattern that serves as the primary diagnosis for approximately 85% of cases and may develop into a secondary progressive type over 10-15 years (Tanabe et al., 2019, Wimmer et al., 2019). Immigrant cells of both innate and adaptive immune systems play a crucial role in MS progression (Dendrou et al., 2015, Marik et al., 2007, Schirmer et al., 2009).

MS is primarily modelled in mice using Experimental Autoimmune Encephalomyelitis (EAE). Initiation of inflammation in EAE is predominantly through the activation of MHC class II-restricted autoreactive T cells, triggered either by the injection of encephalitogenic antigens or by adoptive transfer of encephalitogenic $CD4^+$ T cells (Constantinescu et al., 2011). The progression and characteristics of EAE vary, based on the method of induction, the mouse strain and its specific genetic alterations (Burrows et al., 2019, Kipp et al., 2017). However, most EAE models fall short of fully mirroring the intricate pathological features of MS, due to the diverse range of clinical presentations and lesion types observed across various disease stages and anatomical compartments (Lucchinetti et al., 2000, Popescu and Lucchinetti, 2012). These include the uneven distribution of lesions across the brain and spinal cord, the composition of lymphoid cell types involved (Calabrese et al., 2015), and the degree of demyelination in grey matter areas. Furthermore, the extensive grey matter pathology typical in MS patients (Popescu and Lucchinetti, 2012), marked by a demyelination pattern that

includes chronic activation of microglia, lack of leukocyte infiltration, and significant meningeal inflammation, is not accurately reflected in most EAE models (Howell et al., 2011). Despite these limitations, EAE models remain invaluable for elucidating many of the pathological underpinnings of MS and remain the foremost platform for testing new therapeutic strategies (Kipp et al., 2017).

1.4.2.1 Role of monocytes in disease progression: antigen presentation and inflammatory myelin damage

Monocytes play an essential role in the progression of MS (Kuhlmann et al., 2017). In EAE, these cells migrate from the BM to the CNS before symptoms manifest (King et al., 2009, Mildner et al., 2009), indicating their important contribution to the pathogenesis and progression of disease. Their migration, largely driven by CCR2, is essential for the development of EAE. Studies have demonstrated that mice without CCR2 are not susceptible to EAE (Izikson et al., 2000, Mildner et al., 2007, Fife et al., 2000, Greter et al., 2015), emphasizing the significance of monocytes in disease pathogenesis. Monocytes contribute to the disease through various mechanisms, including the activation of T cells through antigen presentation and the breakdown of myelin by inflammation. The various roles of monocytes in autoimmune inflammation, including their RNA and protein phenotypes, are detailed in Table 1.4.

Monocytes have a crucial function in presenting antigens, particularly in activating encephalitogenic T cells, which is essential for inducing disease (Constantinescu et al., 2011). The difference in antigen-presenting roles between CNS-resident DCs and monocyte-derived DCs is not well-defined, but DCs have historically been linked to this function. CNS-infiltrating myeloid cells have been demonstrated to have extended interactions with T cells (Mundt et al., 2019, Jordão et al., 2019), emphasizing their importance in disease progression. Although some research indicates that monocyte-derived DCs may have reduced efficiency in displaying myelin peptides to T cells (Giles et al., 2018, Mundt et al., 2019), their role in activating and differentiating T helper type 17 cells highlights their impact on disease progression (Ko et al., 2014, Miller et al., 2007).

Moreover, the involvement of CNS-infiltrating monocytes and resident microglia in MS is evident through non-specific inflammation and myelin degradation (Nikić et al., 2011, Grassivaro et al., 2020). MCs surrounding the nodes of Ranvier express a pro-inflammatory signature, indicating that these cells actively participate in myelin destruction (Yamasaki et al.,

2014). Recent advances have shown the diversity of monocyte subsets and their roles in causing inflammation, such as a toxic phenotype linked to oxidative stress that exacerbates tissue damage (Mendiola et al., 2020). Interestingly, these monocytes may transition from a pro-inflammatory state to a tissue-repair state (Locatelli et al., 2018), showcasing their versatile function in disease development and recovery.

Monocytes display various phenotypes during EAE, with the surrounding inflammatory milieu playing a decisive role in defining their functional diversity and contribution to the disease process. Such an environment may include cytokines like granulocyte-macrophage colony-stimulating factor (GM-CSF), secreted by surrounding autoreactive T cells at the site of inflammation. GM-CSF signalling is also thought to elicit a distinct transcriptional response in monocytes, critical for initiating disease (Croxford et al., 2015, Komuczki et al., 2019). Monocytes with impaired GM-CSF signalling are not implicated in the degradation of myelin (Greter et al., 2012), indicating that their pathogenic role is heavily reliant on GM-CSF produced by autoreactive T cells. The temporal and spatial dynamics within the inflammatory setting also differentiate the roles of monocyte-derived infiltrates. Tracking studies have shown that cells with pro-inflammatory markers ($iNOS^+$) are primarily found within spinal cord lesions and perivascular regions (Locatelli et al., 2018). Meanwhile, cells bearing anti-inflammatory markers (arginase-1^+) are typically located in the meninges (Locatelli et al., 2018, Ivan et al., 2021). Initially, the pro-inflammatory ($iNOS^+$) phenotype dominates lesion sites, but as the lesion heals, these cells locally adjust, shifting towards an anti-inflammatory phenotype which appears to aid EAE recovery (Locatelli et al., 2018). Interestingly, when introduced into a healthy CNS, pro-inflammatory ($iNOS^+$) cells can rapidly transition to an anti-inflammatory ($Arg1^+$) state, highlighting the influence of the CNS microenvironment on MC (Locatelli et al., 2018). Notably, in the absence of inflammation resolution in lesions, cells with an anti-inflammatory profile can revert to a pro-inflammatory state due to persistent inflammatory conditions (Giladi et al., 2020), likely as a transcriptional response to the complex milieu where tissue damage and repair processes occur simultaneously.

Finally, various studies using single-cell RNA-sequencing and mass cytometry have unveiled the heterogeneity of monocytes in EAE (Jordão et al., 2019, Ajami et al., 2018, Giladi et al., 2020). These cells can adopt highly specialized profiles that are time point-specific and are likely influenced by the changing inflammatory environment that occurs in spinal cord lesions. Indeed, recent studies have found particular types of monocytes with pro-inflammatory

characteristics that play a vital role during the peak of the disease (Table 1.4), indicating the potential for a focused strategy to enhance clinical outcomes (Giladi et al., 2020). This highlights the intricate nature of monocyte functions and how the inflammatory environment impact their function.

Table 1.4. Functions and phenotypes of monocytes in models of multiple sclerosis.

RNA	**Ly6C^{hi}CD11c^{+}MHC-II^{+}CD11b^{+}CD45^{hi} MoDC** **GM-CSF-dependent gene signature:** ↑ *CCL6, CCL17, CCL24* and *Tnfrsf9* (co-stimulatory molecules) ↑ *Mfge8, Cd1d1, Pld1, Scarb1, Clec7a* and *Anxa1 (*phagocytosis-associated genes) ↑ *Asc, NLRP3, and Pycard (*inflammasome-associated genes*)* (peak EAE, next-generation sequencing (Croxford et al., 2015))
	Four MC populations in the parenchyma and perivascular space, all expressing *Ly6c2, Ccr2, Cd44* and *Fcgr1* • **Ly6C^{hi} monocytes:** *Fn1* • **MertK^{+} MoDM subset 1:** *Fn1* and *Mertk* • **MerTK^{+} MoDM subset 2 and 3:** *Fn1, Mertk, Mrc1* and *Ms4a7* • **MoDC:** *Fn1, Kmo* and *Zbtb46* (peak EAE, single-cell RNA seq, (Jordão et al., 2019)
	Seven monocyte populations: • **Ly6C^{hi} monocytes:** *Ly6c2, Sell* and *Ccr2* • **Ly6C^{lo} monocytes**: *Nr4a1* and *Pparg* • **Ifit2^{+} monocytes:** *Ifit1, Ifit2, Ifit3, Usp18* and *Irf7* • **Arg1^{+} macrophages:** *Arg1, Apoc2* and *C1qb* • **Nos2^{+} macrophages:** *Nos2, Gpnmb, Arg1*and *Fabp5* • **Saa3^{+} monocytes:** *Saa3, Plac8* and *Gbp2* • **Cxcl10^{+} monocytes:** *Cxcl9, Cxcl10* and *Il1b* (peak and chronic EAE, MARS-seq, (Giladi et al., 2020)
	Seven monocyte/macrophage (Mp) populations: Top 10 differentially expressed genes and top gene ontology terms associated with each population • **Mp I:** *Clec4n, Inhba, Cd9, Ccl6, Clec7a, Cfb, Bcl2a1d, Il1a, Nos2* and *Arg1* (ROS metabolic process) • **Mp II:** *Cd81, Sparc, Ccl12, C1qa, C1qc, Hexb, Cx3cr1, Ly86, Olfml3* and *Cd63* (inflammatory response) • **Mp III:** *Apoe, C1qc, C1qa, C1qb, Apoc2, Trem2, Ccl5, Ms4a7, H2-Eb1* and *H2-Aa* (antigen processing and presentation via MHC-II) • **Mp IV:** *Apoe, C1qa, Ms4a7, C1qb, C1qc, Lgmn, Cx3cr1, Ccl12, Ly86* and *Trem2* (lipid catabolic process) • **Mp V:** *Plac8, Isg15, Gbp2, Ms4a4c, Ifitm1, Ccr2, Tgm2, Actb, Fgl2* and *Ifit3* (response to interferon-β) • **Mp VI:** *Cxcl10, Ifitm6, S100a4, Lrg1, Ifi203, Gm9733, Ifitm2, Tspan13, Wfdc17* and *Tmem176b* (cytokine production) • **Mp VII:** *S100a9, S100a8, Ngp, Camp, Retnlg, Lcn2, 1100001G20Rik, Ltf, Ifitm6* and *Pglyrp1* (leukocyte migration) (onset EAE, Toxic-RNA seq, (Mendiola et al., 2020)
Protein	Five MC subsets, all expressing CD45^{+}CD11b^{+}Ly6C^{+} • **Subset D:** PD-L1^{+}MHC-II^{+}Axl^{hi}MerTK^{int}TREM2^{int} CD86^{hi}CD80^{hi}CD206^{lo}CD39^{hi}CD38^{hi} • **Subset E:** PD-L1^{+}MHC-II^{-}Axl^{hi}MerTK^{int}TREM2^{int}CD86^{hi}CD80^{hi}CD206^{lo}CD39^{hi}CD38^{hi} • **Subset F:** PD-L1^{-}CD88^{-}IL-17R^{-}Axl^{-}MerTK^{-}TREM2^{-}CD86^{int}CD80^{-}CD206^{-}CD39^{int}CD38^{lo}

	• **Subset G:** PD-L1^{-}CD88^{+}IL-17R^{-}Axl^{-}MerTK^{-} TREM2^{lo}CD86^{lo}CD80^{lo}CD206^{-} CD39^{lo}CD38^{int} • **Subset H:** PD-L1^{-}CD88^{+}IL-17R^{+}Axl^{lo}MerTK^{lo} TREM2^{lo}CD86^{int}CD80^{lo}CD206^{lo}CD39^{int}CD38^{int} (pre-symptomatic, peak, recovery and chronic EAE, CyTOF, (Ajami et al., 2018)
	Two MC subsets • MerTK^{+} MC: MerTK^{+}CD64^{+}Ly6C^{+}CD44^{+} • CD209^{+} MC: CD209^{+}CD64^{+}Ly6C^{+}CD44^{-} (peak EAE, flow cytometry, (Jordão et al., 2019)
	CD45^{hi}CD11b^{+}F4/80^{+} macrophages • Upregulation of MHC class II (JHM strain murine heptatitis virus-induced demyelination, flow cytometry, (Savarin et al., 2018)
Neuro-protective roles	• NO^{+} and Arg1^{+} MCs may represent CD11b^{+}Ly6C^{hi}Ly6G^{-}F4/80^{+}CD93^{+} cells, a subset of myeloid-derived suppressor cells, capable of suppressing CD4^{+} and CD8^{+} T cells through the production of NO in culture (Zhu et al., 2007). • Adoptively transferred monocytes treated with the MS drug, glatiramer acetate, reversed EAE paralysis by inducing MHC II-restricted regulatory T cells and T helper 2 cells in an antigen-independent manner (Weber et al., 2007).
Neuro-toxic roles	• CCR2- (Izikson et al., 2000, Mildner et al., 2007, Fife et al., 2000, Greter et al., 2015) or CD49e (Ajami et al., 2018)-dependent Ly6C^{hi} monocyte infiltration into the spinal cord is necessary for EAE induction (Ajami et al., 2018, Izikson et al., 2000, Mildner et al., 2007, Fife et al., 2000, Greter et al., 2015) and exacerbates disease severity (Ajami et al., 2018). • MCs initiate myelin destruction at the Nodes of Ranvier (Yamasaki et al., 2014). • CD11c^{+}CCR2^{+} MCs may stimulate myelin-reactive T cells, as selective deletion of MHC-II on both peripheral and CNS-resident CD11c^{+} myeloid cells, but not CNS-resident myeloid cells alone, prevented EAE induction, and CCR2^{+} peripheral myeloid cells preferentially show long-lasting interactions with autoreactive CD2^{+} T cells (Jordão et al., 2019). • GM-CSF-stimulated MCs contribute to EAE induction (Croxford et al., 2015), and clinical disease severity (Croxford et al., 2015), and participate in de-myelination (Spath et al., 2017, Croxford et al., 2015) via the production of IL-1β and ROS (Spath et al., 2017).

1.4.2.2 Metabolic profiles of monocytes in demyelinating disease

In the study of MS pathogenesis, particularly within the EAE model, MCs are implicated in critical immune functions, such as the production of inflammatory cytokines, phagocytosis of apoptotic debris, remyelination processes, and antigen presentation (Spiteri et al., 2021b) (Figure 1.7). These processes necessitate substantial energy and specialized biosynthesis, correlating with unique metabolic demands in MCs.

Glycolysis is closely linked to inflammation in MS. Patients with relapsing-remitting MS exhibit a pronounced upregulation of the glycolytic pathway, as evidenced by elevated serum levels of glycolysis-related metabolites, which were shown to correlate with episodes of neuroinflammation (Zahoor et al., 2022). In exploring the therapeutic potential of glycolytic inhibition, 2-deoxy-D-glucose (2DG)—a known inhibitor of this pathway—was utilized in the

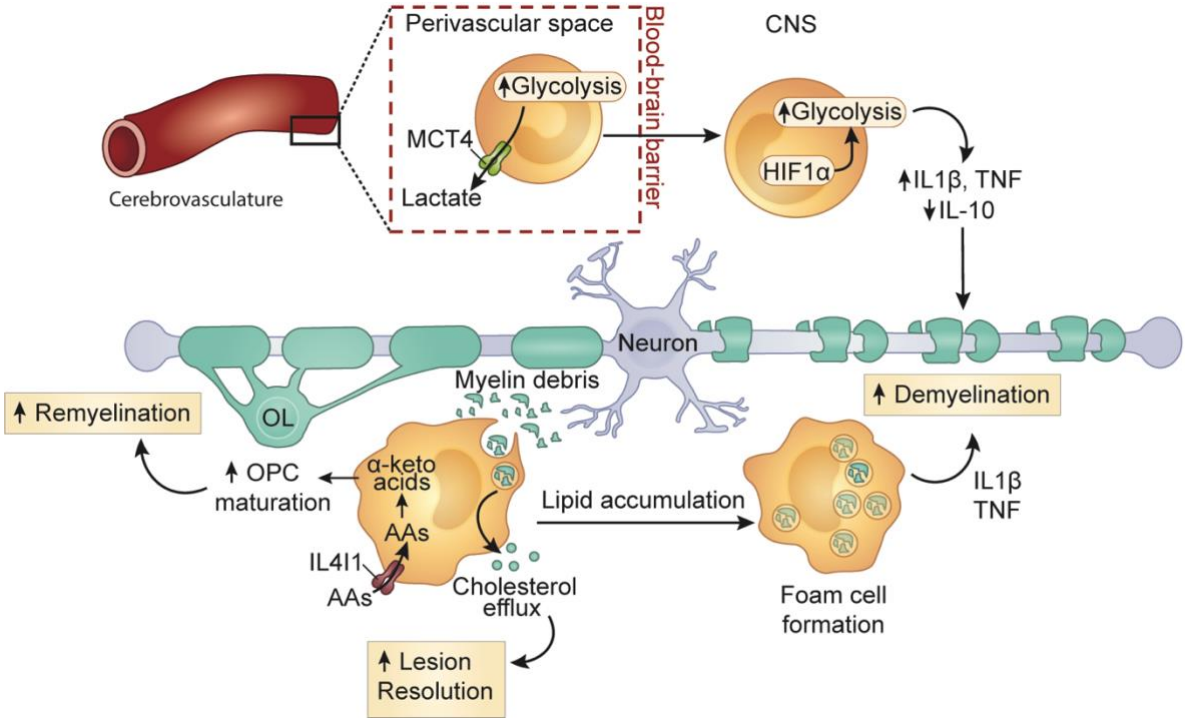

Figure 1.7 Monocyte metabolic profiles in autoimmune neuroinflammation.

Glycolysis facilitates monocyte transmigration across the BBB, where cells express lactate dehydrogenase A (LDHA) and monocarboxylate transporter 4 (MCT4) for lactate efflux. Post-BBB crossing, monocyte-derived cells adopt a HIF1α-driven glycolytic phenotype, promoting inflammatory cytokines and suppressing anti-inflammatory IL-10. Initially, phagocytosis of myelin debris is initially pro-resolving, but excessive myelin leads to cholesterol recycling impairment and foam cell formation, exacerbating inflammation and demyelination. Remyelination may be aided by amino acid metabolism; monocytes IL41I convert amino acids into α-keto acids, promoting oligodendrocyte progenitor cell (OPC) maturation and remyelination.

EAE model. Treatment with 2DG not only attenuated myelin-specific immune cell proliferation and the production of proinflammatory cytokines but also enhanced the generation of the anti-inflammatory cytokine IL-10 (Zahoor et al., 2022). Moreover, it significantly reduced the pro-inflammatory phenotype of monocytes/macrophages, which aligned with a reduction in glycolytic activity, as indicated by decreased glucose and lactate levels and lower expression of glycolytic enzymes (Zahoor et al., 2022). Crucially, monocytes treated with 2DG, when adoptively transferred into EAE mice, led to milder EAE symptoms (Zahoor et al., 2022), emphasizing the therapeutic promise of glycolysis inhibition in mitigating acute inflammatory phases in MS progression by promoting an anti-inflammatory monocyte phenotype.

Glycolysis not only promotes a pro-inflammatory phenotype but is also essential for monocyte transmigration across the BBB in EAE. Monocytes located in perivascular cuffs exhibit elevated lactate dehydrogenase A expression, an enzyme critical for the glycolytic conversion of pyruvate to lactate during inflammatory responses (Kaushik et al., 2019). Additionally, these cells expressed significant levels of monocarboxylate transporter-4, a transporter important for lactate efflux from glycolytically active cells (Tan et al., 2015). Intriguingly, such expression is localized to the perivascular spaces, not the CNS parenchyma, with similar patterns observed in MS patient brains (Nijland et al., 2014), emphasizing the importance of glycolysis in migrating across endothelial barriers. Glycolytic dependency is further evidenced by the reduced transmigration following lactate dehydrogenase A and monocarboxylate transporter-4 knockdown (Kaushik et al., 2019). Sites of inflammation in MS are often hypoxic and acidic, and accordingly, show increased expression of hypoxic markers and expression of glucose transporters compared to healthy patients, most likely due to increased glycolysis of infiltrating cells (Nijland et al., 2014). HIF1α, a regulator of glycolysis under hypoxic conditions, is also stabilized in these inflammatory macrophages. As the switch toward aerobic glycolysis in activated macrophages is at least in part orchestrated by HIF1α, this suggests a complex glycolytic reprogramming that supports monocyte infiltration into the brain in MS pathology.

Notably, glycolysis-associated signaling molecules such as lactate (Zhang et al., 2019b) and HIF1α (Cheng et al., 2014) have been linked to metabolic regulatory mechanisms in monocytes and macrophages. Signalling between lactate and HIF1α has been shown to have potent immunosuppressive effects on infiltrating myeloid cells in EAE (Sanmarco et al., 2023). DCs in the CNS showed increased levels of HIF1α and associated signaling, and deletion of *Hif1a*

in DCs led to exacerbated EAE symptoms and increased numbers of pro-inflammatory T cells in the CNS. Lactate, as a metabolite, was identified as a stabilizing factor for HIF1α. It was observed that lactate treatment reduced the expression of pro-inflammatory cytokines by T cells in a HIF1α-dependent manner. This suggests that lactate triggers a regulatory loop in DCs via HIF1α, which can limit inflammation. Exploring the potential for clinical application, a probiotic *E. coli* strain producing D-Lactate was engineered, which, when administered orally, increased HIF1α and improved EAE symptoms, supporting the role of this pathway in CNS autoimmunity and highlighting its therapeutic potential.

In demyelinating diseases such as MS, damaged myelin is cleared by phagocytes and new myelin sheaths are generated from existing or newly-differentiated oligodendrocytes. Cholesterol is a major component of myelin membranes (Dietschy, 2009). As this lipid cannot be degraded by mammals, the cholesterol from degenerating myelin is either locally recycled, or exported from the brain. Experimental interference at distinct levels of cholesterol/lipid metabolism has demonstrated a complex interplay between myelin membrane destruction, intracellular cholesterol/lipid trafficking, efflux and recycling, as well as the inflammatory profile of phagocytes (Cole et al., 2017, Bogie et al., 2020, Colombo et al., 2021). Uptake of myelin by macrophages and microglia temporarily skews phagocytes towards a disease-resolving phenotype, while sustained intracellular accumulation of myelin induces a lesion-promoting phenotype (Bogie et al., 2020). This phenotypic shift is mediated by fatty acid-associated enzymes that contribute to reduced cholesterol efflux in phagocytes, promoting a pro-inflammatory phenotype (Bogie et al., 2020). Similarly, uptake of cholesterol from myelin debris in the proinflammatory environment of actively demyelinating lesions increases the sterol synthesis pathway, occurring exclusively in phagocytes (Berghoff et al., 2021). Interestingly, functional CNS phagocyte sterol synthesis following myelin uptake mediates cholesterol efflux and limits inflammation (Berghoff et al., 2021). Genetic loss of sterol synthesis leads to the appearance of proinflammatory, lipid-laden foamy phagocytes due to downregulated efflux transporters (Berghoff et al., 2021). In chronic lesions, local cholesterol and lipid metabolism is strikingly different; they contain numerous foam cells with internalized myelin, suggesting suboptimal lipid recycling (Berghoff et al., 2022). Similarly, monocytes derived from the blood of patients with relapsing-remitting MS demonstrate reduced expression of lipid-sensing nuclear receptors, such as peroxisome proliferator-activated receptors, which was found to be related to foam cell formation via its impact on cholesterol metabolism (Wouters et al., 2020). Together, these findings support a complex and tightly

regulated interplay between intracellular lipid metabolism and the pro- or anti-inflammatory phenotype of phagocytes during CNS remyelination and demyelination.

Although myeloid cells are often linked to a pro-inflammatory phenotype resulting in demyelination, recent studies demonstrate these cells also contribute to the remyelination, which is associated with a distinct amino acid-associated metabolic profile. Interleukin-4-induced one (IL4I1) is a molecule that converts aromatic amino acids, such as phenylalanine, into α-keto acids. It was demonstrated that IL4I1, mostly produced by myeloid cells during the phase of remyelination (Hu et al., 2024), is essential in reducing demyelination and promoting the resolution of inflammation during a chemical demyelination model of MS (Hu et al., 2024, Psachoulia et al., 2016). IL-4 signaling was shown to induce IL4I1 expression in myeloid cells, resulting in an anti-inflammatory phenotype that regulated $CD4^+$ T cell polarization towards an immunomodulatory T helper type 2 cell phenotype (Psachoulia et al., 2016). This facilitated CNS remyelination and reduced disease severity. The immunomodulatory effect of IL4I1 was associated with α-keto acids, which are the enzymatic byproducts of IL4I1 (Hu et al., 2024). These α-keto acids were shown to affect the metabolic profile of myeloid cells, particularly lipid metabolism (Hu et al., 2024), a phenotype that is associated with resolving inflammation and assisting in remyelination (Penkert et al., 2021, Grajchen et al., 2020). However, whether the origin of this amino acid metabolism-associated anti-inflammatory phenotype arises from MCs or microglia, has yet to be determined (Psachoulia et al., 2016).

1.4.3 Viral encephalitis

Viral encephalitis, which is inflammation of the brain parenchyma caused by viral infection, has a mortality rate of 5-30%. Those who survive frequently suffer from severe neurological consequences, such as memory problems (Vora et al., 2014, Madden, 2003, Samaan et al., 2016, Weatherhead et al., 2015, Garber et al., 2019). The infection process begins when a virus enters brain tissue and replicates within neurons or glial cells, causing the release of cytokines. These cytokines subsequently recruit a variety of leukocytes, including monocytes and lymphocytes, to help eliminate the virus (Klein et al., 2019). This immune response can be overexuberant (King et al., 2011), causing additional neurological damage, as seen in WNV encephalitis, where the influx of immune cells coincides with tissue damage, swelling, and seizures (Getts et al., 2014, Getts et al., 2012, Getts et al., 2008, Getts et al., 2007).

Murine models are commonly used to explore immune responses to viral encephalitis, although they have significant limitations in reflecting human disease. The mode of viral inoculation often differs greatly, even with the same virus, and may not accurately reflect the natural infection routes in humans, altering how the virus spreads and the body's immunological response (Burke et al., 2004, Davison and King, 2011, Diamond et al., 2003, King et al., 2007, Wang et al., 2003). Furthermore, the use of several mouse strains and genetically modified mice provides a diversity in immunological responses that may not be consistent with human responses (Diamond et al., 2003, Burke et al., 2004). Variations in virus strains between laboratories, the historical usage of only female mice, and the selection of mice at an age often based on convenience rather than comparable phases of immune system development may all impinge on results to confound their translation. Furthermore, factors such as food make-up and circadian rhythms might influence immunological responses (Tan et al., 2021b, Tan et al., 2021a, Labrecque and Cermakian, 2015), adding a degree of complexity due to differences in laboratory circumstances. These characteristics make it difficult to draw direct parallels between animal models and human diseases. Nonetheless, given the unpredictable nature of the onset of disease, its clinical development and detection in humans, due in part to the influence of wide background genetics, as well as the restrictions on sample collection, animal models continue to be an important supplement to human studies in studying viral encephalitis.

1.4.3.1 Monocytes in viral encephalitis

Encephalitis caused by flaviviruses elicits robust neuroinflammatory responses, characterized by the recruitment of a substantial number of monocytes from the periphery, exceeding 50% of the total cells recruited to the CNS (Getts et al., 2008, Getts et al., 2012). The presence of monocytes is additionally observed in human cases of severe encephalitis during postmortem examination (Armah et al., 2007, Omalu et al., 2003, Sampson et al., 2000). Monocytes, in conjunction with lymphocytes and microglia, play essential roles in the processes of inflammation and antiviral defence, which are imperative for the elimination of the virus (Klein et al., 2019). However, it should be noted that these responses may not always be beneficial, as an excessively vigorous inflammatory response may lead to a fatal outcome in encephalitis. The various roles of monocytes in viral encephalitis, in addition to their phenotype (RNA and protein) are detailed in Table 1.5.

MCs infiltrating the virus-infected brain have two primary functions: they can present viral antigen and help activate $CD4^+$ and/or $CD8^+$ T cells to eliminate the virus, or they can directly

destroy infected cells by releasing inflammatory substances such as NO and interleukin-6 (IL-6) (Chen et al., 2001, Lim et al., 2011a, Bardina et al., 2015, Ben-Nathan et al., 1996). While these functions can be advantageous in eliminating the virus, they can also result in significant neurodegeneration (Waltl et al., 2018, Howe et al., 2012, Cusick et al., 2013, Getts et al., 2008, Getts et al., 2012, Getts et al., 2007). For example, in the context of WNV infection in mice, the infiltration of Ly6C^{hi} monocytes into the brain serves as a preliminary stage leading to the development of lethal encephalitis (Getts et al., 2008, Getts et al., 2012). The cells are attracted to the CNS through pathways involving C-C Motif Chemokine Ligand 2 (CCL2) and very late antigen-4 (VLA-4). Once in the CNS, they exacerbate damage to neuronal cells by promoting sustained production of NO (Getts et al., 2008, Getts et al., 2012). Utilizing anti-CCL2 and anti-VLA-4 antibodies, or inhibiting NOS2 with aminoguanidine hemisulphate, effectively hinders the infiltration of monocytes into the brain or prevents their inflammatory activity, respectively. These strategies significantly enhance survival rates in affected mice without

Table 1.5. Functions and phenotypes of monocytes in viral encephalitis

RNA	**CD45^{hi}CD11b^{+} macrophages** ↑ 'macrophage-specific' genes relative to microglia: *Gzmb*, *Il2ra*, *Nos2*, *Oas3*, *Ms4a8a*, *Arg2*, *Trem-1*, *Ly6c2*, *Ccr2*, *Vim*, *Ifi204*, *S100a10* and *Msrb1* (TMEV-infection, dpi 6, RNAseq, (DePaula-Silva et al., 2019)
Protein	**CD45^{hi}CD11b^{+} macrophages** ↑ MHC II (TMEV-infection, dpi 6, flow cytometry, (DePaula-Silva et al., 2019)
	Bead^{+}CD45^{int}CD11b^{+} macrophages ↓Ly6C ↑ MHC II and CD86 (Sarafend strain, WNV-infection, dpi 7, flow cytometry, (Getts et al., 2008)
Neuro-protective roles	• CCL2 and CCL7-dependent monocyte migration to the brain is required for effective viral clearance and survival in WNV encephalitis (neurotropic WNV99) (Bardina et al., 2015). • CNS-infiltrating macrophages prevent viremia and enhance survival in WNV encephalitis (neurotropic WNV) (Ben-Nathan et al., 1996). • CCR2-dependent Ly6C^{hi} monocyte infiltration into the brain is required for effective viral clearance, survival, and anti-viral CD4^{+} and CD8^{+} T cell responses in MHV (Chen et al., 2001)- and WNV-encephalitis (neurotropic WNV) (Lim et al., 2011a).
Neurotoxic roles	• CNS-infiltrating Ly6C^{hi} monocytes and macrophages contribute to seizure incidence, seizure severity, memory deficits or hippocampal neuron damage in TMEV-induced encephalitis (Waltl et al., 2018, Howe et al., 2012, Cusick et al., 2013). • IL-6-producing CD45^{hi}CD11b^{+} myeloid cells correlate with seizure development in TMEV encephalitis (Cusick et al., 2013, DePaula-Silva et al., 2017). • Ly6C^{+} MCs trafficking into the brain correlates with mortality in WNV encephalitis (Sarafend strain) (Getts et al., 2008, Getts et al., 2012). • Infiltration of NO-producing Ly6C^{+} MC into the CNS correlates with mortality in lethal WNV encephalitis (Sarafend strain) (Getts et al., 2012).

altering the viral load (Getts et al., 2008, Getts et al., 2012). This further supports the notion that MCs play a crucial role in causing damage in WNV infection.

The detrimental impact of monocytes following infection appears to be limited to the CNS (Getts et al., 2012), despite the crucial function of these cells in controlling WNV in the initial peripheral stages of infection (Davison and King, 2011). This observation is consistent with previous research showing a decrease in monocyte migration into the CNS in mice with deficiencies in CCR2, CCL2, and CCL7, as well as an increase in viral levels when the virus is delivered peripherally (Ben-Nathan et al., 1996, Lim et al., 2011a, Bardina et al., 2015). Monocytes that migrate into the infected brain express MHC-II, CD80, and CD86 molecules. This enables them to effectively present antigens and induce the proliferation of T cells (Getts et al., 2012), thereby providing evidence for their involvement in initiating antiviral T cell responses. The impact of MCs on WNV encephalitis may vary depending on factors such as the virus strain, dosage, and route and dose of infection. However, due to their delayed entry into the CNS (Getts et al., 2012), it is still unclear whether they have a role in eliminating the virus within the CNS.

It is widely believed that monocytes have a substantial impact on hippocampal neurodegeneration (Waltl et al., 2018, Cusick et al., 2013) and the onset of seizures (Howe et al., 2012) observed in cases of viral encephalitis, including those induced by Theiler's Murine Encephalomyelitis Virus (TMEV). This harmful function is emphasized by research demonstrating that the depletion of myeloid cells using anti-Gr-1 antibodies or the administration of anti-inflammatory substances such as wogonin and minocycline can preserve cognitive function and decrease the frequency of seizures (Waltl et al., 2018, Cusick et al., 2013, Howe et al., 2012). While the findings of this study indicate the potential advantages of decreasing monocyte migration to the brain, the non-selective depletion techniques employed made it impossible to rule out the potential involvement of other infiltrating blood cell types like neutrophils. The implementation of an alternative monocyte depletion strategy involving clodronate liposomes, which effectively eliminates phagocytes from the bloodstream, spleen, and BM (Van Rooijen, 1989, Van Rooijen and Sanders, 1994, van Rooijen and van Nieuwmegen, 1984), resulted in a decrease in the severity of seizures. However, this approach did not effectively prevent the degeneration of the hippocampus (Waltl et al., 2018). This suggests that the influence of monocytes on this particular pathological condition is contingent upon the specific depletion technique employed. Hence, the precise etiology of seizures,

whether they originate from infected neurons or from stimuli originating from infiltrating cells, remains incompletely understood (Waltl et al., 2018, Howe et al., 2012, Cusick et al., 2013, Getts et al., 2008, Getts et al., 2012, Getts et al., 2007). Consequently, further focused investigation is required to elucidate the specific roles of monocytes in the initiation of seizures associated with viral encephalitis.

1.4.3.2 Metabolic pathways supporting anti-viral innate immunity

As key players in the anti-viral immune response, monocytes must adapt their metabolism to fulfill various roles. These roles include directly phagocytosing viral particles, to antigen presentation, and the production of inflammatory mediators. Despite the limited research on monocyte metabolic responses to CNS viral infection, valuable insights can be drawn from peripheral infection studies and *in vitro* anti-viral functions in monocytes (Figure 1.8).

Nutrient availability plays a significant role in monocyte functionality during *in vivo* viral infection. For instance, studies in mice have shown that a fibre rich diet substantially increases the production of $Ly6C^-$ monocytes in the BM during influenza A infection (Trompette et al., 2018). This is associated with increased expansion of alternatively activated macrophages in the lungs, reduced tissue damage, and reduced neutrophil influx post-infection, resulting in improved survival and increased viral defence (Trompette et al., 2018). Altering dietary components, therefore, holds potential for influencing BM myelopoiesis and priming the inflammatory capacity of monocytes prior to their infiltration into inflamed tissues. This effect may be virus or dose-dependent, however, as a high-fibre diet was shown to have minimal impact on monocyte-mediated immunopathology in flavivirus infection (Ni et al., 2022).

Moreover, recent work has highlighted the role of glucose availability in dictating the inflammatory function of monocytes during severe acute respiratory syndrome-related coronavirus 2 (SARS Cov-2) infection. In the context of SARS Cov-2, monocytes contribute to immunopathology via the production of pro-inflammatory cytokines (Bost et al., 2020). This leads to the detrimental “cytokine storm”. Particularly in the context of diabetic individuals, high blood glucose levels are a prominent risk factor for severe coronavirus disease (Zhu et al., 2020), pointing to the local glucose levels as a determining factor in monocyte function and virus replication. Indeed, SARS-Cov-2-infected monocytes produce high levels of pro-inflammatory cytokines, which is regulated by local glucose availability (Codo et al., 2020). This results in a shift to aerobic glycolysis – a metabolic phenotype that is sustained by the stabilisation of HIF1α by mitochondrial ROS, ultimately enhancing the expression of

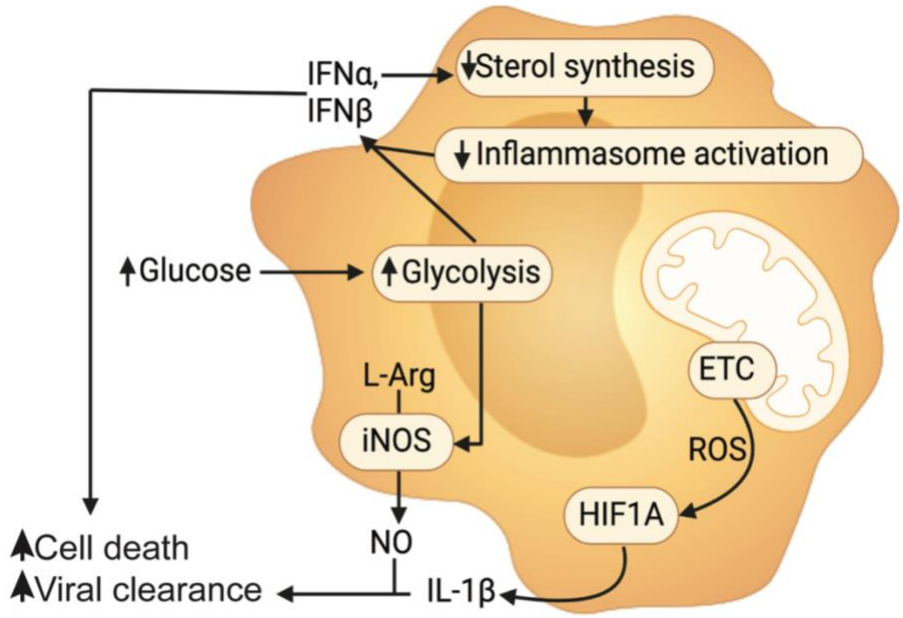

Figure 1.8 Metabolic profiles supporting the anti-viral response in monocyte-derived cells.

Glucose availability enhances glycolysis, leading to mitochondrial ROS production, which stabilizes HIF1α and increases IL1β production, contributing to the cytokine storm observed in coronavirus disease. NO production, driven by glycolysis-promoted catalysis of arginine by iNOS, destroys infected cells but can also cause inflammatory damage. Glycolysis also boosts type I IFNs, enhancing the efferocytosis of virus-infected cells. Additionally, IFN downregulates cholesterol synthesis, which restrains inflammasome activation and further increases type I IFN production.

glycolysis-associated genes and IL-1β (Codo et al., 2020). Given that the pro-inflammatory monocyte phenotype is common across various CNS infections, including WNV encephalitis, strategies that limit glucose availability or inhibit its metabolic pathway—such as by using glycolysis inhibitors such as 2-DG—may offer a promising approach to dampen an overexuberant inflammatory response in monocytes and mitigate immune-mediated damage during viral encephalitis.

The production of inflammatory mediators, such as NO, is an additional important component of the anti-viral response. Classical *in vitro* activation [M(LPS+IFN-γ)] of murine macrophages elicits the expression of iNOS, generating large amounts of NO and disrupting mitochondrial respiration (Kelly and O'neill, 2015). Upregulation of glycolysis and a disrupted TCA cycle underpin this switch to a pro-inflammatory phenotype. iNOS catalyzes arginine, a non-essential amino acid, into NO and citrulline, providing macrophages with 'cytotoxic' potential (MacMicking et al., 1997). In this process, NO reacts with oxygen or ROS spontaneously, leading to the formation of numerous antimicrobial species (Schairer et al., 2012). The citrulline produced by iNOS is recycled back into arginine through the activity of argininosuccinate synthase 1, thereby maintaining NO production (Qualls et al., 2012). Sustained NO production, however, can lead to hyperinflammation and tissue damage in certain diseases, such as severe influenza virus infection, severe coronavirus disease, and WNV encephalitis (Perrone et al., 2013, Xu et al., 2020, Getts et al., 2012).

In addition to the production of inflammatory cytokines, signaling initiated by viral nucleic acids, followed by the activation of type I IFNs, play a central role in the innate immune response against viral infections. These signaling events trigger metabolic adaptations within MCs, providing crucial support for antiviral defences. Cytosolic viral recognition occurs through secondary IFN signaling, leading to a preferential increase in glycolytic activity in macrophages (Jiang et al., 2016). This metabolic shift involves the induction of the glycolytic activator known as 6-phosphofructose-2-kinase and fructose-2,6-bisphosphatase. Glycolysis driven by this enzyme serves as a selective enhancer of the antiviral capacity of macrophages by facilitating efferocytosis of virus-infected cells (Jiang et al., 2016).

Increasing evidence suggests that lipid metabolism plays a critical role in regulating the type I IFN response. During viral infection, IFN signalling modifies cholesterol synthesis in macrophages through the degradation of key biosynthetic pathway enzymes (Blanc et al., 2013, York et al., 2015). Reprogramming of sterol metabolism by IFN signalling has been shown to

facilitate cellular resistance to viral invaders and can intrinsically promote IFN-mediated inflammation (Reboldi et al., 2014, Blanc et al., 2013, York et al., 2015, Xiao et al., 2020). Mechanistically, downregulation of *de novo* cholesterol synthesis during macrophage activation restrains engagement of the inflammasome, thereby ensuring that effective type I IFN signalling proceeds (Dang et al., 2017). Hence, inhibiting cholesterol synthesis pathways appears to be a key factor in enhancing the type I IFN response and ensuring the elimination of viruses. Interesingly, viruses such as flaviviruses modulate fatty acid and cholesterol biosynthesis during replication (Osuna-Ramos et al., 2018), although it is unclear whether this contributes to viral immune evasion via the type I IFN pathway.

Type II IFN, IFN-γ, also plays a critical role in the anti-viral response. IFN-γ is crucial in antiviral immunity, primarily by activating immune cells, enhancing antigen presentation, and directing T helper cells towards a T helper type 1 response, which is vital for fighting viral infections. Recently, it was shown that mitochondrial respiration, and in particular complex I, was essential for IFN-γ responses in APCs (Kiritsy et al., 2021). Complex I was required for the IFN-γ-mediated induction of important co-signalling molecules and expression of MHC-II on APCs and is necessary for antigen presentation and T cell activation (Kiritsy et al., 2021).

Finally, it is essential to acknowledge the specificity of metabolic responses to viral recognition by monocytes, which are tailored rather than generic. The Warburg effect describes that glycolysis is increased in pro-inflammatory macrophages, whereas OXPHOS is increased in anti-inflammatory macrophages at the expense of glycolysis (Warburg et al., 1927). This effect has been traditionally viewed as a universal metabolic adaptation to microbial stimulation, aimed to promote cytokine production, macrophage polarization, and microbial killing (Galván-Peña and O'Neill, 2014). However, a shift from OXPHOS to glycolysis has only been observed in LPS-stimulated monocytes (i.e., TLR4 stimulation) and not monocytes stimulated with alternative TLR activation (e.g., TLR2 via Pam3CysSK4) or other bacterial lysates (Table 1.6) (Lachmandas et al., 2016). Interestingly, IL-1β and phagocytosis are sustained by OXPHOS when monocytes are stimulated with Pam3CysSK4, but this metabolic pathway was dispensable for these functions upon LPS challenge (Lachmandas et al., 2016). Furthermore, glycolysis inhibition does not impede the phagocytic capabilities of these monocytes, which suggests that OXPHOS is the principal metabolic process supporting monocyte phagocytosis (Lachmandas et al., 2016). Interestingly, macrophages have been shown to have the capacity to respond to distal versus proximal stimuli, which is mediated by metabolic reprogramming.

Distal threats (associated with soluble factors such as LPS), which requires immune cell trafficking, induced a different metabolic program that proximal threats, such as whole uropathogenic *E. coli* (Das Gupta et al., 2023). This effect was found to be mediated by the histone deacetylase 7 enzyme (Das Gupta et al., 2023). Thus, pathogen-specific metabolic adaptation leads to distinct functional outputs such as phagocytosis and cytokine production, and can be triaged towards either antimicrobial or inflammatory threats. Consequently, the systemic metabolic response to viral or bacterial infections is tailored to support varying inflammatory functions. For example, restricting glucose during bacterial inflammation promotes ketogenesis, enhancing resilience to ROS-induced brain damage and reducing death, while during viral inflammation, glucose utilization counters ER stress induced by type I IFN signalling, thus preventing neuronal damage and death (Wang et al., 2016). This demonstrates that while glucose metabolism is vital for surviving viral infection, it can be harmful during bacterial challenges. Thus, inflammatory responses to different microbial stimuli seem to have specific metabolic requirements to provide optimal protection.

Table 1.6. Metabolic and functional responses to stimulation of different toll-like receptors

Stimulus	**Pathogen-recognition receptor**	**Metabolic pathways**	**Metabolic enzymes**	**Cytokines**	**Functional output**	**Refs**
LPS	TLR4	↑ Glycolysis ↑ HIF1A, AKT ↑ FAS ↓ OXPHOS, ETC	↓ IDH1 ↓ SDH ↑ IRG1 ↑ ACAC	↑TNF, IL-6, IL-1β, IL-10	↑ Cytokine production ↓Phagocytosis	(Lachmandas et al., 2016, Yeudall et al., 2022)
Poly(I:C)	TLR3	↑ Glycolysis ↑↓OXPHOS ↑ TCA cycle	↑ *Hif1a*	↑*Il1b, Il6, Il8, Tnf*	IFN response	(Lachmandas et al., 2016, Pantel et al., 2014, Guo et al., 2022)
Pam3CysSK4	TLR2	↑ Glycolysis ↑ HIF1A, AKT ↑ OXPHOS, ETC	↓ SDH	↑ TNF, IL-6, IL-1β, IL-10	↑ Phagocytosis ↓ Cytokine production	(Lachmandas et al., 2016)

1.5 West Nile virus encephalitis as model for monocyte-mediated immunopathology

1.5.1 West Nile virus

WNV belongs to the Flaviviridae family (Petersen et al., 2013b) and like almost all members, is transmitted by arthropods. It is part of the *Japanese encephalitis serocomplex*, which

includes Japanese encephalitis virus, St Louis encephalitis virus, Murray Valley encephalitis virus, and Alfuy virus (Petersen et al., 2013b). WNV has a single-stranded, positive-sense ribonucleic acid (RNA) genome approximately 11,000 nucleotides long. Upon entering a host cell, this genome functions as messenger RNA, directly producing a single long polyprotein. This polyprotein is then divided into three structural proteins, namely capsid, premembrane/membrane, and envelope, as well as seven non-structural proteins (NS), including NS1, NS2A, NS2B, NS3, NS4A, NS4B, and NS5 (Habarugira et al., 2020). The non-structural proteins have multiple functions, including assisting in viral propagation, assembly, and evading the immunological response of the host.

1.5.2 Disease, incidence and prevalence of WNV infection

WNV can result in a range of disease in humans, varying from asymptomatic or mild infections to serious neuroinvasive disorders (Petersen et al., 2013b). Most WNV infections in humans are subclinical, indicating that they are asymptomatic and go unreported. Around 25% of infected individuals develop West Nile fever, a temporary flu-like illness (Zou et al., 2010). This illness is marked by symptoms such as fever, headache, body aches, joint pains, vomiting, diarrhoea, or rash (Bai et al., 2019). Although the majority of individuals who contract West Nile fever make a full recovery, they may experience prolonged periods of lethargy and weakness that can persist for several weeks or even months (Bai et al., 2019).

Approximately 1 out of every 150-250 infected individuals progress to neuroinvasive disease that impacts the CNS (Petersen et al., 2013a, Mostashari et al., 2001). WNV is a major cause of viral encephalitis on a global scale, and WNV encephalitis is considered one of the most severe consequences of WNV infection. Encephalitis can give rise to profound neurological manifestations like headache, elevated body temperature, neck stiffness, confusion, unconsciousness, tremors, convulsions, or loss of muscle function. The neuroinvasive manifestation of WNV is exceptionally dangerous and poses a significant mortality risk, particularly among older adults, individuals with compromised immune systems, and those with pre-existing health conditions (Bai et al., 2019, Lindsey et al., 2010). The mortality rate of WNV encephalitis fluctuates, with fatality rates for individuals with the neuroinvasive form of the disease ranging from around 10% to greater rates in outbreaks with exceptionally potent strains or in groups that are more susceptible (Lindsey et al., 2010). Individuals who survive WNV encephalitis may encounter long-lasting or irreversible consequences, including cognitive decline, alterations in personality, or impairments in motor skills (Petersen et al.,

2013b). These consequences have a significant impact on overall well-being and can result in prolonged impairment that necessitates comprehensive rehabilitation, making WNV a significant public health concern.

1.5.3 Pathogenesis

Studies using animal models of infection have identified three distinct phases of WNV pathogenesis – initial infection and spread, peripheral viral amplification, and neuroinvasion (Petersen et al., 2013b, Samuel and Diamond, 2006). These phases are broadly thought to reflect the natural disease course in humans following infection by a mosquito.

WNV, being an arbovirus, is transmitted through a mosquito vector, often of the Culex genus, during its life cycle (Muñoz et al., 2012). The virus is perpetuated in an inherent cycle between avian species, which serve as amplifying reservoir hosts, and mosquitoes (Suthar et al., 2013). When a mosquito ingests the blood of an infected bird, the virus enters and reproduces in the mosquito's midgut, eventually spreading to the salivary glands (Girard et al., 2005, Hall-Mendelin et al., 2016). WNV is subsequently transmitted to humans (terminal host) and other mammals when they are bitten by infected mosquitoes in search of a blood meal. During this process, a mosquito injects saliva, which contains virus particles, into the prospective host. Mosquito saliva has components that not only interfere with blood coagulation and the immune defences of the host, but also inhibit inflammation and can disrupt the local immune response of the host, resulting in a decrease in defence mechanisms and altered production of cytokines. This disruption has an impact on the recruitment of neutrophils, DCs, and T cells to the specific location of infection (Schneider et al., 2010, Schneider and Higgs, 2008). Thus, mice receiving intradermal injections of WNV, having been bitten by mosquitoes such as Culex or Aedes species, exhibit faster infection progression, elevated viral levels in the bloodstream, and accelerated transmission to the nervous system, compared to mice given WNV without mosquito bites (Schneider et al., 2006, Styer et al., 2011).

Understanding of the disease process of WNV in humans remains incomplete. However, comprehensive animal models have provided insights into the mechanisms by which WNV induces disease. The transmission of WNV by mosquitoes is commonly simulated in these models through the injection of the virus into the footpad of rodents. However, alternative approaches have been employed by other research groups, such as direct abdominal cavity (intraperitoneal) or bloodstream (intravenous) injections, which circumvent the usual entry points of the virus through the skin and associated lymphatic system. Additionally, intranasal

inoculation of the virus restricts disease to the CNS. Peripheral inoculation of the virus begins with viral replication in skin cells, specifically keratinocytes and several types of skin-derived DCs, such as dermal DCs and Langerhans cells (Lim et al., 2011b, Johnston et al., 2000). Subsequently, the virus undergoes rapid replication inside adjacent lymph nodes, resulting in the development of viremia and subsequent dissemination to several organs, which serves as a crucial location for viral replication in peripheral tissue (Diamond et al., 2003).

The capacity of the virus to infiltrate and induce pathology in brain tissue signifies a pivotal phase in the progression of the infection. In order to create neuroinvasive disease, WNV must initially penetrate the CNS. There are various hypotheses regarding the mechanism by which WNV invades the CNS. These include direct viral entry through the compromised BBB facilitated by cytokines (Diamond et al., 2003, Wang et al., 2004), traverse through endothelial cells of the BBB (Verma et al., 2009), the 'Trojan horse' approach, in which virus-laden macrophages are transported across the BBB into the brain parenchyma (Bai et al., 2010), and transmission of the virus along nerves to the CNS from sensory points such as the olfactory nerve or peripheral nervous tissue (Getts et al., 2008, Samuel et al., 2007b).

1.5.4 Immune response to WNV

1.5.4.1 Contribution of CNS resident cells to the immune response during WNV encephalitis

Upon WNV infection of the CNS, resident immune cells, such as microglia, astrocytes and neurons are among the first to recognize viral particles through PRRs, such as TLRs and retinoic acid-inducible gene 1 (RIG1)-like receptors. Stimulation of these molecular pathways induces the production of pro-inflammatory cytokines, including type I IFNs, TNF, and chemokines that facilitate the recruitment of additional immune cells to the site of infection, as well as enhancing the anti-viral state of uninfected neighboring cells.

Neurons are the primary target of WNV infection, and apoptosis of virus-infected neurons contributes to viral spread in the CNS. Neuronal death in WNV infection is a complex process and involves activation of caspase 3/9-dependent apoptosis via intrinsic and extrinsic pathways (Samuel et al., 2007a). Although these mechanisms are not fully understood, apoptotic neuronal death is thought to occur directly via virus infection or due to bystander injury caused by cytotoxic factors released by non-neuronal cells (Kumar et al., 2010, Zhang et al., 2010). In addition to their roles as targets for viral infection, neurons play an important role in the immune response to WNV. They express PRRs that recognise virus, resulting in the production

of IFNs and other antiviral signaling molecules that limit viral replication and spread. Neurons from mice with genetic deletions in either *Irf3* or *Irf7*, which control critical interferon-responsive transcriptional programs, results in reduced expression of antiviral genes and increased WNV infection (Daffis et al., 2007, Daffis et al., 2008). This is further supported by *in vitro* studies demonstrating that WNV infection stimulates neuronal secretion of IL-1β, IL-6, IL-8, TNF, and CXCL10, which increases neuronal apoptosis and induces astrocyte activation (Kumar et al., 2010, Van Marle et al., 2007). Furthermore, neurons release factors and cytokines that signal distress and facilitate the recruitment and activation of microglia and astrocytes to the site of infection.

Although they are not the primary target for WNV, astrocytes can be infected, although this is generally limited (Van Marle et al., 2007). Astrocytes are typically activated by infected or injured neurons, other glial cells, and infiltrating immune cells. Upon activation, astrocytes enhance the expression of antiviral molecules, including type I IFNs (Hussmann et al., 2013), and secrete a range of cytokines and chemokines that further modulate the immune response and can also contribute to the repair and regeneration of the BBB (Phares et al., 2006). Furthermore, the production of IL-1 in WNV-infected astrocytes during the convalescent stage of WNV infection decreases neurogenesis and ultimately leads to memory dysfunction (Garber et al., 2018).

Endothelial cells of the BBB are involved in the immune response by regulating the entry of immune cells into the CNS. In response to cytokines and chemokines produced by microglia, astrocytes, and infected neurons, endothelial cells upregulate adhesion molecules (e.g., intracellular cell adhesion molecule 1, vascular cell adhesion molecule 1, E-Selectin) and chemokine expression, facilitating the transmigration of peripheral immune cells such as T cells, B cells, and monocytes into the brain (Roe et al., 2014). This selective permeability is crucial for allowing immune cells to access infected regions of the brain while maintaining the protective barrier function of the BBB.

Microglia, as the resident immune cells of the CNS, play a pivotal role in the body's defence against WNV infection. Upon neuroinvasion by WNV, microglia are among the first cells to respond, acting as sentinels that detect viral presence through their expression of PRRs such as TLRs and RIG-I-like receptors (Town et al., 2006, Furr et al., 2008). In humans, evidence of microglial activation is demonstrated by their increased proliferation and the presence of microglial nodules (Fratkin et al., 2004). Detection of viral RNA via PRRs triggers microglial

activation and the subsequent release of a variety of cytokines and chemokines, which are crucial for initiating and orchestrating an inflammatory response aimed at controlling and clearing the viral infection (Stonedahl et al., 2020). Cytokines such as type I IFNs and TNF help to establish an antiviral state in neighbouring cells, reducing viral replication and spread.

Microglia can have both neuroprotective and neurotoxic roles during WNV infection. In WNV-infected *ex vivo* slice cultures, microglia display an amoeboid and phagocytic phenotype that promoted the engulfment and destruction of viral particles, infected cells, and cellular debris (Stonedahl et al., 2020), which is vital for mitigating the infection and facilitating recovery of the CNS. However, this phagocytic response of microglia is a double-edged sword: while essential for controlling the virus, an overactive or prolonged microglial response can lead to neuroinflammation, potentially resulting in neuronal damage and contributing to the severity of WNV-associated neurological disorders. Indeed, microglia have been shown to inappropriately phagocytose hippocampal synapses following WNV infection, leading to spatial-learning deficits and the development of post-viral cognitive dysfunction (Garber et al., 2019).

Complicating the study of the role of microglia in WNV infection is the use of non-specific identification methods and reagents lacking microglia specificity that do not enable discrimination of microglia from monocyte-derived infiltrates. For instance, the CSF1R inhibitor PLX5622, designed to specifically deplete microglia, has been discovered to affect the production of monocytes in the BM (Spiteri and King, 2023, Spiteri et al., 2022a). This complicates distinguishing the functions of microglia from those of peripheral myeloid cells during WNV infection. Although PLX5622 initially seemed to alleviate the disease severity of WNV, subsequent examination indicated that this effect was mostly caused by its inadvertent inhibition of myelopoiesis (Spiteri et al., 2022a). This led to a reduction in the number of monocytes in the brain, which are cells that play a significant neurotoxic role in WNV infection, particularly through the production of NO.

Recent research shows that the neuroprotective role of microglia in the acute phase of WNV infection evolves over time. They initially display an antiviral phenotype, characterized by the expression of antiviral genes such as *Oas2*, *Ifitm2*, and *Ifitm3* (Spiteri et al., 2023b). Additionally, they phagocytose infected neurons with their ramified processes, thereby facilitating the elimination of the virus (Spiteri et al., 2023b). This antiviral function is further supported by investigations demonstrating the phagocytosis of virus by microglia in human

tissue infected with WNV (Omalu et al., 2003). In addition to directly aiding in viral clearance, microglia play a crucial role in coordinating the generation of IFN-γ by $CD4^+$ T cells and potentially enhancing the proliferation of and antigen presentation to $CD8^+$ T cells (Spiteri et al., 2023b). This ultimately strengthens the process of T cell-mediated elimination of WNV.

1.5.4.2 Contribution of peripherally-derived immune cells to the immune response during WNV encephalitis

1.5.4.2.1 T cells

T cells have an essential function in the context of WNV infection. These cells comprise approximately 10% of the neuroinflammatory infiltrate and are recruited to the CNS in a C-C chemokine receptor type 5-dependent manner. Studies have demonstrated that mice deficient in $CD8^+$ T cells display increased viral spread throughout the CNS, highlighting the crucial function of these cells in limiting viral dissemination (Shrestha and Diamond, 2004). This protective effect was further highlighted by studies demonstrating that mice deficient in CXCL10 and its receptor C-X-C motif chemokine receptor 3, a chemotactic pathway that facilitates $CD8^+$ T cell migration into the CNS, increased viral load in the brain and increased mortality (Klein et al., 2005, Zhang et al., 2008).

$CD8^+$ T cell-mediated viral clearance is likely mediated by both cytolytic and non-cytolytic mechanisms. While not completely understood, mechanisms likely include killing virus-infected cells by apoptosis, either via perforin release or through cell surface expression of TNF-related apoptosis-inducing ligand (TRAIL, CD253) interacting with their respective receptors, Fas (CD95) and TRAILRI/II, on the infected target cell (Shrestha et al., 2006, Shrestha and Diamond, 2007, Shrestha et al., 2012).

However, the beneficial impact of cytotoxic $CD8^+$ T cells in the CNS against WNV is attended by the risk of inducing significant harm to the CNS by loss of neurons and structural damage. In the case of neurons, however, they would have to express MHC-I in order to be recognized by anti-viral $CD8^+$ T cells and this may represent some defence against cytoxic T cell killing. Experiments with less virulent strains of WNV indicate that mice lacking $CD8^+$ T cells or depleted of $CD8^+$ T cells exhibit prolonged survival compared to wild type mice (Wang et al., 2003, Szretter et al., 2012). Furthermore, $CD8^+$ T cell depletion in mice deficient in the interferon-stimulated gene *Ifit1* resulted in improved survival following WNV infection, suggesting that $CD8^+$ T cells play a role in immunopathogenesis (Wang et al., 2003). This

suggests that $CD8^+$ T cells may play a role in inducing immunopathology in the context of WNV infection.

$CD4^+$ T cells are of significant importance in the immune response against WNV infection. The crucial role of $CD4^+$ T cells in initiating and sustaining the WNV-specific IgM and IgG antibody responses, as well as supporting the activity of $CD8^+$ T cells in the CNS has been substantiated through research on mice with specific genetic deletions (e.g., genetic deletion of CD4 or MHC class II) or those with diminished antibody levels (Sitati and Diamond, 2006). The precise protective mechanisms of $CD4^+$ T cells against WNV are not fully understood, however previous studies have demonstrated that these cells eliminate target cells tagged with WNV-peptides through mechanisms involving perforin and the CD95-CD95L pathway. *In vitro*, $CD4^+$ T cells produce IFN-γ and IL-2 upon exposure to WNV peptides, albeit in limited quantities (Brien et al., 2008). The complete understanding of the specific influence of these secreted factors on viral defence remains incomplete, particularly due to the observation that the absence of these factors in adoptively transferred cells does weaken protection against WNV (Brien et al., 2008).

Additionally, subsequent investigations have uncovered the involvement of regulatory T cells in the regulation of the immune response during the acute stage of WNV infection (Lanteri et al., 2009). The clinical symptoms of WNV in human instances have been linked to an imbalance in the proliferation of regulatory T cells (Lanteri et al., 2009). Significantly, symptomatic WNV-infected individuals have lower numbers of regulatory T cells compared to asymptomatic individuals. This highlights the importance of regulatory T cell responses in regulating the immunopathogenesis of WNV disease. A comparable increase in regulatory T cells has been observed in mice between the sixth and eighth day following WNV infection (Suthar et al., 2010). Conditional depletion of these cells has resulted in exacerbated disease severity and an increase in WNV-specific $CD8^+$ T cell populations (Lanteri et al., 2009). The evidence highlights the significant importance of regulatory T cells in maintaining a balance between the effective eradication of infection via cellular immune responses and the intensity of these responses that might worsen the disease outcome for the individual.

1.5.4.2.2 Monocytes

Research conducted on experimental models of WNV encephalitis have demonstrated a significant accumulation in monocyte numbers in the infected brain, with a nearly ten-fold increase detected at the peak of disease (Spiteri et al., 2021a). Comprising approximately 60%

of the immune cell infiltrate (Spiteri et al., 2021a), these monocytes have a vital function in defence and contribute significantly to the observed immunopathology.

During WNV infection, the BM undergoes a massive myelopoietic response, which supplies the significant recruitment of monocytes to the inflamed brain. This phenomenon, referred to as emergency myelopoiesis, is triggered to counterbalance the reduction in myeloid cells in the BM. As mentioned previously, monocytes can originate from either GMP or MDP progenitors. The former exhibits a greater resemblance to neutrophils, in their enhanced ability to combat bacterial infections, while the latter resemble DC more closely, with an improved capability to combat viral infections (Yáñez et al., 2017, Weinreb et al., 2020). The stimulation that initiates emergency myelopoiesis can impact the direction of this process. For instance, LPS treatment, a bacterial PAMP, enhances the generation of GMP-derived monocytes which display a neutrophil-like phenotype (Yáñez et al., 2017). On the other hand, stimulation with CpG DNA, a TLR9-activating PAMP, leads to an augmentation of MDP-derived monocytes, which are primed to differentiate into DCs, and play a crucial role in combating viral infections (Yáñez et al., 2017). Pathogen-specific myelopoietic responses have been observed in several diseases. For example, influenza virus induces monopoiesis while reducing the production of DCs, resulting in an increased presence of inflammatory monocytes. These monocytes play a crucial role in eliminating the virus from the lungs (Beshara et al., 2018). However, this response concurrently diminishes conventional DCs, rendering the host more vulnerable to subsequent bacterial infections. The impact of WNV on BM myelopoiesis is not fully understood, although it is probable that the activation of different PRRs (Yáñez et al., 2017) or the generation of certain inflammatory mediators, such as interferons (de Bruin et al., 2012), during infection contributes to the generation of distinct monocyte phenotypes (Swann et al., 2024). For instance, IFN-γ can inhibit neutrophil production and promote monopoiesis by enhancing expression of IRF8 (de Bruin et al., 2012). As it has been demonstrated that WNV-infected, IRF8-deficient mice have significantly reduced MCs in the brain, it is possible that WNV infection induces BM skewing via this differentiation pathway (Terry et al., 2015). This process may lead to the differentiation of monocyte subtypes, including those with NO-producing capabilities–historically known as Tip-DCs, but now identified as $iNOS^{+}$ MCs (Guilliams et al., 2014)–to potentially enhance viral defence in the CNS.

The migratory patterns of $Ly6C^{hi}$ inflammatory monocytes during WNV infection are regulated by several chemokines and their receptors. C-C chemokine receptor type 5 (CCR5), a receptor

expressed on Ly6C^{hi} monocytes, is of significant importance since it plays a crucial role in their migration towards inflammatory foci (Glass et al., 2005). During WNV infection, the brain has elevated levels of chemokine C-C motif ligand 5 (CCL5), which is the ligand for CCR5 (Glass et al., 2005). In addition, monocyte egress to the bloodstream from the BM is facilitated by the CCL2-CCR2 axis. CCL2 is generated by WNV-infected neurons and structural cells in the WNV-infected skin and contributes to inflammatory monocyte recruitment to these sites (Getts et al., 2008, Davison and King, 2011). While the inhibition of CCL2 reduces the infiltration of monocytes into the brain, it is possible for monocytes to utilize alternative chemokine pathways to enter the brain as there are still a small number of monocytes that are capable of migrating to the brain with CCL2 neutralization (Getts et al., 2008). This suggests that diapedesis across the BBB is not purely dependent on CCR2. Indeed, both wild-type and CCR2-deficient monocytes have the ability to migrate into the brain of CCR2-deficient animals infected with WNV (Lim et al., 2011a). This observation, in conjunction with other studies, suggests that integrins, specifically VLA-4 and lymphocyte function-associated antigen 1 (Getts et al., 2012), play a crucial role in the process of endothelial migration across the BBB, rather than the CCR2-CCL2 axis.

Upon entering the WNV-infected brain, monocytes can differentiate into various functionally distinct phenotypes. Predominantly, they assume an NO-producing phenotype, which is linked to significant immunopathology, morbidity, and mortality. Approximately 72% of monocytes in the WNV-infected brain adopt this phenotype, perpetuating immunopathology by the sustained generation of NO (Getts et al., 2012). Interventions aimed at impeding inflammatory monocyte infiltration into the brain or attenuating their inflammatory responses, such as the inhibition of CCL2 or the suppression of NO synthesis, can substantially improve survival rates in mice without affecting the viral load (Getts et al., 2008, Getts et al., 2012, Terry et al., 2015, Getts et al., 2014, Spiteri et al., 2023b). This highlights the crucial involvement of these cells in inflammatory damage rather than direct viral control.

The adoption of specific phenotypes by monocytes that infiltrate the CNS can be controlled by various parameters. These factors include the microenvironments of the BM and brain, the timing of their migration to the brain after infection, and the duration of their residence within the infected CNS. During WNV infection, it was demonstrated that monocytes also display an antigen-presenting phenotype that may indirectly aid in the elimination of viruses by promoting an efficient T cell response (Getts et al., 2012, Spiteri et al., 2023b). Monocytes may first

assume an antigen-presenting profile at day 5 of post-infection, followed by a change to an immune-cell recruiting or inflammatory phenotype by day 7 post-infection (Spiteri et al., 2023b). In addition, monocytes have been shown to adopt a microglia-like phenotype during infection (Getts et al., 2008, Spiteri et al., 2021a), as these cells can upregulate nominal "microglia-specific" markers such as TMEM119 (Spiteri et al., 2021a). Although the functional role of these microglia-like MCs is poorly defined, it has been suggested that prolonged exposure to the CNS microenvironment induces a phenotype reminiscent of the sentinel macrophages of the CNS parenchyma, which undergo apoptosis during WNV infection (Spiteri et al., 2021a). Overall, this suggests that the functional characteristics of monocytes may be influenced by the microenvironment in the BM and bloodstream before they enter the CNS, depending on the time point at which they migrate to the CNS, or influenced by ongoing exposure to the changing CNS microenvironment.

Finally, it is crucial to acknowledge that the influence of monocytes on WNV infection is substantially influenced by the route of viral inoculation. For example, the reduction of monocytes in mice peripherally infected with WNV significantly decreases survival rates (Ben-Nathan et al., 1996, Lim et al., 2011a), suggesting that monocytes have distinct temporal roles in peripheral tissues as opposed to the brain. In peripheral infection, this may serve to reduce the probability of virus getting into the brain in the first place and/or substantially reduce the number of virions that gain access to the brain, making early innate and later adaptive defence more effective and manageable for the CNS. If this is case, the large monocyte numbers that subsequently infiltrate into the CNS in our model reflects the lack of lead time these cells would normally have to accomplish this task in classical peripheral infection.

1.6 Research objectives

The field of immunometabolism is emerging as a dynamic area of research with significant potential to unveil new therapeutic targets and strategies. Immunometabolism explores the interplay between metabolic processes and immune cell function, offering insights into how metabolic pathways influence immune responses in various diseases.

MCs exhibit remarkable functional heterogeneity, especially in the context of CNS disease. Advances in high-dimensional techniques, such as single-cell RNA sequencing (scRNA-seq) and immune profiling technologies, have shed light on this diversity. However, it remains unclear whether MCs adopt distinct functional states that are conserved across different pathologies. Additionally, the extent to which these cells are functionally distinct from resident microglia in the context of CNS disease is not well understood.

Macrophage metabolism, a relatively new field, has primarily been explored through the lens of the M1/M2 paradigm, which categorizes macrophages into pro-inflammatory (M1) and anti-inflammatory (M2) states. This binary classification oversimplifies the complexity of macrophage function *in vivo*, where these cells rarely conform strictly to M1 or M2 phenotypes. This complexity is particularly evident in the context of CNS infections, emphasizing the need for a more nuanced understanding of macrophage metabolism-function relationship and its implications for disease processes and therapeutic interventions.

The primary objective of this research is to elucidate the relationship between MC function and metabolism within the context of CNS disease. To achieve this, my first aim was to identify, compare, and contrast the shared MC functions (Results Chapter I) and metabolic profiles (Results Chapter II) aof these cells across different pathologies. This approach was intended to enhance our understanding of the functional diversity of MCs and the interplay between metabolism and function, potentially uncovering common therapeutic targets across various CNS diseases. Subsequently, I aimed to develop and validate a method for evaluating MC metabolism using flow cytometry, taking advantage of the significant flow cytometric expertise of this lab (Results Chapter III). This single-cell analysis technique is essential to accurately define the heterogeneity of MCs, allowing me to investigate these cells on an individual basis. Finally, utilizing this method, I sought to characterize the metabolic profiles of monocytes during WNV infection and formulate a metabolism-focused therapeutic strategy (Results

Chapter IV). This strategy aims to selectively target these cells based on the insights gained into their metabolic phenotype and its correlation with their functional status.

Chapter 2: Materials & Methods

2.1 Animals

Female 9 to 10-week-old C57BL/6 mice were obtained from Animal BioResources (NSW, Australia) or Ozgene (South Australia, Australia). All experiments involving mice were approved by the University of Sydney Animal Ethics Committee (Protocol 1696). Mice were housed at 20-24°C and 40-70% humidity in a 12/12-hr light/dark cycle and received standard food and water *ad libitum*. All mice were allowed to acclimatize for 7 days before each experiment. We elected to use female mice as animals are required to be housed together for ethical reasons and scientific purposes. Inflammatory injuries associated with housing dominant males in groups produces background immunological reactions which may confound results in this inflammatory model.

2.2 WNV Infection

The original stock of WNV (Lineage II, Sarafend Strain) was acquired from the John Curtin School of Medical Research (ACT, Australia). Virus was isolated via propagation *in vivo* in C57BL/6 suckling mouse brains and *in vitro* in Vero cells. Virus stock was stored at -80°C, thawed, and diluted in PBS prior to use. Mice were anaesthetised with 5% isoflurane with 1L/min of oxygen until deeply anaesthetised. WNV (Lineage II, Sarafend strain) was delivered intranasally in 10 µL of PBS (5 µL per nostril). Mice were infected with 3×10^4 plaque-forming units (PFU), a dose which is lethal in 100% of animals (LD_{100}). Mock-infected mice were given 10 µL of sterile PBS (vehicle control). Following infection, isoflurane levels were reduced to 1.5% and animals were returned to a chamber for a further 10 minutes. Mice were euthanised at the indicated timepoints over the disease course and disease scored according to the criteria in Table 2.1.

2.3 Animal Treatments

2.3.1 Glycolysis inhibition by 2-deoxy-d-glucose treatment

Mice were randomly assigned into treatment or vehicle control groups. 2-deoxy-D-glucose (2-DG, Sigma-Aldrich, USA) was made up in sterile phosphate-buffered saline (PBS) at a concentration of 0.2 g/mL fresh before each injection. 2-DG was injected intraperitoneally once daily from 4 to 7-8 days post-infection (dpi) at a dose of 2g/kg body weight. In some

experiments, 2-DG (2g/kg) was administered once at 7 dpi at either 4.5 hours or 5.5 hours before euthanasia. To ensure blood glucose levels remained stable with 2-DG treatment, blood glucose monitoring was performed the day before 2-DG treatment as a baseline, and then daily following 2-DG treatment after a 2-hour recovery period. Blood sampling was performed from the tail tip.

Table 2.1. Criteria for WNV disease score.

Score	Criteria
0	No evidence of disease
1	Weight loss ≤ 3%
2	Weight loss ≤ 4%
3	Weight loss ≤ 5%
4	Weight loss ≥ 5% Add 0.1 for each disease sign: ruffled fur, hyperaemic face, hunched posture or shaking Add 0.2 for each disease sign: no reaction upon pulling tail or stumbles when walks
4.9	Weight loss ≥ 5% and incapacitated

2.3.2 Detection of proliferating cells with Bromodeoxyuridine

A stock of Bromodeoxyuridine (BrdU) (Sigma-Aldrich, USA, 10 mg/mL) was made by dissolving BrdU in sterile PBS, then stored at -80°C and thawed prior to use. The stock solution was diluted to a dose of 1 mg prepared in 200 μL of sterile PBS and injected intraperitoneally 3 hours before sacrifice at dpi 7.

2.3.3 Tracking recently infiltrated cells into the CNS with PKH26

PKH26 cell linker was combined with diluent C (Sigma-Aldrich, USA) at a 10-fold higher concentration than the manufacturer's recommendation and injected intravenously via the lateral tail vein 2 hrs before euthanasia, as previously described (Spiteri et al., 2022a).

2.4 Tissue Isolation, Processing, and Cell Counting

2.4.1 Dissection and perfusion

Mice were anaesthetised with avertin and transcardially perfused 10 mL of sterile 1X PBS using a 27G needle to clear organs of circulating leukocytes and red blood cells (RBC). Organs of interest were collected as indicated.

2.4.2 Organ collection for PCR

Half-brains were collected in a 2.5 mL tube that was immediately placed on dry ice, then stored at -80°C until further processing.

2.4.3 Organ collection for plaque assay

Half-brains were weighed and immediately frozen in dry ice in Roswell Park Memorial Institute 1640 media (RPMI, Lonza Bioscience).

2.4.4 Leukocyte isolation

2.4.4.1 Brain

Brains were collected in a petri dish and cut into ~1 mm pieces with 10 µL of PBS before being placed in 1X PBS in a C-tube (Miltenyi Biotec, USA). Tissue was homogenised on the gentleMACS dissociator for 30 minutes at 37°C with collagenase type IV (C5138, Sigma-Aldrich, USA, 5 mg/mL) and DNase (DN25, Sigma-Aldrich, 0.1 mg/mL), which was freshly defrosted from storage in a -30 freezer before each use. After homogenisation, brain tissue was topped up with FACS and centrifuged at 500 xg for 10 mins at 4°C. The pelleted cells were then resuspended in 30% percoll, carefully layered onto 80% percoll, and then isopycnically separated by centrifugation (1825 xg, 25 mins, no brake, room temperature). Brain leukocytes were collected from the 30%/80% percoll interface using a pipette and then resuspended in 250 µL of FACS buffer.

2.4.4.2 BM and spleen

The femur and tibia were collected, and both ends of the bone were removed by transection with a scalpel. The BM was flushed with 6 mL of sterile 1X PBS using a 5 mL syringe with a 30½ G needle.

Spleens were collected into a 12-well plate in sterile PBS, then each gently mashed through a 70 µm sieve using the plunger of a 5 mL plastic syringe and the filtrate collected in sterile PBS in a 50 mL Falcon tube.

BM and spleens were stored on ice until further processing. Splenocytes and BM cells were pelleted by centrifugation (500 xg, 5 mins, 4°C), resuspended in 1 mL of 1X RBC lysis buffer (Pharm Lyse Buffer, BD) and incubated for 5 mins. Samples were topped up with 10 mL of FACS buffer, pelleted by centrifugation (500 xg, 5 mins, 4°C) and then resuspended in 3 mL (spleen) or 1 mL (BM) of FACs buffer.

2.4.4.3 Cervical lymph nodes

Cervical lymph nodes were collected in ice cold PBS and gently forced through a 70 µm sieve using the plunger of a 5 mL plastic syringe and the filtrate collected in sterile PBS in a 50 mL

Falcon tube. Cells were pelleted by centrifugation (500 x g, 5 min, 4°C) and the pellet was resuspended in 250 µL of FACS buffer.

2.4.5 Cell counting

Processed samples were vortexed or gently mixed with a pipette and 10 µL of sample was mixed with 10 µL of 0.4% trypan blue. The number of live (unstained) and dead (stained) cells were counted in a haemocytometer and where relevant the proportion of live cells determined.

2.5 Primary Cell Culture

Primary cell culture was performed on isolated leukocytes from the cervical lymph nodes, spleen, and BM, where indicated. The reagents used for primary cell culture are shown in Table 2.2.

Table 2.2. Reagents for primary cell culture.

Reagent	Source	Catalogue number
Carboxyfluorescein succinimidyl ester	Invitrogen	C34554
Concanavalin A	Sigma-Aldrich	L7647-25MG
HEPES	Sigma-Aldrich	SRE0065
L-Glutamine	Thermo Fisher Scientific	25030081
D-(+)-Glucose	Sigma-Aldrich	G8270-100G
2-deoxy-D-glucose	Sigma-Aldrich	D8375-5G
Lipopolysaccharides from *Escherichia coli* K12	InvivoGen	NC9355258
Purified interferon gamma	Biolegend	575308
Dimethyloxalylglycine (DMOG)	Sigma-Aldrich	D3695-10MG
Chrysin	Abcam	ab141230-1g
Oligomycin	Sigma-Aldrich	75351-5MG
Carbonyl cyanide 4-(trifluoromethoxy)phenylhydrazone (FCCP)	Sigma-Aldrich	C2920-10MG
Palmitic acid	Sigma-Aldrich	P0500-10G
Bovine serum albumin (BSA)	Sigma-Aldrich	A7906-100G
5-(Tetradecyloxy)-2-furoic acid (TOFA)	Sigma-Aldrich	T6575-5MG
C75	Sigma-Aldrich	C5490-5MG
L-leucine	Sigma-Aldrich	L8912-25G
L-isoleucine	Sigma-Aldrich	I7403-25G
L-valine	Sigma-Aldrich	V0513-25G
L-histidine	Sigma-Aldrich	H5659-25G
L-methionine	Sigma-Aldrich	M5308-25G
L-phenylalanine	Sigma-Aldrich	P5482-25G
L-tyrosine	Sigma-Aldrich	T8566-25G
L-tryptophan	Sigma-Aldrich	T8941-25G
Ultra-low adherence 96-well plates	Corning	3474
RPMI 1640 Medium with L-glutamine	Lonza Biosciences	12-702Q
DMEM, no glucose	Sigma-Aldrich	D5030-10X1L

2.5.1 T cell proliferation assay

Five million cells from the cervical lymph nodes were aliquoted into a 50 mL Falcon tube, pelleted (500 xg, 5 mins, 4°C), and resuspended in 3 mL (WNV-infected samples) or 250 μL (mock-infected samples) of PBS supplemented with 5% foetal calf serum (FCS). A stock concentration of carboxyfluorescein succinimidyl ester (CFSE, Life Technologies) made up in PBS was stored at -30 °C and thawed before use. CFSE staining solution was prepared at 2X the working concentration in 3 mL (WNV-infected samples) or 250 μL (mock-infected samples) of PBS and allowed to stand at room temperature. The CFSE staining solution was then added to cells (final concentration 1.5 μM), vortexed briefly, and incubated at room temperature for 5 mins. Each sample was gently agitated twice by inversion throughout the incubation time. Samples were quenched with PBS with 5% FCS and placed on ice for 15 minutes, washed twice (500 xg, 5 mins, 4°C), then resuspended in either 3 mL (WNV-infected samples) or 250 μL (mock-infected samples) of RPMI (Lonza Biosciences, USA) supplemented with 10 mM of 4-(2-Hydroxyethyl)piperazine-1-ethanesulfonic acid (HEPES) (Sigma-Aldrich, USA), 5% FCS, 0.1 M of β-mercaptoethanol (Gibco), penicillin G (0.06 g/L, Thermofisher Scientific) and streptomycin sulfate (0.1 g/L, Thermofisher Scientific). CFSE-stained cells were then plated in a flat-bottom 96-well plate in duplicate (5×10^5 cells/well). Cells were then pelleted by centrifugation (500 xg, 5 mins, 4°C). WNV stock solution (1.7×10^9 PFU/mL) was thawed and diluted in media to a concentration of 1 PFU/cell in 50 μL. The WNV solution or media alone was added to each well, resuspended, and cultured for 1 hr at 37°C and 5% CO_2 with agitation every 10 minutes. Unbound virus was then washed off and cells were cultured for a further 72 hours in media alone or media supplemented with 1 ug/mL of Concanavalin A (Sigma-Aldrich), as a positive control for T cell proliferation. After incubation, live cells from each well were counted on a haemocytometer using trypan blue (0.4%) to enumerate live cells.

2.5.2 BM stimulation

BM cells from PBS-treated or 2-DG-treated mice were plated at a seeding density of 1.2×10^6 cells/well in duplicate in a flat-bottom, ultra-low adherence 96-well plate (Corning). Cells were pelleted (500 xg, 5 mins, 4°C) and resuspended in 200 μL of RPMI media (Lonza Biosciences, USA) supplemented with 10 mM HEPES (Sigma-Aldrich, USA), 5% FCS, 0.1 M of β-mercaptoethanol (Gibco), and 1x penicillin/streptomycin (Thermofisher Scientific) and 100 ng/mL of IFN-γ and incubated for four hours at 37°C and 5% CO_2. Cells were then washed

twice in complete RPMI and resuspended in 200 µL of complete RPMI media containing 100 ng/mL of LPS (InvivoGen) and incubated for 16 hours at 37°C and 5% CO_2.

2.5.3 Metabolic stimulation experiments

BM cells or splenocytes were plated at a density of 1.2 x 10^6 cells per well in flat-bottom, ultra-low adherence 96-well plates (Corning). The cells were cultured in custom glucose-free RPMI media at 37°C with 5% CO_2 and humidified air, except where indicated. For each condition, the media was supplemented with 10 mM of HEPES (Sigma-Aldrich), 2 mM glutamine (Thermo Fisher Scientific), 1% FCS, and 2 mg/mL glucose, and the cells were incubated at 37°C with 20% oxygen unless otherwise stated.

For glycolysis and iNOS experiments, BM cells were pre-treated with 10 mM 2-DG (Sigma-Aldrich) or PBS for 1 hour. Following pre-treatment, the cells were cultured with 100 ng/mL IFN-γ (Biolegend, USA) and 10 mM 2-DG or PBS for 4 hours, followed by 100 ng/mL LPS (InvivoGen) with 10 mM 2-DG or PBS for an additional 16 hours. Alternatively, cells were cultured in custom glucose-free media with or without 2 mg/mL glucose and 100 ng/mL LPS or PBS as a vehicle control. To validate HIF1α signalling, BM cells were cultured in media supplemented with either 0.2 mM Dimethyloxalylglycine (DMOG, Sigma-Aldrich) or PBS in 3% oxygen, or 0.01 mM Chrysin (Abcam) or PBS in 20% oxygen. For TCA cycle experiments validating isocitrate dehydrogenase 1 (IDH1), cells were cultured with 2 µM oligomycin (Sigma-Aldrich) or vehicle control for 4 hours to prevent the induction of glycolysis, which occurs after 6 hours of incubation (Hao et al., 2010). To validate cytochrome C as a marker of the ETC, BM cells were cultured with 1 µM carbonyl cyanide 4-(trifluoromethoxy)phenylhydrazone (FCCP, Sigma-Aldrich) for 4 hours. For experiments involving fatty acid metabolism, 2 mM palmitic acid (Sigma-Aldrich) was conjugated with 20% bovine serum albumin (BSA) (Scientifix Australia) before use. To validate carnitine palmitoyltransferase 1A (CPT1A) as a marker for fatty acid oxidation, BM cells were cultured with 167 µM palmitate conjugated to BSA or BSA alone, ± 10 mM 2-DG, and ± 3 µM etomoxir or vehicle control for 16 hours. In some experiments, CPT1A expression was assessed in splenocytes cultured in glucose-free Dulbecco's Modified Eagles Medium (DMEM, Sigma-Aldrich) supplemented with palmitate conjugated to BSA (0.175 mM) and/or 4.5 g/L glucose. To validate acetyl-coA carboxylase (ACAC) as a marker of fatty acid synthesis, BM cells were cultured with the indicated concentrations of either C75 (Sigma-Aldrich) or 5-(Tetradecyloxy)-2-furoic acid (TOFA, Sigma-Aldrich) with 100 ng/mL LPS and 100 ng/mL IFN-γ for 16 hours.

To validate CD98 as a marker of amino acid uptake, BM cells were cultured with 100 ng/mL LPS in custom RPMI media free of large neutral amino acids or supplemented with large neutral amino acids at normal RPMI levels: L-leucine (0.3817 mM), L-isoleucine (0.3817 mM), L-valine (0.1709 mM), L-histidine (0.097 mM), L-methionine (0.1006 mM), L-phenylalanine (0.0909 mM), L-tyrosine (0.1111 mM), and L-tryptophan (0.0245 mM) (all from Sigma-Aldrich).

2.6 Spectral Flow Cytometry

2.6.1 Surface staining

Samples of 3 x 10^6 cells were seeded in a 96-well U-bottom plate, pelleted by centrifugation (500 xg, 5 mins, 4°C), then resuspended in 50 µL of Zombie UV Fixable Viability dye (Biologend, USA) (1/1000 in PBS for BM, spleen, and cervical lymph nodes and 1/500 for brain) and anti-CD16/32 (fluorescently conjugated or unconjugated, Biolegend, USA at 1/100) for 30 minutes on ice, topped up with 150 µL PBS and washed twice with 250 µL of PBS (500 xg, 5 mins, 4°C). Cells were then resuspended in 50 µL of a cocktail of fluorescently-labelled surface-stain antibodies in FACS buffer on ice for 30 minutes (see Table 2.3). Cells were then topped up with 150 µL of FACS buffer and then washed twice in FACS buffer. If cells were not being permeabilised for intracellular staining, cells were resuspended in Fixation Buffer (Biolegend) for 20 mins at room temperature. Cells were then topped up and washed once in FACS. Cells were then resuspended in 180-200 µL of FACS buffer and stored overnight at 4°C. Cells were then run on the 5-laser Aurora (Cytek Biosciences) the next day.

2.6.2 Detection of nitric oxide

NO was detected by using 4-Amino-5-Methylamino-2',7'-Difluorofluorescein diacetate (DAF-FM diacetate) (Invitrogen, USA), which is a cell-permeable fluorescent probe that is nonfluorescent until it reacts with NO. Cells were resuspended in DAF-FM (5 nmol/mL) in PBS for 30 min at room temperature, prior to cell surface staining. DAF-FM staining was detected flow cytometrically.

2.6.3 Detection of mitochondrial reactive oxygen species

Mitochondrial ROS production was detected using MitoSOX Red (ThermoFisher Scientific), a fluorogenic dye, which upon oxidation by mitochondrial superoxides, exhibits bright red fluorescence when excited by 396 nm wavelength light. MitoSOX powder was stored at -30°C

protected from light, and stock solutions were prepared dissolving vial contents in 13 μL of dimethyl sulfoxide (DMSO) to make a 5mM MitoSOX reagent solution. MitoSOX reagent solutions were prepared fresh before each experiment to avoid oxidation. Cells were resuspended in MitoSOX (1/4000, 1.25 uM) in PBS for 30 mins at 37°C, prior to cell surface staining. MitoSOX staining was detected flow cytometrically.

Table 2.3. Antibodies used for flow cytometry staining.

Antibody	Company	Catalogue	Concentration
Surface stain antibodies			
Anti-CD11b (clone M1/70) – BUV395	BD	Cat # 563553	1:100
Anti-CD11b (clone M1/70) – PE-Cy7	Biolegend	Cat # 101216	1:100
Anti-CD45 (clone 30-F11) – BUV661	BD	Cat # 612975	1:100
Anti-CD45 (clone 30-F11) – PE/Cy7	Biolegend	Cat # 103114	1:200
Anti-CD45 (clone 30-F11) – AF700	Biolegend	Cat # 103128	1:200
Anti-CD45.2 (clone 104) – BV650	Biolegend	Cat # 109835	1:50
Anti-CD11c (clone F10/21A3) – BUV737	BD	Cat # 748723	1:100
Anti-CD98 (clone H202-141) – BUV615	BD	Cat # 752360	1:100
Anti-CD8a (clone 53-6.7) – BUV805	BD	Cat # 612898	1:100 (Brain) 1:200 (BM, LN, spleen)
Anti-MHC-II (clone MP6-XT22) – BV510	Biolegend	Cat # 506339	1:200
Anti-MHC-II (M5/114.15.2) – BV480	BD	Cat # 566088	1:200
Anti-Ly6C (clone HK1.4) – BV605	Biolegend	Cat # 128036	1:100
Anti-Ly6G (clone 1A8) – BV650	Biolegend	Cat # 127641	1:200
Anti-Ly6G (clone 1A8) – FITC	Biolegend	Cat # 127606	1:200
Anti-CD4 (clone GK1.5) – BV750	Biolegend	Cat # 100467	1:100
Anti-CD4 (clone RM4-5) – BV570	Biolegend	Cat #100542	1:100 (Brain) 1:200 (BM, CLN, spleen)
Anti-B220 (clone RA3-6B2) – BV785	Biolegend	Cat # 103245	1:200
Anti-B220 (clone RA3-6B2) – BV570	Biolegend	Cat # 100542	1:100
Anti-B220 (clone RA3-6B2) – PE-Cy5	Biolegend	Cat #103210	1:100 (Brain) 1:200 (BM, LN, spleen)
Anti-B220 (clone HL32) – BUV737	BD	Cat # 612796	1:100 (Brain) 1:200 (BM, LN, spleen)
Anti-NK1.1 (clone PK136) – PE-Cy5	Biolegend	Cat # 108716	1:100 (Brain) 1:200 (BM, LN, spleen)

Anti-CD64 (clone X54-5/7.1) – PE/Dazzle594	Biolegend	Cat # 139319	1:200
Anti-CD64 (clone X54-5/7.1) – PE-Cy7	Biolegend	Cat # 139313	1:200
Anti-CD3e (clone 500A2) – AF700	BD	Cat # 557984	1:100 (Brain) 1:200 (BM, LN, spleen)
Anti-CD3e (clone 145-2C11) – PE-Cy5	Biolegend	Cat # 100310	1:100 (Brain) 1:200 (BM, LN, spleen)
Anti-CD3e (clone 145-2C11) – PE/Dazzle 594	Biolegend	Cat # 100348	1:100 (Brain) 1:200 (BM, LN, spleen)
Anti-CX3CR1 (clone SA011F11) – APC/Fire750	Biolegend	Cat # 149040	1:100
Anti-CX3CR1 (clone SA011F11) – BV421	Biolegend	Cat # 149023	1:100
Anti-CD44 (clone IM7) – FITC	Biolegend	Cat # 103006	1:100
Anti-CD44 (clone IM7) – BV650	Biolegend	Cat # 103049	1:100
Anti-P2RY12 (clone S16007D) – PE	Biolegend	Cat # 848004	1:100
Anti-P2RY12 (clone S16007D) – APC	Biolegend	Cat # 848006	1:100
Anti-CD62L (MEL-14) – APC	Biolegend	Cat # 104412	1:100
Anti-CD62L (MEL-14) – BV605	Biolegend	Cat # 104438	1:100
Anti-CD69 (H1.2F3) – APC/Cy7	Biolegend	Cat # 104526	1:100
Anti-CD69 (clone H1.2F3) - BV786	BD	Cat # 564683	1:100
Anti-FoxP3 (MF-14) – PE	Biolegend	Cat # 126404	1:100
Anti-IFNy (XMG1.2) – APC	Biolegend	Cat # 505810	1:100
Anti-CD48 (HM48-1) – BUV563	BD	Cat # 741258	1:100
Anti-CD48 (clone HM48-1) – APC	Biolegend	Cat # 103412	1:200
Anti-CD48 (clone HM48-1) – APC/Cy7	Biolegend	Cat # 103432	1:200
Anti-CD34 (clone RAM34) – BV421	BD	Cat # 562608	1:100
Anti-Sca-1 (clone D7) – BV711	Biolegend	Cat # 108131	1:200
Anti-CD117 (clone 2B8) – PE-Cy5	Biolegend	Cat # 105810	1:100
Anti-CD117 (clone 2B8) – BV421	Biolegend	Cat # 105828	1:100
Anti-CD115 (clone AFS98) – APC/Fire750	Biolegend	Cat # 135535	1:100
Anti-CD115 (clone AFS98) – PE	Biolegend	Cat #135506	1:100
Anti-CD16/32 (clone 2.4G2) – FITC	Biolegend	Cat # 553144	1:100
Anti-CD16/32 (clone 93) – purified	Biolegend	Cat # 101301	1:100
Anti-CD25 (clone PC61) – PE-Cy7	Biolegend	Cat # 102016	1:200
Anti-CD49d (clone R1-2) – PE	Biolegend	Cat # 103607	1:100
Anti-Siglec H PerCP/Cy5.5 (clone 551)	Biolegend	Cat # 129614	1:100
Anti-CD81 (clone Eat-2) – PE	Biolegend	Cat # 104906	1:100
Anti-CD81 (clone Eat-2) – APC	Biolegend	Cat # 104910	1:100
Anti-CD86 (clone GL-1) – APC/Cy7	Biolegend	Cat # 105030	1:100
Intracellular and intranuclear antibodies			
Anti-CD206 (clone C068C2)	Biolegend	Cat # 141729	1:100
Anti-iNOS (clone CXNFT) – BV421	Invitrogen	Cat # 404-5920-82	1:100
Anti-GAPDH (clone W17079A) – AF488	Biolegend	Cat # 607905	1:100
Anti-IDH1 (clone RMab 3) - PE	BD	Cat # 567019	1:80
Anti-HIF1α (clone 241812) – APC	R&D systems	Cat # IC1935A	1:100
Anti-IDO1 (clone 2E2) – AF647	Biolegend	Cat # 654003	1:100
Anti-Cytochrome C (clone 6H2.B4) – AF647	Biolegend	Cat # 612310	1:100

Anti-CPT1α (clone 8F6AE9) – Purified	Abcam	Cat # ab128568	1:100
Anti-ACAC– Purified	Abcam	Cat # ab72046	1:50, 1:100
Anti-rabbit IgG – DyLight800	Invitrogen	Cat # **SA5-10036**	1:50
Anti-rabbit IgG (clone Poly4064) – Dylight594 (Secondary Ab for ACAC)	Biolegend	Cat # 406418	1:300
Anti-mouse IgG2b (clone RMG2b-1) – PE-Cy7 (Secondary Ab for CPT1A)	Biolegend	Cat # 406713	1:100
Anti-FoxP3 (MF-14) – PE	Biolegend	Cat # 126404	1:100
Anti-IFNy (XMG1.2) – APC	Biolegend	Cat # 505810	1:100
BrdU – APC	BD	Cat # 51-23619L	1:100
Isotype controls			
Anti-Rat IgG2a, k – BUV615	BD	Cat # 751544	1:100
Anti-Rat IgG2a, k – BV421	ThermoFisher Scientific	Cat # 404-4321-81	1:100
Anti-Rat IgG2a, k – AF488	Biolegend	Cat # 400525	1:100
Anti-Mouse IgG1, k – PE	Biolegend	Cat # 400111	1:32
Anti-Mouse IgG2b, k – purified	Biolegend	Cat # 401201	1:100
Anti-Mouse IgG1, k – APC	Biolegend	Cat # 400121	1:100
Anti-Mouse IgG1, k – AF647	Biolegend	Cat # 400130	1:100
Anti-Rabbit IgG – purified	Biolegend	Cat #026102	1:500
Other dyes and reagents			
Zombie UV™ Fixable Viability Kit	Biolegend	Cat # 423107	1:500 (Brain) 1:200 (BM, LN, spleen)
MitoSOX Red	ThermoFisher Scientific	Cat # M36008	1:4000
DAF-FM diacetate	Invitrogen	Cat # D23844	1:1000

2.6.4 Intracellular staining

Cells were permeabilized with True-Nuclear 1x Fix Concentrate (Biolegend, USA) for one hour at room temperature and washed twice with 1X perm wash buffer (Biolegend, USA) diluted in milli-Q water. Cells were resuspended in 50 µL of intracellular/intranuclear antibody cocktails (see Table 2.3) made up in 1X perm wash buffer for 1 hour on ice, washed twice, and then stained with secondary antibodies targeting ACAC (anti-rabbit IgG conjugated to DyLight594 or DyLight800) and CPT1α (anti-mouse IgG2b conjugated to PE-Cy7) (see Table 2.3) for 1 hr on ice. After incubation, samples were topped up with 150 µL of 1X perm wash, washed twice in 1X perm wash and once in FACS buffer, and then resuspended in 180-200 µL of FACS buffer. Cells were stored protected from light at 4°C until acquisition with the 5-Laser Aurora spectral cytometer (Cytek Biosciences, USA).

2.6.5 Detection of proliferating cells with BrdU

BrdU staining was performed on samples obtained from animals injected with BrdU before organ collection. Cells previously stained with surface markers were pelleted by centrifugation

and resuspended in 1X CytoFix/CytoPerm buffer (BD Biosciences) for 20 mins at 4°C in the dark, then topped up with 150 µL of perm wash buffer (BD Biosciences). Subsequently, cells were permeabilised by resuspending them in CytoPerm Buffer Plus (BD Biosciences) for 10 minus on ice, topped up with 150 µL of perm wash, pelleted and then resuspended in CytoFix/Cytoperm (BD Biosciences) for 5 mins at room temperature. Cells were then pelleted by centrifugation with perm wash buffer and resuspended in a 1 mg/mL DNase solution (Sigma-Aldrich, USA; 30 units/sample, >400 units per mg of DNase) at 37°C for 1 hr. Cells were then topped up and washed with perm wash buffer, and then resuspended in an intracellular antibody cocktail mixture containing APC-BrdU (BD Biosciences) in perm wash buffer and incubated for 30 mins at room temperature. Finally, cells were topped up with 150 µL of perm wash buffer, washed twice with perm wash buffer and once with FACS buffer, and then resuspended in 180-200 µL of FACS buffer. Cells were stored at 4°C protected from the light until data acquisition with the 5-laser Aurora (Cytek Biosciences, USA).

2.6.6 Sample acquisition by spectral flow cytometry

Prior to sample acquisition, cells were filtered into FACS tubes through a 70 µm Nytex filter (Merck Millipore, MA, USA). Cells were run on the 5-laser Aurora (Cytek Biosciences, USA) using the SpectroFlo software (Cytek Biosciences, USA). Unstained controls for each specific condition were used as reference controls for spectral unmixing in each experiment. For some experiments, unstained samples were acquired for each sample.

2.7 Single-Cell RNA Sequencing

2.7.1 Cell Sorting

Monocytes, microglia and MCs were isolated from WNV-infected murine brains and BM at the designated dpi. To ensure ample cells were available for sorting, tissues from two animals were combined per sample. Brain and BM were processed into single-cell suspensions as described in section 2.4.2. Single cell suspensions underwent CD16/32 blocking and Zombie UV viability staining (Biolegend, USA) before incubation with a cocktail of fluorescently-conjugated surface stain antibodies (Spiteri et al., 2023b). Cells were washed twice in FACS buffer, filtered, and adjusted to a concentration of 1 x 10^7 cells per mL before sorting. Sorting was performed on a 10-laser Influx Cell Sorter (BD Bioscences, USA) using the FACS Diva Program (BD Biosciences, USA). Samples were sorted in 500 µL of FBS and kept on ice until further processing. Samples were then barcoded with a mouse multiplexing kit using an anti-

CD45 antibody (BD Biosciences, USA), as previously described (Spiteri et al., 2023b). To avoid interference with the anti-CD45 barcode, cells were stained with anti-CD45.2 for cell sorting.

After barcoding sorted cells, samples were counted and pooled in equal numbers. The pooled sample was subsequently stained with Calcein AM (2 mM) (ThermoFisher) and Draq7 (0.3 mM) and loaded on a INCYTO^{TM} disposable hemocytometer and placed in the BD Rhapsody Scanner to measure cell concentration and viability. Quality control metrics for the Rhapsody scanner were as follows: number of cells loaded into cartridge, 51675; doublet rate, 8.3%; viability, 53.28%; number of single cells loaded into the cartridge, 22217; number of cells captured in the cartridge, 15386; number of individual cells attached to a single capture bead, 14711.

2.7.2 Cell Capture

The BD Rhapsody Express system was used to capture single-cell transcriptomics on a BD Rhapsody Cartridge (BD Biosciences) following the manufacturer's instructions. Viable cells included those that were single cells with beads captured in wells. After lysing the cells with a lysis buffer containing DDT (BD Biosciences), cell capture beads (BD Biosciences) were collected and washed before reverse transcription and exonuclease I treatment (BD Biosciences). The final libraries were generated using microbead-captured single cell transcriptomes as per the manufacturer's protocol using the BD Rhapsody cDNA Kit (BD Biosciences) and the BD Rhapsody Targeted mRNA Amplification Kit (BD Biosciences). The BD Rhapsody Immune Response Panel (cat. # 633753), consisting of 397 genes, and an additional 67 custom genes were used. Following PCR1, the transcripts were separated into mRNA or Sample Tag libraries based on amplicon size using DNA double-sided size selection. PCR2 was then carried out to further enrich both mRNA and Sample Tag libraries, after which each library was indexed for sequencing.

2.7.3 Library Preparation

For sequencing, libraries were quantified using a Qubit Fluorometer (ThermoFisher Scientific) and KAPA Library Quantification Kit (Roche), adjusted to 2nM, and pooled in a mRNA:sample tag ratio of 12.5:1. The average fragment size of the mRNA targeted library was quantified using the KAPA Library Quantification Kit. This showed that the fragment distribution was approximately 290-600 bps for sample mRNA and approximately 290 bps for

the Sample Tag index PCR products, which is the expected size of the Sample Tag index PCR products. Sequencing was performed on an Illumina NextSeq1000, with stringent QC metrics such as 93.28 %Q30 and 81.73 %PF achieved. The run yielded 131 million reads with a high loading efficiency (98.4%).

2.8 Plaque Assay

Baby Hamster Kidney (BHK) fibroblasts were used to perform WNV plaque assays, as previously described (Getts et al., 2008). Briefly, BHK cells were inoculated with brain tissue homogenates in a series of ten-fold dilutions for 1 hr, washed, then subsequently overlaid with agarose. After a 3-day incubation, cells were fixed with 10% formalin (Sigma-Aldrich, USA), then stained with 1% crystal violet solution. Viral load, expressed as PFU per gram of brain tissue, was calculated by quantifying the number of visible plaques and accounting for inoculum volume and dilutions used.

2.9 RNA Extraction and Real-Time Quantitative Polymerase Chain Reaction

Brain samples were homogenized using 1 mL of TRI Reagent (Sigma Aldrich, USA), stainless steel beads, and a tissue homogenizer (TissueLyzer, Qiagen, DE) at 50 Hz for 2 rounds of 40 seconds. The High-Capacity cDNA Reverse Transcription Kit (ThermoFisher Scientific, USA) was used to synthesize cDNA and The Power SYBR Green PCR Master Mix (ThermoFisher Scientific, USA) was then used for real-time quantitative polymerase chain reaction (qPCR) using primers detailed in Table 2.4. This was conducted using the LightCycle® 480 Instrument II (Roche, CH). Gene expression values were normalized to *Rpl13a*.

2.10 Flow Cytometry Data Analysis

The FCS files were compensated and gated down to individual cell populations prior to exporting cell proportions and MFI in FlowJo (BD Biosciences, USA). Cell proportions and live cell counts were used to quantify cell numbers. MFIs from positive populations, as determined both by the isotype and fluorescence minus one (FMO) control, were used to quantify and validate protein expression of metabolic targets. Statistical analyses were carried out in GraphPad Prism (version 10.2.0 for Mac, GraphPad Software, Boston, Massachusetts USA, www.graphpad.com) and the statistical tests used are indicated in each figure legend.

Table 2.4. Primer sequences used for qPCR

Primer	NM	Primer set sequence for F 5'-3'	Primer set sequence for R 5'-3'
Tnf	NM_013693.3	ATGGCCTCCCTCTCATCAGT	GTTTGCTACGACGTGGGCTA
Il6	NM_038165.2	CCTCTCTGCAAGAGACTTCCAT	ASTOTCOTCTOOGGACTTOT
Il1b	NM_008361.4	TGCCACCTTTTGACAGTGATG	TGATGTGCTGCTGCGAGATT
Ifng	NM_008337.4	GCAAAAGGATGGTGACATGA	TTCGCCTTGCTGTTGCTGA
Ccl2	NM_011333.3	CAAGATGATCCCAATGAGTAG	TTGGTGACAAAAACTACAGC
Ccl3	NM_011337	CCATATGGAGCTGACACCCC	GAGCAAAGGCTGCTGGTTTC
Ccl5	NM_013653	TGCTCCAATCTTGCAGTCGT	GCAAGCAATGACAGGGAAGC
Ccl7	NM_013654	CTCTCTCACTCTCTTTCTCC	TCTGTAGCTCTTGAGATTCC
Cxcl10	NM_021274	AAAAAGGTCTAAAAGGGCTC	AATTAGGACTAGCCATCCAC
Cxcl16	NM_023158.6	CCATTCTTTATCAGGTTCCAG	CTTGAGGCAAATGTTTTTGG

For Results Chapter I, histograms, dot plots (showing surface markers) and tSNE plots (using default settings) were created in FlowJo (BD Biosciences, v10.8). The clustered heatmap shown in Figure 3.8 was made in R using the pheatmap package (v1.0.12) (Kolde, 2012).

For Results Chapter III, the FCS files were compensated in FlowJo and gated down to monocytes ($CD45^+$, $Ly6G^-$, $SSCA^{low}$, $CD3e^-$, $NK1.1^-$, B220-, $CD11c^{low}$, $CD11b^+$, $Ly6C^{+/-}$) or T cells ($CD45^+$, $Ly6G^-$, $SSCA^{low}$, $NK1.1^-$, $B220^-$, $CD11b^-$, $CD11c^-$, $CD3e^+$). For stained samples, autofluorescence was extracted during spectral unmixing to obtain an aggregated measure of autofluorescence across 64 raw fluorescence parameters. Gating and analysis of datasets was performed in FlowJo. MFI was exported from FlowJo, and the correlation between unmixed autofluorescence MFI and GAPDH MFI was calculated via Pearson R in Prism 9 (GraphPad).

For Results Chapter IV, the FCS files were compensated and gated in FlowJo (BD Biosciences, USA). Monocytes (for BM samples) or MCs and microglia (for brain samples) were then exported and downsampled to a total of $3x10^5$ cells ($1.5x10^5$ per organ). FCS files were formatted with the CyCombine package (Pedersen et al., 2022) and Arcsinh transformed (cofactor = 6000) before being converted into a Seurat object using a custom R script using Seurat (v4.0) (Hao et al., 2021). Two independent experiments were then batched integrated

using rPCA in Seurat using all markers as integration anchors. All subsequent analysis was performed on data as a Seurat object using the Seurat pipeline (Hao et al., 2021). Uniform manifold approximation and projection (UMAP) and clustering analysis was performed using only metabolic features.

2.10.1 Analysis of unstained samples

To examine changes in autofluorescence, unstained samples for nutrient stimulation and inhibition experiments were stored in the online analysis platform OMIQ as Aurora 5L raw FCS files (CBInsights). Off-scale or debris events were excluded from analysis using scatter gating. The analysis was carried out on 50,000 non-debris, non-erythrocyte single cells per sample using the OMIQ fluorescence parameter scaling (arcsinh, cofactor = 6000). Opt-SNE was performed using the following OMIQ settings: maximum iterations = 1000, opt-sneEnd = 5000, perplexity = 30, Theta = 0.5, components = 2, verbosity = 25, and random seed values.

2.11 Analysis of transcriptomic data

The tools, online platforms, software, and R and Python packages used to analyse transcriptomic data are detailed in Table 2.5.

2.11.1 Single-cell RNA-sequencing

2.11.1.1 Pre-processing and normalisation

For Results Chapter I and II, count matrices were downloaded from the Gene Expression Omnibus (GEO) (Barrett et al., 2013). The R toolkit Seurat v4.0 (Hao et al., 2021) was used for quality control processing, graph-based clustering, visualizations and differential gene expression analyses of scRNA-seq and performed in R (v.4.0.3). Each scRNA-seq dataset was processed separately. Samples were filtered to remove cells that were either empty droplets or possible doublets/multiples or had a higher percentage of reads mapping to the mitochondrial genome. Cells in each dataset were included if the number of unique genes detected per cell were between 250 and 25000 and the percentage of mitochondrial reads were less than 5%. As mitochondrial genes were not present in Keren-Shaul et al. (2017), this dataset was filtered only by the number of unique genes per cell. The number of cells in each dataset before and after filtering is shown in Table 2.6.

For Results Chapter IV, raw sequencing reads exported from the Illumina NextSeq 1000 were processed through the SevenBridges Targeted Analysis pipeline to generate a count matrix.

The R toolkit Seurat v4.0 was used for pre-processing and downstream analyses in R (v.4.0.3). Samples were filtered to remove cells that were possible doublets/multiplets or had a higher percentage of reads mapping to mitochondrial genes. Cells in each dataset were included if the number of unique genes and percent of mitochondrial genes detected per cell were between -3 to +3 median absolute deviations of the median. Normalization and variance stabilization were performed using the *sctransform*() function in Seurat. Mitochondrial gene expression and total number of reads per cell were regressed out to control for confounding sources of variation.

Table 2.5. Software and algorithms used for analysis of transcriptomic data.

Item	Source	Identifier
DESeq2	Love et al., 2014; Galaxy Version 2.11.40.6+galaxy1	https://usegalaxy.org/root?tool_id=toolshed.g2.bx.psu.edu/repos/iuc/deseq2/deseq2/2.11.40.6+galaxy1
featureCounts	Liao et al., 2014; Galaxy Version 2.0.1	https://usegalaxy.org/root?tool_id=toolshed.g2.bx.psu.edu/repos/iuc/featurecounts/featurecounts/2.0.1
annotatemyIDs	Galaxy Version 3.12.0	https://usegalaxy.org/root?tool_id=toolshed.g2.bx.psu.edu/repos/iuc/annotatemyids/annotatemyids/3.12.0
CutAdapt	Martin, 2011; Galaxy Version 3.4+galaxy0	https://usegalaxy.org/root?tool_id=toolshed.g2.bx.psu.edu/repos/lparsons/cutadapt/cutadapt/3.4+galaxy0
HISAT2	Kim et al., 2015; Galaxy Version 2.1.0+galaxy7	https://usegalaxy.org/root?tool_id=toolshed.g2.bx.psu.edu/repos/iuc/hisat2/hisat2/2.1.0+galaxy7
FastQC	Andrews, 2010; Galaxy Version 0.72+galaxy1	https://usegalaxy.org/root?tool_id=toolshed.g2.bx.psu.edu/repos/devteam/fastqc/fastqc/0.72+galaxy1
Seurat v4	Hao et al., 2021	https://satijalab.org/seurat/
Spectre	Ashhurst et al., 2021	https://immunedynamics.io/spectre/
LIGER v0.5.0	Welch et al., 2019	https://CRAN.R-project.org/package=rliger
topGO v2.44.0	Alexa and Rahnenfuhrer, 2021	https://bioconductor.org/packages/topGO/
pheatmap v1.0.12	Kolde, 2012	https://cran.r-project.org/web/packages/pheatmap/index.html
Python (version)	Vanrossum and DeBoer, 1991	https://www.python.org
TPMCalculator	Vera Alvarez et al., 2019	https://github.com/ncbi/TPMCalculator
UpSetR v1.4.0	Conway et al., 2017	https://cran.r-project.org/web/packages/UpSetR/index.html
ViSEAGO v1.6.0	Brionne et al., 2019	https://bioconductor.org/packages/ViSEAGO
RankProd 2.0	Del Carratore et al., 2017	https://www.bioconductor.org/packages/devel/bioc/html/RankProd.html
ggplot2 v3.3.5	Wickham, 2006; Wickham and Wickham, 2007	https://ggplot2.tidyverse.org/
Galaxy	Afgan et al., 2016; Jalili et al., 2020	https://usegalaxy.org.au
Slingshot v1.8	Street at al., 2018	https://bioconductor.riken.jp/packages/3.8/bioc/html/slingshot.html

2.11.1.2 Clustering and cell type annotation

After normalization and variance stabilization, linear dimensionality reduction was performed using principal component analysis (PCA) on the top 2000 highly variable genes (Results Chapter I and II) or all genes if the total number of genes was less than 2000 (Results Chapter IV). Principal components (PCs) were calculated using the 'RunPCA' Seurat function. Each

Table 2.6. Number of single cells passing quality control metrics in each single-cell RNA-sequencing dataset.

First author	GSE #	Disease model	# cells before QC	# cells after QC	# QC myeloid cells
Mendiola et al.	GSE146113	EAE	9,079	6,859	3,297
Hammond et al.	GSE121654	LPC-induced demyelination	5,510	5,408	5,408
Keren-Shaul et al.	GSE98969	5xFAD transgenic mice	10,146	9,636	3,958
Keren-Shaul et al.	GSE98969	$SOD1^{G93A}$ transgenic mice	2,820 (day 80 only)	2,693	1,091
Milich et al.	GSE162610	Spinal cord injury	66,428	54,049	35,518
Somebang et al.	GSE175430	Traumatic brain injury	99,769	90,998	17,097

Acronyms: 5xFAD, 5 familial AD mutations; EAE, experimental autoimmune encephalomyelitis; LPC, lysophosphatidylcholine; QC, quality control.

PC represents a "metagene" that reduces information across a correlated gene set (identified as the top variable genes). PC selection for downstream clustering was defined by elbow plots. The 'elbow' was defined by taking the larger value of the point where the (1) principal components cumulatively contribute to 90% of the standard deviation and (2) percent change in variation between the consecutive PCs is less than 0.1%.

For Results Chapter I and II, UMAP was performed using the first 29 principal components to visualize the pre-processed and normalized scRNA-seq data in two-dimensional space. We used *FindNeighbours*() and *FindClusters*() functions with default parameters to perform graph-based clustering on a shared nearest-neighbour graph. The optimal clustering resolution was determined by selecting the lowest resolution separating distinct clusters by a decision tree. Cell type annotation of clusters was performed using unbiased gene marker analysis. We performed differential expression analysis using the *FindAllMarkers*() function in Seurat with default parameters, which implements a Wilcoxon rank-sum test comparing gene expression of cells within a given cluster versus all other cells. For a given cluster, genes with adjusted $p<0.05$ and log2 fold change (FC)>0.25 were considered as markers for that cluster. Cell type annotation for myeloid cells were made based on expression of microglial- and MC-specific genes. For downstream integration with LIGER and RankProduct analysis, datasets were subsetted so that only myeloid populations ('MC' or 'microglial' clusters) were present in the datasets.

For Results Chapter IV, 13 PCs were used for the initial dataset, which included both microglia and MCs. UMAPs and clustering were performed on the PCA-reduced data using the

RunUMAP, *FindNeighbours* and *FindClusters* at resolutions ranging from 0.25 to 4, which generated 8 to 39 individual clusters. The resolution producing the smallest number of clusters that separated by tree-based clustering (0.75) was chosen. Cell types were defined by (1) sample tag label, e.g., "Ly6C^{hi} monocyte", which denotes the sorted population and (2) expression of cell type-specific and lineage markers. MCs were subsetted from microglia and contaminating T cells, and then re-clustered as described above. For this dataset, 9 PCs and clustered at a resolution of 0.25.

2.11.1.3 Trajectory inference

The R package Slingshot (v1.8) (Street et al., 2018) was used to define computationally imputed pseudotime trajectories in MCs. For this analysis, dpi 7 for the brain and the BM was segregated from the dataset and used for trajectory analysis. A Seurat wrapper was used to integrate the above UMAP into slingshot, considering *Mo3* as a root state when calculating the trajectories and pseudotime. Lineages were determined using the function *getLineages()* using the UMAP dimensions and cluster labels in the annotated dataset (e.g., Mo1-3, MC1-4). Principal curves were determined by using the function getCurves(), with applying thresh = 0.01, stretch = 0.8, allow.breaks = F, and shrink = 0.99. DEGs that change with pseudotime were determined using *startVsEndTest()*. Genes with similar expression patterns were determined by using the function *clusterExpressionPatterns()*.

2.11.1.4 Module scoring

Genes for all functional and metabolic pathways were downloaded from the Mouse Genome Informatics database (Blake et al., 2021). Genes related to pathways associated with each of the metabolic and functional pathways were derived by searching for the key word. For metabolic modules, these included "amino acid metabolism", "ATP biosynthesis", "Citric Acid Cycle", "Electron Transport Chain", "fatty acid oxidation", "fatty acid synthesis", "Glycolysis", and "Pentose Phosphate Pathway". For functional modules, these included "antigen presentation", "response to virus", "acute inflammatory response", "nitric oxide production", "myeloid cell development", "myeloid cell differentiation", "macrophage migration", "proliferation". For all modules except for myeloid cell differentiation, genes associated with the negative regulation of the module of interest was filtered out. This is because negative regulators of cellular differentiation may be important for the specification of cellular fate. Each of the gene sets were then filtered by the genes available in both the LIGER integrated and WNV datasets. Module scores for a particular functional or metabolic

module were derived by running the function *AddModuleScore* in Seurat. For the LIGER integrated dataset (Results Chapter II), 100 control genes and 24 bins (default parameters) were used. For the WNV dataset (Results Chapter IV), 16 control genes and 24 bins were used due to the limited number of genes available in this dataset.

2.11.1.5 Single-cell RNA sequencing integration using LIGER

Aligned, raw single-cell RNA-sequencing datasets were obtained from the gene expression omnibus (GEO) (a list of all datasets used are shown in Supplementary Table 3.1). Datasets from each disease model were downsampled to the limiting cell number (469 microglia from Mendiola et al.) to ensure equal representation of each disease model in the integrated dataset. For Results Chapter I, absolute cell numbers for each disease model prior to downsampling were 685 MCs and 1,960 microglia in LPC-induced demyelination; 3,234 MCs and 1,468 microglia in EAE; 182 MCs and 3,620 microglia in 5xFAD; and 72 MCs and 1,136 microglia in $SOD1^{G93A}$, 14,243 MCs and 17,739 microglia in SCI; and 612 MCs and 8,434 microglia in TBI. Microglia from each of the six disease models were downsampled to 469 cells (2,814 microglia total) and 469 MCs were selected from EAE, TBI, SCI (1,407 MC total), since MCs were negatively 'sorted' from the myeloid population in 5xFAD, $SOD1^{G93A}$, and LPC-induced demyelination disease models. For Results Chapter II, datasets from each disease model were downsampled to the limiting cell number of 612 prior to integration. The absolute cell numbers for each disease model before downsampling were 3498 MCs in WNV, 3234 MCs in EAE and 612 MCs in TBI. From EAE, TBI, SCI, and WNV, a total of 2,448 MCs were selected.

The R package rliger v0.5.0 (Welch et al., 2019) was employed to align and integrate the pre-processed and subsetted MCs from scRNA-seq datasets, with only samples from disease conditions included in the analysis. The integration of data was carried out following a protocol described previously by the Welch Lab (Liu et al., 2020). Briefly, the normalization, variable gene selection, and scaling of individual genes were performed with default parameters on the combined dataset. The function suggestK (num.cors = 4, lambda = 5) was used to determine the optimal number of factors (k), and suggestLambda was used to determine the optimal regularization parameter, λ. Integrative non-negative matrix factorization was performed on the normalized and scaled dataset using optimal parameters $k = 12$ and $\lambda = 5$ to define dataset-specific and shared metagenes (i.e., factors) that correspond to genes defining particular cell types and subsets. The resulting factors were utilized to jointly cluster cells and perform quantile normalization by dataset, factor, and cluster using the LIGER function

quantile_norm(). The LIGER-integrated dataset was converted to a Seurat object for downstream visualization and differential expression analysis. The integrated scRNA-seq data plots were constructed using Seurat (v4.0.1) or rliger (v0.5.0).

2.11.2 Analysis of Bulk RNA Sequencing Data

2.11.2.1 Bulk RNA dataset pre-processing and normalisation

FASTQ files were downloaded from the GEO (Barrett et al., 2013) and loaded into the online Galaxy platform (Afgan et al., 2016, Jalili et al., 2020). Cutadapt (v 1.16.6) (Martin, 2011) was used to trim known adaptor and primer sequences from raw reads and filter low quality (minimum quality cutoff=20) and short reads (minimum length=20 bp after trimming). All reads passed quality control checks using FastQC (v0.72+galaxy1) (Andrews, 2010). Trimmed and filtered reads were then aligned to the built-in mm10 reference genome using HISAT2 (v2.1.0+galaxy7) (Kim et al., 2015). FeatureCounts was used to generate counts from HISAT2 output files using the built-in mm10 gene annotation file (v2.0.1) (Liao et al., 2014) and known genes were annotated with AnnotateMyIDs (v3.12.0). Transcripts per million mapped reads (TPM) values were calculated using TPMCalculator (Vera Alvarez et al., 2019) in Python (Vanrossum and DeBoer, 1991). The same pre-processing, alignment and normalisation pipeline was used for each bulk RNA-sequencing study.

2.11.2.2 Nanostring data pre-processing and normalisation

Nanostring data was acquired from Kraseman et al. (2017) already pre-processed and normalised using nSolver™ software. Data was not re-analysed from raw files since it was uniformly processed by a single study.

2.11.3 Differential expression testing and GO analysis

Identification of differentially expressed genes (DEGs) and gene ontology (GO) enrichment analysis was performed on myeloid clusters identified in the LIGER-integrated dataset. To identify marker genes for each cluster, the *FindAllMarkers*() function implemented in the Seurat v4.0.1 package was implemented with default parameters. DEGs for myeloid clusters were calculated using the Seurat function *FindAllMarkers*() using, and defined as positively enriched, genes with an adjusted $p<0.01$ and $log2FC > 0.25$ (Wilcox sum rank test), which represents genes enriched in the cluster versus all other clusters.

Functional GO enrichment analysis from DEGs of each population (by cluster or by bulk cell population for each disease model) was performed using the VISEAGO (v1.4.0) and topGO (v2.42.0) packages in R. GO biological process term enrichment was performed using the VISEAGO *create_topGOdata*() relative to the background gene expression, which was defined as the full list of genes expressed in the LIGER-integrated dataset. Enrichment tests were performed with Fisher's exact test using both the "classic" and "elim" algorithms. Enriched GO terms were defined as terms with a minimum of ten genes mapping to a term and an adjusted p-value less than 0.01. For visualization of GO terms, GO terms for each population were combined into a single matrix using the ViSEAGO function *build_GO_SS*() (Brionne et al., 2019) and annotated using the Bioconductor *org.Mm.eg.db* database package for the mouse species (Carlson, 2019). UpSet visualization was performed on the significantly enriched GO term matrices using the UpSetR package (v1.4.0) (Conway et al., 2017), and the significance of intersections was calculated using the SuperExactTest (v1.0.7) R package, which reports one-tailed *P* values (Wang et al., 2015).

2.11.4 Using a Rank product statistic to generate gene ranks

To compare datasets from different origins and sequencing platforms, we applied a Rank product (RP) statistic to genes common to all studies (319 genes). To increase our gene list (7804 genes) we excluded the dataset with the limiting number of genes (Krasemann et al., 2017) and reapplied the same RP analysis. A RP is a non-parametric statistical test that ranks gene by their fold-change values, adjusted p-value and percentage of false discovery (Del Carratore et al., 2017, Hong et al., 2006). The RP output consists of two tables: genes ranked in order of upregulation and genes ranked in order of downregulation. Genes more likely to be up- or down-regulated in each table have a lower RP value and thus are more highly ranked. A RP was applied to normalised expression values using a two-class setting (*i.e.*, control vs disease) and a single (samples originating from one study) function. Only studies with a minimum of two replicates per condition could be included in this analysis, necessitating the exclusion of DePaula Silva et al., 2019 (Supplementary Table 3.1).

2.11.5 2D visualisation of gene ranks

Data from the single-origin RP analysis on the common gene list A (319 genes) were used for hierarchical clustering and heatmap visualization, bubble plots and UMAPs. Clustered heatmaps were generated in R Studio using the pheatmap package (v1.0.12) (Kolde, 2012). Rows and/or columns were clustered on for hierarchical clustering using the complete

parameter for clustering_method() and euclidean parameter for clustering_distance(). Bubble plots were made using the ggplots2 package (v3.3.3) in R studio (Wickham, 2006, Wickham and Wickham, 2007). The R package, Spectre (Ashhurst et al., 2021), was used to perform dimensionality reduction by UMAP on data clustered by k-means clustering with FlowSOM (xdim=5; ydim=5; meta.k=auto) on the common gene list.

2.11.6 GO analysis and UpSet visualization of gene ranks

Functional gene ontology (GO) enrichment analysis was performed on differentially expressed, upregulated genes ($log_2FC>1$, $pval<0.05$). The enriched biological process results were obtained using a Fisher's exact test with elim algorithm developed in the topGO package. Significantly enriched GO terms were defined as terms with a minimum of five significantly enriched upregulated genes mapping to a term and an enrichment $p<0.05$ relative to the gene background (all expressed genes in the population). For GO analysis in Results Chapter I, GO terms for each population were combined into a single matrix using the ViSEAGO function *build_GO_SS*() (Brionne et al., 2019) and annotated using the Bioconductor *org.Mm.eg.db* database package for the mouse species (Carlson, 2019). UpSet visualization was performed on the significantly enriched GO term matrices using the UpSetR package (Conway et al., 2017).

2.11.7 Identification of differentially enriched genes

To define cell type-enriched markers, only studies that processed RNA from MCs and microglia in the same disease state were included in our analysis. These included (1) Locatelli et al., (2018), (2) Mendiola et al., (2020), (3) Werner et al., (2020), (4) Milich et al, (2021), (5) Somebang et al, (2021) and (6) DePaula-Silva et al., (2019). For all bulk RNA-seq datasets, differential expression analysis comparing MCs to microglia was performed in DESeq2 on the online Galaxy platform from HISAT2 outputs (v2.11.40.6+galaxy1) (Love et al., 2014). For the scRNA-seq dataset, fold-change values from RP outputs were used, since scRNA-seq data was incompatible with DESeq2 in the online Galaxy platform. DEGs common to all studies were identified and filtered for genes with a $log_2FC>1$ and $p<0.05$. Membrane-expressed DEGs were identified by annotating gene names in Uniprot (UniProt, 2021). Total enriched genes were filtered for 1) the term *cell membrane* in the Uniprot category *subcellular location* and 2) the terms *integral component of plasma membrane* or *cell surface* in the Uniprot category *Gene ontology*. The expression of identified DEGs by microglia and MCs was confirmed at the single-cell level in the LIGER-integrated scRNA-seq dataset.

2.12 Identification and selection of eligible gene expression datasets for meta-analysis

Gene expression studies of acutely isolated microglia and MCs from adult mouse brains or spinal cords in various disease conditions were considered for our analysis. We systematically mined PubMed database for microarray, bulk RNA-seq, and scRNA-seq expression profiling. In addition, publicly availably transcriptomic datasets were searched in the NCBI GEO database (http://www.ncbi.nlm.nih.gov/geo/). The following search terms were used: “neuropath*"[Title/Abstract], “neuroinflammation"[Title/Abstract], “neuroinflammatory diseases"[Title/Abstract], “cns pathology"[Title/Abstract], “spinal cord injury"[Title/Abstract], “stroke"[Title/Abstract], “viral encephalitis"[Title/Abstract],“multiple sclerosis"[Title/Abstract], “encephalitis"[Title/Abstract],“Alzheimer’s disease"[Title/Abstract], “Parkinson’s disease"[Title/Abstract],“amyotrophic lateral sclerosis"[Title/Abstract],“motor neuron disease"[Title/Abstract], “neurodegeneration"[Title/Abstract], “neurodegenerative disease"[Title/Abstract], "macrophage"[Title/Abstract],"myeloid"[Title/Abstract],"monocyte-derived"[Title/Abstract], "monocyte "[Title/Abstract],“microglia”[Title/Abstract], "single cell rna seq"[Title/Abstract] ,"single cell rna sequencing"[Title/Abstract] ,"scRNA-seq"[Title/Abstract] "single cell transcriptom*"[Title/Abstract]),“RNA seq"[Title/Abstract],“RNA sequencing"[Title/Abstract] , “Bulk transcriptom*"[Title/Abstract],“Gene Expression Profiling” [Title/Abstract] ,“Transcriptome”[Title/Abstract], "gene expression"[Title/Abstract]. References of identified articles were additionally searched. Studies were eligible for inclusion if: (1) raw data was accessible on a public data repository, (2) data was acquired by nanostring, bulk or single-cell RNA-sequencing technologies; and (3) data included either microglia in disease and control conditions or both microglia and MCs in disease conditions. Exclusion criteria for all eligible studies included (1) additional comorbidities (*e.g*., diabetes, obesity, etc.); (2) adoptively transferred microglia or monocytes; (3) gene knock-out or mutant models, but not excluding transgenic mice *e.g.,* APP/PS1, 5xFAD, $SOD1^{G93A}$; (4) transcriptomes from pharmacologically-treated mice, unless data from non-treated disease and homeostatic controls were available; (5) single-cell RNA-sequencing data included a minimum of 600 single cells passing quality-control metrics (see *single-cell RNA-sequencing analysis, pre-processing and normalisation*). Lists of excluded studies and reasons for exclusion, along with all study metadata characteristics for included studies (including time points at which mice were sacrificed, sorting methods and other possible

confounding variables) are provided in Supplementary Table 3.1. Excluded data included 19 samples from Keren-Shaul et al., 2017 (see Supplementary Table 3.1 for sample details and reasons for exclusion of each sample). Ten transcriptomic datasets from eight separate studies were integrated to identify conserved and disease-specific transcriptional signatures and/or for differential expression analysis (see Supplementary Table 3.1). The following information was extracted from each identified study: GEO expression number, cell type, disease model, mouse strain, mouse age (weeks), mouse sex, sequencing method, sequencing platform, layout (single vs. paired), scRNA-seq protocol, library size, cell sorting strategy, anatomical region, and tissue processing (Supplementary Table 3.1). We additionally determined the FAST QC results for bulk RNA-seq datasets and the median percent mitochondrial gene expression, median number of unique genes per cell, and total number of molecules per cell for all included scRNA-seq data. For Results Chapter II, we applied the same criteria as above, but we limited studies to those including MCs and that used single-cell RNA-sequencing only, which gave three disease models: EAE (Mendiola et al, GSE146113), SCI (Milich et al., GSE162610), and TBI (Somebang et al., GSE175430).

2.13 Data handling and statistical analyses

A standardized statistical approach was applied to all datasets except those in Section 2.11 ("Analysis of Transcriptomic data"), which required specific bioinformatics methods detailed therein. Prior to analysis, outliers were identified using the ROUT method (Robust regression and Outlier removal). For each analysis, normality was tested using the Shapiro-Wilk test. Where data followed a normal distribution, parametric tests were used (unpaired t-test for two groups or one-way ANOVA for multiple groups). Where the normality assumption was violated, non-parametric alternatives were employed (Mann-Whitney U test for two groups or Kruskal-Wallis test for multiple groups). For experimental designs where samples were matched or paired (e.g., cells from the same mouse subjected to different treatment conditions), paired t-tests (two conditions) or repeated measures one-way ANOVA (multiple conditions) were used. This approach ensures appropriate statistical testing based on both the distribution and experimental design of each dataset.

Chapter 3: Results I

3.1 Integrating transcriptomic datasets across neurological disease identifies unique subpopulations driving disease-specific signatures

The following chapter is presented as the following manuscript:

Wishart, C.L.*, Spiteri, A.G.*, Locatelli, G. & King, N.J.C., Integrating transcriptomic datasets across neurological disease identifies unique myeloid subpopulations driving disease-specific signatures. *Glia* 71, 4 (2023).

3.1.1 Overview

Microglia and BM-derived monocytes are key elements of CNS inflammation, both capable of enhancing and dampening immune-mediated pathology. However, the study-specific focus on individual cell types, disease models or experimental approaches has limited our ability to infer common and disease-specific responses. This meta-analysis integrates bulk and single-cell transcriptomic datasets of microglia and monocytes from disease models of autoimmunity, neurodegeneration, sterile injury, and infection to build a comprehensive resource connecting myeloid responses across CNS disease. We demonstrate that the bulk microglial and monocyte program is highly contingent on the disease environment, challenging the notion of a universal microglial disease signature. Integration of six scRNA-seq datasets revealed that these disease-specific signatures are likely driven by differing proportions of unique myeloid subpopulations that were individually expanded in different disease settings. These subsets were functionally-defined as a neurodegeneration-associated, inflammatory, interferon-responsive, phagocytic, antigen-presenting, and lipopolysaccharide-responsive cellular state, revealing a core set of myeloid responses at the single-cell level that are conserved across CNS pathology.

Showcasing the predictive and practical value of this resource, we performed differential expression analysis on microglia and monocytes across disease and identified *Cd81* as a new neuroinflammatory-stable gene that accurately identified microglia and distinguished them from MCs across all experimental models at both the bulk and single-cell level. Together, this resource dissects the influence of disease environment on shared immune response programmes to build a unified perspective of myeloid behaviour across CNS pathology.

3.1.2 Introduction

Inflammation is a hallmark of many neuropathologies, irrespective of disease etiology (Spiteri et al., 2022b). Microglial activation and the infiltration of BM-derived monocytes into the CNS are key elements of this inflammatory response, with both cell types capable of promoting tissue healing and repair, as well as disease pathogenesis and cell damage. However, despite the pervasive representation of these two cell types in CNS disease (McQuade and Blurton-Jones, 2019, Marioni et al., 2018, Zhang et al., 2014), the interplay between resident microglia and recruited MCs, and the precise contribution to pathology of each cell remain poorly resolved.

Microglia and MCs are ontogenetically distinct cell types. Microglia are CNS-resident tissue macrophages arising from uncommitted KIT^+ erythromyeloid precursors (Kierdorf et al., 2013) that seed the CNS from the yolk sac during embryogenesis (Ginhoux et al., 2010). These CNS-resident cells self-renew *in situ*, independently of BM-derived HSC (Ajami et al., 2007). By contrast, monocytes are derived from the fetal liver during embryogenesis and are continuously renewed throughout postnatal life from HSCs in the adult BM (Geissmann et al., 2010).

Despite microglia and MCs arising from precursors with distinct developmental trajectories, these cells often adopt similar phenotypes and morphologies during neuroinflammation, confounding definitive discrimination between them. Recent advances in scRNA-seq technologies have shed light on some uniquely-expressed microglial genes, including Fc receptor-like S (*Fcrls*), *P2ry12* (Butovsky et al., 2014), *Sall1* (Buttgereit et al., 2016), sialic acid-binding immunoglobulin-type lectin H (*Siglech*) and transmembrane protein 119 (*Tmem119*) (Bennett et al., 2016). This has substantially aided the identification and resolution of these myeloid populations. During inflammation, however, many of these homeostatic markers are downregulated in microglia (Jordão et al., 2019, Masuda et al., 2019, Krasemann et al., 2017, Friedman et al., 2018, Vankriekelsvenne et al., 2022) or upregulated by MCs

(Werner et al., 2020, Chen et al., 2020, Spiteri et al., 2021a), making their transcriptomic and phenotypic profiles highly overlapping, highlighting the need for a more comprehensive insight into the biological processes defining distinct myeloid cells during homeostasis and across pathologies.

Along these lines, in the last few years transcriptomic sequencing uncovered a possible universal 'disease-associated microglia' (DAM) (Keren-Shaul et al., 2017) or 'microglial neurodegenerative' (MGnD) (Krasemann et al., 2017) signature that is argued to be conserved across neurodegeneration (Tay et al., 2018), demyelinating disease (Poliani et al., 2015) and aging (Holtman et al., 2015). These universal DAM/MGnD signatures characteristically have downregulated homeostatic genes, including *P2ry12*, *Tmem119* and *Cx3cr1*, and upregulated inflammatory program genes, including *Trem2*, *Apoe*, *Axl*, *Lpl*, *Itgax* and *Clec7a* (Keren-Shaul et al., 2017, Krasemann et al., 2017).

In contrast, more recent findings suggest microglia develop heterogenous signatures highly specific to a disease state that may individually drive immune-mediated pathology or promote tissue repair, rather than adopting a universal disease signature (Friedman et al., 2018, Sobue et al., 2021, Olah et al., 2020, Sousa et al., 2018, Yang et al., 2021, Sanin et al., 2022). However, these studies have focused on individual cell types in specific diseases, using disparate experimental approaches and sequencing platforms, which considerably limits our ability to convincingly compare the identified myeloid signatures and their associated functions more widely across CNS pathologies. Connecting these disease-associated signatures across different studies is an essential unmet need of current research on neuroinflammation and would allow us to uncover intrinsic myeloid response programs to CNS perturbation, that could realistically inform the development of novel therapeutic and diagnostic tools.

To address this issue, we present a detailed meta-analysis integrating the transcriptomes of resident and CNS-infiltrating myeloid cells from demyelinating, ischemic, neurodegenerative, traumatic injury, and infectious conditions. Using high-parameter data integration and visualization techniques, including clustering algorithms and dimensionality reduction techniques, we compared these unique profiles to understand the relationship between disease models and cell types. Specifically, we demonstrate that microglia and monocyte transcriptomes are highly divergent across pathologies, emphasising the importance of individual disease environments in shaping myeloid immune responses. We suggest that these specialised disease-specific signatures shown in bulk populations are driven by the differential

proportional expansion of unique subpopulations, identified by scRNA-seq integration, in different disease contexts. Further, differential expression analysis between microglia and monocytes across pathologies enabled the identification of the tetraspanin gene, *Cd81,* as a microglia-enriched transcript that reliably discriminates between microglia and infiltrating monocytes across all examined CNS disease models, thereby showcasing the predictive and practical value of this resource.

3.1.3 Results

3.1.3.1 Integrating studies across CNS disease with gene rank analysis

To determine how microglial and MC responses converge or diverge across different pathological settings, we performed an integrative meta-analysis on eight published studies from independent laboratories describing different disease models and/or different experimental approaches. In our analysis, we included transcriptomic datasets from murine models of acute inflammation and chronic neurodegeneration, including photothrombosis (PT)-induced focal ischemia (Werner et al., 2020), SCI (Milich et al., 2021) and TBI (Somebang et al., 2021) models of sterile injury, EAE (Krasemann et al., 2017, Locatelli et al., 2018, Mendiola et al., 2020) and LPC-induced demyelination (Hammond et al., 2019) models of MS, 5xFAD (Keren-Shaul et al., 2017) and APP/PS1 (Krasemann et al., 2017) transgenic models of Alzheimer's disease, and the $SOD1^{G93A}$ model of amyotrophic lateral sclerosis (Krasemann et al., 2017, Keren-Shaul et al., 2017) (Figure 3.1A, B and Supplementary Table 3.1). This data was obtained from three different sequencing platforms, including nanostring, scRNA-seq or bulk RNA-sequencing technologies (Figure 3.1B).

Direct comparison of gene expression or fold-change data acquired from different sequencing technologies, laboratories and disease models is highly challenging, as global normalisation often fails to overcome lab-specific batch effects. To surmount this, we integrated datasets from multiple origins using a rank product approach on genes common to all studies (Figure 3.1C). This method employs a simple non-parametric test to generate a single-origin RP statistic, which ranks genes in order of upregulation and downregulation for each study using fold-change, adjusted p-value and percentage of false predictions (Del Carratore et al., 2017, Hong et al., 2006). Thus, a comparison of gene ranks or RP values across different studies enables a reliable determination of which genes are likely to be regulated across different CNS disease models.

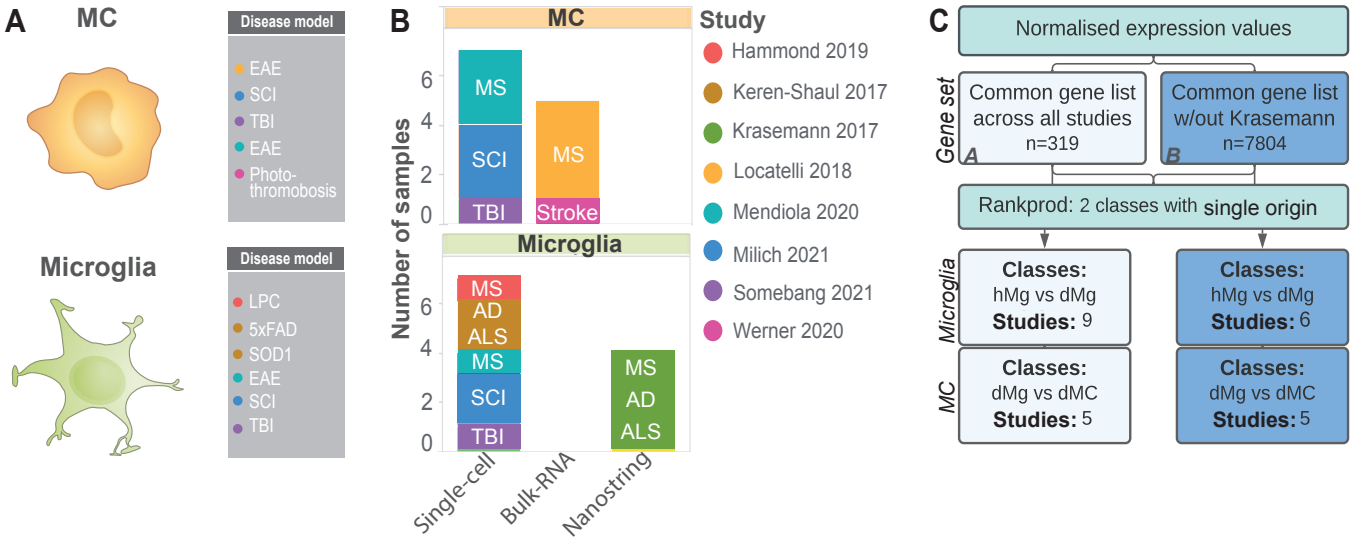
A
MC
Disease model
EAE
SCI
TBI
EAE
Photo-thromobosis
Microglia
Disease model
LPC
5xFAD
SOD1
EAE
SCI
TBI
B
MC
Microglia
Number of samples
0
2
4
6
MS
SCI
TBI
MS
Stroke
MS
AD
ALS
MS
SCI
TBI
MS
AD
ALS
Single-cell
Bulk-RNA
Nanostring
Study
Hammond 2019
Keren-Shaul 2017
Krasemann 2017
Locatelli 2018
Mendiola 2020
Milich 2021
Somebang 2021
Werner 2020
C
Normalised expression values
Gene set
Common gene list across all studies n=319
A
Common gene list w/out Krasemann n=7804
B
Rankprod: 2 classes with single origin
Microglia
Classes: hMg vs dMg
Studies: 9
Classes: hMg vs dMg
Studies: 6
MC
Classes: dMg vs dMC
Studies: 5
Classes: dMg vs dMC
Studies: 5

Figure 3.1 Integrating studies across CNS disease with gene rank analysis.

(**A-B**) Summary of datasets used in the single origin rank product (RP) analysis including cell type, disease and disease model, number of samples, study origin and sequencing modality used. (**C**) Flow chart of analysis pipeline. Single origin RP analysis was performed on normalised expression values on a common gene list from eight datasets (n=319 genes, Common Gene set A) or seven datasets (n=7804 genes, Common Gene set B), including or excluding Krasemann et al., 2017, respectively. Microglia fold-change calculations were made between microglia from disease (dMg) and control conditions (hMg). MC fold-change calculations were made between MCs from disease conditions (dMC) and microglia from disease conditions (dMg).

We performed a single-origin RP analysis on transcriptomic data sequenced from both microglia and MCs (Figure 3.1A-C). Within each study, fold-change calculations were made between microglia from disease (dMg) and control conditions (hMg) (Figure 3.1C). However, the absence of peripherally-derived MCs in control brains meant this control was unavailable for MCs in these studies. Therefore, fold-change calculations were instead made between MCs from disease conditions (dMC) and microglia from disease conditions (dMg) (Figure 3.1C). While disease-related microglia are a suboptimal control for disease-related MCs, such comparisons are used to assess MC gene expression in the brain in most studies, as more suitable controls (*i.e.*, blood or BM-derived monocytes) are rarely included in published work. However, this decision illustrates the intrinsic challenges underlying a comprehensive meta-analysis of published data. Thus, while this approach aligns with previously published work (DePaula-Silva et al., 2019, Yamasaki et al., 2014, Schlachetzki et al., 2018), accurately understanding MC biology will require consensus MC controls to be included by future investigators.

Integrating datasets by genes common to all eight studies narrowed our gene list to 319 genes (*Common Gene set A*). This limited number of genetic candidates was dictated by the small dataset published by Krasemann et al., 2017. Thus, to broaden the scope of our analysis, we performed a parallel analysis where we excluded the smallest dataset (Krasemann et al., 2017, n = 411 genes), thereby increasing our gene list 24-fold (n=7804 genes) (*Common Gene set B*), but reducing the number of studies to 7 (Figure 3.1C).

3.1.3.2 Cell type-specific programs are dependent on disease-specific perturbation for microglia and MCs

To compare the disease signature of microglia and MCs to the nominal universal microglial signature, as defined in Krasemann *et al.,* 2017 we first used the *Common Gene set A* (n=319 genes). Strikingly, we observed few similarities between disease-specific signatures. This is shown by the minimal overlap in the top 10 highest and lowest ranked genes and the trajectory of gene ranking, as visualised by the plateau phases and slopes of the bubble plots (Figure 3.2A). Notably, no commonly upregulated genes were identified across diseases between either microglia or MC populations. This suggests that microglia and MCs adopt separate, highly specific responses to unique disease settings, with minimal overlap across pathologies that is distinct from the universal microglial signature identified in Krasemann *et al.,* 2017.

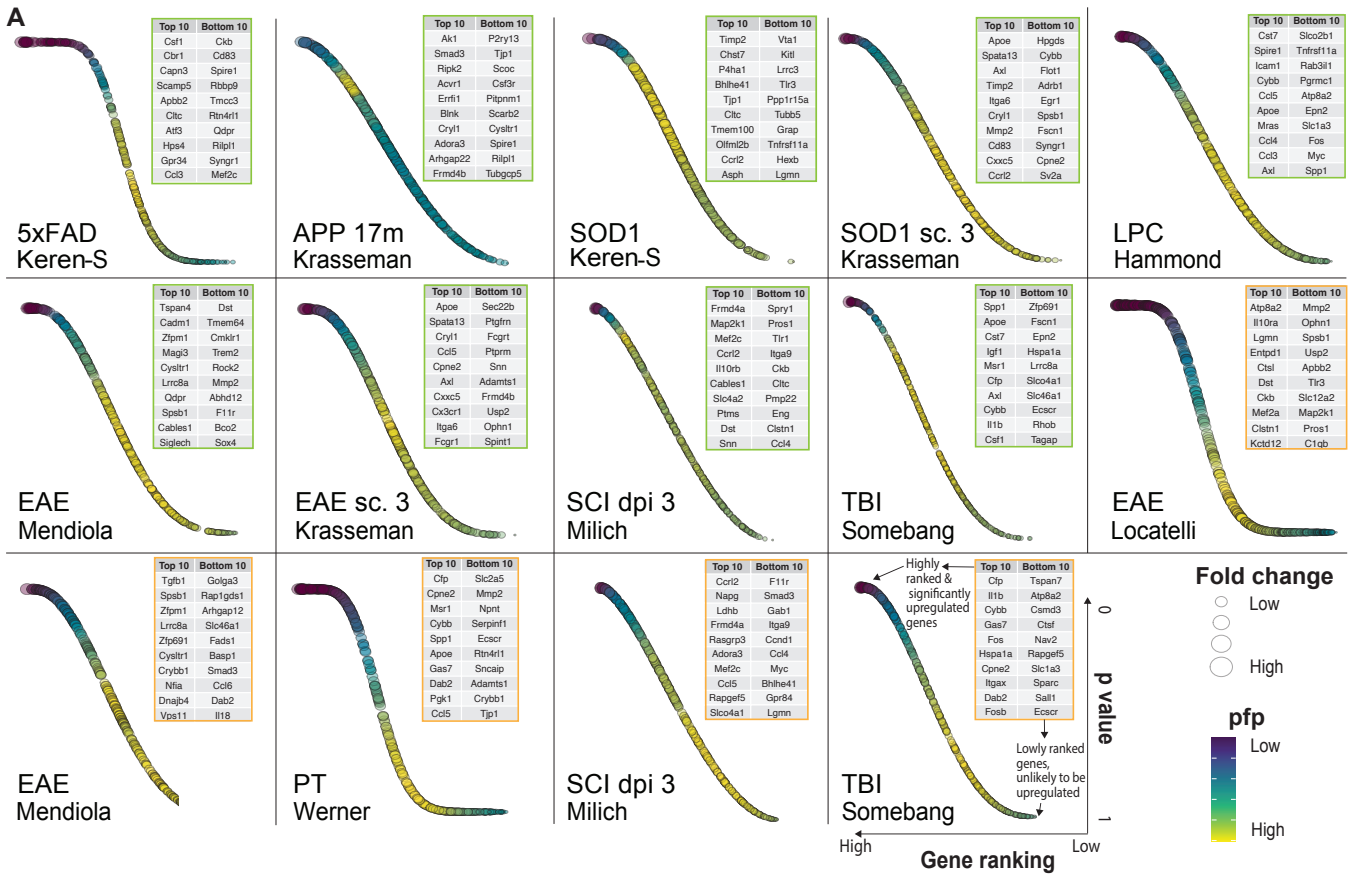
A
5xFAD Keren-S
APP 17m Krasseman
SOD1 Keren-S
SOD1 sc. 3 Krasseman
LPC Hammond
EAE Mendiola
EAE sc. 3 Krasseman
SCI dpi 3 Milich
TBI Somebang
EAE Locatelli
EAE Mendiola
PT Werner
SCI dpi 3 Milich
TBI Somebang
Highly ranked & significantly upregulated genes
Lowly ranked genes, unlikely to be upregulated
p value
0
1
High
Low
Gene ranking
Fold change
Low
High
pfp
Low
High

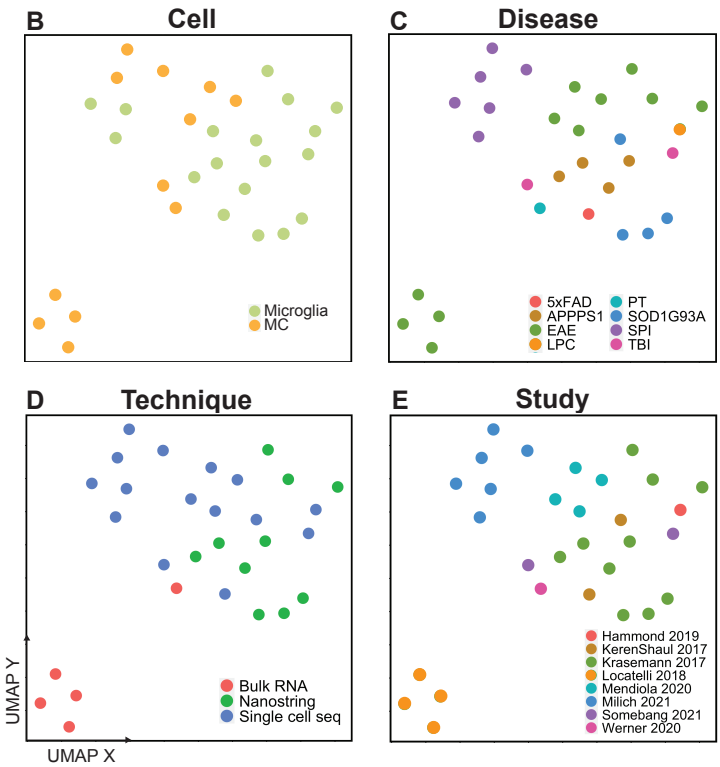
B
Cell
Microglia
MC
C
Disease
5xFAD
APPPS1
EAE
LPC
PT
SOD1G93A
SPI
TBI
D
Technique
Bulk RNA
Nanostring
Single cell seq
UMAP Y
UMAP X
E
Study
Hammond 2019
KerenShaul 2017
Krasemann 2017
Locatelli 2018
Mendiola 2020
Milich 2021
Somebang 2021
Werner 2020

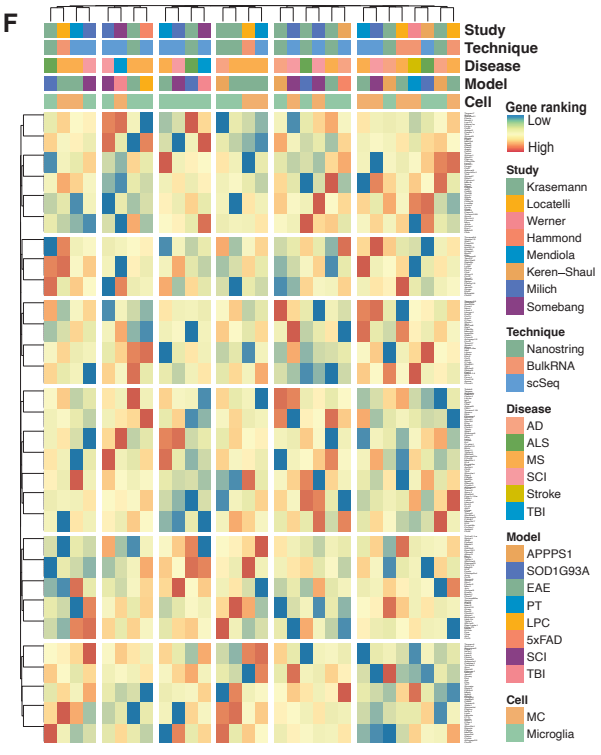
F
Study
Technique
Disease
Model
Cell
Gene ranking
Low
High
Study
Krasemann
Locatelli
Werner
Hammond
Mendiola
Keren–Shaul
Milich
Somebang
Technique
Nanostring
BulkRNA
scSeq
Disease
AD
ALS
MS
SCI
Stroke
TBI
Model
APPPS1
SOD1G93A
EAE
PT
LPC
5xFAD
SCI
TBI
Cell
MC
Microglia

Figure 3.2 Clustering analysis connects the transcriptomic responses adopted by microglia and MCs in disease.

(**A**) Bubble plots showing gene ranking using Common Gene set A by order of upregulation (x-axis) with associated p-values (y-axis), fold-change (bubble size) and percentage of false predictions (pfp) values (bubble color) for selected MC (the cell type indicated by orange boxes) and microglia (indicated by green boxes) populations. The top- and bottom-ranked genes are listed in these boxes, placed at the top right of each plot, for MC (orange boxes) and microglia (green boxes). (**B**-**E**) UMAP plots of 18 microglia and 12 MCs samples pseudocolored by cell type (**B**), disease (**C**), sequencing technology (**D**) or study (**E**). UMAPs were run on gene rank values for the 319 genes of Common Gene set A. See also Table S2 for a list of populations used with their study and disease origins. (**F**) Heatmap showing gene rank values for the 319 genes of Common Gene set A in order of upregulation for MC and microglial populations. Clustering was performed on both rows (genes) and columns (populations). See also Table S2 for a list of populations used with their study and disease origins in order of the clustering arrangement shown in the heatmap.

Next, to confirm these disease-specific responses we coupled our gene rank analysis with an unbiased approach using unsupervised dimensionality reduction, *k*-means clustering and hierarchical clustering (Figure 3.2B-F). Importantly, clustering analysis of individual myeloid populations showed intermixing of different studies and sequencing platforms, suggesting little or no bias specific either to sequencing technology or laboratory in this analysis (Figure 3.2D, 3.2E, 3.2F and Supplementary Table 3.1). Notably, MC and microglial populations did not cluster by cell type or by disease model (Figure 3.2B, C, F), supporting the notion that myeloid populations adopt unique profiles.

We confirmed disease-specific signatures in *Common Gene set B* (n=7804 genes) (Supplementary Table 3.3), demonstrating that these differences are not specific to the smaller dataset. We then assessed functional similarities between these unique transcriptional profiles by GO enrichment analysis on the upregulated genes (log_2 FC >1, p-value <0.05) from the larger gene set (*Common Gene set B*, n=7804 genes) and evaluated overlap in GO terms between diseases using an UpSet plot (Figure 3.3). We observed no significant overlapping biological functions between any two microglia populations in any diseases. Significant overlap in these functions, however existed between microglia and MCs in TBI, and between MCs in both TBI and stroke (Figure 3.3, red intersections and Supplementary Table 3.3). This emphasizes that the transcriptional profiles of microglia and MCs are contingent upon the disease environment, but may converge in a disease-dependent manner. Overall, however, the limited set of significant intersecting lines between populations indicate more uniquely-enriched than shared functions across diseases (Figure 3.3).

3.1.3.3 Integration of scRNA-seq data connects myeloid signatures across disease

We next wanted to evaluate whether these disease-specific signatures were reflected at the single cell level. We therefore used LIGER (Welch et al., 2019, Liu et al., 2020) to integrate myeloid populations from six scRNA-seq datasets investigating LPC-induced demyelination (Hammond et al., 2019), EAE (Mendiola et al., 2020), 5xFAD, $SOD1^{G93A}$ (Keren-Shaul et al., 2017), TBI (Somebang et al., 2021) and SCI (Milich et al., 2021) (Figure 3.4A). This approach enabled us to (1) assess gene expression data independent of gene ranking, (2) assess MCs independently of their comparison to disease-related microglia, and (3) examine microglia and MC subpopulations that may be unique to, or conserved across, multiple disease states, which may be missed at the bulk population level. Prior to data integration, all scRNA-seq studies underwent the same pre-processing, normalisation, and clustering workflow. Microglia and

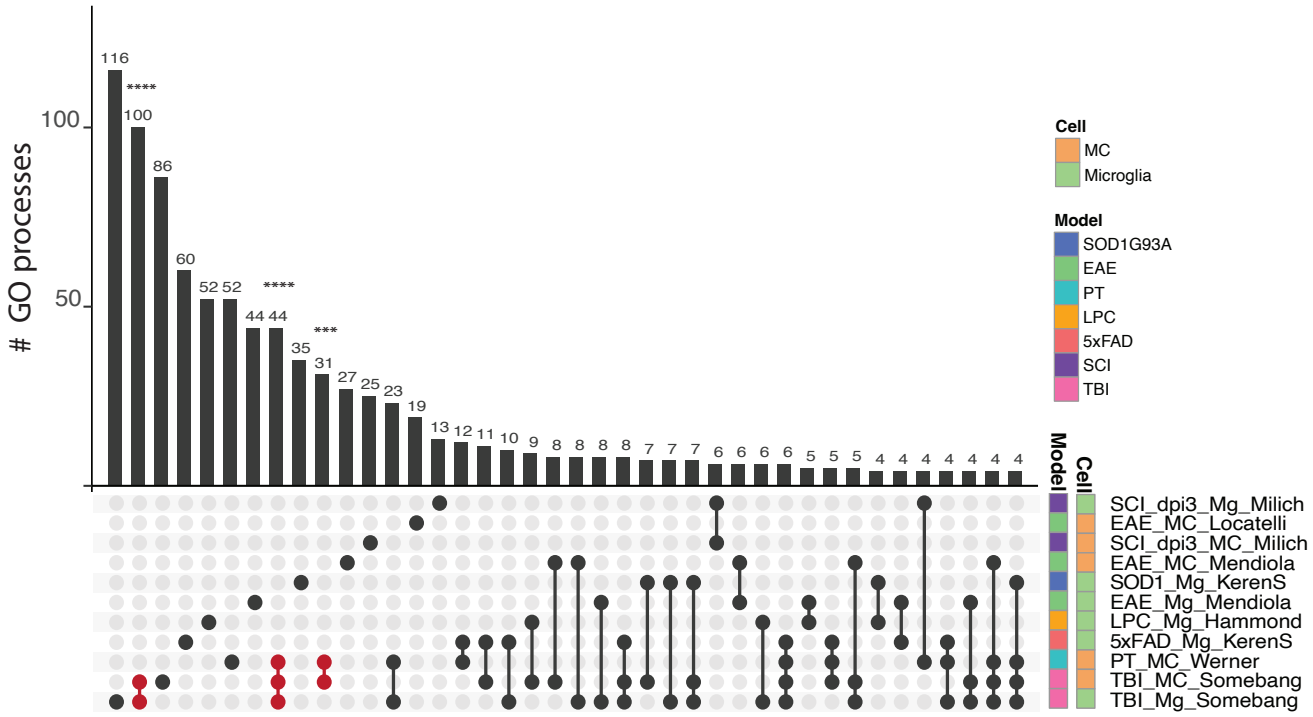
GO processes
100
50
116
****
100
86
60
52 52
****
44 44
***
35
31
27
25
23
19
13
12
11
10
9
8 8 8 8
7 7 7
6 6 6 6
5 5 5
4 4 4 4 4 4
Cell
MC
Microglia
Model
SOD1G93A
EAE
PT
LPC
5xFAD
SCI
TBI
Model
Cell
SCI_dpi3_Mg_Milich
EAE_MC_Locatelli
SCI_dpi3_MC_Milich
EAE_MC_Mendiola
SOD1_Mg_KerenS
EAE_Mg_Mendiola
LPC_Mg_Hammond
5xFAD_Mg_KerenS
PT_MC_Werner
TBI_MC_Somebang
TBI_Mg_Somebang

Figure 3.3 Cell type-specific programs are dependent on disease-specific perturbation.

UpSet plot showing shared and unique GO biological processes associated with genes significantly upregulated ($p<0.05$, $\log_2FC>1$) by microglial and MC populations out of the 7804 genes of the Common Gene set B. Populations are colored by cell type and disease-model membership and arranged in order of increasing to decreasing number of biological processes associated with each population. The number of shared or unique GO biological processes ($p<0.05$) are shown by the bar graph and the corresponding population(s) are indicated by the dot plot panel below. Lines connecting populations indicate shared GO processes.

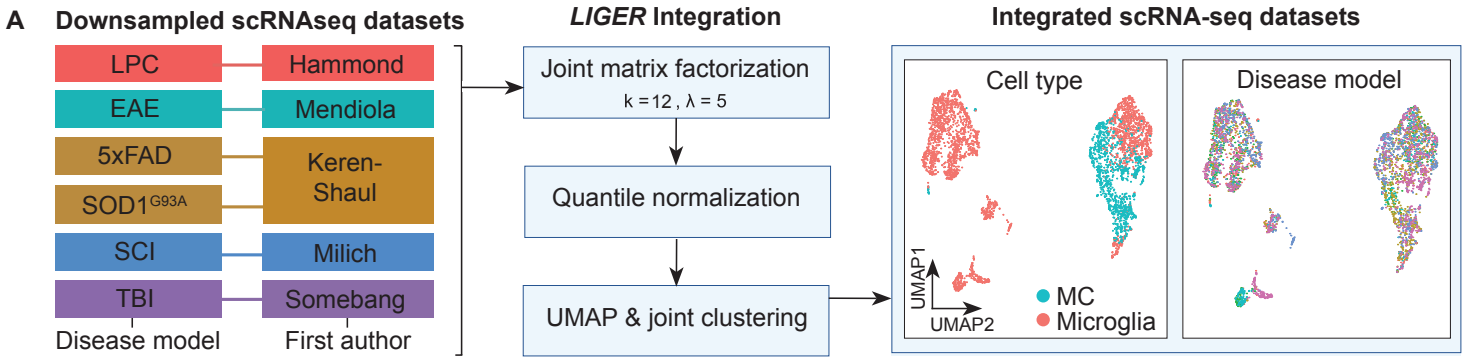
A
Downsampled scRNAseq datasets
LPC
EAE
5xFAD
SOD1G93A
SCI
TBI
Hammond
Mendiola
Keren-Shaul
Milich
Somebang
Disease model
First author
LIGER Integration
Joint matrix factorization
k = 12 , λ = 5
Quantile normalization
UMAP & joint clustering
Integrated scRNA-seq datasets
Cell type
Disease model
UMAP1
UMAP2
MC
Microglia

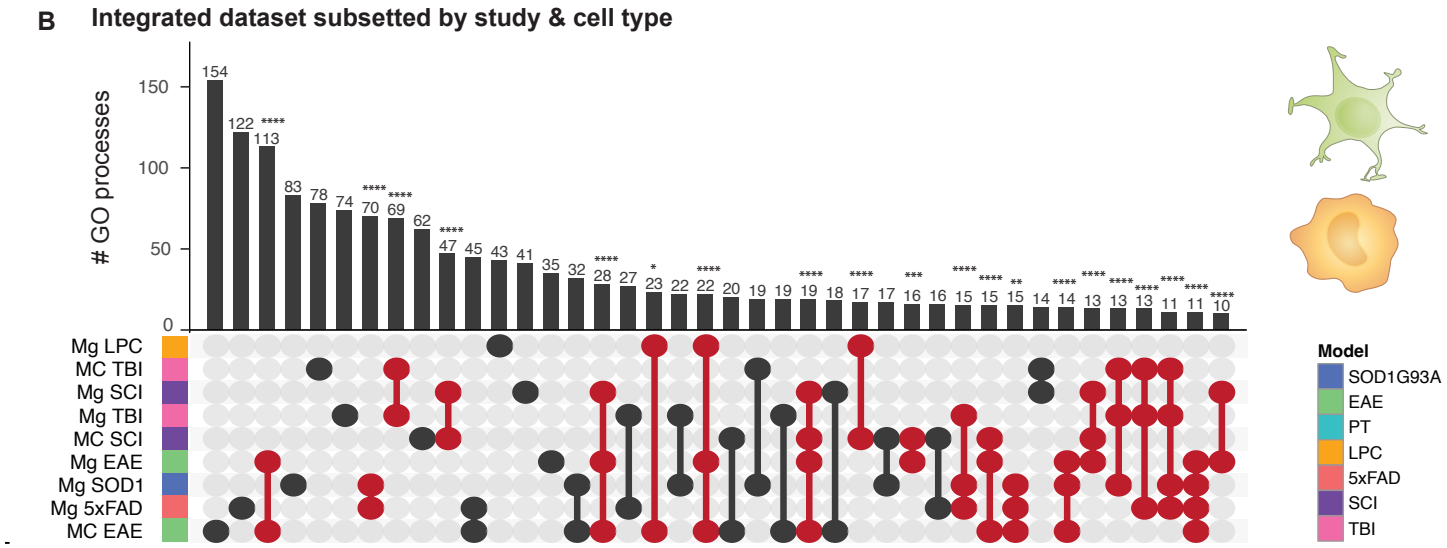
B
Integrated dataset subsetted by study & cell type
GO processes
Mg LPC
MC TBI
Mg SCI
Mg TBI
MC SCI
Mg EAE
Mg SOD1
Mg 5xFAD
MC EAE
Model
SOD1G93A
EAE
PT
LPC
5xFAD
SCI
TBI

Figure 3.4 Single-cell RNA-sequencing integration workflow with LIGER.

(**A**) Myeloid cells from six disease models from five separate studies were integrated using LIGER. Data sets were downsampled prior to integration to ensure equal representation across disease models (469 microglia from each six disease models, 469 MCs from EAE, TBI, and SCI). Optimal k and lambda values were determined prior to clustering (Supplementary Figure 3.1). Data sets were then integrated with LIGER and subjected to joint matrix factorisation (k=12, lambda=5), quantile normalisation, dimensionality reduction and joint clustering (data set alignment = 0.878). UMAPs of the LIGER-integrated dataset show representation of both cell types intermixed across the six disease models. (**B**) UpSet plot showing overlap in the number of enriched GO terms for microglia and/or MCs from six disease models from the LIGER-integrated dataset. GO term enrichment was performed on the differentially expressed genes on bulk cell populations from each disease versus every other disease. Samples are colored by disease-model membership and arranged in order of increasing to decreasing number of biological processes associated with each population.

MCs were defined by their expression of microglia-specific genes, *P2ry12, Tmem119, Sparc, Hexb, Fcrls, Siglech* and monocyte-specific/enriched genes, *Ly6c2, Plac8, Vim, Cd44*, respectively, and the lack of expression of border- and CNS-associated macrophage-specific genes (e.g., *Cd163*, *Cd206*) (Supplementary Figure 3.1) and other cell lineage markers. Identified cell populations did not cluster by anatomical region, suggesting these population are not spatially-dependent (Supplementary Figure 3.1). Pre-defined myeloid populations from the above disease conditions were then integrated into a single dataset and downsampled to the limiting cell number. Joint matrix factorisation, quantile normalisation, dimensionality reduction and joint clustering were then performed on 2,814 microglia and 1,407 MCs (Figure 3.4A and Supplementary Figure 3.1) in our integrated dataset.

To compare our integrated scRNA-seq dataset to our gene rank analysis on bulk populations, we first created pseudo-bulk microglia/MC populations by combining single-cell datasets from the same study and disease model and performed differential gene expression and GO term enrichment analysis (Figure 3.4B). This revealed a similar pattern to our gene rank approach, demonstrating overall that the majority of populations had more unique than shared biological functions across pathology. When more shared than unique processes existed, these were between microglia and MCs in the same disease setting, e.g., microglia and MCs in EAE, TBI and SCI (Figure 3.4B). Supporting our RP analysis, this suggests that microglia and MC responses are principally disease- and disease model-specific, with the disease environment bearing an important role in shaping similar profiles of these cells within the same disease.

3.1.3.4 Differing proportions of unique myeloid subtypes drive disease-specific signatures in bulk populations

To understand what drives the identified disease-specific signatures, we performed clustering analysis on individual single-cells in the LIGER-integrated scRNA-seq. This enabled us to identify myeloid subpopulations that are shared across or unique to each of the six disease models (Figure 3.5A).

This revealed a core set of microglia and MC clusters, defined by their differential expression of subset-defining markers (Figure 3.5B) and enriched GO pathways (Figure 3.6 and Supplementary Table 3.4). Among the 8 microglial clusters, we identified interferon-related (*Mg2*), inflammatory (*Mg3, Mg8*), phagocytic (*Mg4*) and DAM-related *(Mg6)* microglia, each of which displayed unique genetic and functional programs (Figure 3.6A and 3.6C). Although we identified the DAM-related cluster (*Mg6*) (Supplementary Figure 3.2), argued to be a

universal microglia disease state, this was only one of 8 microglia subpopulations that was shared across diseases, suggesting that there are other signatures that are conserved. For MCs, we identified four clusters that included inflammatory (*MC3*), antigen-presenting (*MC4*), and LPS-responsive (*MC2*) states. Importantly, these clusters were consistently detected in each disease model (Figure 3.5C), demonstrating that microglia and MCs can acquire a variety of functionally different and unique states throughout the course of a disease. However, the proportions of these clusters differed in each disease (Figure 3.5C and 3.5D), suggesting functionally distinct populations are individually expanded in response to different disease settings.

We observed that the expansion of individual myeloid subtypes was highly specialised to microenvironmental cues in each disease model. For instance, *Mg4* (phagocytic *Mg*) was the most prevalent microglial subset in 5xFAD (35.1% of all myeloid cells), which was shared with LPC-induced demyelination (28.6%) and TBI (19.5%) (Figure 3.5C and 3.5D), potentially representing a cell state important for debris clearance in these disease models. In contrast, *Mg3* (inflammatory *Mg*) was the most common microglia population (18.8%) (Figure 3.5C and 3.5D) in $SOD1^{G93A}$, pointing to important differences between this model and other neurodegenerative diseases, such as the 5xFAD model of Alzheimer's Disease that may induce a more phagocytic cellular state. *Mg2* clustered separately from the other microglia (Figure 3.5A) and was enriched for interferon-related genes (*Ifit3*, *Ifit2*, *Ifit1*, *Irf7*) (Figure 3.5B) and genes related to the negative regulation of viral genome replication, response to bacterium, cellular response to LPS, cellular response interferon-γ, and defence response to protozoan (Supplementary Table 3.4), potentially suggesting that this population may be uniquely expanded in response to infectious stimuli (e.g., viruses, bacteria, and protozoa), but persists at low levels in neurodegeneration, sterile injury, and demyelinating disorders. Despite filtering out low quality cells (i.e., cells with high mitochondrial gene expression and low relative RNA content), microglial populations, *Mg1* and *Mg7* show a high differential expression of ribosomal genes (Figure 3.5B). These populations could represent cells important for transcriptional regulation of terminal cell differentiation.

In contrast to microglia, the four MC clusters demonstrated overlap in their transcriptional and functional states, despite unique MC clusters dominating each disease model (Figure 3.5C and 3.5D). In TBI, for instance, *MC4* was the most prevalent MC population (17.6% of all myeloid cells) and was enriched for genes related to antigen processing and presentation of exogenous

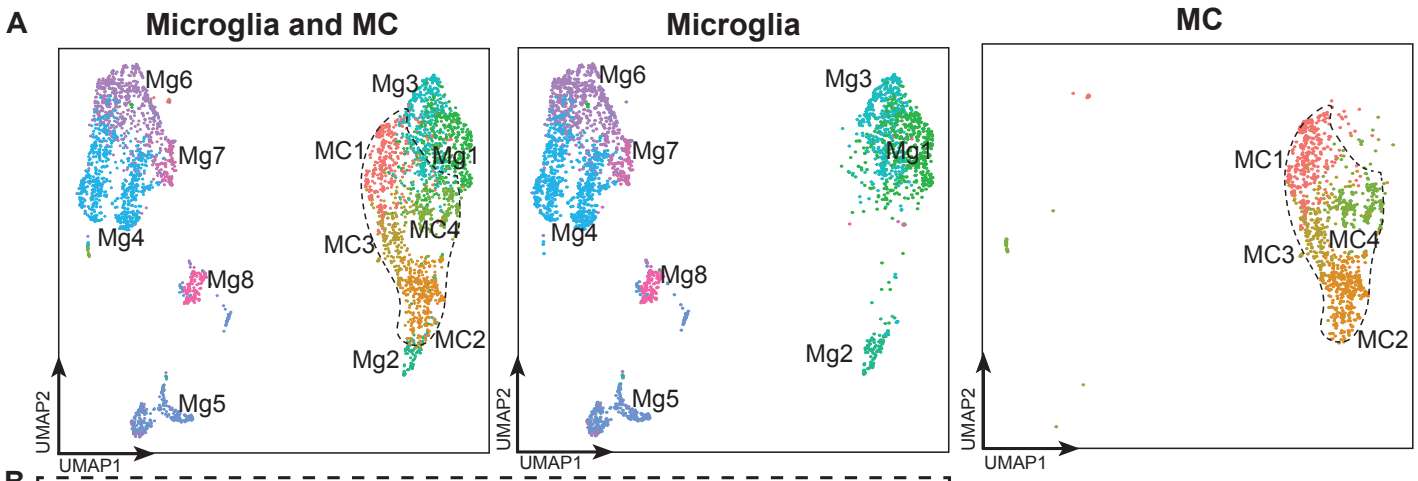

B

MC1		MC2		MC3		MC4	
Klrd1	*Clec10a*	*S100a4*	*S100a10*	*Nos2*	*Cfb*	*Klrd1*	*Clec10a*
Flt3	*Napsa*	*Vcan*	*Ifitm6*	*Inhba*	*Ass1*	*Flt3*	*Napsa*
Cd209a	*Kmo*	*S100a6*	*Ifitm2*	*Ifi205*	*Il1rn*	*Cd209a*	*Kmo*
Jaml	*Dpp4*	*Ccr2*	*Anxa2*	*Upp1*	*Slc7a2*	*Jaml*	*Dpp4*
Cd7	*P2ry10*	*S100a11*	*Crip1*	*Irg1*	*Slc7a11*	*Cd7*	*P2ry10*

Mg1		Mg2	
Apoe	*Rps9*	*Ifit3*	*Cmpk2*
Rpl18a	*Rps5*	*Rsad2*	*Mx1*
Rpl32	*Rpl4*	*Ifit1*	*Pydc4*
Rpl23	*Rpl10*	*Usp18*	*Irf7*
Rps14	*Rps15*	*Ifit2*	*Oasl1*

Mg3		Mg4		Mg5		Mg6		Mg7		Mg8	
Ms4a7	*Wdfy3*	*Cst3*	*Gpr34*	*X1110038B12Rik*		*Cst7*	*Grn*	*Impdh2*	*Nop56*	*Egr1*	*Ccl4*
Rapsn	*Idh1*	*P2ry12*	*Cd81*	*Csf1r*	*Ssh2* *Tgbr1*	*Ctsd*	*C1qa*	*Ccl12*	*Rps26.ps1*	*Nfkbiz*	*Atf3*
Cib2	*Acp5*	*Selplg*	*Cx3cr1*	*Macf1*	*Arhgap5*	*Lpl*	*Cadm1*	*Ranbp1*	*Ran*	*Jun*	*Ier5*
Lipa	*Gna12*	*Hexb*	*Sparc*	*Srgap2*	*Rhob*	*Cd9*	*C1qc*	*Srm*	*Rps18.ps3*	*Ppp1r15a*	*Tnf*
Serpinb6a	*Slc17a5*	*Olfml3*	*Tmem119*	*Cx3cr1*	*Ndufb1.ps*	*Ctsz*	*Syngr1*	*Ncl*	*Rpl23a.ps3*	*Junb*	*Btg2*

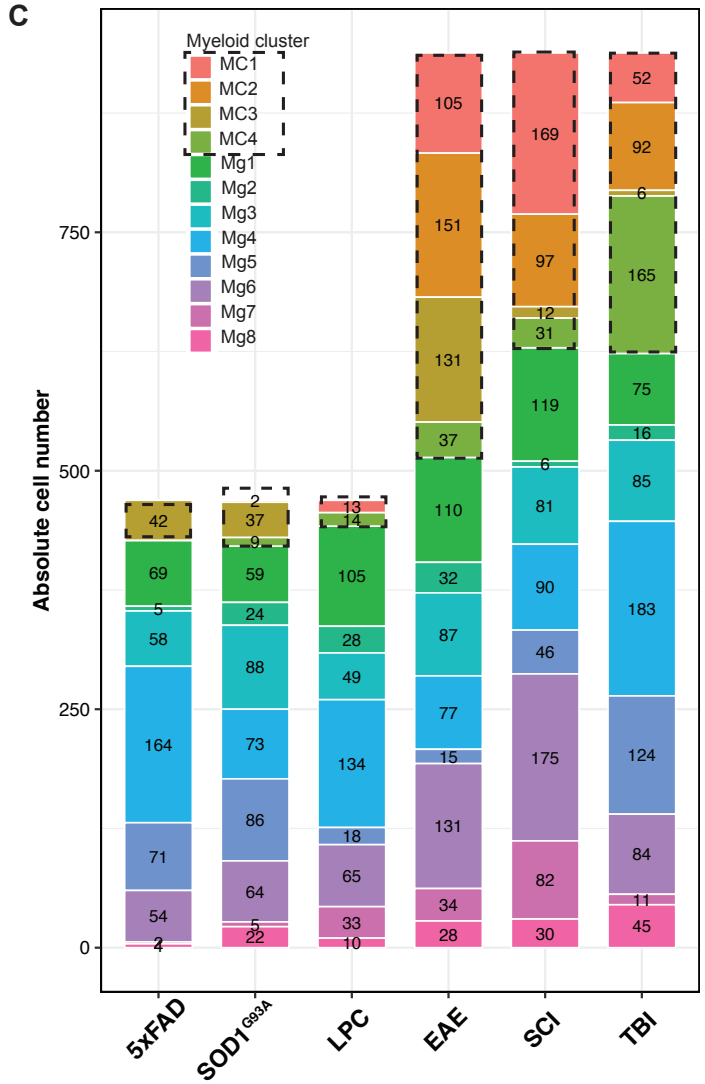

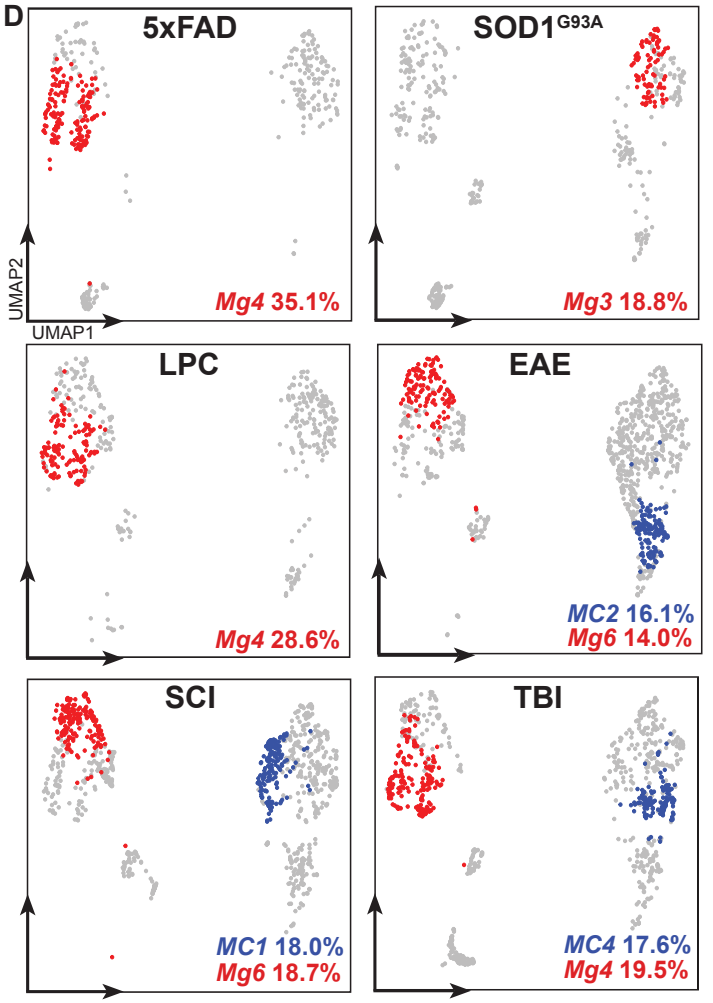

Figure 3.5 Integrative analysis of single-cell RNA-sequencing datasets identifies conserved and disease-specific MC and microglial clusters across six disease models.

(**A**) UMAPs of myeloid cells from the downsampled LIGER-integrated dataset overlaid by either microglia (2,814 cells) and/or MC clusters (1,407 cells). See also Figure S1 for the expression of cell type-specific genes used to annotate cell types. (**B**) Top 10 differentially expressed genes per cluster. Differentially expressed genes were defined as genes enriched in a cluster versus all other clusters (log2FC > 0.25, pvalue < 0.01) by Wilcoxon rank sum test. (**C**) Absolute cell numbers of microglial and MC clusters across the six disease models. Data sets were downsampled prior to integration to ensure equal representation across disease models (469 microglia from each six disease models, 469 MCs from EAE, TBI, and SCI). Absolute cell numbers for each disease model prior to downsampling were 685 MCs and 1960 microglia in LPC-induced demyelination; 3234 MCs and 1468 microglia in EAE; 182 MCs and 3620 microglia in 5xFAD; and 72 MCs and 1136 microglia in $SOD1^{G93A}$, 14,243 MCs and 17,739 microglia in SCI; and 612 MCs and 8,434 microglia in TBI. (**D**) Highest proportional representation of MC (blue) and microglia (red) clusters for each disease model overlaid onto UMAPs of myeloid cells from each disease model. Numbers represent the relative percentage of each of the myeloid clusters of the total myeloid pool in each disease model. Disease models 5xFAD, SOD1G93A, and LPC-induced demyelination contain only microglia (469 cells per disease model), whereas EAE, TBI and SCI contain both microglia and MCs (938 cells per disease model).

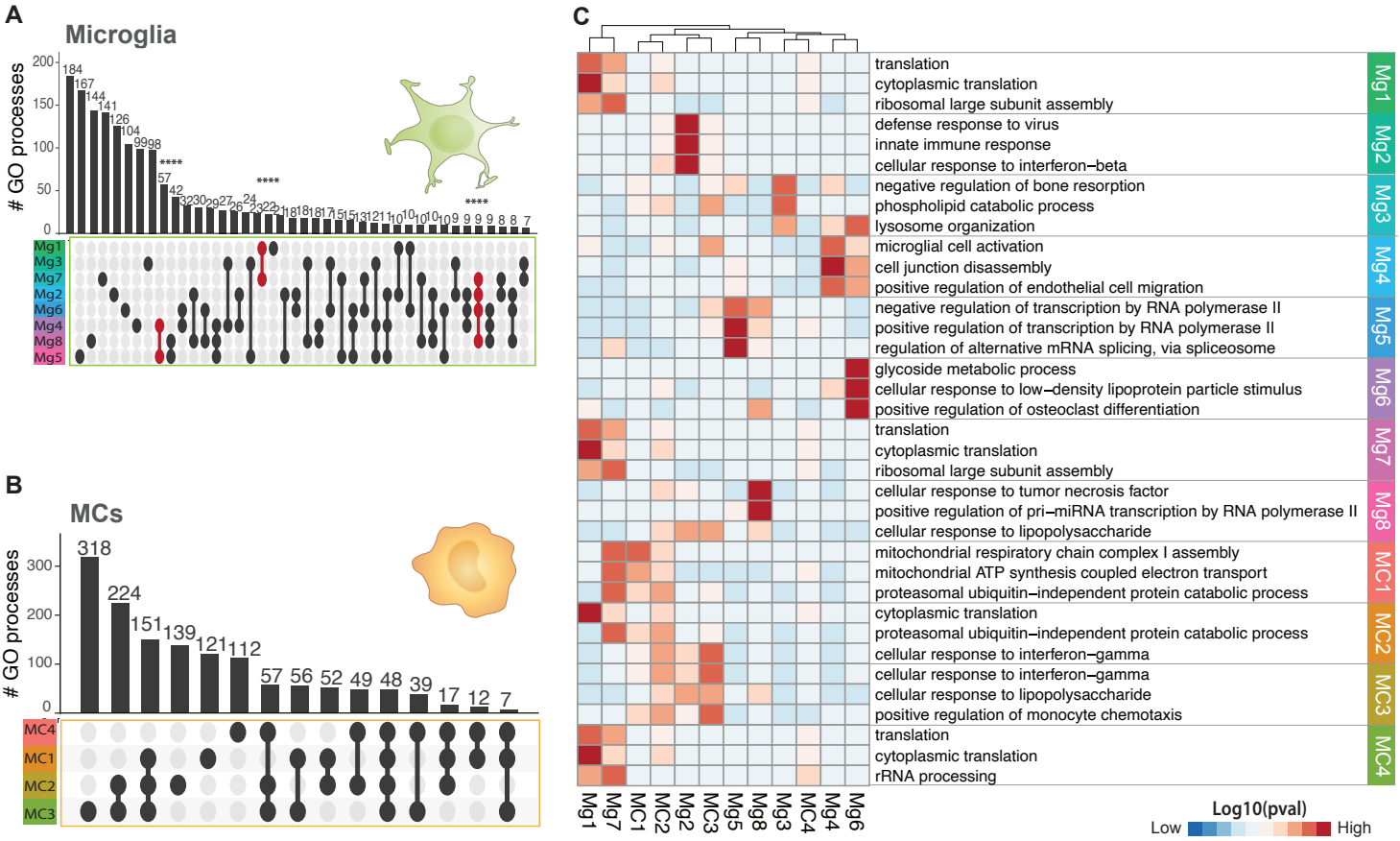
A
Microglia
GO processes
200
150
100
50
0
184
167
144
141
126
104
99
98
****
57
42
32
30
29
27
26
24
23
22
21
18
18
18
17
15
15
13
12
11
10
10
10
10
9
9
9
9
8
8
7
****
Mg1
Mg3
Mg7
Mg2
Mg6
Mg4
Mg8
Mg5
B
MCs
GO processes
300
200
100
0
318
224
151
139
121
112
57
56
52
49
48
39
17
12
7
MC4
MC1
MC2
MC3
C
translation
cytoplasmic translation
ribosomal large subunit assembly
defense response to virus
innate immune response
cellular response to interferon−beta
negative regulation of bone resorption
phospholipid catabolic process
lysosome organization
microglial cell activation
cell junction disassembly
positive regulation of endothelial cell migration
negative regulation of transcription by RNA polymerase II
positive regulation of transcription by RNA polymerase II
regulation of alternative mRNA splicing, via spliceosome
glycoside metabolic process
cellular response to low−density lipoprotein particle stimulus
positive regulation of osteoclast differentiation
translation
cytoplasmic translation
ribosomal large subunit assembly
cellular response to tumor necrosis factor
positive regulation of pri−miRNA transcription by RNA polymerase II
cellular response to lipopolysaccharide
mitochondrial respiratory chain complex I assembly
mitochondrial ATP synthesis coupled electron transport
proteasomal ubiquitin−independent protein catabolic process
cytoplasmic translation
proteasomal ubiquitin−independent protein catabolic process
cellular response to interferon−gamma
cellular response to interferon−gamma
cellular response to lipopolysaccharide
positive regulation of monocyte chemotaxis
translation
cytoplasmic translation
rRNA processing
Mg1
Mg2
Mg3
Mg4
Mg5
Mg6
Mg7
Mg8
MC1
MC2
MC3
MC4
Mg1
Mg7
MC1
MC2
Mg2
MC3
Mg5
Mg8
Mg3
MC4
Mg4
Mg6
Log10(pval)
Low
High

Figure 3.6 Differing proportions of unique myeloid subtypes drive disease-specific signatures in bulk populations.

(**A** and **B)** UpSet plot showing overlap in the number of enriched GO terms for each of the (**A**) eight microglia (n = 2,814 single cells) or (**B**) four MC (n = 1,407 single cells) clusters identified in the LIGER-integrated scRNA-seq dataset from six disease models. GO term enrichment was performed on the differentially expressed genes for each cluster (log2FC > 0.25, pval < 0.01) and enriched GO terms were defined as terms with more than 10 genes mapping to a term and a pvalue less than 0.01 (Fisher's exact test, elim algorithm). Populations that share GO terms are indicated by connecting lines in the dot plot. Individual populations are indicated by a singular dark circle with no intersecting lines. Significance of intersections are calculated by SuperExact Test. See also Table S5 for a list of the significance of each intersection shown. Samples are colored by cell cluster and arranged in order of increasing to decreasing number of biological processes associated with each population. (**C**) Heatmap showing the top three GO terms for each microglia and MC cluster. See also Table S4 for a list of all GO processes. Clustering was applied to columns only.

peptide antigen, a functional state partially shared with *MC3*, represented at much lower numbers in in TBI (Figure 3.5C, 3.5D and Supplementary Table 3.4). *MC2*, on the other hand, was the most prominent MC subset in EAE (16.1% of all myeloid cells) and was enriched for genes related to cellular response to interferon-β and LPS (Figure 3.5C, 3.5D and Supplementary Table 3.4). *MC1* was the most prevalent population in SCI (18.0% of all myeloid cells) and was enriched for genes related to cell redox homeostasis and aerobic respiration (Figure 3.5C, 3.5D and Supplementary Table 3.4). Notably, UpSet analysis on enriched GO terms for each cluster demonstrated 48 shared functional pathways between the four MC clusters, which included interferon-responsive, oxidative stress, innate immune responses, cytokine production, and inflammatory signalling cascade pathways (Figure 3.6B, 3.6C, Supplementary Table 3.4 and 3.5). We observed small variations in this core MC state between clusters, often with pathway overlap between two or more clusters (Supplementary Table 3.5), possibly indicating a continuous population rather than a series of distinct MC subtypes.

Together, this work suggests that the microenvironment drives the expansion of unique myeloid subtypes that drive disease-specific signatures in bulk populations.

3.1.3.5 Cross-disease comparison reveals CD81 as a microglia-enriched marker in neuroinflammation

Considering that some nominal microglia-specific markers are downregulated during pathology (Spiteri et al., 2021a, Vankriekelsvenne et al., 2022, Krasemann et al., 2017), we sought to find a novel and stably-expressed microglia marker to reliably identify these cells in disease at both RNA (Werner et al., 2020) and protein level. We performed differential expression analysis on individual bulk and scRNA-seq studies to evaluate the genes highly enriched in microglia versus MCs across CNS disease (Figure 3.7A). For this analysis, only studies that examined both microglia and MCs in the CNS simultaneously were used. This included the additional infectious disease model, using Theiler's encephalomyelitis virus.

This analysis identified 192 and 119 genes differentially enriched in MCs and microglia, respectively, that were conserved across five models of CNS pathology, including EAE, SCI, TBI, PT and Theiler's encephalomyelitis virus infection (Figure 3.7A and Supplementary Table 3.6). Filtering these genes by their cellular localization on the plasma membrane revealed 12 and 22 MC and microglia differentially enriched membrane markers, respectively (Figure 3.7A-C), including previously identified MC markers *Cxcr4* and *Cd44* that have been used to

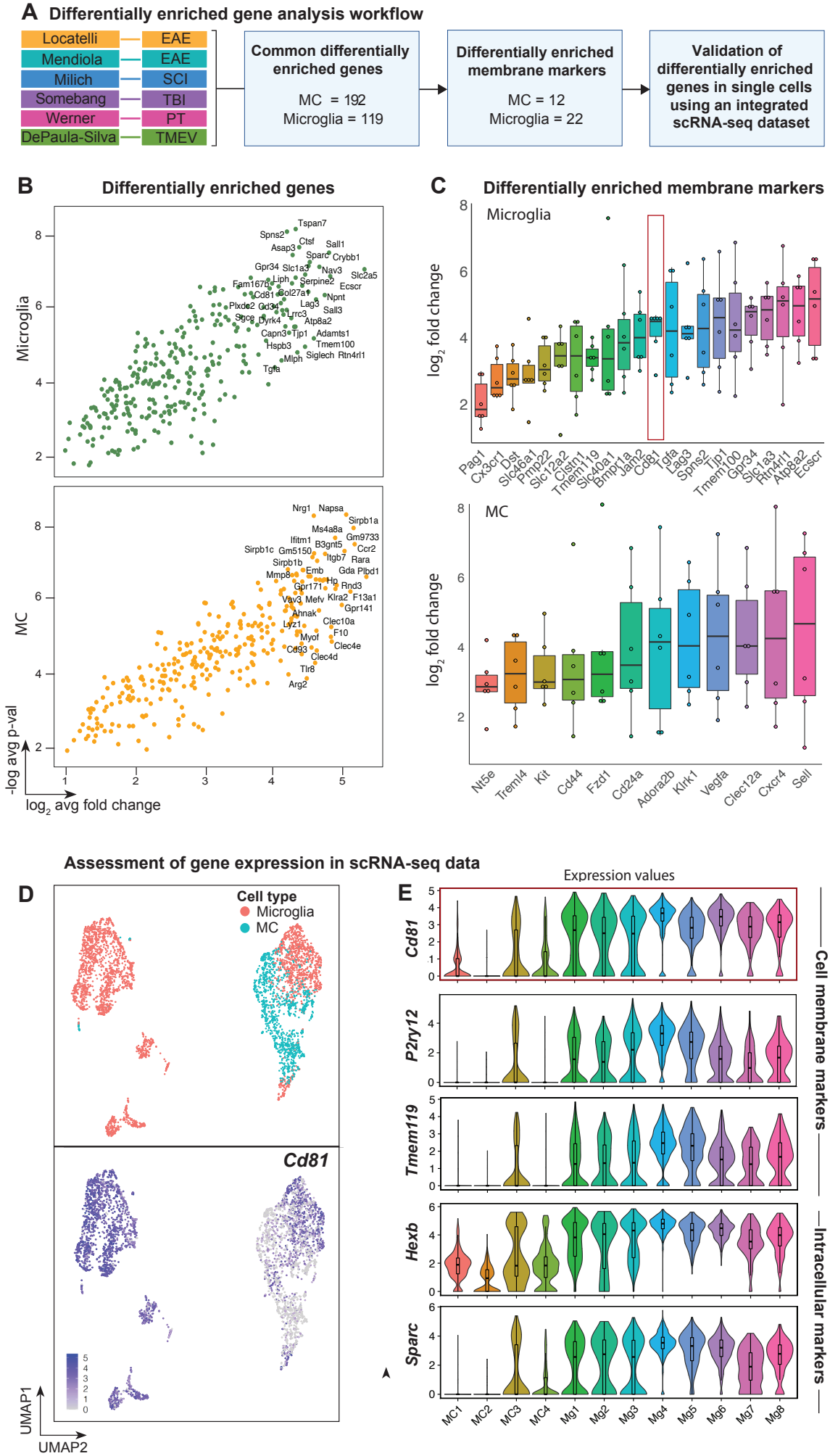
A Differentially enriched gene analysis workflow
Locatelli EAE
Mendiola EAE
Milich SCI
Somebang TBI
Werner PT
DePaula-Silva TMEV
Common differentially enriched genes
MC = 192
Microglia = 119
Differentially enriched membrane markers
MC = 12
Microglia = 22
Validation of differentially enriched genes in single cells using an integrated scRNA-seq dataset
B Differentially enriched genes
Microglia
MC
-log avg p-val
log2 avg fold change
C Differentially enriched membrane markers
Microglia
MC
log2 fold change
Pag1 Cx3cr1 Dst Slc4a1 Pmp22 Slc12a2 Cisd1 Tmem119 Slc40a1 Bmpr1a Jam2 Cd81 Tgfa Lag3 Sprns2 Tjp1 Tmem100 Gpr34 Slc1a3 Rtn4rl1 Atp8a2 Ecscr
Nt5e Treml4 Kit Cd44 Fzd1 Cd24a Adora2b Klrk1 Vegfa Clec12a Cxcr4 Sell
Assessment of gene expression in scRNA-seq data
D
Cell type
Microglia
MC
Cd81
UMAP1
UMAP2
E
Expression values
Cd81
P2ry12
Tmem119
Hexb
Sparc
Cell membrane markers
Intracellular markers
MC1 MC2 MC3 MC4 Mg1 Mg2 Mg3 Mg4 Mg5 Mg6 Mg7 Mg8

Figure 3.7 Cross-disease analysis reveals Cd81 as a microglial-enriched gene in neuroinflammation.

(**A**) Flow chart analysis pipeline used to identify differentially enriched microglial and MC genes in the inflamed brain. Six studies that simultaneously analysed microglia and MCs in the CNS were used to identify 192 and 119 differentially enriched ($p<0.05$, $log2FC>1$) MC and microglia genes, respectively. This gene list was filtered in uniprot to identify membrane expressed genes, which were subsequently validated with expression data using an integrated scRNA-seq dataset. (**B**) Volcano plots showing all genes differentially enriched by microglia and MCs in EAE, SCI, TBI, PT and TMEV. The top 35 differentially enriched genes are annotated. See also Table S6 for a list of these genes. (**C**) Box plots showing differentially enriched surface/plasma membrane-expressed genes for microglia and MCs. (**D**) UMAPs showing single-cell gene expression overlays for Cd81 in MC and microglial clusters identified in the integrated single-cell RNA-sequencing dataset. (**E**) Violin plots showing the expression of *Cd81* relative to nominal microglia-specific genes in the 16 myeloid clusters.

distinguish these cells from microglia in stroke (Werner et al., 2020) and EAE (Lewis et al., 2014) (Figure 3.7C). Of interest, *Cd81* was stably expressed by microglia across all models of CNS inflammation, with a 25-fold higher median expression relative to MCs (Figure 3.7C). While *Lag3* also showed relatively stable microglial expression across disease models (Figure 3.7C), the higher expression of *Cd81* and more distinct separation between microglia and MCs make it particularly promising as a discriminating marker. In addition, this marker is a species-conserved microglial-enriched tetraspanin gene (Geirsdottir et al., 2020) expressed on the cell surface, reagents for which are commercially available for flow cytometric and RNA detection, making this a potentially suitable marker for detecting this cells multimodally across species.

We confirmed the differential expression of *Cd81* at the single-cell level in our LIGER-integrated scRNA-seq dataset and observed that *Cd81* remained highly expressed by all microglial clusters (*i.e.*, *Mg1* to *Mg8*), but remained expressed only at low levels by MCs during neuroinflammatory conditions (Figure 3.7D and 3.7E). Importantly, previously identified membrane markers for yolk-sac-derived microglia (e.g., *P2ry12*, *Tmem119*) showed variable expression in all microglia clusters relative to *Cd81* expression (Figure 3.7E). Although genes such as *Spar*c (Jordão et al., 2019) and *Hexb* (Masuda et al., 2020) were also enriched in all microglia populations (Figure 3.7E), the intracellular localization of their encoded protein products do not allow antibody binding in live cells without lethal cell permeabilization, thus precluding downstream live cell experimental approaches (*e.g.,* after flow cytometric sorting) in the absence of specific genetic manipulation (Masuda et al., 2020).

To validate *Cd81* as a microglia-enriched marker for flow cytometry during pathology, we investigated the expression of CD81 protein on microglia and CNS-infiltrating MCs in a mouse model of flaviviral encephalitis (Figure 3.8). Since many microglia-specific markers are either downregulated by microglia or upregulated by MCs during inflammation, we used a highly inflammatory model of CNS disease with a significant monocytic infiltrate to validate the differential protein expression of this marker on these cells. WNV encephalitis causes a severe inflammatory response characterised by a ~10-fold increase in the number of leukocytes in the brain, with approximately 50% of this infiltrate comprising $Ly6C^{hi}$ inflammatory macrophages (Terry et al., 2012, Terry et al., 2015, Getts et al., 2008, Getts et al., 2012, Getts et al., 2014, Getts et al., 2007). Examination of $CD45^{+}$ cells in the virus-infected brain on day 7 post-infection confirmed that CD81 was expressed at high levels only on microglia (Figure 3.8B-E) and not on $Ly6C^{hi}$ MCs or microglia-like MCs (*i.e.*, myeloid cells of non-microglial origin

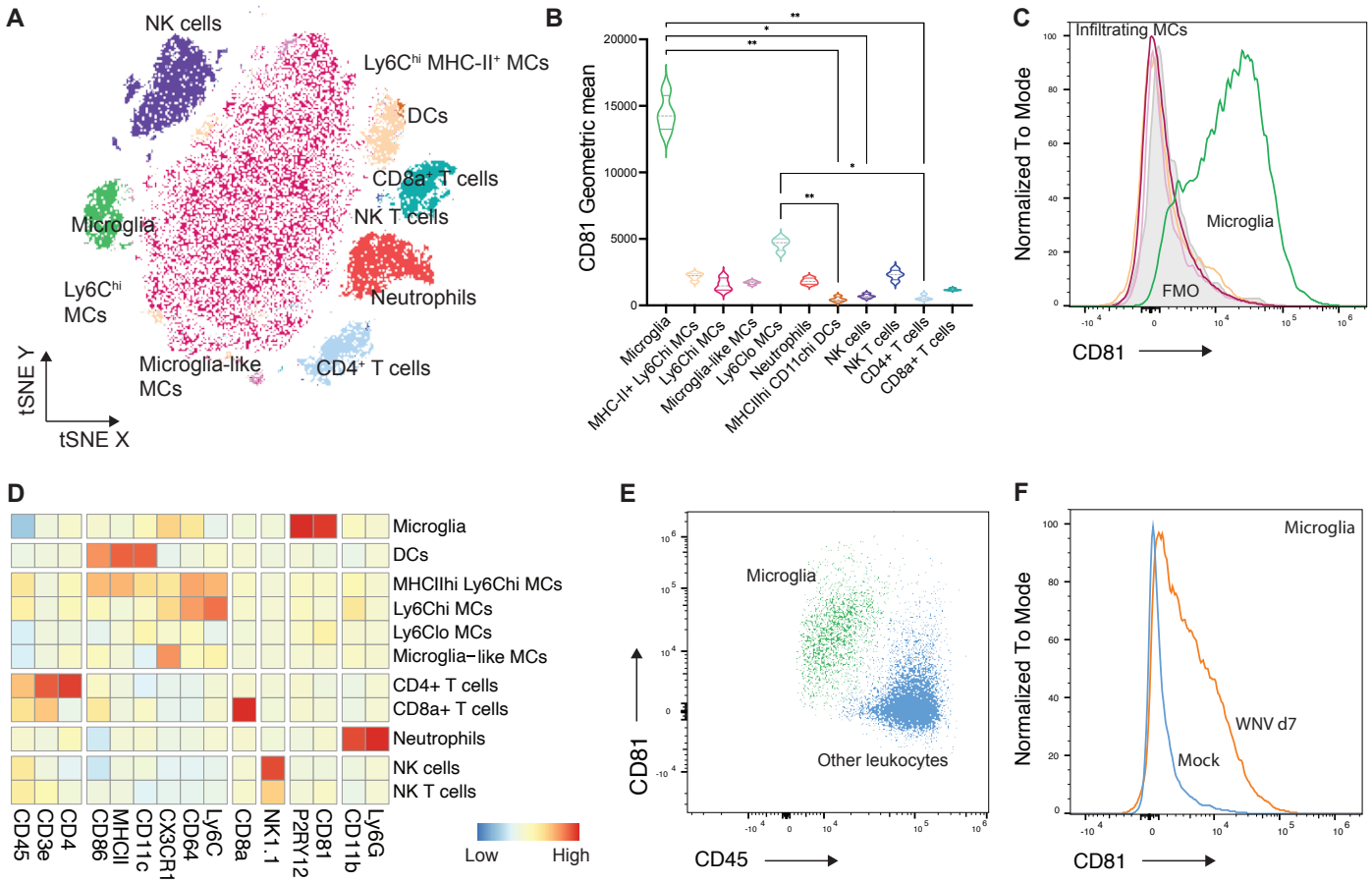
A
NK cells
Ly6C^hi MHC-II^+ MCs
DCs
CD8a^+ T cells
NK T cells
Microglia
Ly6C^hi MCs
Neutrophils
Microglia-like MCs
CD4^+ T cells
tSNE Y
tSNE X
B
CD81 Geometric mean
20000
15000
10000
5000
0
Microglia
MHC-II+ Ly6Chi MCs
Ly6Chi MCs
Microglia-like MCs
Ly6Clo MCs
Neutrophils
MHCIIhi CD11chi DCs
NK cells
NK T cells
CD4+ T cells
CD8a+ T cells
C
Infiltrating MCs
Normalized To Mode
Microglia
FMO
CD81
D
Microglia
DCs
MHCIIhi Ly6Chi MCs
Ly6Chi MCs
Ly6Clo MCs
Microglia−like MCs
CD4+ T cells
CD8a+ T cells
Neutrophils
NK cells
NK T cells
CD45
CD3e
CD4
CD86
MHCII
CD11c
CX3CR1
CD64
Ly6C
CD8a
NK1.1
P2RY12
CD81
CD11b
Ly6G
Low
High
E
Microglia
Other leukocytes
CD81
CD45
F
Microglia
Normalized To Mode
WNV d7
Mock
CD81

Figure 3.8 CD81 is a microglial-enriched protein expressed in neuroinflammation.

(**A**) tSNE plot showing WNV-infected brains with resident and infiltrating $CD45^+$ leukocyte populations overlaid. (**B**) Violin plots showing the expression of CD81 on cell populations identified on the tSNE plot. (**C**) Histogram showing the expression of CD81 by microglia relative to infiltrating macrophage populations and FMO for CD81 in infected brains. See also Supplementary Figure 3.3 and Supplementary Figure 3.4 showing CD81 expression by leukocyte populations in the bone marrow and spleen, respectively. (**D**) Heatmap showing the expression of markers on cell populations shown in (**A**). (**E**) FACs plot showing the expression of CD81 and CD45 on microglia and other $CD45^+$ leukocytes in infected brains. (**F**) Histogram showing the expression of CD81 on microglia from mock and infected brains at day 7 post infection.

present in the infected brain with a $CD45^+$, $CX3CR1^+$ and $CD11b^+$ profile similar to microglia, but absent in the homeostatic brain) (Spiteri et al., 2021a).

Interestingly, CD81 was not detectable on microglia during homeostasis (Figure 3.8F), despite the homeostatic expression of RNA for this molecule (Geirsdottir et al., 2020), suggesting that the induction of protein expression occurs only during inflammation. Furthermore, while CD81 is microglia-enriched out of all CNS resident and infiltrating leukocytes, this protein is expressed by a number of cells in the BM and spleen, suggesting that CD81 is downregulated by infiltrating myeloid cells upon entry into the CNS (Figure 3.8B, Supplementary Figure 3.3 and 3.4). Taken together, while other disease models need to be investigated, this data suggests that under highly inflammatory conditions, the differential expression of CD81 in combination with previously reported CD45, Ly6C, CX3CR1 or P2RY12 (Spiteri et al., 2021a) in the CNS, enables a novel and simple method for discriminating microglia from other leukocytes by flow cytometry, as well as for live cell sorting and imaging.

3.1.4 Discussion

Despite decades of research and recent technical advances, the differential and shared contributions of microglia and MCs to disease and disease resolution are still poorly understood. While their immense functional and phenotypic diversity make this problem intrinsically complex, this is further exacerbated by the wide range of technologies and analytical approaches used to describe these cells in different fields of research. To address this problem, we have systematically integrated the transcriptional and functional profiles of resident and CNS-infiltrating myeloid cells obtained from demyelinating, neurodegenerative, ischemic, traumatic and infectious conditions across three sequencing modalities. Concatenating the gene expression profiles across these models identified a quorum of genes and their associated functions that were principally disease-specific.

In contrast to the proposed universal microglia signature, we observed that individual disease environments drive microglia to adopt highly specialized signatures with minimal overlap across CNS conditions. Analysis of bulk microglia populations demonstrate limited overlap in gene expression profiles and biological functions between diseases. More detailed examination of scRNA-seq populations suggest that these disease-specific bulk populations may be a result of the distinct composition of differing proportions of unique subpopulations in each disease setting, including interferon-related, inflammatory, phagocytic, and DAM-related microglia

identified in this report. Indeed, concatenating microglia populations from each scRNA-seq study, demonstrated more unique than shared biological functions across pathologies, confirming that although each disease state shared these subpopulations, the differing proportions drove unique signatures when pooled together. While these disease-specific microglia populations showed limited overlap across pathologies, they demonstrated convergence with MC populations in the same disease, suggesting that various activation states are regulated by the disease setting. The notion of diverse myeloid activation signatures has been previously proposed by other studies including a meta-analysis integrating various animal disease models (Friedman et al., 2018) and in human Alzheimer's Disease, where they identified homeostatic, interferon-, LPS-, neurodegeneration- or proliferation-related modules (Olah et al., 2020), closely resembling the activation states reported here. It remains an important task to understand the signalling pathways driving the distinct functional specialization of microglia. This could help restore beneficial functions such as phagocytic functions in the handling of myelin debris associated with senescence (Safaiyan et al., 2016) or amyloid plaques that arise during Alzheimer's Disease (Grubman et al., 2021, Ennerfelt et al., 2022), or prevent maladaptive responses such as the production of ROS or reactive nitrogen species that may underlie tissue damage in MS (Mendiola et al., 2020) or viral encephalitis (Getts et al., 2012), respectively.

Intriguingly, microglia and MCs adopt more distinct than shared expression profiles and functions across pathologies, despite being exposed to similar inflammatory settings. This may relate to their unique ontogenies and regulatory signalling patterns (Bennett et al., 2018, Butovsky et al., 2014, Buttgereit et al., 2016). In contrast to microglia, MCs showed more similarities across models of acute neuroinflammation, potentially relating to the limited time spent in the CNS, compared to microglia, that would normally be required for adaptation and specialisation to environmental cues. Previous single-cell studies show multiple transcriptionally diverse MCs within a single disease (Jordão et al., 2019, Mendiola et al., 2020, Giladi et al., 2020). The accumulation of CNS-infiltrating monocytes in anatomically distinct CNS compartments may contribute to this previously reported transcriptomic heterogeneity (Ivan et al., 2021, Locatelli et al., 2018, Jordão et al., 2019). Alternatively, these distinct transcriptional programs may represent a trajectory of maturation within the CNS, where MCs adapt more subtly in response to changes in the local microenvironment with disease progression (Locatelli et al., 2018) from an initially conserved, functional program that generally enables rapid, if generic, control of an acute insult (Sanin et al., 2022).

Single-cell transcriptomics has uncovered nominally microglia-specific markers. However, several of these markers are downregulated during inflammation (Jordão et al., 2019, Keren-Shaul et al., 2017, Krasemann et al., 2017) or also expressed by peripherally-derived cells (Chen et al., 2020, Spiteri et al., 2021a), making them unreliable for the unambiguous identification of microglia in the inflamed CNS. Highlighting the practical value of our cross-disease analysis, we here identified *Cd81* as a novel and conserved RNA marker distinguishing microglia from MCs during neuroinflammation. Indeed, interrogation of other publicly available human and mouse datasets show a stable expression of *Cd81* across disease states (Srinivasan et al., 2020, Li et al., 2018a, Zhang et al., 2014). Notably, *Cd81* is a microglial marker conserved at least across the evolutionary span of sheep, mice and humans (Geirsdottir et al., 2020). It is not upregulated by monocytes that engraft the brain (Cronk et al., 2018), suggesting that *Cd81*, in combination with other microglia-enriched genes, is a robust marker for distinguishing microglia from MCs under a range of disease conditions.

Importantly, of all the $CD45^+$ cells in the inflamed brain, CD81 protein was highly expressed only on microglia. While other disease models require further investigation, this work validates the use of CD81 along with other differentially expressed microglia proteins for cytometric identification of these cells during WNV encephalitis. While other cells also express this tetraspanin (Maecker et al., 1997), its function appears to be cell type-specific (Dijkstra et al., 2000, Mordica et al., 2009). The upregulation and expression of CD81 by microglia in the WNV-infected brain (Figure 3.8), human Alzheimer's Disease (Mathys et al., 2019) and in SCI in the rat (Dijkstra et al., 2000), may relate to their activation/transformation (Dijkstra et al., 2000), enhanced proliferative capacity (Dijkstra et al., 2001, Geisert et al., 2002, Ma et al., 2010) and mobility (Maecker et al., 1997) and/or the release of extracellular vesicles (Paolicelli et al., 2019, Clayton et al., 2021, Muraoka et al., 2021) during disease. The consistent expression of CD81 on microglia across disease states likely reflects its fundamental role in microglial biology — as a tetraspanin protein, it helps organize membrane microdomains and regulate membrane protein trafficking, which are crucial for microglial functions including phagocytosis, cytokine secretion, and cell-cell communication. Given the multi-functional role employed by microglia in CNS diseases, where they may adopt a range of functional profiles, the stable expression of CD81 may be a reflection of its importance across multiple functional states in microglia, from homeostatic surveillance to inflammatory responses.

While our analysis is informative, it has several limitations. Firstly, we were unable to dissect the contribution of gender or mouse strain per se to the identified gene profiles. Secondly, given our stringent criteria for data incorporation (see Materials and Methods and Supplementary Table 3.1), several studies were not included, restricting our evaluation of other cell types and diseases. For example, the unexplored contribution of border-associated macrophages to disease (Ivan et al., 2021) and how their gene expression profiles may relate to those of microglia and MCs remains unclear. Thirdly, we were unable to investigate microglia or MCs in certain diseases either due to the lack of the relevant homeostatic controls or due to a statistically insufficient number of biological replicates. Fourthly, further characterisation of these clusters is still required, including functional analyses, to determine the biological importance of these subsets. It is also critical to determine whether specific myeloid clusters identified here are spatially localised and/or timepoint dependent. Lastly, to translate these findings into a clinically relevant setting, parallel analysis of human data would be required, however the potential discordance of animal models and human disease will require further integrative techniques that can accurately align biological differences between humans and mice. While additional characterisation is required, we believe this work provides a cornerstone for building a consensus to enable more accurate classification of myeloid populations in pathological settings.

Additionally, the technical and methodological discrepancies between incorporated datasets have limited more direct comparisons. This argues for a unified approach in processing, sorting, and analysis of these cell types to enable integration across broader, often segregated disease research fields. For instance, the use of standard tissue processing procedures, standard gating strategies to identify and sort populations for subsequent transcriptomic analysis, and in the absence of appropriate controls, the use of homeostatic, peripheral blood monocytes as standardized controls for CNS-infiltrating populations in the inflamed brain, would resolve many of these issues. A consensus defining a set of standards for the field to unify experimental and analytical procedures would go a considerable way to begin this process, as previously attempted for macrophage activation nomenclature, transcriptomic profiling of brain barriers and flow cytometry standards (Murray et al., 2014, Cossarizza et al., 2019, Francisco et al., 2020).

Together, our meta-analytical approach integrates data across fields of research and technology to enable comparison of myeloid behaviour in different experimental models of

neuroinflammation. As a resource, this work highlights the importance of cross-disease comparison to better characterize the conserved and divergent microglial and MC responses in CNS disease and contributes to the creation of a unified perspective of the behaviour of these cells across CNS conditions. We demonstrate that microglia and monocyte transcriptomes are disease-dependent, with differing proportions of unique myeloid subpopulations driving these bulk population signatures. These include 8 microglia clusters and 4 monocytes clusters that were functionally-defined and conserved across disease settings, identifying a core set of myeloid responses. This paves the way for identifying myeloid “archetypes” across CNS pathologies, which may enable us more precisely to dissect the influence of disease environments on functional programs that influence progression. This is also crucial to inform the ongoing development of targeted therapeutic approaches.

Supplementary Figures

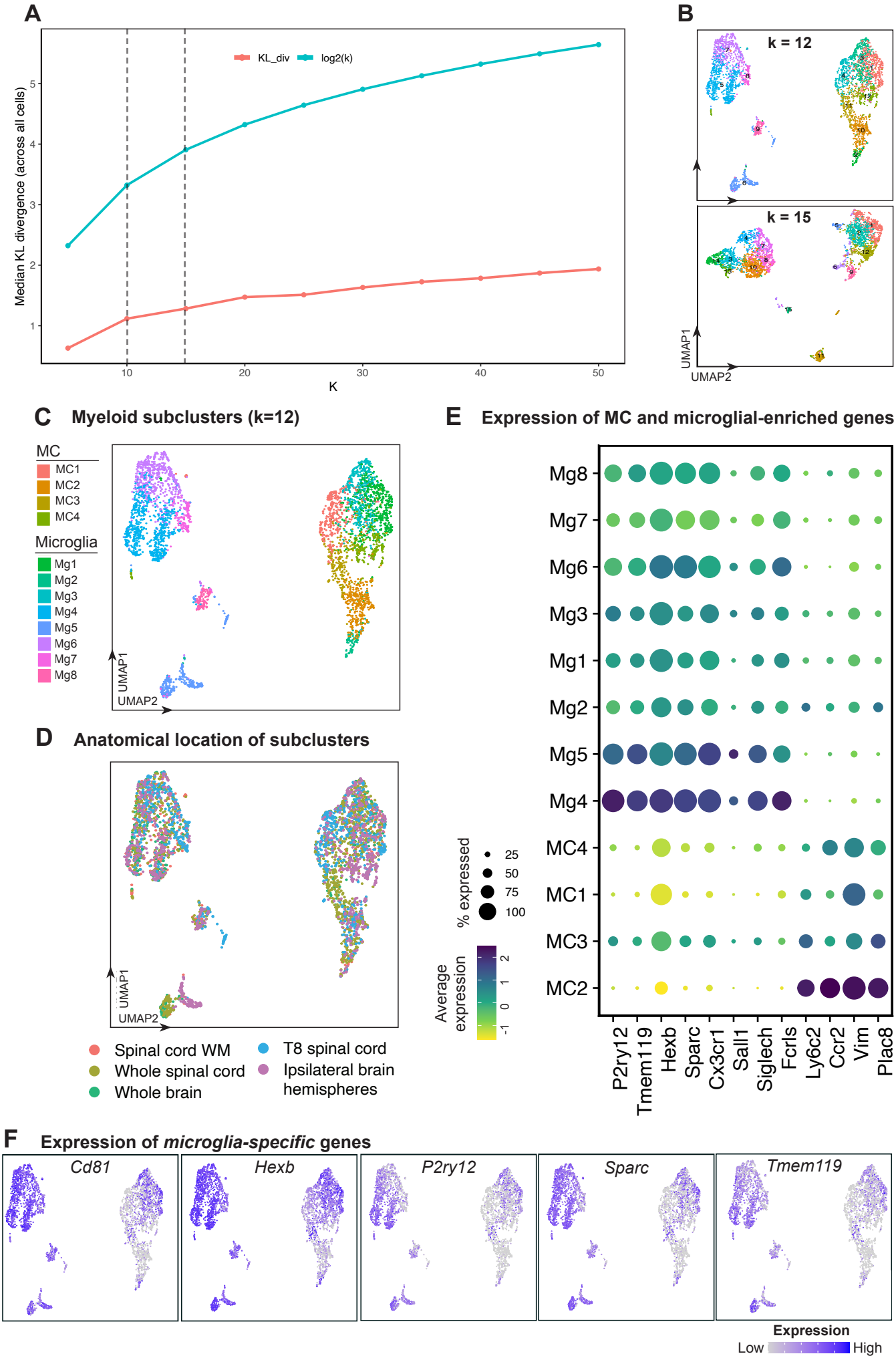
A
KL_div
log2(k)
Median KL divergence (across all cells)
K
B
k = 12
k = 15
UMAP1
UMAP2
C
Myeloid subclusters (k=12)
MC
MC1
MC2
MC3
MC4
Microglia
Mg1
Mg2
Mg3
Mg4
Mg5
Mg6
Mg7
Mg8
D
Anatomical location of subclusters
Spinal cord WM
Whole spinal cord
Whole brain
T8 spinal cord
Ipsilateral brain hemispheres
E
Expression of MC and microglial-enriched genes
% expressed
Average expression
P2ry12
Tmem119
Hexb
Sparc
Cx3cr1
Sall1
Siglech
Fcrls
Ly6c2
Ccr2
Vim
Plac8
F
Expression of microglia-specific genes
Cd81
Hexb
P2ry12
Sparc
Tmem119
Expression
Low
High

Supplementary Figure 3.1 Clustering parameters used for defining myeloid subtypes of the LIGER-integrated scRNA-seq dataset.

(**A**) Parameter selection for the number of factors k versus the median Kullback-Leibler (KL) value across all cells for the LIGER-integrated data set of six disease models. The tuning parameter, lambda, was kept at the recommended value of 5 (Liu et al., 2020). The optimal value of k is defined as the 'elbow' of the plot, i.e., the k value at which the median KL value becomes negligible (defined between k = 10-15, dashed lines). (**B**) UMAP showing the clusters for two optimal k values, k=12 (alignment = 0.878) and k=15 (alignment=0.837). The optimal number of factors chosen was k=12 based on improved alignment between datasets and based on prior biological knowledge of clustering (Liu et al., 2020). (**C**) UMAP of myeloid cells from the downsampled LIGER-integrated dataset (k=12) overlaid by either microglia (2,814 cells) and/or MC clusters (1,407 cells). (**D**) UMAP showing the anatomic location myeloid subclusters were isolated from during CNS tissue processing and cell sorting. (**E**) Dot plot heatmap showing the average expression of microglia-specific genes and highly expressed MC genes in identified clusters. Clusters have been ordered by unsupervised hierarchical clustering. (**F**) UMAPs showing single-cell gene expression overlays for microglia-specific genes, P2ry12, Tmem119, Hexb and Sparc, in MC and microglial clusters.

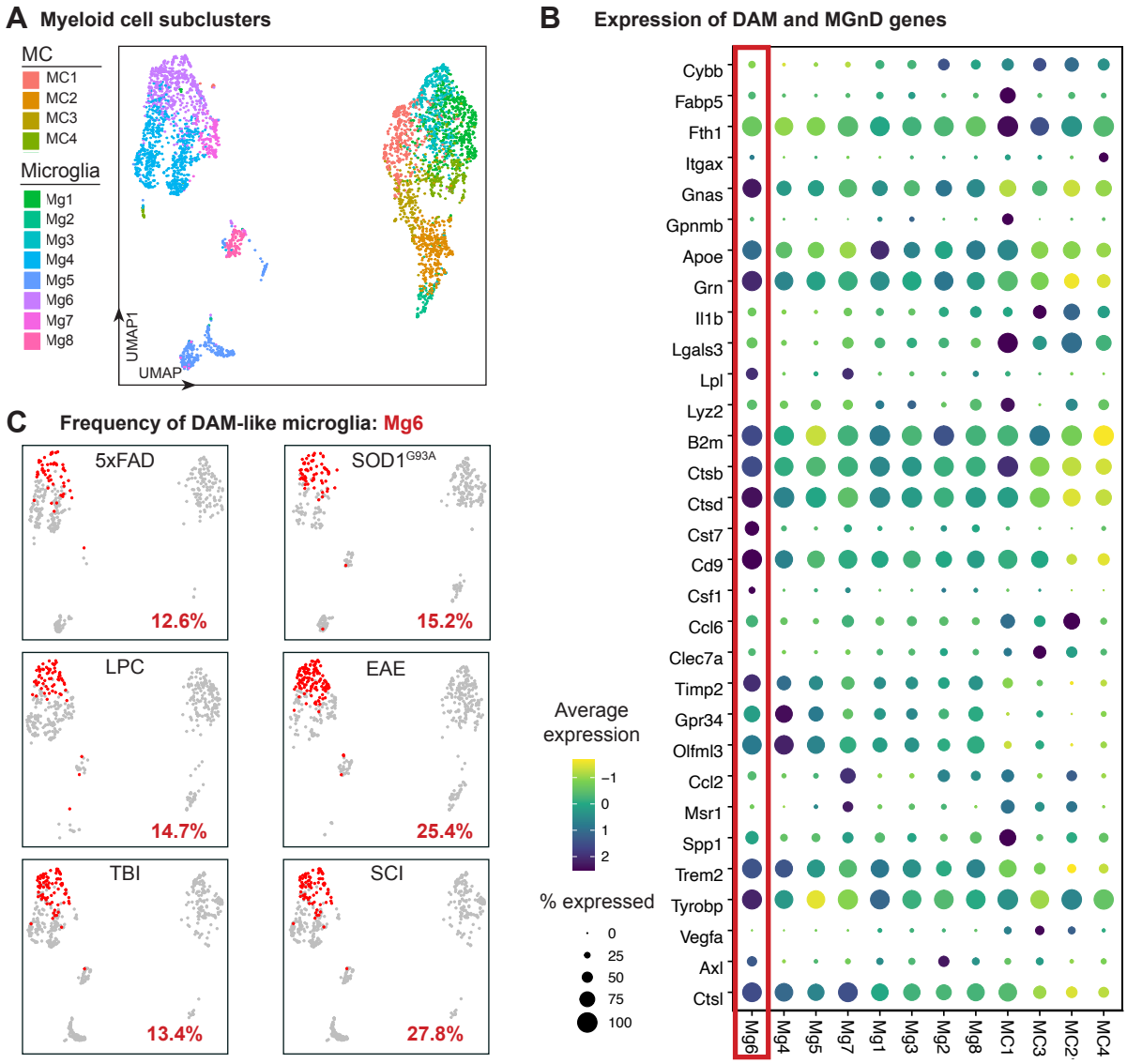
A Myeloid cell subclusters
MC
MC1
MC2
MC3
MC4
Microglia
Mg1
Mg2
Mg3
Mg4
Mg5
Mg6
Mg7
Mg8
UMAP1
UMAP
B Expression of DAM and MGnD genes
Cybb
Fabp5
Fth1
Itgax
Gnas
Gpnmb
Apoe
Grn
Il1b
Lgals3
Lpl
Lyz2
B2m
Ctsb
Ctsd
Cst7
Cd9
Csf1
Ccl6
Clec7a
Timp2
Gpr34
Olfml3
Ccl2
Msr1
Spp1
Trem2
Tyrobp
Vegfa
Axl
Ctsl
Mg6
Mg4
Mg5
Mg7
Mg1
Mg3
Mg2
Mg8
MC1
MC3
MC2
MC4
Average expression
−1
0
1
2
% expressed
0
25
50
75
100
C Frequency of DAM-like microglia: Mg6
5xFAD
12.6%
SOD1G93A
15.2%
LPC
14.7%
EAE
25.4%
TBI
13.4%
SCI
27.8%

Supplementary Figure 3.2 Expression of universal microglial signatures by single-cell RNA-seq myeloid clusters.

(**A**) UMAP of 4,221 myeloid cells (downsampled) with clusters annotated and pseudocolored based on cell type cluster. (**B**) Dot plot heatmap showing the average expression of DAM and MGnD genes in all myeloid clusters. Clusters have been ordered by unsupervised hierarchical clustering. Microglial clusters with high expression of DAM/MGnD genes are annotated as DAM-like microglia (*Mg6*, red box). (**C**) DAM-like microglia *Mg6* (red) overlaid onto UMAPs of microglia clusters from each disease model. Numbers represent the relative frequency percentage of *Mg6* out of the microglial pool within each disease model.

Bone marrow

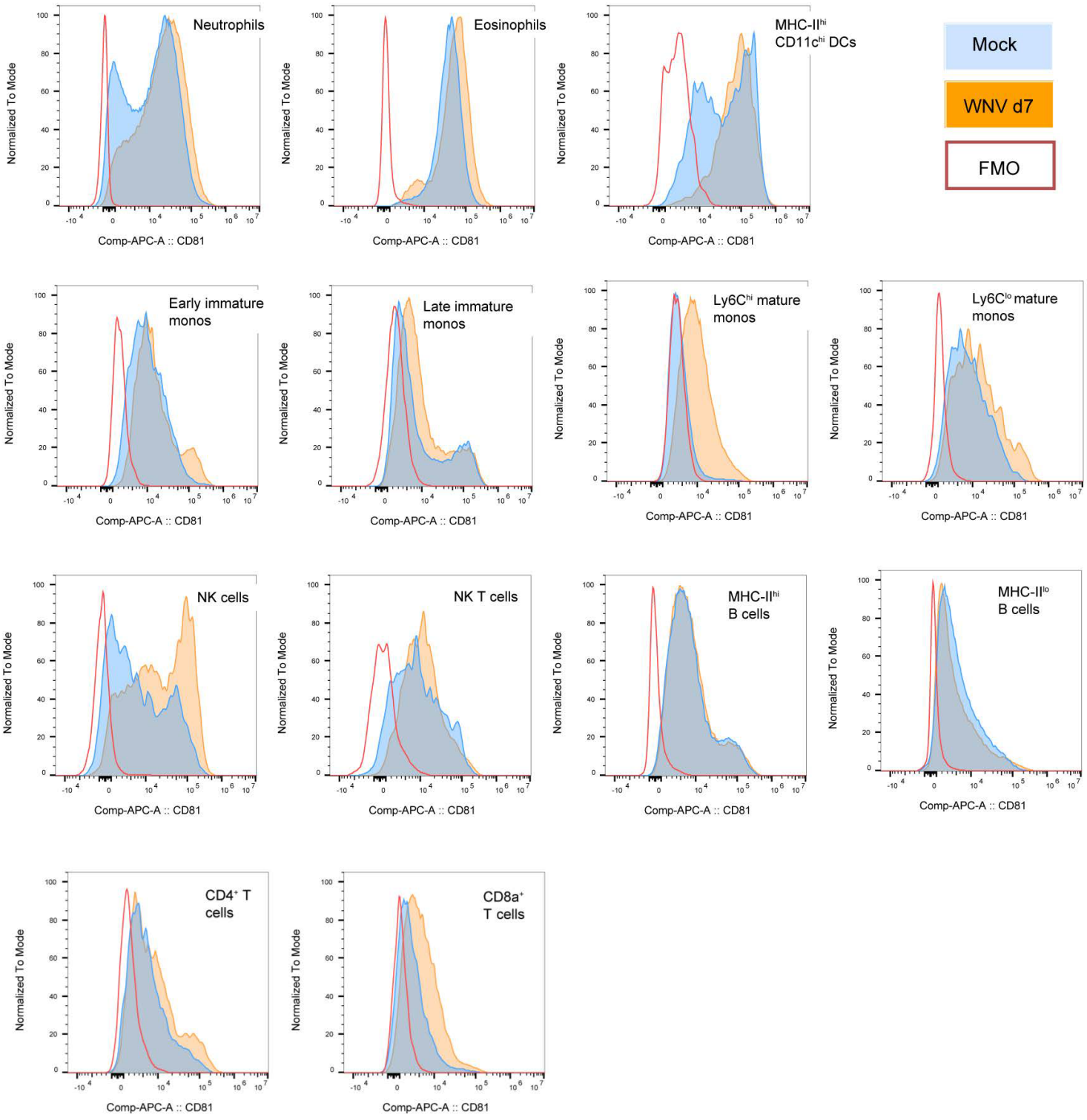
Neutrophils
Eosinophils
MHC-II^{hi} CD11c^{hi} DCs
Mock
WNV d7
FMO
Early immature monos
Late immature monos
Ly6C^{hi} mature monos
Ly6C^{lo} mature monos
NK cells
NK T cells
MHC-II^{hi} B cells
MHC-II^{lo} B cells
CD4^{+} T cells
CD8a^{+} T cells
Normalized To Mode
Comp-APC-A :: CD81

Supplementary Figure 3.3 Histograms showing the expression of CD81 on CD45+ cell types in the non-infected and WNV-infected bone marrow at dpi 7.

SPLEEN

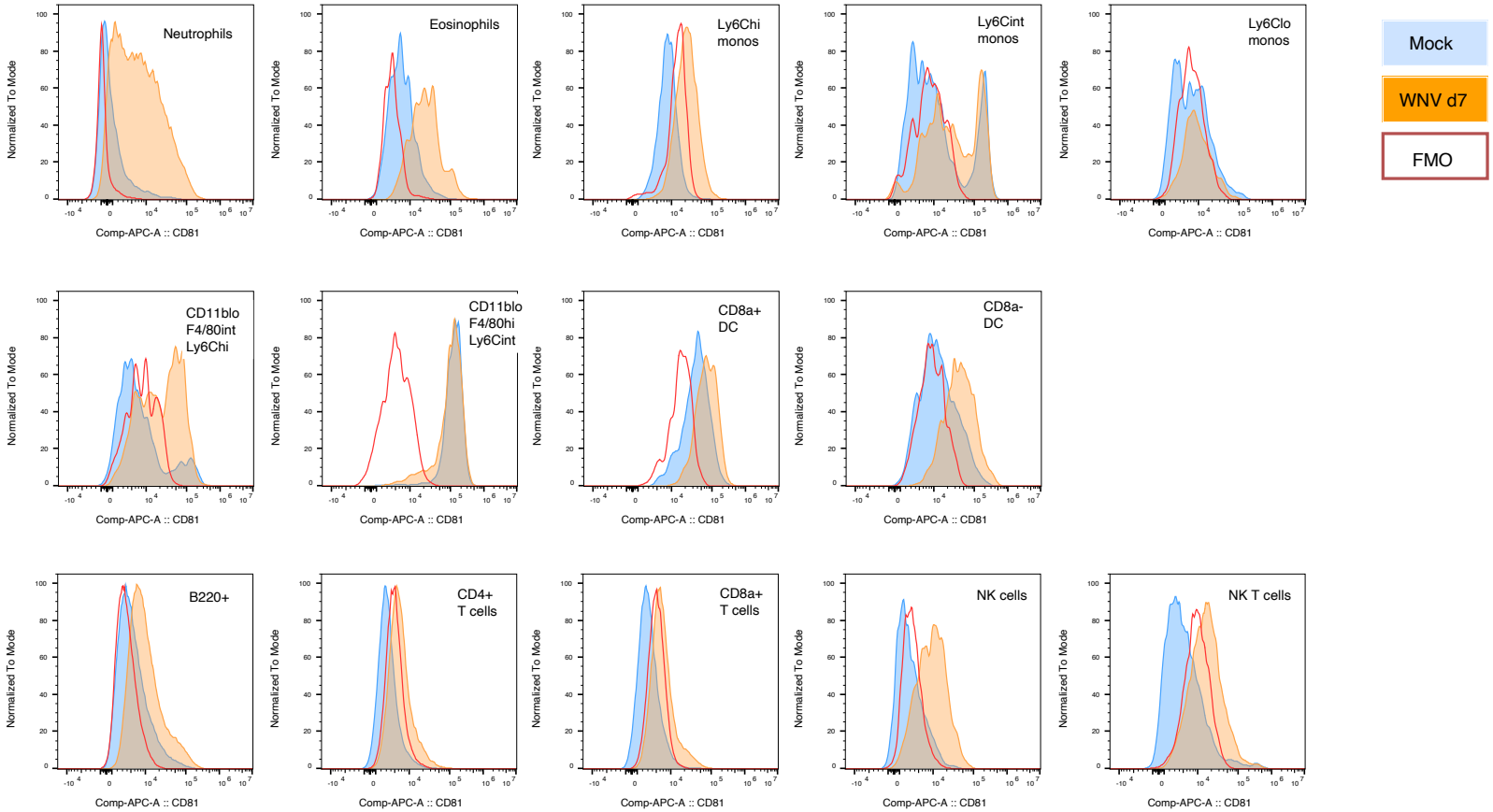
Neutrophils
Eosinophils
Ly6Chi monos
Ly6Cint monos
Ly6Clo monos
CD11blo F4/80int Ly6Chi
CD11blo F4/80hi Ly6Cint
CD8a+ DC
CD8a- DC
B220+
CD4+ T cells
CD8a+ T cells
NK cells
NK T cells
Normalized To Mode
Comp-APC-A :: CD81
Mock
WNV d7
FMO

Supplementary Figure 3.4 Histograms showing the expression of CD81 on CD45+ cell types in the non-infected and WNV-infected spleen at dpi 7.

Chapter 4: Results II

4.1 MC heterogeneity in the diseased CNS microenvironment is linked to distinct metabolic profiles

The following chapter is formatted into a manuscript.

4.1.1 Overview

MCs are a major cellular component of the microenvironment in CNS diseases. However, the relationship between the functional and metabolic profiles of these cells remains poorly understood across and within CNS pathologies. The *in vitro* M1 and M2 paradigm of macrophage activation is traditionally used to characterize MC function. It is unclear, however, whether this polarization paradigm accurately characterizes the functional and metabolic heterogeneity of these cells in the context of *in vivo* disease scenarios in the CNS. We performed single-cell transcriptomic integration of CNS MCs from murine models of MS, viral encephalitis, TBI, and SCI. Our study reveals that the M1/M2 paradigm fails to adequately characterize MC metabolic responses in CNS diseases, as they often display mixed or absent M1 and M2 signatures. Instead, our approach identified significant heterogeneity in transcription, metabolism, and function among these cells. Specific functional responses showed distinct metabolic associations with antigen presentation, inflammatory response, phagocytosis, NO production, and wound healing. Notably, we found that glycolysis, typically linked to the M1-like response, is differentially regulated across these functions in the CNS. While strongly associated with NO production and phagocytosis, glycolysis is not linked to antigen presentation. This suggests that MCs utilize metabolic pathways based both on specific and temporal energy demands of their functions, challenging the traditional M1/M2 activation model and highlighting the complexity and adaptability of MC functions in the context of CNS diseases.

4.1.2 Introduction

MCs are important components of the immune response in the CNS. Unlike microglia, the resident myeloid cells of the CNS parenchyma, MCs originate from HSCs in the BM. During CNS inflammation, monocytes are recruited in varying numbers via CCL2/CCR2-dependent mechanism, contributing to various aspects of CNS pathobiology, including inflammation,

antigen presentation, wound healing, and response to pathogens (Spiteri et al., 2021b). These cells have a profound impact on both the generation, exacerbation and resolution of inflammation in various diseases. Consequently, therapeutic strategies aimed at depleting or reprogramming MCs have garnered significant interest.

MC subsets within CNS disease exhibit specialized functions, yet the mechanisms underlying this heterogeneity remain largely unexplored. Advances in immunometabolism suggest that cellular metabolism plays an important role in driving specific functional MC states. Traditionally, MC metabolism is dichotomised into inflammatory (M1) and alternatively-activated (M2) profiles, induced and characterized under controlled *in vitro* conditions. Pro-inflammatory M1 MCs, induced by LPS and interferon IFN-γ, exhibit increased phagocytic capacity, release of pro-inflammatory cytokines, higher capacity for antigen presentation, and produce high levels of ROS (Rodríguez-Prados et al., 2010, Freemerman et al., 2014, Palsson-McDermott et al., 2015, Viola et al., 2019). Metabolically, M1 MCs favour glycolysis over OXPHOS, have increased fatty acid synthesis and increased activity of the oxidative arm of the PPP (Van den Bossche et al., 2017, Viola et al., 2019). Conversely, anti-inflammatory M2 MCs, induced by interleukin IL-4 or IL-13, release anti-inflammatory cytokines (e.g., IL-10) and growth factors (e.g., TFG-β), produce low levels of ROS and NO and can promote stem cell proliferation and differentiation (Mills et al., 2000, Stein et al., 1992, Corraliza et al., 1995), thus they are typically associated with wound healing. Metabolically, M2 MCs exhibit lower glycolysis, increased OXPHOS, and a greater reliance on fatty acid oxidation and glutaminolysis (Viola et al., 2019, Huang et al., 2014, Wang et al., 2018).

However, applying the M1/M2 nomenclature to *in vivo* CNS disease poses significant challenges (Devanney et al., 2020). Firstly, these profiles are derived from controlled *in vitro* stimulation, whereas *in vivo* stimuli are more complex and difficult to identify. This is particularly relevant in the complex environment of the inflamed CNS, where environmental factors such as hypoxia, nutrient availability, and the presence of other immune cells, signals, and pathogens significantly influence MC function and metabolism. These factors vary considerably according to the disease microenvironment, leading to differential regulation of MC subsets and unique metabolic and functional signatures. Secondly, MCs exhibit high plasticity, moving along a continuum of activation and adaptating to changing microenvironments. Indeed, single-cell transcriptional profiling has demonstrated that MCs can concurrently express both M1 and M2 markers in CNS disease (Locatelli et al., 2018, Kim

et al., 2016) and can transition between these states (Locatelli et al., 2018). Finally, recent studies have highlighted specific metabolic profiles associated with various MC functions *in vitro* and in non-CNS diseases, including cytokine production (Yeudall et al., 2022, Lachmandas et al., 2016), antigen presentation (Everts et al., 2014), phagocytosis (Lee et al., 2018, Lachmandas et al., 2016), and anti-viral responses (Xiao et al., 2020, Peng et al., 2021, Shen et al., 2021), highlighting the complex relationship between metabolism and immune cell function. However, despite their crucial role in regulating MC functions, the metabolic characteristics of MCs *in vivo*, particularly in CNS diseases, remains largely unexplored. Understanding the metabolic underpinnings of these functional states is particularly relevant given recent advancements in therapeutic strategies targeting metabolic reprogramming of cells in CNS disease (Kelly et al., 2015, Zahoor et al., 2022).

Transcriptome profiling at the single-cell level provides valuable insights into intracellular signalling responses, cell type-specific pathways, possible/likely function, and activity of major metabolic pathways. Here, we applied scRNA-seq to MCs isolated from the brains of mice with WNV encephalitis and integrated this dataset with publicly available scRNAseq datasets investigating MCs from murine models of MS, TBI, and SCI to investigate the metabolic and functional states of MCs across acute CNS disease. Our findings reveal that the M1/M2 paradigm does not accurately capture MC profiles in these CNS diseases. We demonstrate a complex relationship between MC function and metabolism, highlighting the metabolic and functional heterogeneity of MCs, with glycolysis serving as a key differentiator between inflammatory and antigen-presenting MCs.

4.1.3 Results

4.1.3.1 Investigating M1/M2 metabolic signatures across CNS disease models

To investigate metabolic responses of MCs across CNS disease, we integrated our in-house scRNA-seq dataset of total MCs in WNV encephalitis, a model of severe neuroinflammation, with total MCs isolated from the CNS across three murine disease models, including the EAE model of MS and experimental models of SCI and TBI (Figure 4.1A). From each disease, MCs were derived at the disease peak coinciding with significant monocyte infiltration: WNV (day post-infection 5 & 7), EAE (disease onset), SCI (day post-injury 1, 3, and 7) and TBI (day post-injury 4). MCs were identified by their expression of *Ly6c2*, *Plac8*, *Vim*, and *Cd44* and distinguished from microglia by their lack of expression of microglia-specific genes (*P2ry12*,

Tmem119, *Sparc*, *Hexb*, *Fcrls*, *Siglech*, *Cd81*) and border- and CNS-associated macrophage-specific genes (e.g., *Cd163*, *Cd206*), as previously described (Wishart, 2022). MCs did not cluster by disease, showing successful cross-disease integration (Figure 4.1B).

MC metabolism is commonly assessed using M1/M2 polarizing stimulation *in vitro*, yet the question of how metabolic responses to these stimuli translate to disease microenvironments in the CNS remains largely unanswered. To comprehensively evaluate these signatures, we selected a publicly available gene set, derived from *in vitro*-polarised BM-derived macrophages from C57BL/6 mice using specific activation protocols, comprised of classically activated (M1: LPS, 100 ng/mL + IFN-γ, 20 ng/mL, 24 h) or alternatively-activated (M2: IL-4, 20 ng/mL, 24 h) macrophages (Orecchioni et al., 2019, Jablonski et al., 2015). This gene set was selected to comprehensively assess the relevance of the *in vitro* M1/M2 paradigm to MCs in CNS diseases.

Using this *in vitro* gene set, we scored the expression of M1 (443 genes) and M2 (331 genes) gene sets across all the diseases (Figure 4.1C) to generate a module score. The M1 and M2 module scores for each disease was calculated using the average expression of all the genes from the *in vitro* M1/M2 gene sets relative to the aggregated expression of randomly-selected control genes outside the gene set (Tirosh et al., 2016). Examination of MCs aggregated across all diseases by UMAP showed inverse differential expression of M1 and M2 *in vitro* scores (Figure 4.1D, 4.1E), suggesting differential polarization between these two transcriptional states. MCs derived from EAE and/or viral encephalitis showed the highest M1 scores (Figure 4.1F), which aligns with the known pro-inflammatory role of these cells in these diseases, in which their overexuberant pro-inflammatory response contributes to neuronal injury by exacerbating inflammation and tissue damage (Wishart, 2022). On the other hand, M2 scores were notably elevated in TBI and SCI (Figure 4.1F), consistent with their wound-healing role in sterile injury (Wishart, 2022).

As the M1 and M2 sets contain genes pertaining to both functional and metabolic pathways, we next examined the expression of genes related to distinct metabolic pathways across each disease (Figure 4.1G), including *amino acid metabolism*, *ETC*, *TCA cycle*, *fatty acid oxidation*, *fatty acid synthesi*s, and *glycolysis*. Genes for each of these pathways were selected by the Mouse Genome Informatics Database (Tirosh et al., 2016), with scores being calculated as before, based on the average expression of the gene set relative to the aggregated expression

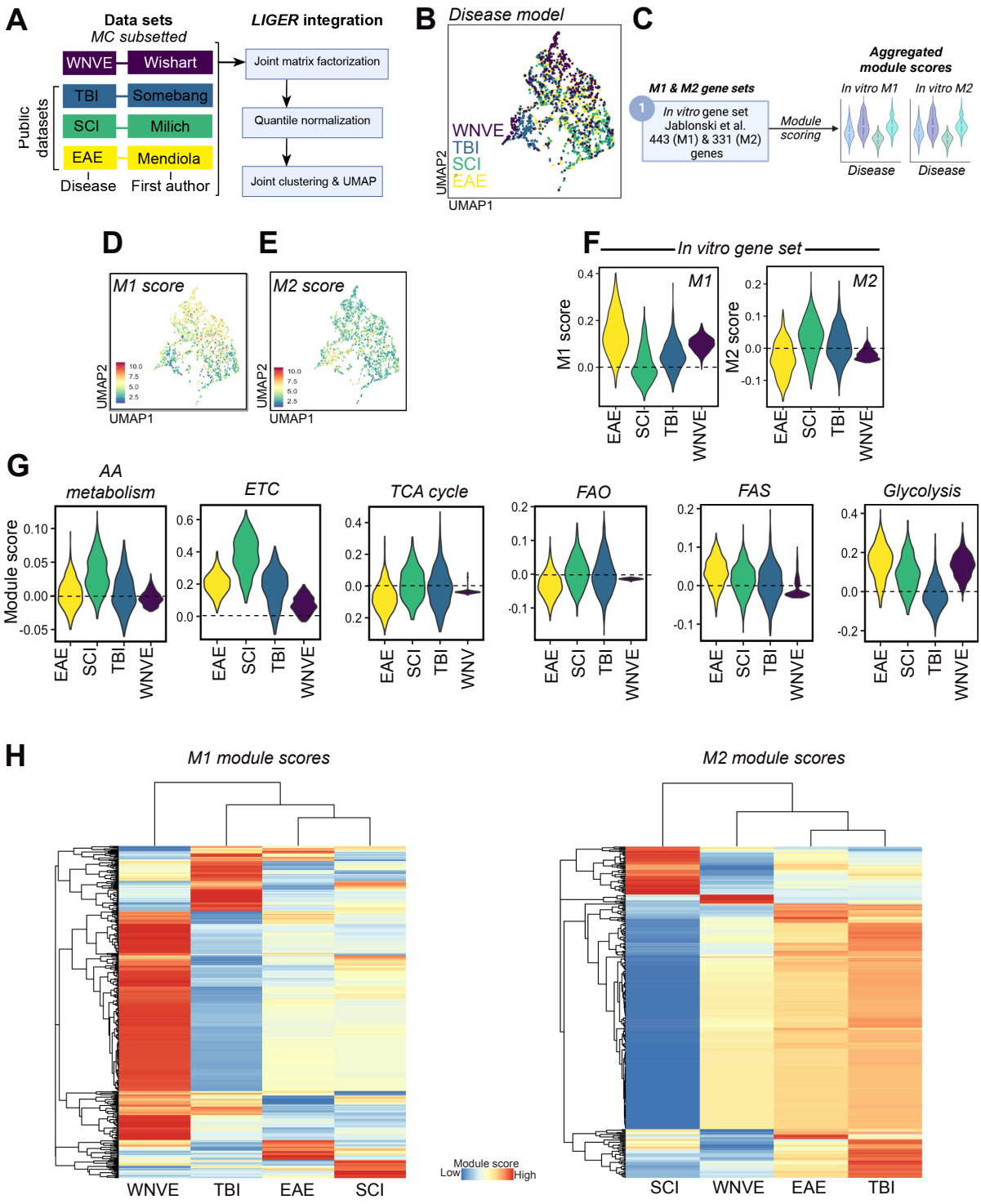
A
Data sets
MC subsetted
LIGER integration
WNVE
Wishart
TBI
Somebang
SCI
Milich
EAE
Mendiola
Public datasets
Disease
First author
Joint matrix factorization
Quantile normalization
Joint clustering & UMAP
B
Disease model
WNVE
TBI
SCI
EAE
UMAP2
UMAP1
C
M1 & M2 gene sets
In vitro gene set Jablonski et al. 443 (M1) & 331 (M2) genes
Module scoring
Aggregated module scores
In vitro M1
In vitro M2
Disease
Disease
D
M1 score
UMAP2
UMAP1
E
M2 score
UMAP2
UMAP1
F
In vitro gene set
M1
M2
M1 score
M2 score
EAE
SCI
TBI
WNVE
G
AA metabolism
ETC
TCA cycle
FAO
FAS
Glycolysis
Module score
EAE
SCI
TBI
WNVE
H
M1 module scores
M2 module scores
Module score
Low
High
WNVE
TBI
EAE
SCI
SCI
WNVE
EAE
TBI

Figure 4.1 Bulk M1/M2 polarization of MCs across CNS disease.

(**A**) Schematic workflow of dataset integration. (**B**) UMAP pseudocoloured by disease origin. (**C**) Schematic workflow of M1 and M2 gene set origin and module scoring. (**D**, **E**) UMAP pseudocoloured by module score for *in vitro* M1 (**D**) and M2 (**E**) gene sets. (**F**) *In vitro* M1 and M2 module scores across each of the disease models. (**G**) Module scores for the identified metabolic pathways across the indicated disease models. (**H**) Heatmap displaying the expression level of all M1-associated genes (173 genes) or M2-associated genes (174 genes) across each of the four disease models. AA, amino acid; FAO, fatty acid oxidation; FAS, fatty acid synthesis; WNVE, West Nile virus encephalitis.

of randomly-selected control genes. While each of these pathways may be distinctly regulated based on functional requirements, they are thought to have specific associations with either M1 or M2 polarization. Consistent with the M1 and M2 paradigm, M2-associated metabolic pathways (e.g., *amino acid metabolism*, the *ETC*, the *TCA cycle*, and *fatty acid oxidation*) were higher in SCI and TBI (Figure 4.1G), further supporting the notion that MCs derived from these diseases show a predominant M2-like metabolic signature. On the other hand, *glycolysis*, which is typically associated with an M1-like signature (Figure 4.1G), was highest in EAE and WNV encephalitis, consistent with the predominant M1-like signature of these cells.

Examination of each of the M1 and M2 *in vitro* gene sets revealed significant variability in the expression of genes within the sets, with cells from each disease showing high expression of genes belonging to both M1 and M2 gene sets (Figure 4.1H). Notably, EAE and WNV encephalitis clustered separately based on their expression of M1 genes, suggesting that although both of these diseases showed primarily M1 signatures, the functional and metabolic status of these cells may differ significantly (Figure 4.1H). We observed a similar pattern for SCI and TBI, which clustered separately based on their expression of M2 genes, suggesting that the nominal "M2-like" diseases have distinct gene expression patterns. In addition, the evident variability in the M1 and M2 gene sets within each disease suggests the presence of transcriptionally distinct subsets that cannot be captured by the M1 and M2 polarization signatures.

4.1.3.2 Metabolic heterogeneity of MCs in the diseased CNS environment

Given the variability in the M1 and M2 signatures, we next aimed to investigate MC subset heterogeneity within each disease. To this end, MCs were clustered across the four diseases, revealing seven separate MC subsets (Figure 4.2A). Importantly, these subsets did not cluster by disease membership, but could each be detected across the four disease models at different prevalence (Figure 4.2B). For instance, in TBI, *MC4* had the highest prevalence, whereas in SCI, *MC5* was highest. *MC3* was highest in WNV, whereas *MC2* was highest in EAE. Despite these differences in proportions, each of these subsets could be detected in each of the disease models, supporting the transcriptional heterogeneity of MCs across these four conditions.

Examination of the M1 and M2 gene sets for each subset also showed a spectrum of activation. In support of our findings demonstrating differential M1 and M2 module scores by each disease (Figure 4.1F), we found that MC subsets with elevated M1 scores (*MC3*, *MC6*) (Figure 4.2C, 4.2D) were predominantly present in WNV and EAE (Figure 4.2B). *MC4*, the subset with

elevated M2 scores (Figure 4.2C), showed higher prevalence in TBI (Figure 4.2B). However, various MC subsets did not fall distinctly into either M1 or M2 categories, with *MC1*, *MC2*, and *MC7* showing high or intermediate expression of both M1 and M2 gene sets (Figure 4.2C). Notably, *MC5*, highest in SCI, seemed to lack expression of both M1 and M2 gene sets (Figure 4.2C). Examination of typical M1- and M2-associated genes, *Nos2* and *Arg1*, respectively, revealed co-expression among individual cells and no distinct polarization in the expression of these two genes (Figure 4.2D). These data suggest a complexity in the activation and metabolic states of MCs within CNS diseases that extends beyond a binary classification. Further supporting this, examination of a select number of genes typically associated with M1 or M2 states showed similar expression patterns, with *MC3* and *MC6* showing the highest expression of M1 genes (Figure 4.2E), although notably, *MC6* highly expressed shared M2-associated genes, such as *Arg1*, *Il10* and *Socs2* (Figure 4.2E).

To further elucidate the metabolic profiles of MC subsets within CNS disease, we conducted gene set enrichment analysis (GSEA) on MC subsets across thirty-nine metabolic pathways using the REACTOME database (Milacic et al., 2024) (Figure 4.2F). The aim of this analysis was to provide a comprehensive overview of the metabolic pathway activity independent of M1/M2 categorization. We initially examined the five major metabolic pathways (i.e., a*mino acid metabolism*, *TCA cycle*, *fatty acid metabolism*, *glycolysis*, and *nucleotide metabolism*) to provide a broad overview of metabolic pathway activity (Figure 4.G). This showed that MCs could be grouped based on their metabolic signatures. *MC3* and *MC6* showed high expression of *glycolysis* and *nucleotide metabolism* but could be distinguished by their differential upregulation of *fatty acid metabolism* (Figure 4.2G). On the other hand, both *MC4* (M2-like subset) and *MC5* showed high expression of *amino acid metabolism*, *TCA cycle*, and *fatty acid metabolism*, but showed differential upregulation of *glycolysis* (Figure 4.2G).

More detailed examination of the 39 metabolic pathways showed further heterogeneity in the MC subsets (Figure 4.2H). For instance, the nominal M1-like MCs, *MC3* and *MC6*, clustered together by hierarchical clustering, but showed vastly different upregulation of metabolic pathways (Figure 4.2H). *MC3* showed upregulation across almost all amino acid metabolic pathways, excluding glutamate and glutamine metabolism, a pathway typically associated with an M2-like phenotype (Jha et al., 2015) (Figure 4.2H). On the other hand, *MC6* showed higher upregulation of almost all glucose metabolism pathways, in addition to the production of mitochondrial-derived ROS and nucleotide metabolic pathways (Figure 4.2H). However, this

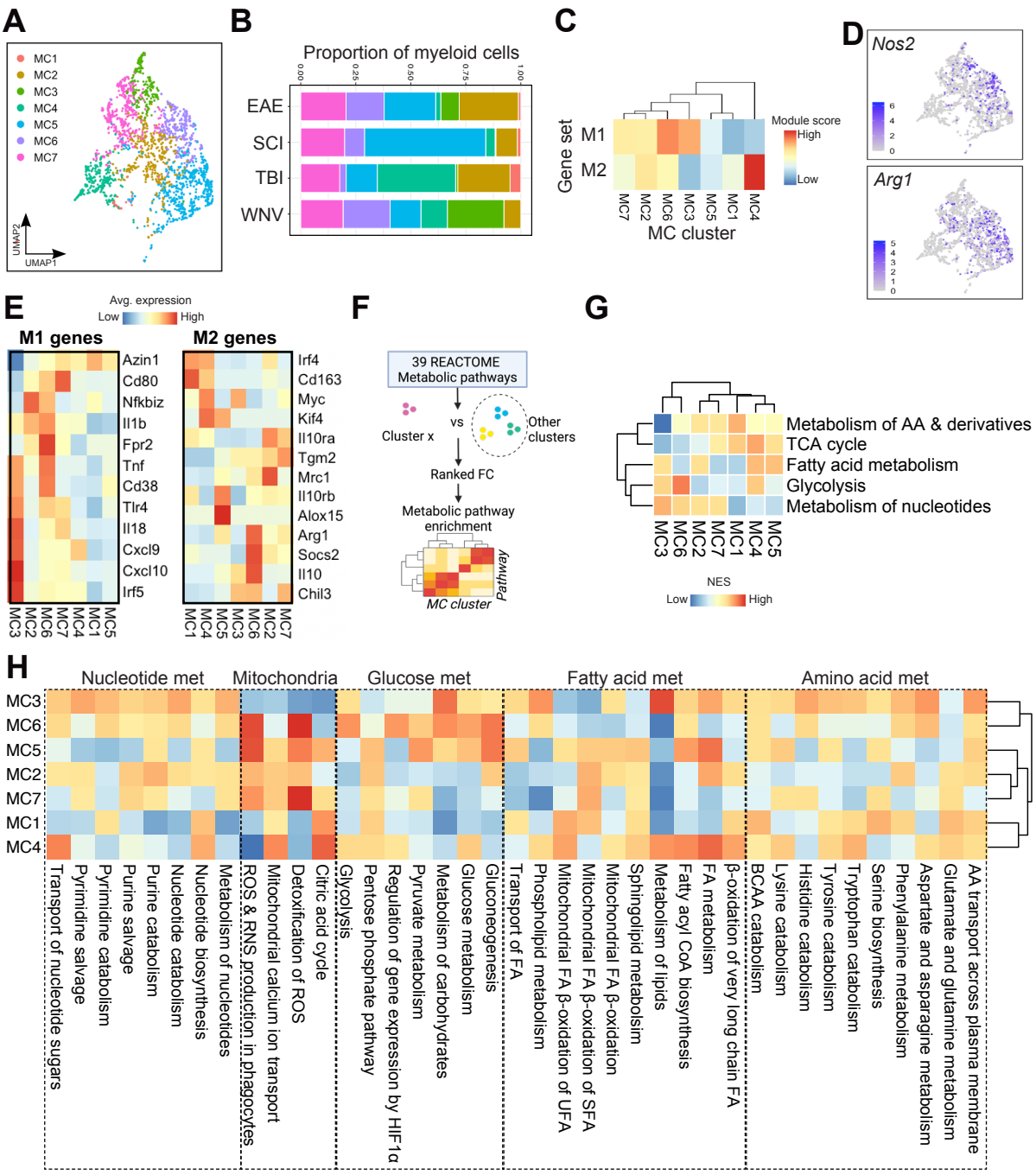
A
MC1
MC2
MC3
MC4
MC5
MC6
MC7
UMAP2
UMAP1
B
Proportion of myeloid cells
0.00
0.25
0.50
0.75
1.00
EAE
SCI
TBI
WNV
C
Gene set
M1
M2
MC7
MC2
MC6
MC3
MC5
MC1
MC4
MC cluster
Module score
High
Low
D
Nos2
Arg1
E
Avg. expression
Low
High
M1 genes
M2 genes
Azin1
Cd80
Nfkbiz
Il1b
Fpr2
Tnf
Cd38
Tlr4
Il18
Cxcl9
Cxcl10
Irf5
Irf4
Cd163
Myc
Kif4
Il10ra
Tgm2
Mrc1
Il10rb
Alox15
Arg1
Socs2
Il10
Chil3
MC3
MC2
MC6
MC7
MC4
MC1
MC5
MC1
MC4
MC5
MC3
MC6
MC2
MC7
F
39 REACTOME Metabolic pathways
Cluster x
vs
Other clusters
Ranked FC
Metabolic pathway enrichment
Pathway
MC cluster
G
Metabolism of AA & derivatives
TCA cycle
Fatty acid metabolism
Glycolysis
Metabolism of nucleotides
MC3
MC6
MC2
MC7
MC1
MC4
MC5
NES
Low
High
H
Nucleotide met
Mitochondria
Glucose met
Fatty acid met
Amino acid met
MC3
MC6
MC5
MC2
MC7
MC1
MC4
Transport of nucleotide sugars
Pyrimidine salvage
Pyrimidine catabolism
Purine salvage
Purine catabolism
Nucleotide catabolism
Nucleotide biosynthesis
Metabolism of nucleotides
ROS & RNS production in phagocytes
Mitochondrial calcium ion transport
Detoxification of ROS
Citric acid cycle
Glycolysis
Pentose phosphate pathway
Regulation of gene expression by HIF1α
Pyruvate metabolism
Metabolism of carbohydrates
Glucose metabolism
Gluconeogenesis
Transport of FA
Phospholipid metabolism
Mitochondrial FA β-oxidation of UFA
Mitochondrial FA β-oxidation of SFA
Mitochondrial FA β-oxidation
Sphingolipid metabolism
Metabolism of lipids
Fatty acyl CoA biosynthesis
FA metabolism
β-oxidation of very long chain FA
BCAA catabolism
Lysine catabolism
Histidine catabolism
Tyrosine catabolism
Tryptophan catabolism
Serine biosynthesis
Phenylalanine metabolism
Aspartate and asparagine metabolism
Glutamate and glutamine metabolism
AA transport across plasma membrane

Figure 4.2 Metabolic heterogeneity of MCs across CNS disease.

(**A**) UMAP pseudocoloured by MC cluster ID. (**B**) Proportion of each MC cluster comprising the total MC pool by each disease. (**C**) Scaled module scores of *in vitro*-derived M1 and M2 gene sets. Hierarchical clustering is performed by column (i.e., MC cluster). (**D**) UMAP pseuodocolored by *Nos2* or *Arg1* expression level. (**E**) Heatmap depicting the expression level of the indicated M1 and M2-associated genes. Hierarchical clustering is performed by row (gene) and column (MC cluster). (**F**) Schematic representing the workflow of metabolic activity analysis for each MC cluster. (**G, H**) Landscape of the activity of different metabolic pathways across MC subsets. Enrichment analysis by gene set enrichment analysis (REACTOME). Colour of each heatmap represents the scaled value calculated with the formula +/-Log_2|NES/FDR|. Hierarchical clustering is performed by column (MC cluster) and row (pathway) (**G**) or row (MC cluster) only (**H**). FDR, false discovery rate; NES, normalised enrichment score.

subset showed minimal expression of fatty acid metabolic pathways, excluding fatty acyl coA biosynthesis (Figure 4.2H), which is required for pro-inflammatory stimulation. Fatty acid synthesis can promote membrane fluidity for phagocytosis and cell migration (Schumann, 2016, Wei et al., 2016), in addition to the production of lipid inflammatory mediators (Yeudall et al., 2022). Both *MC4* and *MC5* showed highest expression of β oxidation of fatty acids (Figure 4.2H), a typical M2-associated pathway (Viola et al., 2019), although they also upregulated fatty acyl coA biosynthesis (Figure 4.2H), suggesting that these pathways can be concurrently upregulated in MCs. Similar to *MC6*, *MC5* also upregulated glucose-associated metabolic pathways and ROS production, although *MC5*, similar to *MC4*, upregulated the TCA cycle (i.e., citric acid cycle) (Figure 4.2H). Mitochondrial metabolic processes were particularly prominent in clusters *MC2*, *MC5*, *MC6*, and *MC7* (Figure 4.2H), suggesting a substantial role of these pathways in their metabolic reprogramming. Collectively, these findings emphasize the metabolic diversity of MC subsets in various CNS disease microenvironments, reflecting a multifaceted interplay between metabolic demands that may dictate function.

4.1.3.3 Metabolic profiles correlate with distinct functional MC programs

To examine the association between the metabolic profiles of MCs and their functions in CNS disease, we manually queried several M1 functional programs, such as *antigen presentation* (93 genes), *inflammatory response* (115 genes), *viral response* (281 genes), *NO production* (147 genes), and *phagocytosis* (209 genes), against gene modules from the Mouse Genome Informatics database. This analysis revealed functional heterogeneity among MCs, with *MC2* and *MC4* being involved in *antigen presentation*, and *MC3* and *MC6* in the *inflammatory response*, further delineating *MC3* as particular to *viral response*, and *MC6* with *NO production* (Figure 4.2A), reflecting their distinct metabolic signatures. Upregulation of these key pathways was confirmed with unbiased GO enrichment analysis (Ashburner et al., 2000, Aleksander et al., 2023), which showed each of these pathways within the top 5 upregulated pathways for the selected subsets (Figure 4.3B). Together, this shows that the seven MC subsets have distinct functional signatures, presumptively related to their separate metabolic requirements in CNS disease.

4.1.3.4 Glycolysis is selectively upregulated across M1-like functions

The findings above suggest that M1-like profiles encompass a wide range of functions, including antigen presentation, phagocytosis, and NO production, regulated by various

metabolic pathways. These pathways may be susceptible to reprogramming by various metabolic inhibitors, leading to an improvement in disease outcomes. Since glycolysis is typically considered to be uniformly associated with the inflammatory activity of MCs, it represents an obvious therapeutic target, but it is important that inhibition does not supress elements important to disease resolution. As it is unclear to what extent glycolysis is used differentially among these functionally-distinct subsets, we examined the association of glycolysis with each of these functional pathways. Mixed model analysis identified that glycolysis was significantly predicted by NO production (coefficient = 0.56, 95% CI [0.50, 0.62], p-value = 1.16×10^{-65}), inflammatory response (coefficient = 0.36, 95% CI [0.31, 0.40], p-value = 8.3×10^{-50}), and phagocytosis (coefficient = 0.43, 95% CI [0.36, 0.50], p-value = 9.7×10^{-34}), but not antigen presentation (coefficient = 0.015, 95% CI [-0.024, 0.055], p-value = 0.445) (Figure 4.4A), indicating a stronger relationship between glycolysis and other M1-like functions compared to antigen presentation. Further supporting this, differential expression analysis of metabolic genes across 39 REACTOME pathways highlighted a skewing of inflammatory MCs (*MC3, MC6*) towards carbohydrate metabolism and amino acid transport (Figure 4.4B). In contrast, antigen-presenting cells (*MC2, MC4*) were associated with the TCA cycle and lipid metabolism (Figure 4.4B). Thus, these results suggest a close coupling of MC metabolism and function, with nominal M1-associated functions, i.e., inflammation and antigen presentation, having distinct metabolic signatures, suggesting nuanced regulation of metabolism that may ordain function and having important implications for therapeutic reprogramming.

4.1.4 Discussion

Despite the widely recognized limitations surrounding *in vitro* experiments, a prolonged lag in pushing towards *in vivo* studies has hindered advances in MC immunometabolism in CNS disease. In this work, we have integrated MC transcriptomic profiles across four CNS diseases at their peak, revealing that glycolysis delineates between pro-inflammatory and antigen-presenting MC populations, emphasizing the metabolic and functional heterogeneity of these cells.

Most metabolism studies have focused on *in vitro* polarized MCs, which considers M1/M2 MCs as the two extremes of a spectrum of activation states (Jha et al., 2015, Liu et al., 2017a, Seim et al., 2019, Viola et al., 2019). However, complex CNS disease microenvironments drive myeloid subsets with functionally distinct characteristics (Spiteri et al., 2021b, Wishart, 2022),

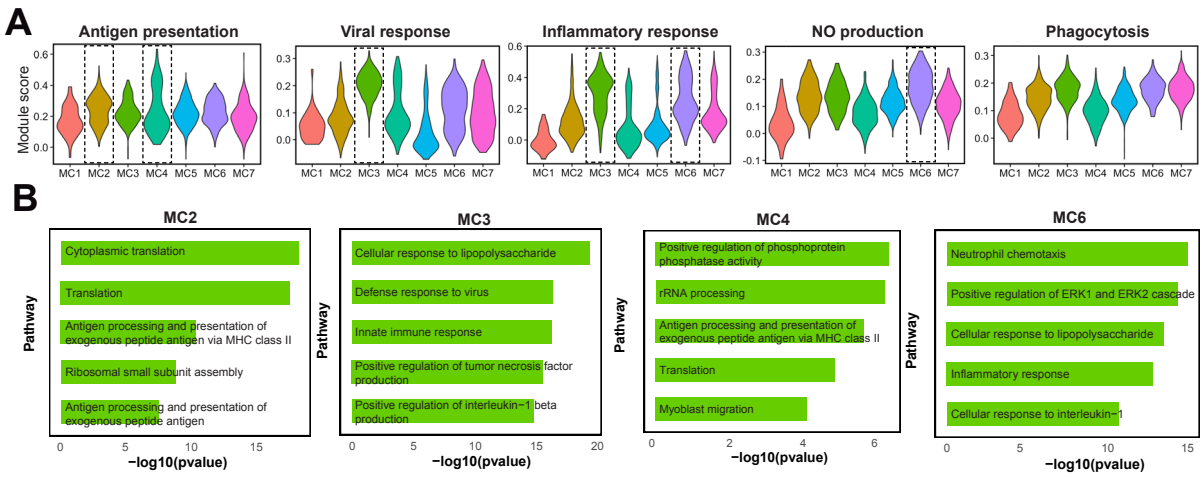
A
Antigen presentation
Viral response
Inflammatory response
NO production
Phagocytosis
Module score
MC1 MC2 MC3 MC4 MC5 MC6 MC7
B
MC2
Cytoplasmic translation
Translation
Antigen processing and presentation of exogenous peptide antigen via MHC class II
Ribosomal small subunit assembly
Antigen processing and presentation of exogenous peptide antigen
MC3
Cellular response to lipopolysaccharide
Defense response to virus
Innate immune response
Positive regulation of tumor necrosis factor production
Positive regulation of interleukin−1 beta production
MC4
Positive regulation of phosphoprotein phosphatase activity
rRNA processing
Antigen processing and presentation of exogenous peptide antigen via MHC class II
Translation
Myoblast migration
MC6
Neutrophil chemotaxis
Positive regulation of ERK1 and ERK2 cascade
Cellular response to lipopolysaccharide
Inflammatory response
Cellular response to interleukin−1
Pathway
−log10(pvalue)

Figure 4.3 MCs adopt distinct metabolic profiles across CNS disease.

(**A**) Module scores for the indicated functional pathways across MC subsets. Dotted box indicates population(s) with the highest module scores. (**B**) Bar graph depicting the top five significantly upregulated gene ontology (GO) biological processes upregulated by the indicated MC subsets ($p<0.05$) associated with genes upregulated greater than two-fold relative to every other MC cluster.

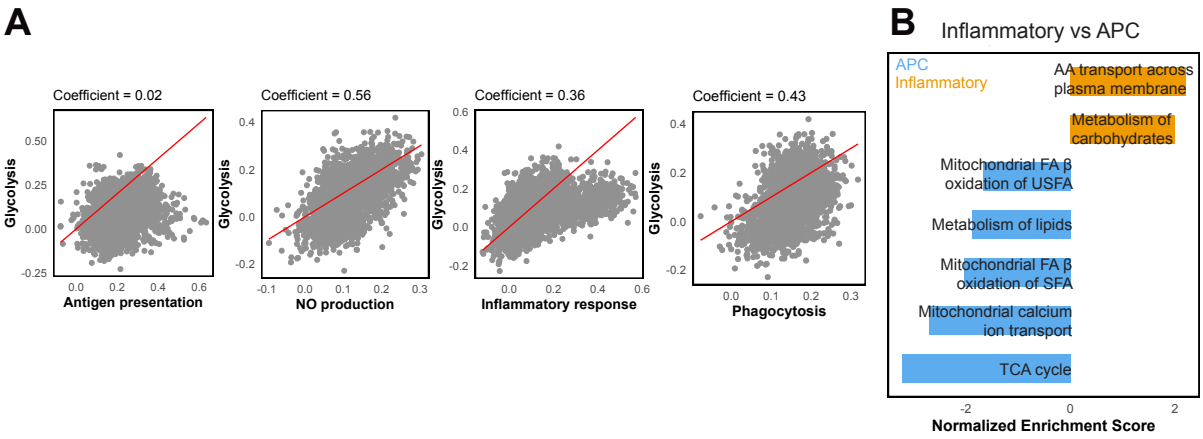
A
Coefficient = 0.02
Glycolysis
Antigen presentation
Coefficient = 0.56
NO production
Coefficient = 0.36
Inflammatory response
Coefficient = 0.43
Phagocytosis
B
Inflammatory vs APC
APC
Inflammatory
AA transport across plasma membrane
Metabolism of carbohydrates
Mitochondrial FA β oxidation of USFA
Metabolism of lipids
Mitochondrial FA β oxidation of SFA
Mitochondrial calcium ion transport
TCA cycle
Normalized Enrichment Score

Figure 4.4 Antigen presenting and inflammatory MCs have distinct metabolic requirements across CNS disease.

(**A**) Mixed-effects linear models, which included random effects to account for variations across studies and meta-clusters, evaluating the relationship between glycolysis and the indicated functional pathways. The red line indicates the predicted values of a one-to-one correlation. (**B**) Gene set enrichment analysis showing enriched metabolic pathways in inflammatory (*MC3*, *MC6*) versus antigen-presenting (*MC2*, *MC4*) MCs. Upregulated pathways (orange) indicate pathways upregulated in inflammatory MCs, whereas downregulated pathways (blue) indicate pathways upregulated in antigen-presenting MCs.

challenging the relevance of the M1/M2 paradigm to CNS disease. Our work demonstrates that MCs from disease models of MS, SCI, TBI, and viral encephalitis cannot be accurately captured by the rigid M1/M2 polarization framework. Nonetheless, we observed that each CNS disease exhibited skewing towards either an M1 or M2 state. MCs derived from WNV and EAE displayed predominantly M1-associated signatures, while MCs from TBI and SCI showed more M2-associated signatures. This could be attributable to observations that MCs from EAE and WNV play more pathogenic roles in the acute stages of disease, whereas MCs from SCI and TBI are more involved in wound healing (Spiteri et al., 2021b). However, detailed examination of genes associated with M1 or M2 gene sets revealed significant variability, suggesting multiple transcriptionally and functionally heterogeneous subsets. Overall, we argue that the current M1/M2 paradigm fails to capture the metabolic and functional heterogeneity of MCs in acute CNS diseases.

While diseases could not be grouped by pure M1 or M2 polarization signatures, *MC3* and *MC6* showed the highest transcriptional similarity to the M1-like state. Nevertheless, these populations displayed clear distinctions even though both upregulated inflammatory response pathways: *MC3* was strongly linked to the anti-viral response, while *MC6* was more strongly linked to NO generation. These functional differences were also reflected metabolically, as *MC3* had high nucleotide and amino acid metabolism scores, while *MC6* had higher mitochondrial ROS production and glycolysis scores. Additionally, *MC6* displayed increased expression of genes related to regulation by the transcription factor HIF1α, which has been shown to interact with the NO-producing enzyme iNOS in a positive feedback loop to upregulate aerobic glycolysis in response to IFN-γ *in vitro* (Braverman and Stanley, 2017). Both *MC3* and *MC6* were prevalent in WNV, consistent with the anti-viral response, critical to combat progressive CNS infection and the concurrent NO production by MCs, which is a major contributor to immunopathology that ultimately results in neuronal damage and death (Getts et al., 2008, Getts et al., 2012, Terry et al., 2015). In EAE, the "NO-producing" *MC6* was more prevalent. Similar NO-producing MC states have been identified throughout both the acute and chronic stages of EAE (Locatelli et al., 2018, Giladi et al., 2020), and blocking glycolysis—a pathway enriched in *MC6*—markedly decreased the number of $iNOS^+$ MCs in the CNS and improved overall clinical outcomes (Zahoor et al., 2022). Interestingly, *MC6* also expressed M2-associated genes, such as *Il10* and *Arg1*. This may be linked to the finding that, in response to local inflammatory signals originating from astrocytes, inflammatory $iNOS^+$ MCs can transition into anti-inflammatory $Arg1^+$ MCs (Locatelli et al., 2018). Since arginase depletes

the substrate (L-arginine) for NO production, the expression of arginase and iNOS are functionally mutually exclusive. Consistent with this, the phenotypic evolution of $iNOS^+$ MCs to $Arg1^+$ MCs coincided with the development and resolution of neuroinflammatory lesions (Locatelli et al., 2018). These findings highlight the complex interplay between MC metabolism and inflammatory function, which seems to be specialized rather than generic.

The expression of lipid metabolism-associated genes is particularly relevant in the context of CNS diseases with mechanical and inflammatory damage, such as EAE, SCI and TBI, due to the efferocytosis of lipid-rich structural cells, such as oligodendrocytes. Correspondingly, we identified *MC5*, which was prevalent across SCI, TBI, and EAE. This population showed a distinctive metabolic profile associated with an increased lipid metabolism signature (e.g., fatty acid oxidation), in addition to the expression of genes related to glucose metabolism and amino acid metabolism. Lipid scavenging in the CNS is associated with increased expression of the lipid scavenger receptor CD36 (Beuker et al., 2022, Woo et al., 2016), increased activity of fatty acid oxidation (Zhang et al., 2019c), and activation of the sterol pathway (Noelia et al., 2009). While beneficial in the acute stages of injury, chronic lipid scavenging can lead to progressive lipid overload and foam cell formation (Berghoff et al., 2021, Bogie et al., 2020, Berghoff et al., 2022), which ultimately exacerbates inflammation, increases oxidative stress, and hinders oligodendrocyte regeneration. Monocytes derived from the blood of patients with relapsing-remitting MS show inflammation-induced reduction in lipid-sensing nuclear receptors, such as peroxisome proliferator-activated receptors, was associated with foam cell formation via its impact on lipid metabolism, resulting in a negative impact on MS lesion progression (Wouters et al., 2020). Correspondingly, we observed that in addition to its lipid metabolic profile, *MC5* also upregulated genes associated with ROS generation, suggesting an inflammatory profile that may ultimately contribute to secondary damage of structural cells. This emphasizes the finding that M2-associated metabolic pathways, such as fatty acid oxidation, is likely involved in a tightly-regulated interplay between intracellular lipid stores and pro- or anti-inflammatory states of myeloid cells during CNS remyelination or demyelination.

Glycolysis has traditionally been associated with M1-polarisation and inflammatory function (Viola et al., 2019). However, we found that glycolysis was not uniformly linked to all M1 functions. Glycolysis had the weakest association with antigen presentation relative to other pathways such as NO production, the inflammatory response, and phagocytosis. Instead, MCs

with high antigen-presenting scores (*MC2*, *MC4*) were enriched in fatty acid oxidation, lipid metabolism, and the TCA cycle relative to inflammatory MCs (*MC3*, *MC6*), which were more enriched in amino acid transport and carbohydrate metabolism, such as glycolysis. The lack of a glycolytic signature in antigen-presenting MCs aligns with findings that monocytes decrease glycolytic activity and increase mitochondrial dependence as they increase their expression of antigen-presenting and co-stimulatory molecules, such as MHC-II and CD86 (Adamik et al., 2022). Blocking the ETC, essential to OXPHOS, led to apoptosis during DC differentiation and partially prevented the development of an antigen-presenting DC phenotype (Zaccagnino et al., 2012, Del Prete et al., 2008). Thus, in an inflammatory environment, there is a metabolic co-ordination that includes the downregulation of glycolysis and upregulation of mitochondrial OXPHOS, collectively promoting the differentiation of monocytes into an antigen-presenting state. This may be distinct from other functional pathways, in which rapid energy generation provided by glycolysis may support production of inflammatory mediators derived from amino acids, such as NO generation from L-arginine. Given that antigen-presenting and inflammatory MCs can play distinct and often opposing roles in CNS diseases, such as in viral encephalitis (Spiteri et al., 2021b), the potential differential employment of glycolysis between these two functional states may enable a targeted therapeutic approach that can optimize viral clearance while minimizing collateral inflammatory damage. However, it may be important to note that inhibition of glycolysis, while being potentially advantageous in viral encephalitis, could have undesirable effects in MS.

The observed heterogeneity of MCs across CNS diseases can be attributed to several factors. Firstly, ontogenic differences between MC states may exist. Although we differentiated MCs from resident microglia and border-associated macrophages using cell type-specific gene expression patterns, these cells can upregulate or downregulate these genes under inflammatory conditions, potentially confounding their accurate identification (Jordão et al., 2019, Masuda et al., 2019, Krasemann et al., 2017, Friedman et al., 2018, Chen et al., 2020, Werner et al., 2020, Spiteri et al., 2021a). This is crucial in metabolic profiling since MCs have vastly different metabolic underpinnings compared to their tissue-resident counterparts (Li et al., 2022b, Heieis et al., 2023, Li et al., 2022a). Secondly, the timing of investigation matters. MCs were evaluated at different timepoints depending on the disease: SCI (dpi 1, 3, and 7), TBI (dpi 4), EAE (disease onset), and WNV (dpi 5 & 7). Although these timepoints correspond to peak monocyte infiltration in these diseases (Beck et al., 2010, Kigerl et al., 2006, Milich et al., 2019, Hsieh et al., 2014, Kigerl et al., 2009, Zhu et al., 2015, Spiteri et al., 2022a), the cellular

and molecular environments change significantly over the disease course, influencing MC function. Additionally, anatomical localization, such as different brain or spinal cord regions, can induce vastly different phenotypes (Jordão et al., 2019, Locatelli et al., 2018, Ivan et al., 2021). For instance, in SCI, the infiltration route of monocytes can determine whether they adopt a 'protective' or 'detrimental' phenotype, as protective monocytes infiltrate the brain through the choroid plexus, whereas potentially damaging monocytes enter through the spinal cord leptomeninges (Shechter et al., 2013). Finally, MC states are fluid. For example, in EAE, MCs can initially adopt a toxic $iNOS^+$ state but later transition into an $arginase^+$ state resembling an M2-like phenotype (Locatelli et al., 2018), paralleling the lesion microenvironment transition from active to resolved. The M1/M2 model does not accurately represent this plasticity or the reversibility of MC phenotypes, which is crucial for understanding their roles in CNS diseases.

This work has several limitations. We focused on acute stages of inflammatory CNS diseases, neglecting chronic stages of disease and other chronic neurological diseases such as Alzheimer's and Parkinson's disease, although these diseases typically have minimal contributions from inflammatory monocytes (Spiteri et al., 2021b). Furthermore, metabolic pathway activity is regulated by a variety of factors, such as metabolic protein expression levels, enzymatic activity, and post-transcriptional and post-translational mechanisms. Given we assessed metabolic activity by mRNA expression, our analysis may not accurately reflect these pathways, although metabolic mRNA expression has been shown to correlate highly with the expression of their respective proteins (Schwanhäusser et al., 2011), which may minimise this limitation. Nonetheless, it is important to validate these findings using additional single-cell methods. Metabolic analysis by flow or mass cytometry – which measures single-cell metabolism indirectly by examining the expression of rate-limiting enzymes, nutrient transporters, and transcription factors across various metabolic pathways (Ahl et al., 2020, Levine et al., 2021, Hartmann et al., 2021) – may enable a more comprehensive picture of metabolic pathway activity at the protein level. In this context, these approaches are more informative than gold-standard metabolic techniques such as metabolomics and extracellular flux assays, which produce population averages rather than single-cell measurements.

Together, our approach integrates data across four acute CNS diseases to provide a comprehensive picture of MC metabolic and functional heterogeneity. This work illustrates for the first time that the *in vitro*-derived M1/M2 paradigm is inadequate for characterising MCs

in the CNS. Instead, we reveal a complex metabolism-function relationship where functionally distinct MCs are tightly regulated by specific metabolic pathways. This nuanced understanding may open new therapeutic avenues, enabling the selective regulation of MC functional states through targeted metabolic pathways. This approach holds the potential to intervene even before monocytes infiltrate the brain, offering a proactive strategy for managing acute inflammatory CNS disease.

Chapter 5: Results III

5.1 Deep metabolic profiling of immune cells by spectral flow cytometry – a comprehensive validation approach

The following chapter is formatted into a manuscript.

5.1.1 Overview

Immunometabolism is a rapidly expanding field that investigates the intimate link between cellular metabolism and function. While methodologies such as extracellular flux assays and metabolomics provide valuable insights into population dynamics, they lack individual cell-specific information. This can mask considerable heterogeneity within a population and thus function. Cytometric approaches, using spectral or conventional flow cytometry, enable the investigation of metabolism at the single-cell level in phenotypically defined cells identified simultaneously. These techniques provide a surrogate measurement of metabolism by the expression of key rate-limiting enzymes, signalling molecules, transporters, transcription factors and dyes staining for metabolic substrates. Here, we present an in-depth metabolic panel designed to study the metabolism of murine leukocytes using spectral flow cytometry, comprising commercially available antibodies with cross-species reactivity that target a range of key metabolic proteins. This provides insight into eight critical metabolic pathways in a single spectral cytometry panel and includes glycolysis, the TCA cycle, the ETC, HIF1-α signalling, amino acid uptake, fatty acid synthesis and oxidation, and NO production. All metabolic markers were meticulously validated using specific reagents to inhibit or amplify relevant metabolic pathways. Using this approach, we further identify a unique autofluorescent cellular signature associated with glycolysis, allowing measurement of this pathway without perturbation by antibody staining. Altogether, we have developed an essential research tool that enables future researchers to better link metabolism and cellular function, thereby informing more detailed understanding of immunometabolic modulation in disease.

5.1.2 Introduction

Cellular metabolism is intimately tied to function (Buck et al., 2017). Intermediates of metabolic processes activate various signalling pathways, act as substrates for enzymatic reactions and also regulate gene expression, thereby dictating effector functions of cells. They can also act directly as signalling molecules to induce both pro- and anti-inflammatory

functions. This is of particular interest to immunologists, as it has been shown that metabolic reprogramming is required for immune cell differentiation, function and fate. For example, metabolic reprogramming of macrophages and T cell subsets towards anti-inflammatory states has been explored in various disease contexts, *e.g.,* MS (Kelly et al., 2015, Kopf et al., 2007, Gross et al., 2015, Zahoor et al., 2022). These strategies highlight the practical importance of studying cellular metabolism, which has significantly advanced our understanding of immune cell biology and opened new avenues for treatment.

Conventional methods of probing cellular metabolism rely on extracellular flux assays (e.g., Seahorse) or metabolomics. However, these techniques have several limitations. Firstly, these bulk-based assays require homogenous samples, such as sorted cells or cell lines, making it difficult to acquire meaningful data from heterogenous cell populations. Secondly, they require substantial numbers of cells which limits the analysis of rare cell populations. Thirdly, the Seahorse assay interrogates only a select few metabolic pathways; several other pathways important to cellular metabolism are not captured. Finally, the Seahorse assay is an *in vitro* culture system that does not replicate the complex, heterogeneous *in vivo* environment of naturally functioning immune cells.

Metabolic status can also be estimated by the autofluorescence of certain biological molecules, such as NADH. NADH is an intracellular co-enzyme that is a key electron carrier in cellular energy metabolism. In its reduced form as NADH, this molecule exhibits autofluorescence, whereas the oxidized NAD^+ does not (Chance, 1954, Chance and Thorell, 1959). During glycolysis, NAD^+ is reduced to NADH, whereas in the ETC, NAD^+ is produced. Thus, a shift in cellular metabolism towards glycolysis and/or lower mitochondrial respiration corresponds to higher NADH autofluorescence intensity (Schaefer et al., 2019), and can be used to estimate glycolytic status. However, this method has primarily been used in imaging approaches and has not been applied to the study of cellular metabolism by single-cell techniques like flow cytometry (Schaefer et al., 2019). The recent availability of full spectrum cytometry to detect cellular autofluorescence should enable more precise identification of specific autofluorescent signatures linked to unique metabolic states using flow cytometry.

Advances in single-cell technologies have led to the development of several pioneering approaches that overcome the shortcomings of bulk analysis, enabling the analysis of metabolic profile and phenotypic identity simultaneously. The first of these methods leverages scRNA-seq of a wide array of expressed genes, laying out a comprehensive map of potential metabolic

changes at the mRNA level. The second technique, embodied by cytometric methods such as single-cell metabolic regulome profiling (scMEP) (Hartmann et al., 2021) and Met-Flow (Ahl et al., 2020), quantifies rate-limiting enzymes, nutrient transporters, and transcription factors as proxies for different metabolic pathways. These approaches allow for the indirect assessment of metabolic pathway activity at the single-cell level. An additional cytometric approach, single cell energetic metabolism by profiling translation inhibition (SCENITH), combines metabolic inhibitors and protein synthesis quantification to assess the metabolic dependencies on glucose catabolism, mitochondria, and fatty acid/amino acid oxidation in immune cells at the single-cell level (Argüello et al., 2020). These approaches have yielded insights into the relationship between metabolism and function across several cell types (Adamik et al., 2022, Levine et al., 2021, Ahl et al., 2020, Hartmann et al., 2021, Geeraerts et al., 2021, Heieis et al., 2023), thus demonstrating the versatility and reliability of examining cellular metabolism by flow cytometry.

However, the application of cytometry in metabolic studies faces significant challenges, primarily due to the lack of standardized methods for the optimisation and analysis of metabolic targets. The validation of metabolic targets as reliable representatives of their respective pathways has generally focused only on the upregulation of glycolysis or OXPHOS with immune cell activation, often combined with readouts from extracellular flux assays, generally focused on one cell type (Hartmann et al., 2021, Ahl et al., 2020). This approach does not adequately cover other metabolic pathways (e.g., fatty acid metabolism, amino acid metabolism) and may not correlate with single-cell measurements of metabolic proteins, as these assays are limited to bulk measurements. In addition, most metabolic panels necessitate expensive and time-consuming custom conjugation of heavy metals or fluorophores (Adamik et al., 2022, Levine et al., 2021, Ahl et al., 2020, Hartmann et al., 2021, Geeraerts et al., 2021, Heieis et al., 2023), thus restricting their broad accessibility.

In light of these impediments, our study presents the first spectral cytometric metabolic approach that incorporates autofluorescence information to profile immunometabolism. We present a carefully optimized antibody panel for assessing metabolic pathway activity using commercially available reagents that are cross-reactive with other species. A range of metabolic inhibitors was used to confirm the validity of our approach, thereby providing a valuable research tool for future investigators to profile cellular metabolism.

5.1.3 Results

Given the limitations of existing tools to study metabolism at a single-cell level, we developed a high-dimensional spectral cytometry panel to profile metabolic proteins in combination with specific immune cell markers. With the potential to include various additional immune and functional markers, this proof-of-principle panel comprises 12 immune cell identification markers and 8 metabolic markers, including rate-limiting enzymes, nutrient transporters, and transcription factors that have roles in glycolysis, the TCA cycle, the ETC, HIF1α signalling, amino acid uptake, fatty acid synthesis and oxidation, and NO production (Table 5.1). The selected metabolic antibodies are cross-reactive, enhancing their utility for cross-species analysis. Positive staining for each of the metabolic labels was determined relative to both the FMO and isotype control (Supplementary Figure 5.1), and the optimal concentrations for each of the antibodies are shown in Table 2.3.

5.1.3.1 Validation of metabolic targets involved in central carbon metabolism

Carbon metabolism is a central component of cellular metabolism. The uptake of glucose from the extracellular space feeds into various metabolic pathways, including glycolysis, HIF1-α signalling, the TCA cycle, and the ETC (Figure 5.1A, 5.1B).

Glyceraldehyde 3-phosphate dehydrogenase (GAPDH), a key enzyme in the glycolysis pathway responsible for catalysing the sixth step of glycolysis, was selected as a readout of glycolysis. This enzyme plays a crucial role in the conversion of glyceraldehyde 3-phosphate to 1,3-bisphosphoglycerate. Interrogation of staining patterns demonstrated that the majority of cells (>97%) express GAPDH relative to the FMO control (Figure 5.1C). To confirm that GAPDH is an accurate representation of glycolysis, mouse BM cells were stimulated with LPS and IFN-γ in the presence or absence of 2-DG, a competitive inhibitor of hexokinase 1, which is an upstream rate-limiting enzyme in the glycolysis pathway (Figure 5.1D). Interestingly, there was no significant increase in GAPDH expression with IFN-γ plus LPS stimulation (Figure 5.1E); however, GAPDH expression was significantly reduced with glycolysis inhibition by 2-DG in monocytes (Figure 5.1E). Notably, however, 2-DG inhibition did not affect GAPDH expression in T cells (Figure 5.1E). This could indicate that 2-DG does not perturb T cell glycolysis under these baseline conditions and that alternative reagents to stimulate glycolysis are needed to validate GAPDH as a reliable readout of glycolysis in this cell type. Further confirming that GAPDH is a reliable readout of glycolysis in monocytes, we

126 **Table 5.1 Metabolic targets used in this study compared to previously developed metabolic panels**

Target	Name	Pathway	Function in pathway	Inflammatory/anti-inflammatory?	Included in panels?				
					Hartmann et al. (2021)	Levine et al. (2021)	Ahl et al. (2020)	Miller et al. (2017)	Core panel[1,]
GAPDH	Glyceraldehyde 3-phosphate dehydrogenase	Glycolysis & fermentation	Glycolytic enzyme catalyzing the conversion of glyceraldehyde 3-phosphate to 1,3-bisphosphoglycerate	*Inflammatory* (increased dependence on glycolysis)	x	x		x	x
IDH1	Isocitrate dehydrogenase	TCA cycle	TCA break point enzyme, conversion of isocitrate to oxoglutarate	*Inflammatory* (Expression shown to be related to break in TCA cycle that occurs in M1 macrophages) (Jha et al., 2015)	x		x	x	x
CPT1A	Carnitine Palmitoyltransferase 1A	Fatty acid oxidation	Fatty acid shuttling into mitochondria	*Anti-inflammatory* (FA oxidation = reduced FA synthesis)	x		x		x
ACAC/ACC1	Acetyl-CoA carboxylase	Fatty acid synthesis	Acetyl-CoA carboxylase/ fatty acid synthesis	*Inflammatory* (FA synthesis = more inflammatory FA, e.g., prostaglandins)	x		x		x

1 Core metabolic panel of 10 metabolic proteins suggested by Cell Metabolism review (2020) ARTYOMOV, M. N. & VAN DEN BOSSCHE, J. 2020. Immunometabolism in the single-cell era. *Cell metabolism,* 32**,** 710-725.

CD98	CD98	Amino acid metabolism	Essential amino acid transporter	Context dependent	x	x			x
HIF1-α	*Hypoxia-inducible factor 1-alpha*	Metabolic regulation/signaling	Hypoxia and inflammation-induced transcription factor	*Inflammatory*	x	x			x
iNOS	Inducible nitric oxide synthase	Amino acid metabolism	NO production, initial rate-limiting enzyme involved in arginine degradation	*Inflammatory*					
CytoC	Cytochrome C	Electron transport chain	Essential electron carrier	*Anti-inflammatory* (Increased dependence on OXPHOS)	x	x		x	x

127

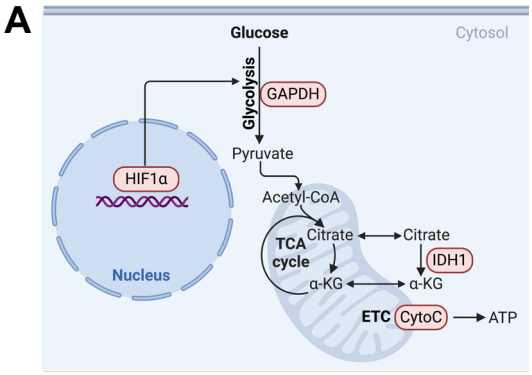

B

Target	Localisation	Pathway
GAPDH	Cytosol	Glycolysis
HIF1α	Nucleus	HIF1α signaling
IDH1	Cytosol	Tricarboxylic acid cycle
CytoC	Mitochondria	Electron transport chain

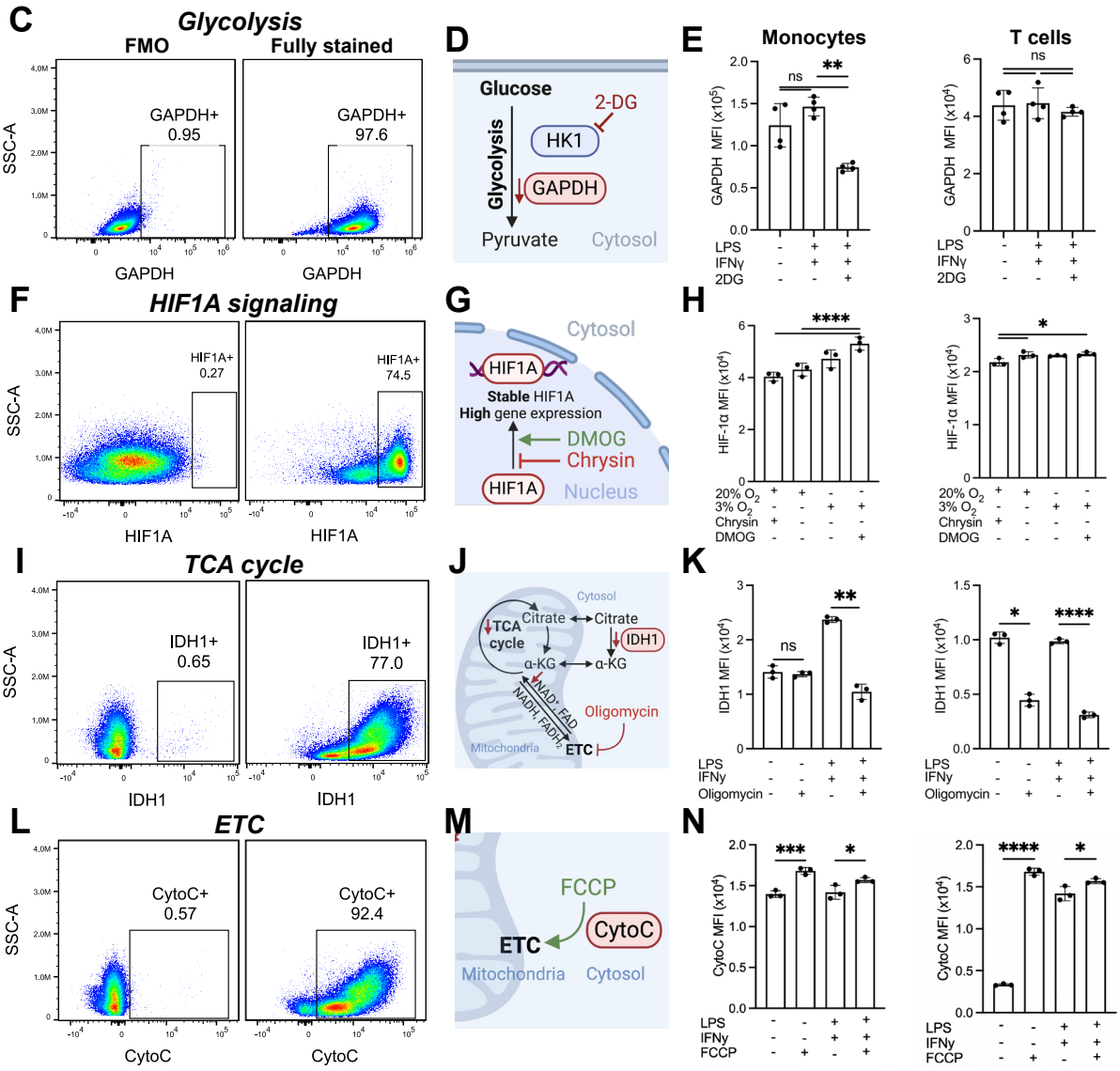

Figure 5.1 Pathway-specific validation of metabolic targets involved in central carbon metabolism.

(**A**) Schematic of central carbon metabolic targets for flow-based analysis. (**B**) Summary of central carbon metabolic targets. (**C**, **F**, **I**, **L**) Dot plots showing positive fluorescent staining of the indicated metabolic targets on cultured $CD45^+$ bone marrow cells relative to the FMO control. (**D**, **G**, **J**, **M**) Mechanistic schematics showing metabolic pathway stimulation (green) or inhibition (red) by the indicated drugs of glycolysis (**D**), HIF1α signalling (**G**), TCA cycle (**J**) and the ETC (**M**). (**E, H, K, N**) Change in median fluorescence intensity (MFI) of positively-stained monocytes and T cells under various culture conditions for GAPDH (**E**), HIF1α (**H**), IDH1 (**K**), and cytochrome C (**N**). Statistics were calculated using RM one-way ANOVA with Tukey's correction for multiple comparisons (**E**, **H**) or paired t-test (**K**, **N**). Each data point represents cells isolated from a different animal, with data points matched across groups within each experiment. Data shows one independent experiment with 3-4 biological samples per group performed in technical duplicate. See methods section 2.5.3 for detailed experimental conditions.

additionally stimulated murine BM cells in glucose-deprived media to evaluate the impact of substrate depletion on GAPDH expression (Supplementary Figure 5.2). This condition, known to reduce glycolysis, resulted in a significant reduction of GAPDH expression in both monocytes and T cells.

We next aimed to evaluate HIF1α signalling, a master metabolic regulator induced during hypoxia. The transcription factor HIF1α is closely linked to glucose metabolism: a disrupted TCA cycle, often seen with inflammatory stimulation, leads to succinate accumulation, which stabilizes HIF1α (Tannahill et al., 2013). Myeloid HIF1α is also a critical regulator of glycolytic metabolism (Lin and Simon, 2016). HIF1α staining demonstrated that this marker was detectable in $CD45^+$ cells and separated well from the FMO control (Figure 5.1F). To validate the induction of HIF1α under hypoxic conditions, BM cells were cultured in either 20% oxygen (normoxia) or 3% oxygen (hypoxia), supplemented with Chrysin, which destabilizes HIF1α, or DMOG, which stabilizes HIF1α expression in the nucleus (Figure 5.1G). Consistent with previous studies, we found that HIF1α was significantly induced under hypoxic conditions (3% O_2) with DMOG, compared to high oxygen conditions (20% O_2) with or without Chrysin in monocytes and, to a lesser extent, in T cells (Figure 5.1H). This demonstrates that HIF1α is a reliable readout of hypoxia-induced metabolic signalling in both T cells and monocytes.

We next aimed to validate markers of OXPHOS, which comprises both the TCA cycle and the ETC. In macrophages, IDH1, an enzyme responsible for converting isocitrate into α-ketoglutarate, has been identified as a critical breaking point in the TCA cycle during inflammatory stimulation (Jha et al., 2015). Therefore, we selected IDH1 as a representative marker of the TCA cycle. Positive staining for this marker showed clear separation from the FMO control (Figure 5.1I). To confirm that IDH1 expression indicates a break in the TCA cycle, we stimulated cells with LPS and IFN-γ in the presence or absence of oligomycin, a known inhibitor of OXPHOS (Figure 5.1J). Notably, oligomycin did not affect IDH1 expression in unstimulated monocytes but significantly reduced IDH1 expression in IFN-γ plus LPS-stimulated monocytes (Figure 5.1K). This supports the notion that IDH1 is a breaking point in the TCA cycle for IFN-γ plus LPS-stimulated macrophages, with inhibition of this pathway being most pronounced under inflammatory polarization. For T cells, we observed that oligomycin-induced inhibition of this pathway was independent of inflammatory stimulation (Figure 5.1K), suggesting that IDH1 may have alternate roles in adaptive immune

cells. Nonetheless, our validation approach demonstrates that IDH1 is a reliable indicator of OXPHOS in both monocytes and T cells.

The ETC, a crucial component of OXPHOS, is central to electron transfer and ATP generation within a cell. We selected cytochrome C, which functions as an essential electron carrier by transferring electrons, thereby facilitating ATP production. Examination of staining patterns demonstrated clear separation from the FMO control (Figure 5.1L). To evaluate whether cytochrome C is a reliable representative of the ETC, we used FCCP, which is a potent uncoupler of mitochondrial OXPHOS that results in uninhibited electron flow through this pathway (Figure 5.1M). Supporting the reliability of cytochrome C, we found that its expression significantly increased in both monocytes and T cells with FCCP treatment (Figure 5.1N). Notably, this effect was less pronounced under inflammatory stimulation with LPS and IFN-γ (Figure 5.1N), consistent with other studies indicating that the ETC is less active under inflammatory stimulation compared to alternative (M2) activation (Van den Bossche et al., 2016).

5.1.3.2 Validation of metabolic targets involved in fatty acid and amino acid metabolism

Fatty acid metabolism includes a major anabolic and catabolic pathway (Figure 5.2A, 5.2B). The catabolism of fatty acids occurs primarily through β-oxidation in the mitochondria, which feeds into the TCA cycle to generate ATP. Conversely, fatty acid synthesis is an anabolic pathway that generates fatty acids through various biochemical processes. For amino acid metabolism, we evaluated CD98, a surface membrane protein that facilitates uptakes of large neutral amino acids such as tryptophan, leucine, and valine, into the cell, and NO production (iNOS), a process which metabolizes the amino acid L-arginine into NO (Figure 5.2A, 5.2B).

The rate-limiting enzyme CPT1A was used as a marker of fatty acid oxidation. CPT1A showed reliable staining relative to the FMO control (Figure 5.2C). To validate this marker, cells were cultured with the fatty acid palmitate, with or without etomoxir, an inhibitor of CPT1A (Figure 5.2D). Given that high concentrations of etomoxir produce off-target effects, a low dose of etomoxir (3 μM) was used, which has been shown specifically to inhibit fatty acid oxidation (Divakaruni et al., 2018). Furthermore, since high levels of glucose in culture media can skew a preference for glucose as an energy source (Adamik et al., 2022), we used 2-DG to inhibit glucose metabolism, thereby promoting utilisation of fatty acids over glucose. We found that monocytes were susceptible to fatty acid oxidation inhibition, leading to a downregulation of

CPT1A (Figure 5.2E), while T cells did not upregulate CPT1A with glycolysis inhibition and were unaffected by etomoxir. Interestingly, however, glucose supplementation alone led to a 50% decrease in the number of CPT1A-expressing splenic T cells cultured with palmitate, but this was not statistically significant in monocytes (Supplementary Figure 5.3). This indicates that glucose availability determines fatty acid oxidation activity in T cells, which may be organ-specific. Despite this, our results suggest that CPT1A is a reliable indicator of fatty acid oxidation in both monocytes and T cells, although this pathway is significantly induced in these cell types under different culture conditions. The negligible effect of etomoxir on T cell fatty acid oxidation contrasts with other studies. However, the previously reported effects of etomoxir on this pathway in T cells and other immune cells have since been attributed to the off-target effects of the drug when used at high doses (> 3 uM) (Yao et al., 2018, Divakaruni et al., 2018, Raud et al., 2018).

Next, we used ACAC as a marker of fatty acid synthesis, given its role as a rate-limiting enzyme catalysing the conversion of acetyl-coA to produce malonyl-coA, a substrate for fatty acid biosynthesis. This marker showed reliable staining relative to the FMO control (Figure 5.2F). Since fatty acid synthesis is upregulated in macrophages under inflammatory conditions, we stimulated BM cells with LPS and IFN-γ, with or without the fatty acid synthase inhibitor C75 at doses known to inhibit fatty acid synthesis (Figure 5.2G, 5.2H) (Rosas-Ballina et al., 2020, Bidault et al., 2021, Rae and Graham, 2008). ACAC expression showed a significant dose-response relationship, with its MFI decreasing with increasing C75 concentrations in both monocytes and T cells, validating its reliability as a marker of fatty acid synthesis across cell types (Figure 5.2H). However, using the ACAC inhibitor TOFA, which directly inhibits this enzyme, only affected ACAC expression at high doses (40 μM) (Supplementary Figure 5.3). This suggests that ACAC activity, which is regulated by its phosphorylation, may not be regulated by direct inhibition alone, whereas C75 globally reduces fatty acid synthesis and ACAC phosphorylation.

Investigation of large-neutral amino acid uptake capacity by CD98 staining demonstrated that this molecule was lowly expressed under homeostatic conditions relative to the FMO control (Figure 5.2I). To evaluate whether this marker is an accurate readout of amino acid uptake capacity, we stimulated BM cells with LPS and IFN-γ in culture media depleted of amino acids or supplemented with amino acids at levels in standard culture media (Figure 5.2J). This demonstrated that the proportion of CD98-expressing monocytes was modestly, but

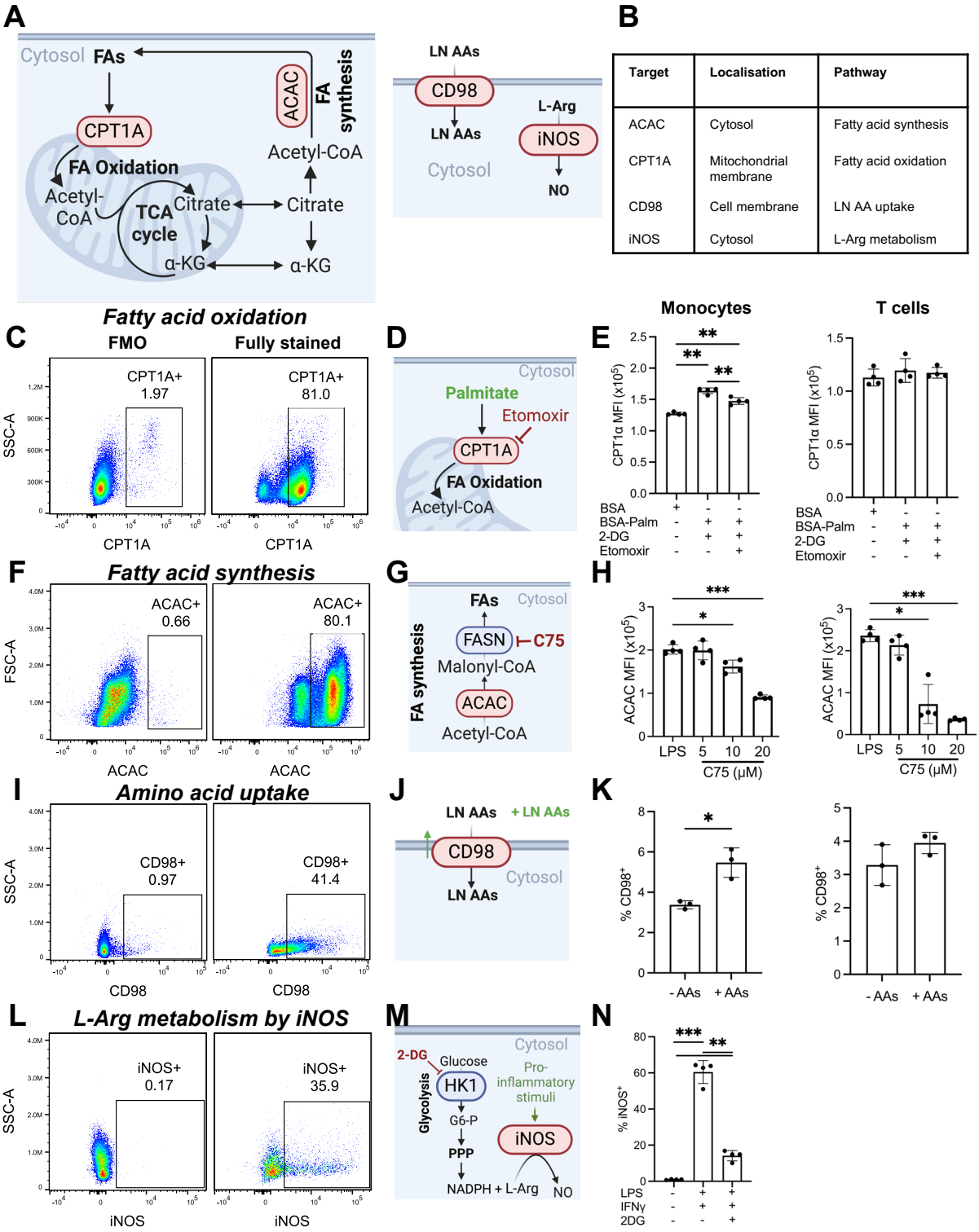
A
Cytosol
FAs
ACAC
FA synthesis
CPT1A
FA Oxidation
Acetyl-CoA
Acetyl-CoA
TCA cycle
Citrate
Citrate
α-KG
α-KG
LN AAs
CD98
LN AAs
Cytosol
L-Arg
iNOS
NO
B
Target
Localisation
Pathway
ACAC
Cytosol
Fatty acid synthesis
CPT1A
Mitochondrial membrane
Fatty acid oxidation
CD98
Cell membrane
LN AA uptake
iNOS
Cytosol
L-Arg metabolism
C
Fatty acid oxidation
FMO
Fully stained
CPT1A+ 1.97
CPT1A+ 81.0
SSC-A
CPT1A
CPT1A
D
Cytosol
Palmitate
Etomoxir
CPT1A
FA Oxidation
Acetyl-CoA
E
Monocytes
T cells
CPT1α MFI (x10^5)
BSA
BSA-Palm
2-DG
Etomoxir
F
Fatty acid synthesis
ACAC+ 0.66
ACAC+ 80.1
FSC-A
ACAC
ACAC
G
FAs
Cytosol
FA synthesis
FASN
C75
Malonyl-CoA
ACAC
Acetyl-CoA
H
ACAC MFI (x10^5)
LPS
5
10
20
C75 (μM)
I
Amino acid uptake
CD98+ 0.97
CD98+ 41.4
SSC-A
CD98
CD98
J
LN AAs
+ LN AAs
CD98
Cytosol
LN AAs
K
% CD98+
- AAs
+ AAs
L
L-Arg metabolism by iNOS
iNOS+ 0.17
iNOS+ 35.9
SSC-A
iNOS
iNOS
M
Cytosol
2-DG
Glucose
Glycolysis
HK1
G6-P
PPP
NADPH + L-Arg
Pro-inflammatory stimuli
iNOS
NO
N
% iNOS+
LPS
IFNγ
2DG

Figure 5.2 Pathway-specific validation of metabolic targets involved in fatty acid and amino acid metabolism.

Schematic summary of fatty acid (FA) and amino acid (AA) metabolic targets for flow-based analysis. (**B**) Summary of metabolic targets for fatty acid and amino acid metabolism. (**C**, **F**, **I**, **L**) Dot plots showing positive fluorescent staining of the indicated metabolic targets on cultured $CD45^+$ bone marrow cells relative to the FMO control. (**D**, **G**, **J**, **M**) Mechanistic schematics showing metabolic pathway stimulation (green) or inhibition (red) of fatty acid oxidation (**D**), fatty acid synthesis (**G**), large neutral (LN) AA uptake (**J**), and L-arginine metabolism by iNOS (**M**). (**E, H, K, N**) Change in median fluorescence intensity (MFI) of positively-stained monocytes and T cells under various culture conditions for CPT1A (**E**) and ACAC (**H**) or percentage of cells expressing CD98 (**K**) and iNOS (**N**). Statistics were calculated using RM one-way ANOVA with Tukey's correction for multiple comparisons (**E**, **H, N**) or paired t-test (**K**). Each data point represents cells isolated from a different animal, with data points matched across groups within each experiment. Data shows one independent experiment with 3-4 biological samples per group performed in technical duplicate. See methods section 2.5.3 for detailed experimental conditions.

significantly, increased with amino acid supplementation (Figure 5.2K), indicating this marker is a reliable readout of amino acid uptake. Although a similar trend was observed in T cells, this effect was not significant (Figure 5.4K).

Finally, we investigated iNOS activity as it is closely linked to inflammation and glycolysis (Figure 5.2M). Inflammatory activity was stimulated with LPS and IFN-γ (Figure 5.2M) and was clearly detected relative to the FMO control (Figure 5.2L). Under homeostatic levels, iNOS, as expected, was expressed by few cells but upon inflammatory stimulation was highly expressed by approximately 60% of monocytes (Figure 5.2N). Importantly, 2-DG treatment reduced these levels to approximately 15% (Figure 5.2N), demonstrating that this molecule is strongly linked to inflammation and glycolysis.

5.1.3.3 Single-cell autofluorescence detected by spectral flow cytometry is linked to glycolytic state

Spectral flow cytometry using the 5-Laser Cytek® Aurora provides the advantage of interrogating cellular autofluorescence over 64 detectors between 365-829 nm, generating 64 usable parameters. Therefore, we hypothesized that this approach would enable the characterisation of metabolism due to the presence of metabolic pathway-associated biological molecules with different emission wavelengths, such as NADH. To characterise the autofluorescent signatures, we clustered unstained cells on 64 different autofluorescence parameters. Strikingly, we found that LPS-induced glycolysis was associated with a distinct autofluorescent signature in BM cells stimulated by LPS (Figure 5.3A). This shift in autofluorescence was found to occur primarily on the B1-B3 detectors (Figure 5.3B) (wavelength of 498-550 nm), consistent with the emission wavelength of NADH (480/540) (Croce and Bottiroli, 2014), a metabolic co-factor used to approximate glycolysis (Alfonso-García et al., 2016, Pavillon et al., 2018, Szulczewski et al., 2016), and accounts for almost the entire autofluorescence signal arising from a cell (Aubin, 1979, Croce and Bottiroli, 2014). Cells could be classified by their levels of autofluorescence intensity in the B2 detector both by clustering (Figure 5.3C) and manual gating (Figure 5.3D). Only $B2^{low}$ and $B2^{int}$ populations increased B2 autofluorescence with LPS stimulation (Figure 5.3E). We observed that B2 autofluorescence could be used to classify major cell types by their forward and side scatter profiles (Figure 5.3F), with $B2^{int}$ cells (*i.e.,* myeloid cells, Figure 5.3F, G) showing the biggest shift in B2 autofluorescence (Figure 5.3E), consistent with their comparatively higher glycolysis associated with LPS stimulation. Total unmixed autofluorescence (Figure 5.3H) showed identical scatter patterns to B2 autofluorescence (Figure 5.3D), emphasizing that the

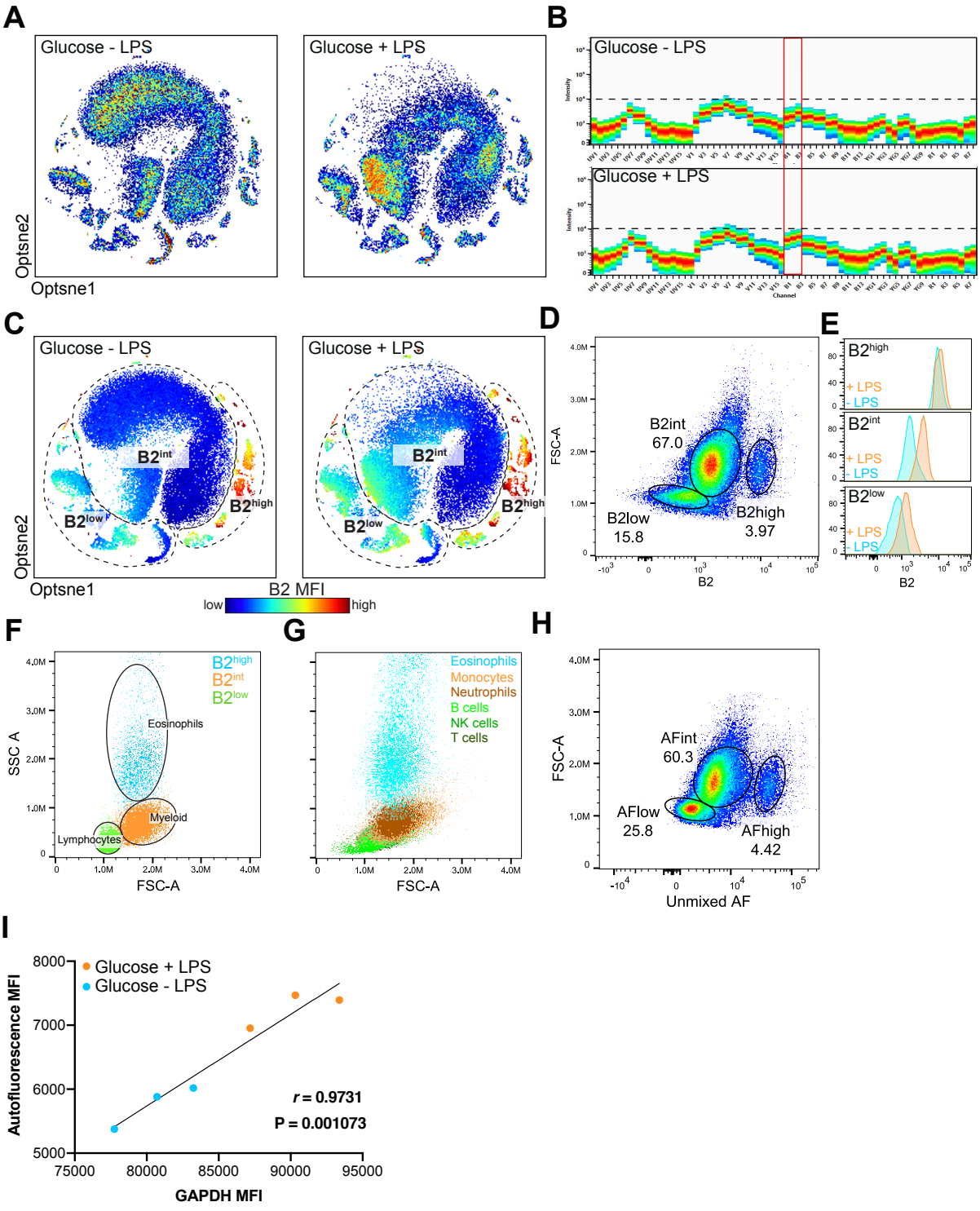
A
Glucose - LPS
Glucose + LPS
Optsne2
Optsne1
B
Glucose - LPS
Glucose + LPS
Intensity
Channel
C
Glucose - LPS
Glucose + LPS
B2int
B2high
B2low
Optsne2
Optsne1
B2 MFI
low
high
D
B2int
67.0
B2low
15.8
B2high
3.97
FSC-A
B2
E
B2high
B2int
B2low
+ LPS
- LPS
B2
F
B2high
B2int
B2low
Eosinophils
Myeloid
Lymphocytes
SSC A
FSC-A
G
Eosinophils
Monocytes
Neutrophils
B cells
NK cells
T cells
FSC-A
H
AFint
60.3
AFlow
25.8
AFhigh
4.42
FSC-A
Unmixed AF
I
Glucose + LPS
Glucose - LPS
r = 0.9731
P = 0.001073
Autofluorescence MFI
GAPDH MFI

Figure 5.3 Enhanced cell type-specific autofluorescence is indicative of glycolysis.

(**A**) OptSNE of unstained cells depicting the change in autofluorescence following stimulation of glycolysis with LPS. OptSNE was performed on autofluorescence across 64 detectors on raw data. (**B**) Spectral signature of stimulated (+LPS) and unstimulated (-LPS) cells. Changes in autofluorescence occurred primarily in the B1-B3 detectors (red box). (**C, D**) Cell events pseudocoloured by median fluorescence intensity in the B2 detector. Cells are classified into three populations based on their autofluorescence in the B2 detector by OptSNE (**C**) and dot plots (**D**). (**E**) Histograms depicting the shift in B2 autofluorescence with LPS stimulation. (**F, G**) Dot plots showing the side (SSC-A) and forward scatter (FSC-A) properties of the $B2^{hi}$, $B2^{int}$ and $B2^{lo}$ cells (**F**) and the immune cell subsets within these gates (**G**). (**H**) Dot plot showing autofluorescence $(AF)^{low}$, AF^{int} and AF^{high} populations on unmixed data. (**I**) Scatter plot depicting the correlation ($r = 0.9731$, $P = 0.001073$) between unmixed autofluorescence MFI and GAPDH MFI on fully stained cells. See methods section 2.5.3 for detailed experimental conditions.

autofluorescence signal from the cell is almost entirely attributable to autofluorescence detected in the B2 detector. Importantly, combining autofluorescence data with our metabolic panel demonstrated a correlation between total unmixed autofluorescence and the expression of the glycolytic enzyme GAPDH (R=0.973) (Figure 5.3I), emphasising the relationship between NADH autofluorescence and glycolysis.

5.1.4 Discussion

The ability to measure the metabolic state of immune cells is essential for a fundamental understanding of cellular function. Here, we present a metabolic spectral flow cytometry panel to simultaneously measure multiple metabolic pathways across diverse immune cell subsets at a protein level in single cells. The metabolic flow cytometry panel presented here employs commercially available reagents, eliminating the need for custom conjugation. We have meticulously validated each metabolic target through targeted inhibition or stimulation, demonstrating that their expression directly correlates with the corresponding pathway activity. This includes glycolysis, the TCA cycle, the ETC, HIF1α signalling, fatty acid oxidation and synthesis, amino acid uptake, and L-arginine metabolism by iNOS. This comprehensive validation approach has not been previously performed in other metabolic panels.

Pioneering flow cytometry-based methods, such as scMEP and MetFlow, have been instrumental in identifying metabolic diversity in various immune cell activation states and subtypes. Despite their utility, these methods have certain limitations, which we have attempted to address in this work. Both scMEP and MetFlow depend on custom fluorophores- or metal-conjugated antibodies, which limits their availability and are liable to inter-lab variability due to differences in conjugation methods. Additionally, the validation of metabolic targets as pathway representatives has been limited. This has primarily involved assessing the upregulation of glycolysis and OXPHOS during immune cell activation by flow cytometry combined with Seahorse assays (Hartmann et al., 2021, Ahl et al., 2020). However, these cytometric approaches have not demonstrated that altering the metabolic pathway through inhibition or substrate depletion affects the expression of metabolic targets, making it difficult to confirm that a marker accurately represents its nominal pathway. Notwithstanding, these platforms offer advantages over the method presented here. scMEP, using mass cytometry, offers a similar advantage to spectral flow cytometry in that it enables highly parametric use of markers and thus can assess a greater number of metabolic proteins, however at a substantially greater cost with extended run times. Additionally, MetFlow, using 10 markers, investigates

additional metabolic pathways not covered in this study, including the PPP, and incorporates the assessment of post-translational modifications, such as phosphorylation status, which is crucial for monitoring signalling pathways playing vital roles in regulating immunometabolism like mTOR and AMPK. Our current panel includes the fundamental pathways that influence immune cell function while defining cell phenotype. However, the use of spectral cytometry permits expansion to include metabolic markers that enable more detailed investigation of major pathways uncovered by the original panel.

In our work, we used targeted metabolic inhibition, stimulation, and nutrient depletion to confirm that our metabolic targets were regulated within the nominated pathway. It is important to note that the validation of each metabolic protein necessitates optimisation for distinct cell types. The culture conditions used here were principally focused on classically activated myeloid cells (e.g., with LPS and IFN-γ) and it is unlikely that indirect activation of T cells by co-culture with these monocytes was sufficient for their activation in all cases. Indeed, although all metabolic targets were validated for monocytes, inhibitors had minimal effects on the T cell expression of metabolic targets for fatty acid oxidation, glycolysis and amino acid uptake. This is likely due to the fact that resting, naïve T cells, as opposed to effector T cells, do not rely on these pathways for survival or function (Chapman et al., 2020), although naïve T cells could be skewed towards fatty acid oxidation with glucose depletion, consistent with previous work (Ecker et al., 2018). Supporting this, mitochondrial pathways primarily used by resting T cells, such as the ETC and TCA cycle (Soriano-Baguet and Brenner, 2023), could be validated without T cell-specific activation. It is thus recommended that the use of metabolic inhibitors for validating selected metabolic targets be performed with culture conditions relevant to activating specific cell types. Nonetheless, validating these metabolic markers allows for the application of our panel in various alternative in vitro and in vivo settings.

We found that metabolic target labelling correlated well with pathway activity in our study, although as mentioned, this may be dependent on cell type and experimental conditions. A recent study comparing co-expression patterns of scMEP markers with SCENITH-derived metabolic capacity in DCs showed that out of 5 measured ETC/TCA regulators, cytochrome C correlated least with mitochondrial dependence (Adamik et al., 2022). On the other hand, CD98 correlated highly with fatty acid/amino acid oxidation capacity. Of the glycolytic enzymes, monocarboxylate transporter 1 and 6-phosphofructo-2-kinase/fructose-2,6-biphosphatase 4 (PFKB4) correlated highest with glycolytic capacity in DCs, although GAPDH, the glycolysis

target used in our study, was not evaluated. However, it is worth noting that GAPDH can also play a role in gluconeogenesis in certain cells, such as hepatocytes in the liver, which should be considered when evaluating glycolysis in non-immune cells. Overall, these findings highlight the importance of validation and optimisation by cell type, metabolic label and experimental conditions to accurately reflect the activity of the pathway of interest. Finally, it should be noted that a lack of correlation may point to other active elements that could uncover useful information about metabolic pathway responses.

The use of spectral flow cytometry demonstrated that autofluorescence can uncover metabolic properties of immune cells. Stimulating glycolysis in vitro with LPS induced a glycolytic-specific autofluorescence signature in BM cells, with autofluorescence intensity associated with increased expression of the glycolytic enzyme GAPDH. This association between autofluorescence and glycolysis is consistent with the emission profile of NADH. Typically, the autofluorescence signal originating in the cell cytoplasm is almost entirely attributable to NADH and flavins (Croce and Bottiroli, 2014, Aubin, 1979). These findings build on established methods of evaluating cell metabolism by NADPH, as both glycolysis and OXPHOS can be approximated by fluorescence-lifetime methods in imaging microscopy (Schaefer et al., 2019). This technique has identified metabolic changes in macrophage polarisation (Alfonso-García et al., 2016, Pavillon et al., 2018, Szulczewski et al., 2016) and T cell activation (Walsh et al., 2021). In addition, glioma stem cells can be sorted and functionally defined by their NADH autofluorescence profiles (Yuan et al., 2019). Thus, cells with higher NADH autofluorescence had a higher capacity for multilineage differentiation, tumorigenesis, and invasive ability (Yuan et al., 2019), consistent with more aggressive tumour cells being highly glycolytic (Hsu and Sabatini, 2008). To our knowledge, however, this is the first study to employ spectral cytometry to assess glycolysis by autofluorescence. This simple and convenient method obviates the need to stain cells with antibodies to measure this pathway. However, the correlation between GAPDH and autofluorescence should be examined first in each experimental setting as a baseline, with the consideration that different organs and experimental conditions may induce molecules with different autofluorescence properties. In itself this may open the way for discovery and future use of other autofluorescent cellular components. By combining different detected autofluorescent signatures enabled by the increasing sensitivity of spectral cytometry, this method can provide a wealth of information about the metabolic status of a cell without the need for additional labelling and manipulation.

This approach not only preserves the natural state of the cell, but also offers insights into its functional identity.

The work here uses antibodies that recognise metabolic targets with mouse-human cross-reactivity. However, iNOS is not commonly expressed in human macrophages, therefore measuring L-arginine metabolism via this enzyme may be inapposite (Gross et al., 2014, Thomas and Mattila, 2014, Verberk et al., 2022). Furthermore, upon LPS activation, human peripheral blood monocyte-derived macrophages utilize OXPHOS rather than glycolysis for ATP production, unlike their mouse counterparts (Vijayan et al., 2019). While there are obvious practical implications of these disparities, it should be noted that they may enable discovery and increase the understanding of the way metabolism has evolved in different species to ordain function. In addition, while our validation approach using metabolic inhibitors and pathway stimulation demonstrates correlation between marker expression and pathway activity, additional controls could further strengthen the specificity of these readouts. For instance, genetic approaches such as knockouts or siRNA targeting specific metabolic enzymes would provide complementary validation of antibody specificity and confirm the precise relationship between marker expression and pathway activity. Moreover, it is important to acknowledge that flow cytometry provides an indirect measure of metabolic activity through protein expression, and changes in protein levels may not always directly correspond to flux through metabolic pathways.

The work presented here provides an additional method for evaluating cell metabolism and can be integrated with other complementary, established methods. For instance, this work could be combined with a parallel flow cytometric panel of fluorescent metabolic probes and analogues of metabolites (Verberk et al., 2022). These include dyes that assess glucose uptake (2-NBDG, -NBDG, 2-(N-(7-Nitrobenz-2-oxa-1,3-diazol-4-yl)Amino)-2-Deoxyglucose), fatty acid uptake and lipid storage (BODIPY, 4,4-difluoro-4-bora-3a,4a-diaza-s-indacene), mitochondrial mass (MitoTracker), mitochondrial membrane potential, and mitochondrial reactive oxygen species production (MitoSOX). These methods are relatively inexpensive, fast, and easily adaptable to different experimental settings (Verberk et al., 2022). In addition, metabolic-based flow cytometry provides an indirect measurement of metabolic pathway activity and does not directly measure the flux of a pathway, which can be investigated by real time respiration or metabolite measurements, for instance, using extracellular flux assays or SCENITH (Argüello et al., 2020, Verberk et al., 2022). Finally, such findings could be supported by targeting

metabolic enzymes with genetic or pharmacological tools, although metabolic redundancy and plasticity may complicate efforts to block a particular transporter or enzyme.

Overall, we present a systematically validated metabolic panel that can be used to investigate the relationship between phenotypic identity and metabolic profile at the single-cell level. This versatile research tool will likely garner significant insights into immune cell biology, but importantly also enable the assessment of the efficacy of therapeutics that induce metabolic reprogramming in cell populations of interest, including pathogenic immune cells and engineered cells like chimeric antigen receptor T or myeloid cells.

5.1.5 Supplementary Figures

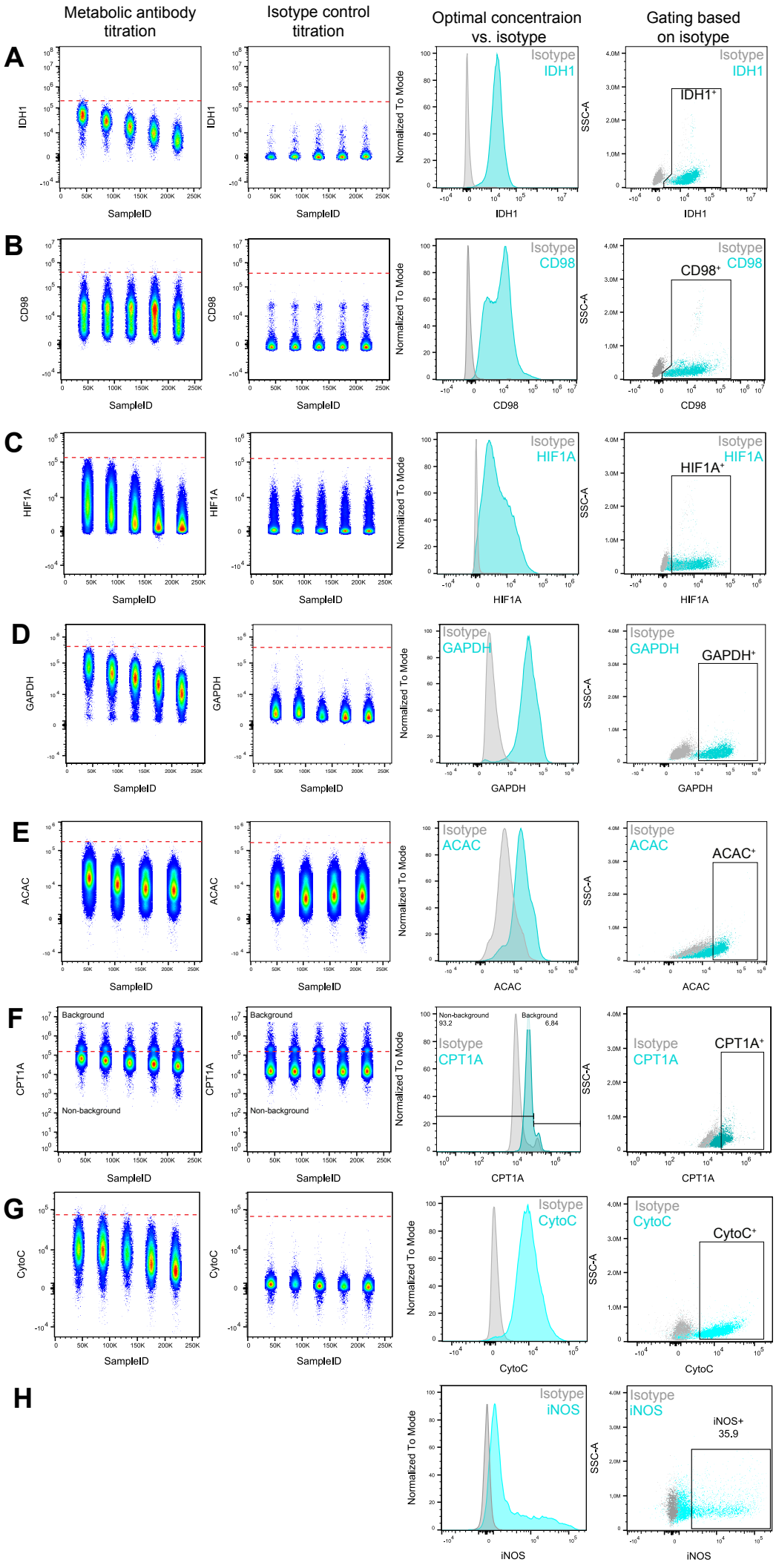
Metabolic antibody titration
Isotype control titration
Optimal concentraion vs. isotype
Gating based on isotype
A
IDH1
SampleID
Normalized To Mode
SSC-A
Isotype
IDH1
IDH1+
B
CD98
Isotype
CD98
CD98+
C
HIF1A
Isotype
HIF1A
HIF1A+
D
GAPDH
Isotype
GAPDH
GAPDH+
E
ACAC
Isotype
ACAC
ACAC+
F
CPT1A
Background
Non-background
Non-background
93.2
Background
6.84
Isotype
CPT1A
CPT1A+
G
CytoC
Isotype
CytoC
CytoC+
H
Isotype
iNOS
iNOS+
35.9

Supplementary Figure 5.1 Metabolic antibody titration and gating strategies.

Bone marrow or spleen cells were processed and stained with Zombie UV Live/Dead and single stains for each metabolic antibody, including IDH1 (**A**), CD98 (**B**), HIF1A (C), GAPDH (**D**), ACAC (**E**), CPT1A (**F**), Cytochrome C (**G**), and iNOS (**H**) Each metabolic antibody and isotype control were titrated at four to five concentrations, ranging from 0.01 ug/μL to 0.16 ug/μL. The optimal concentration for each indicated antibody is the point of lowest concentration at which the cells do not drop below the saturation line (dotted red line). Positive expression for each indicated metabolic antibody is determined by the gate drawn relative to the isotype control. Representative graphs are gated on live, non-debris, non-erythrocyte single cells.

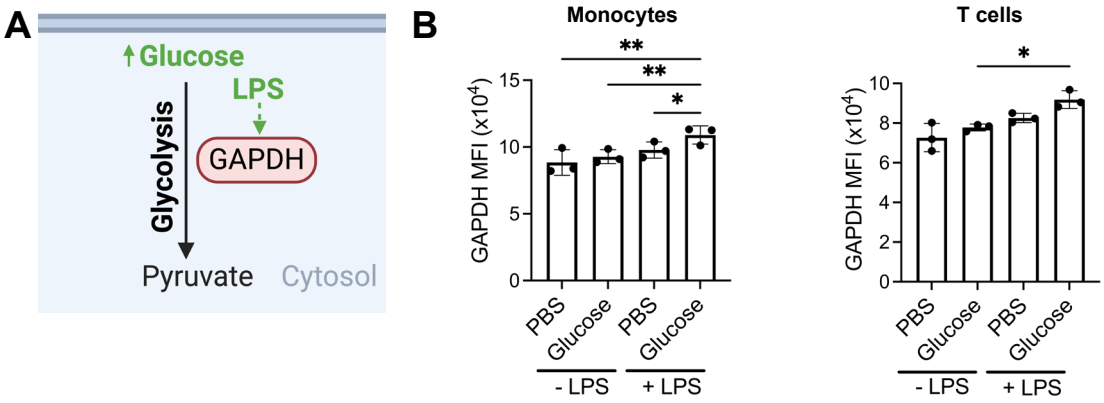
A
Glucose
LPS
Glycolysis
GAPDH
Pyruvate
Cytosol
B
Monocytes
T cells
GAPDH MFI (x10^4)
**
**
*
*
PBS
Glucose
PBS
Glucose
- LPS
+ LPS

Supplementary Figure 5.2 Examination of GAPDH as a marker for glycolysis by glucose depletion.

(**A**) Schematic summary of the mechanism of action of glycolysis stimulation (green) with LPS in the presence of glucose. (**B**) Change in MFI of the GAPDH-positive stained monocytes and T cells. Statistics were calculated using RM one-way ANOVA with Tukey's correction for multiple comparisons. Each data point represents cells isolated from a different animal, with data points matched across groups within each experiment. Data shows one independent experiment with 3-4 biological samples per group performed in technical duplicate.

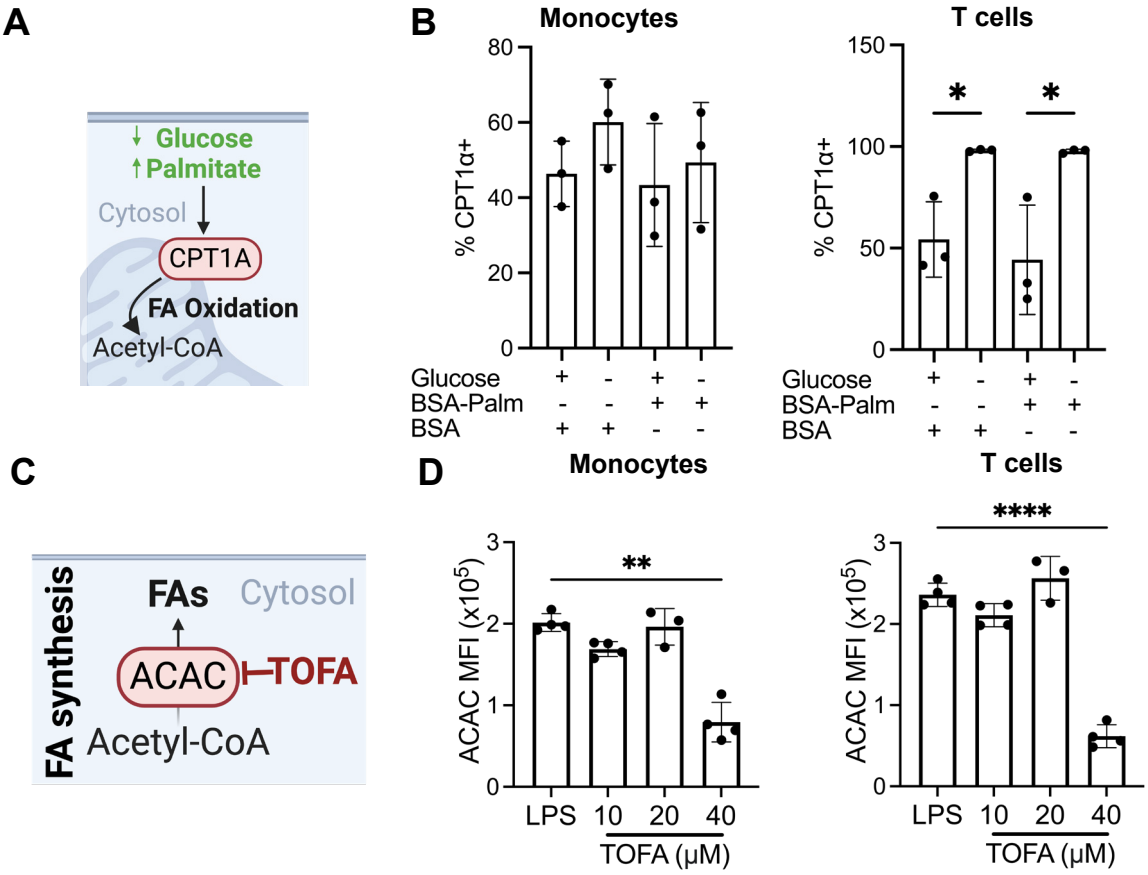
A
Glucose
Palmitate
Cytosol
CPT1A
FA Oxidation
Acetyl-CoA
B
Monocytes
T cells
% CPT1α+
Glucose
BSA-Palm
BSA
C
FA synthesis
FAs
Cytosol
ACAC
TOFA
Acetyl-CoA
D
Monocytes
T cells
ACAC MFI (x10^5)
LPS
10
20
40
TOFA (μM)

Supplementary Figure 5.3 Optimisation of fatty acid metabolic markers.

(**A**, **C**) Mechanistic schematic of metabolic pathway stimulation (green) or inhibition (red) for CPT1A (**A**) and ACAC (**C**). (**B**) Change in the percentage of CPT1A-expressing monocytes and T cells. (**D)** Change in ACAC median fluorescence intensity (MFI) of ACAC-positive stained monocytes and T cells. Statistics were calculated using a paired t-test (**B**) or RM one-way ANOVA with Tukey's correction for multiple comparisons (**D**). Each data point represents cells isolated from a different animal, with data points matched across groups within each experiment. Data shows one independent experiment with 3-4 biological samples per group performed in technical duplicate.

Chapter 6: Results IV

6.1 Therapeutic glycolysis blockade preferentially targets pathogenic monocytes and attenuates CNS inflammation in flavivirus encephalitis

The following chapter is formatted into a manuscript.

6.1.1 Overview

Infiltrating monocytes play a dual role in CNS diseases, both driving and attenuating inflammation. However, understanding how metabolic pathways fuel protective or pathogenic processes is important for therapeutic targeting. We employed scRNA-seq and metabolic flow analysis of brain and BM to map the metabolic signatures of MCs during lethal WNV encephalitis. Trajectory analysis showed progression of BM monocytes through three metabolic profiles before migration to the brain and differentiation into three distinct MC populations. These included a pro-inflammatory HIF1-α^+ MC population that diverged into an iNOS$^+$ M1-like MC with high glycolysis and amino acid metabolism scores, and a glycolytically quiescent, antigen-presenting MC. Daily *in vivo* glycolysis inhibition with 2-DG reduced CNS leukocyte infiltration, neuroinflammation, and disease signs without increasing viral load. This reduction was not due to decreased myelopoiesis, but a preferential decrease in iNOS$^+$ MC migration, compared to antigen-presenting MCs, highlighting different glycolytic dependencies. Importantly, HIF1-α activity was independent of glycolysis, allowing ongoing antigen-presenting MC differentiation, while glycolysis inhibition did not impair antiviral responses by cervical node T cells. This study uncovers coupled MC function and metabolism in viral CNS disease, highlighting novel therapeutic targets during severe inflammation.

6.1.2 Introduction

Monocytes play a pivotal role in both inflammation and maintenance of tissue homeostasis. In the CNS, they replenish a small proportion of tissue-resident macrophages in the dura mater and choroid plexus (Goldmann et al., 2016, Van Hove et al., 2019), and while typically constrained by the BBB, readily infiltrate the CNS during inflammation (Spiteri et al., 2020). MCs, such as monocyte-derived DCs and macrophages, play crucial roles in CNS disorders. Their diverse functions include innate host defence (e.g., phagocytosis of pathogens and tissue

debris), initiation of adaptive defences (antigen presentation) and tissue repair. However, the precise role of cellular metabolism in shaping these functions in the context of CNS disease remains poorly defined.

MC metabolism tends to be dichotomized simplistically into inflammatory (M1) and regulatory (M2) profiles, which are predominantly studied *in vitro* (Jha et al., 2015). In this classification, M2 MCs have regulatory functions that rely on an oxygen-dependent pathway supporting slower, but more efficient, ATP generation, while M1 MCs exert pro-inflammatory functions and rely on glycolysis to meet their high energy demands (Viola et al., 2019). Various M1 stimuli, such as IFN-γ, LPS, tumour necrosis factor, viruses, and granulocyte-macrophage colony-stimulating factor, are characterized by their proinflammatory effects, yet they induce significantly different phenotypes and metabolic responses. This suggests a more complex and nuanced metabolic framework underpinning inflammatory functions. Supporting this, disease environments comprised of diverse inflammatory stimuli give rise to metabolic states tailored to cellular functions (Li et al., 2022b, Heieis et al., 2023). Such functions include NO production, type I IFN responses (Xiao et al., 2020, Peng et al., 2021, Shen et al., 2021), cytokine synthesis (Yeudall et al., 2022, Lachmandas et al., 2016), antigen presentation (Everts et al., 2014), phagocytosis (Lee et al., 2018, Lachmandas et al., 2016, Gonzalez et al., 2023), and migration into inflamed tissues (Semba et al., 2016, Cramer et al., 2003).

WNV is a mosquito-borne, neurotropic flavivirus and one of the most important causative agents of human viral encephalitis worldwide (Saiz et al., 2021). In its neuroinvasive phase, WNV can cause severe encephalitis, the pathogenesis of which is driven by infiltration of M1-like MCs into the CNS. Murine models clearly show that monocytes recruited from the BM migrate to the brain in a CCL2-dependent manner, diapedesing into the CNS via Ly6C and activated VLA-4 expressed on the monocyte surface. Once in the CNS they mediate immune pathology by the sustained production of NO (Getts et al., 2008, Getts et al., 2012, Terry et al., 2015). Strategies that block the entry of inflammatory monocytes into the brain, such as by CCL2, VLA-4 or Ly6C antibody blockade or immune modifying particles, or that attenuate their inflammatory response, such as inhibition of NO production using aminoguanidine hemisulphate, have been shown to improve survival of infected mice markedly without affecting viral load (Getts et al., 2008, Getts et al., 2012, Terry et al., 2015, Getts et al., 2014, Spiteri et al., 2023b), thus emphasizing the role of MCs in causing the inflammatory damage observed in WNV infection. Notably, these cells also adopt an antigen-presenting phenotype

(Spiteri et al., 2023b) and may indirectly aid in viral clearance by promoting an effective T cell response. This effect is more pronounced in peripheral inoculation models, where monocytes exhibit a more protective function (Lim et al., 2011a), in contrast to models in which WNV infection is confined to the CNS, in which viral spread and disease progression is more accelerated. However, it is unclear whether these differential functions are reflected in and effected by distinct metabolic profiles.

Numerous tools exist for the easy assessment of metabolism *ex vivo*. However, traditional methods that measure metabolic respiration in bulk or across whole populations fail to capture the increasingly recognized metabolic diversity of MC populations in the context of disease. To address this, recent technological advancements have enabled single-cell analysis of metabolism through two primary methods. The first uses scRNA-seq for broad analysis of gene expression related to metabolic changes. The second combines cytometric techniques with the detection of key metabolic enzymes, transporters, and transcription factors as a proxy measurement of the metabolic profile (Levine et al., 2021, Miller et al., 2017, Ahl et al., 2020, Hartmann et al., 2021). An additional cytometric approach, SCENITH, combines metabolic inhibitors and protein synthesis quantification to assess the metabolic dependencies of immune cells at the single-cell level (Argüello et al., 2020). The latter approaches overcome the limitations of inferring function from gene expression alone. Nevertheless, comprehensive integration of gene and protein data at the single-cell level is ultimately required to fully elucidate and map the cellular metabolic processes that lead to disease resolution or exacerbation.

In this study, we identify tissue- and time-specific metabolic changes in response to severe flaviviral infection in the CNS, using both scRNA-seq and flow-based metabolic analysis. In particular, we show that MCs with a high glycolytic phenotype exhibited an inflammatory M1-like phenotype that distinguished them from antigen-presenting and other MC populations. Targeting glycolysis as an anti-inflammatory strategy preferentially affected M1-like cells while sparing antigen-presenting populations, resulting in amelioration of disease without increasing viral burden. This selective targeting emphasizes the potential of metabolic interventions in managing the intricate temporal pathogenesis of complex CNS disorders.

6.1.3 Results

6.1.3.1 MCs adopt distinct metabolic and functional profiles in CNS infection

Since BM-derived MCs infiltrating the CNS contribute significantly to immunopathology in WNV encephalitis, we sought to identify the specific metabolic pathways associated with the differentiation and development of these pathogenic responses. MCs were sorted flow cytometrically from the brain at 5 and 7 dpi and identified as Ly6G^{-}, CD49^{hi,} P2RY12^{lo}, NK1.1^{-}, CD3e^{-}, CD11b^{+}, CD64^{+} and CX3CR1^{+}, capturing the entire population of Ly6C^{hi} and Ly6C^{lo} MCs at 5 and 7 dpi (Spiteri et al., 2021a). Mature monocytes from the BM at 7 dpi were identified as CD45.2^{+}, Ly6G^{-}, CD48^{hi}, NK1.1^{-}, CD3e^{-}, B220^{-}, CD11b^{+}, CD117^{-}, CD115^{hi}, as previously described (Spiteri et al., 2023b). We then used a targeted scRNA-seq panel (n = 397 genes and 67 custom genes) to link the metabolic state and functional transcriptional profiles of monocyte subsets in acute viral infection.

Clustering on scRNA-seq data from 3498 MCs and BM monocytes revealed four distinct states in the brain and three in the BM, respectively (Figure 6.1A). Of the brain subsets, we identified 1) an "*APC*" population highly expressing genes involved in antigen presentation, including *H2-Aa*, *H2-Eb1*, *H2-Ab1*, *Cd74*, and *Cd86* (Figure 6.1B), 2) a *"Microglia (Mg)-like MC"* subset resembling microglia, due to its relative expression of microglia-specific markers *Cd81*, *Sparc*, *Hexb*, and *Tmem119* (Wishart, 2022, Spiteri et al., 2021a) (Figure 6.1B), 3) a *Hif1a*-expressing population, and 4) a *Nos2*-expressing population, which likely represented the NO-producing population causing inflammatory damage in this model (Figure 6.1B). While this population showed detectable expression of nominal microglia-specific markers such as *Cd81*, it is important to note that this likely represents either low-level expression relative to *Cd81*-negative cells or potential microglial contamination in the sorted population, as the expression level is negligible when compared to bona fide microglia as demonstrated in Results Chapter I.

The functional status of these cell clusters was supported by manually querying several M1 functional programs, such as *antigen presentation*, *inflammatory response*, and *viral response* against gene modules from the Mouse Genome database (Tirosh et al., 2016) (Figure 6.1C). A high module score represents the average expression of the genes in the module relative to a set number of randomly extracted control genes from the dataset. The *APC MC* cluster had a high antigen-presenting score and viral response score, suggesting this population may be

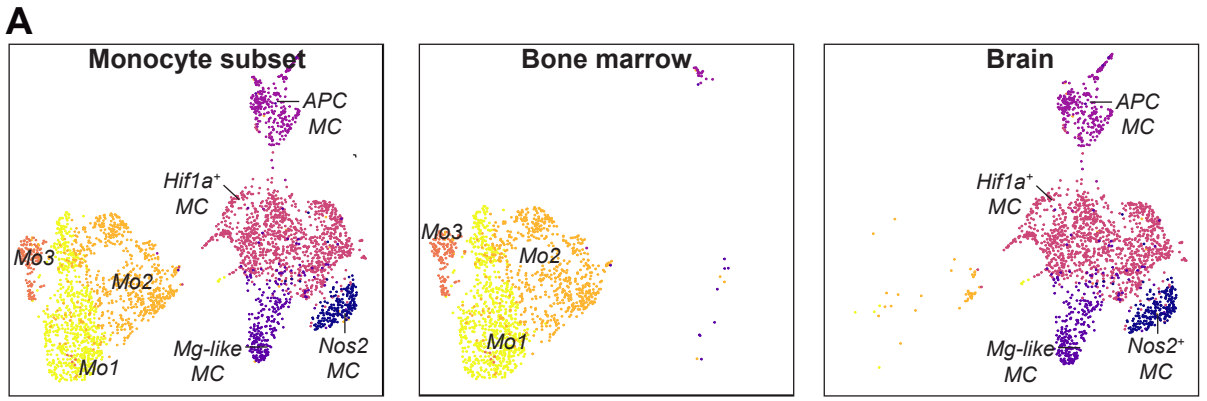

B

Mo1		Mo2		Mo3		Hif1a+ MC		APC MC		Mg-like MC		Nos2+ MC	
Chil3	F13a1	mt.Nd1	Lgals1	S100a8	Top2a	Il1rn	Ccl2	H2.Aa	Cd7	Cd81	Sparc	Cxcl2	Lilrb4a
Fn1	Ccl6	mt.Cytb	Fn1	S100a9	Tyms	Lilrb4a	Hif1a	H2.Eb1	Dpp4	C1qa	Hexb	Ier3	Il7r
Lyz2	Ly6c1	mt.Nd5	Lyz2	Elane	Mki67	Cxcl10	Ccl5	H2.Ab1	Stat4	mt.Rnr2	Cd72	Nos2	Il1rn
Mgst1	S100a10	mt.Co1	Cd52	Chil3	Aurkb	Irf7	Ier3	Cd74	Cd209a	C1qb	Ccl3	Fth1	Rgs1
Il1r2	G6pdx	mt.Nd2	S100a10	X281041-7H13Rik	Mcm2	Mafb	Dusp2	Kmo	Cd86	Tmem119	mt.Co1	Dab2	Dusp2

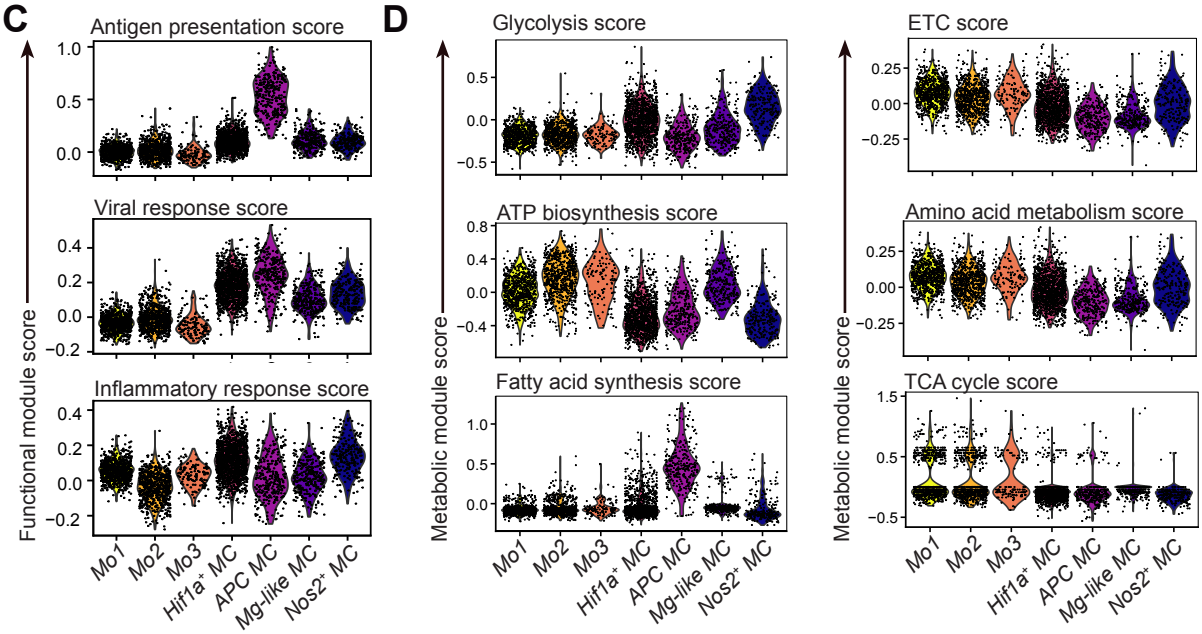

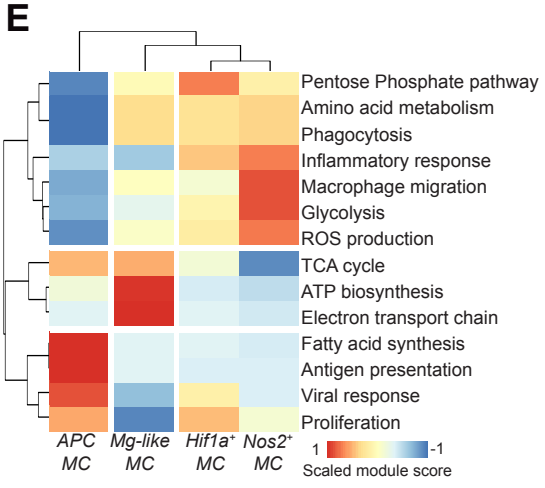

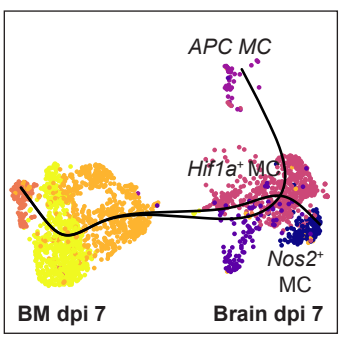

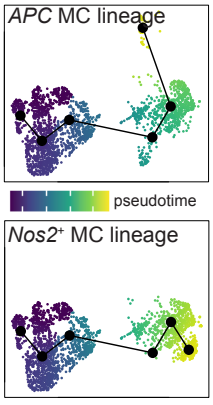

Figure 6.1 MCs adopt distinct metabolic and functional transcriptomic profiles in CNS infection.

(**A**) UMAPs of MCs identified in WNV infection across the BM at 7 dpi and brain at 5 and 7 dpi. **(B**) Top differentially expressed genes per cluster. Differentially expressed genes were defined as genes enriched in a cluster versus all other clusters. (**C, D**). Module scores for functional (**C**) and metabolic (**D**) pathways across each of the identified subsets. (**E**) Heatmap depicting the scaled average module scores for *APC*, *Mg-like*, *Hif1a*$^{+}$, and *Nos2*$^{+}$ MCs in the brain across selected metabolic and functional modules. (**F**) Pseudotime trajectory analysis on BM and brain myeloid cells using Slingshot with *Mo3* set as the root (starting) subset. UMAP is colour-coded by monocyte subsets shown in Figure 6.1B. (**G**) Lineage trajectories from Slingshot analysis, 1) *Nos2*$^{+}$ *MC* and 2) *APC MC.* UMAPs are coloured by pseudotime. Data are from one experiment with four mice per group.

involved in indirectly contributing to viral clearance (Figure 6.1C). By contrast, *Hif1a*$^{+}$ and *Nos2*$^{+}$ MCs exhibited a higher inflammatory response score, supporting a potential inflammatory phenotype that contributes to inflammatory damage in WNV encephalitis (Getts et al., 2012) (Figure 6.1C). All BM monocyte clusters (*Mo1-Mo3*) displayed low M1 functional scores, supporting the notion that these cells are an undifferentiated monocyte state (Figure 6.1C).

As metabolism is coupled with the phenotype and functionality of MCs, we next scored genes involved in several metabolic pathways known to be important in M1- or M2-like functions, including glycolysis, ATP biosynthesis, fatty acid synthesis, ETC, amino acid metabolism, and the TCA cycle (Figure 6.1D). BM monocytes (*Mo1*, *Mo2*, and *Mo3*) and *Mg-like MC* displayed higher expression of metabolic pathways related to homeostatic functions, including the TCA cycle, ATP biosynthesis, and ETC, but also displayed high amino acid metabolism scores (Figure 6.1D and 1E). Inflammatory *Hif1a*$^{+}$ and *Nos2*$^{+}$ MCs displayed higher glycolysis and amino acid metabolism scores with low TCA cycle scores (Figure 6.1D). Expression of these metabolic pathways clustered with typical inflammatory functions, including the *inflammatory response*, *reactive oxygen species production*, and *phagocytosis* (Figure 6.1E), supporting the notion that these *Hif1a*$^{+}$ and *Nos2*$^{+}$ cells adopt a typical M1-like phenotype in WNV encephalitis. On the other hand, *APC MCs* were evidently less reliant on glycolysis and amino acid metabolism pathways, but exhibited higher fatty acid synthesis scores (Figure 6.1D and 1E). This suggests that there exists wide metabolic heterogeneity in typical M1-like functions in CNS infection, including the inflammatory response and antigen presentation, which is likely obscured in bulk *in vitro* systems.

To understand the differentiation pathway of BM monocytes into specific metabolic states in the CNS, we employed trajectory analysis. This showed that BM monocytes progressed through 3 different metabolic profiles before they migrated to the brain, where they underwent a transition towards either *APC* or *Nos2*$^{+}$ *MC* populations in the brain at disease endpoint (Figure 6.1F). Both lineages passed through the *Hif1a*$^{+}$ *MC* population, implying that this population is a transitional state. The *Mg-like MC* population, however, did not align with these pathways, indicating that it is a unique MC population (Figure 6.1F). This distinctness of this 4th population raises the question of contamination by microglial cells. However, we have established that monocytes circulating in the bloodstream can assume a microglial-like

phenotype within the WNV-infected brain, a change attributable to prolonged interaction with the CNS milieu (Spiteri et al., 2021a).

During their differentiation into brain MCs, BM monocytes consistently downregulated genes related to ATP synthesis, the TCA cycle, ETC and PPP, while upregulating genes related to glycolysis (Supplementary Figure 6.2). This indicates a significant metabolic shift as MCs transition from the BM to the infected brain, possibly through a shared *Hif1a*$^{+}$ intermediate, before diverging into functionally distinct pathways towards antigen-presenting (*APC*) or NO-producing (*Nos2*$^{+}$) phenotypes.

6.1.3.2 Application of MetFlow to CNS infection reveals distinct metabolic changes in CNS disease

Given the limitations in existing tools to study metabolism by gene expression alone, we adapted the metabolic panel developed in Results Chapter III, using metabolic marker proteins with high relevance to myeloid cells during inflammation. This comprised 13 immune cell identification markers and 9 metabolic marker proteins, including rate-limiting enzymes, signalling molecules, and transcription factors that have roles in glycolysis, the TCA cycle, hypoxia-induced inflammation, amino acid transport, fatty acid synthesis and oxidation, the kynurenine pathway, NO production, and mitochondrial ROS production (Figure 6.2A, Table 6.1).

To identify metabolic signatures independently of cell lineage and origin, we performed dimensionality reduction on whole brain and BM cell isolates and clustered on metabolic markers (Supplementary Figure 6.2B). Resident microglia (Ly6G^{-}, SSCA^{lo}, NK1.1^{-}, CD3e^{-}, B220^{-}, CD45$^{low\text{-}int}$, CX3CR1^{+}), brain-infiltrating MCs (defined as Ly6G^{-}, SSCA^{lo}, NK1.1^{-}, CD3e^{-}, B220^{-}, CD45^{hi}, CX3CR1^{low}) and BM monocytes (defined as Ly6G^{-}, SSCA^{lo}, NK1.1^{-}, CD3e^{-}, B220^{-}, CD11c^{lo}, MHC-II^{lo}, CD11b^{+}, Ly6C$^{hi/lo}$, CX3CR1$^{hi/lo}$) clustered into 8 distinct metabolic states which varied in proportion across timepoints and were distinctly grouped by organ and lineage/differentiation status (Figure 6.2C-H), demonstrating a significant metabolic adaptation over the course of infection. Within the brain, four dominant MC populations were detected (clusters 2, 4, 6 & 7) (Figure 6.2F, 6.2H), while three predominant monocyte populations were found in the BM (Figure 6.2F). This distribution mirrors the populations revealed by scRNA-seq (Figure 6.1), corroborating our findings across both techniques.

Table 6.1. Metabolic targets included in panel

Target	Name	Pathway	Function in pathway
GAPDH	Glyceraldehyde 3-phosphate dehydrogenase	Glycolysis & fermentation	Rate limiting glycolytic enzyme
IDH1	Isocitrate dehydrogenase	TCA cycle	Rate limiting enzyme in TCA cycle
CPT1A	Carnitine Palmitoyltransferase 1A	Fatty acid oxidation	Fatty acid shuttling into mitochondria
ACAC	Acetyl-CoA carboxylase	Fatty acid synthesis	Acetyl-CoA carboxylase/ fatty acid synthesis
CD98	CD98	Amino acid metabolism	Essential amino acid transporter
HIF1-α	Hypoxia-inducible factor 1-alpha	Metabolic regulation/signaling	Hypoxia and inflammation-induced transcription factor
iNOS	Inducible nitric oxide synthase	Oxidative stress, amino acid metabolism	Nitric oxide production, initial rate-limiting enzyme involved in arginine degradation
MitoSOX	N/A	Free radical superoxide generation	Stains for free radical superoxides, produced in the electron transport chain
IDO1	Indoleamine 2,3-dioxygenase	Amino acid metabolism (kynurenine pathway)	Initial and rate-limiting enzyme for tryptophan degradation to *N*-formylkynurenine in the kynurenine pathway

In the brain, cluster 0 was associated with microglia and was found in the highest proportions in the mock-infected brain (Figure 6.2F, 6.2G). By 7 dpi, microglia predominantly transitioned into cluster 6 (Figure 6.2G). However, the overall proportion of microglia was significantly reduced due to the massive influx of infiltrating MCs in the brain, which exceed microglia by approximately 10-fold at this timepoint (Figure 6.2F). Thus, cell numbers in clusters 1, 2, 4, 5, 6, and 7, predominantly comprising infiltrating MCs, were markedly increased in the brain, compared to mock-infected mice (Figure 6.2I), with numbers in cluster 7 some 8-fold greater than the next largest, cluster 6 (Figure 6.2K). In the BM, clusters 0, 1, 2, 3, 6 and 7 were numerically increased at 7 dpi, relative to mock-infected mice (Figure 6.2J), however, clusters 1, 2, and 3 comprised the majority of BM monocytes at 7 dpi, both numerically and by proportion (Figure 6.2F, 6.2L). These findings demonstrate clear metabolic remodelling both at peripheral sites of monocyte myelopoiesis and inflammatory foci in response to infection.

Supporting our scRNA-seq findings, GAPDH was upregulated in the brain, compared to the BM (Figure 6.2M), emphasizing the importance of glycolysis in the differentiation of MCs. This was most obvious in cluster 7 expressing high levels of iNOS (Figure 6.2N), likely denoting the pathogenic NO-producing MCs implicated in immunopathology. Along with

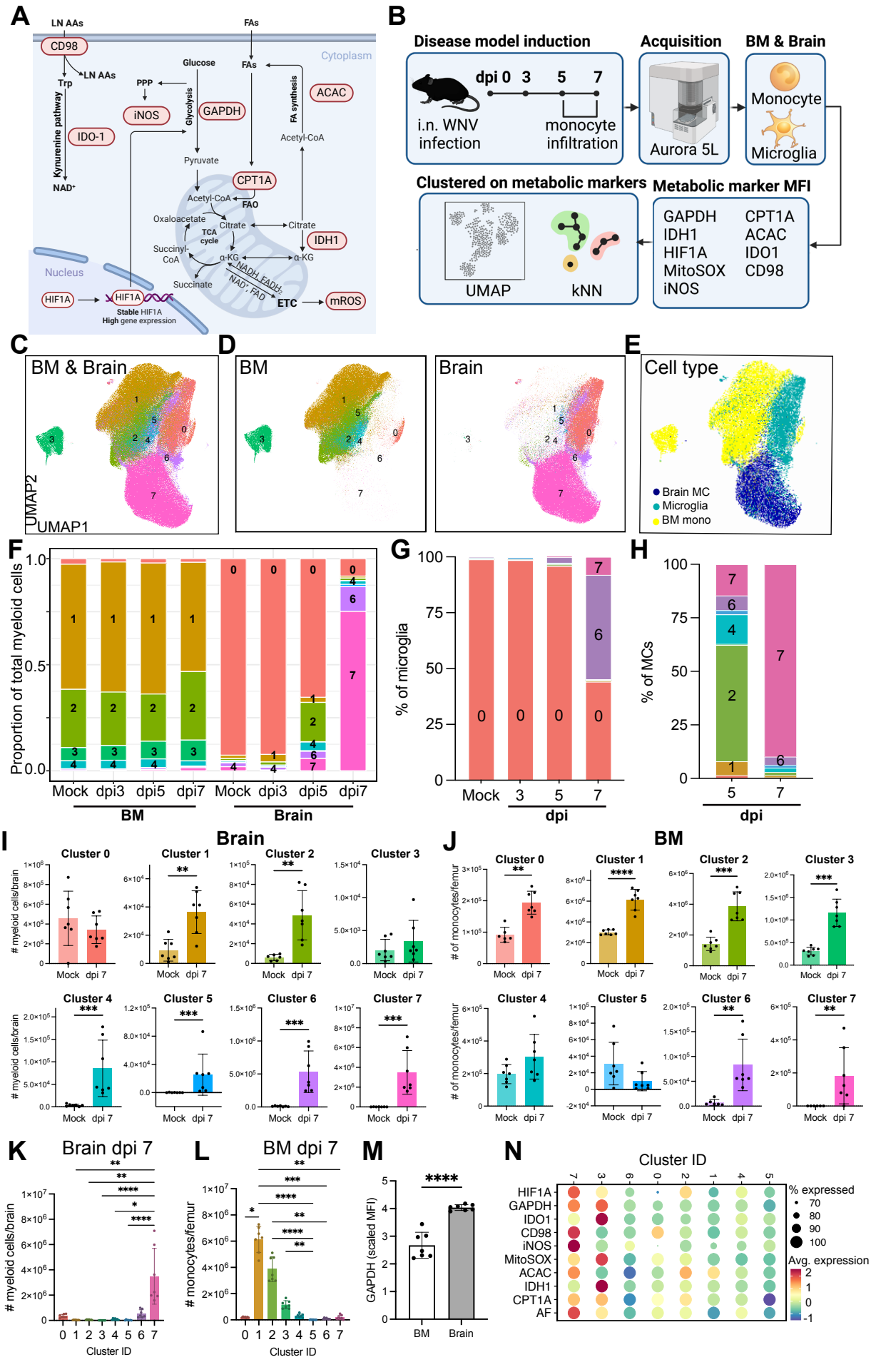
A
LN AAs
FAs
CD98
Cytoplasm
Glucose
FAs
Trp
LN AAs
PPP
FA synthesis
ACAC
iNOS
Glycolysis
GAPDH
Kynurenine pathway
IDO-1
Acetyl-CoA
Pyruvate
NAD+
CPT1A
Acetyl-CoA
FAO
Oxaloacetate
Citrate
TCA cycle
Citrate
IDH1
Succinyl-CoA
α-KG
α-KG
Nucleus
NADH, FADH2
NAD+, FAD
Succinate
HIF1A
HIF1A
ETC
mROS
Stable HIF1A
High gene expression
B
Disease model induction
dpi 0 3 5 7
i.n. WNV infection
monocyte infiltration
Acquisition
Aurora 5L
BM & Brain
Monocyte
Microglia
Clustered on metabolic markers
UMAP
kNN
Metabolic marker MFI
GAPDH
IDH1
HIF1A
MitoSOX
iNOS
CPT1A
ACAC
IDO1
CD98
C
BM & Brain
UMAP2
UMAP1
D
BM
Brain
E
Cell type
Brain MC
Microglia
BM mono
F
Proportion of total myeloid cells
Mock dpi3 dpi5 dpi7 Mock dpi3 dpi5 dpi7
BM
Brain
G
% of microglia
Mock 3 5 7
dpi
H
% of MCs
5 7
dpi
I
Brain
Cluster 0
Cluster 1
Cluster 2
Cluster 3
Cluster 4
Cluster 5
Cluster 6
Cluster 7
myeloid cells/brain
Mock dpi 7
J
BM
# of monocytes/femur
K
Brain dpi 7
myeloid cells/brain
Cluster ID
L
BM dpi 7
monocytes/femur
M
GAPDH (scaled MFI)
BM Brain
N
Cluster ID
HIF1A
GAPDH
IDO1
CD98
iNOS
MitoSOX
ACAC
IDH1
CPT1A
AF
% expressed
Avg. expression

Figure 6.2 Metabolic heterogeneity of MCs in viral infection by spectral flow cytometry.

(**A**) Schematic of metabolic targets for flow-based analysis. (**B**) Experimental workflow. The BM and brain were isolated from mock-infected and WNV-infected mice at 3, 5, or 7 dpi and stained with a metabolic panel. UMAP and k-nearest neighbour clustering was performed on BM monocytes, brain microglia and brain MCs across time points based on arcsinh transformed metabolic protein MFI. (**C-E**) UMAPs pseudocoloured by metabolic cluster ID (**C, D**) and cell types (**E**) in the BM and brain. (**F-H**) Proportion of each metabolic cluster comprising the total myeloid pool across organs and time points (**F**), or the total microglia (**G**), or the MC (**H**) population in the brain. (**I, J**) Number of myeloid cells per brain (**I**) and monocytes per femur (**J**) in each cluster in mock-infected and WNV-infected mice at 7 dpi. (**K, L**) Number of myeloid cells per brain (**K**) and monocytes per femur (**L**) in each cluster at 7 dpi. (**M**) Arcsinh transformed MFI of GAPDH in the BM and brain at 7 dpi. (**N**) Dot plot heatmap depicting the MFI of each metabolic marker across the identified metabolic cluster at 7 dpi. Size of dot represents the percentage of cells in each cluster expressing the metabolic marker. Data are pooled from two independent experiments with 3-4 mice per group. Statistics done using Mann-Whitney test (**I, J, M**) or Kruskal-Wallis test with Dunn's test for multiple comparisons (**K, L**). * $p<0.05$, ** $p<0.01$, *** $p<0.001$, **** $p<0.0001$. Error bars are representative of mean ± SD.

increased iNOS expression, this cluster exhibited elevated GAPDH, HIF1-α, and CD98 levels (Figure 6.2N), reflecting the *Nos2*$^+$ and *Hif1a*$^+$ profiles identified via scRNA-seq (Figure 6.1) and constituted the majority of myeloid cells in the brain, as mentioned above (Figure 6.2K). In contrast to cluster 7, clusters 6, 4, and 2, the next-largest remaining clusters, displayed lower expression of iNOS, HIF1-α and GAPDH (Figure 6.2N), suggesting a deviation from typical pro-inflammatory metabolic pathways. Interestingly, however, cluster 2, which expresses higher HIF1-α, MitoSOX, and fatty acid metabolism markers (Figure 6.2N), is initially present in the brain by 5 dpi, coinciding with significant monocyte infiltration (Figure 6.2F, 6.2H). While remaining significantly elevated compared to controls (Figure 6.2L), cluster 2 had declined in the brain by 7 dpi (Figure 6.2H), coinciding with the appearance of iNOS$^+$ cluster 7, suggesting it may be a precursor to this subset in the brain at 5 dpi.

The metabolic diversity of monocytes in the BM additionally reflects an adaptation to infection. BM cluster 3 is the only BM cluster with high GAPDH expression (Figure 6.2N) and it expands at 7 dpi in the BM (Figure 6.2J, 6.2L), suggesting this cluster is a possible BM precursor for the pathogenic iNOS$^+$ state observed in the brain at 7 dpi. This notion is further supported by the close clustering of these populations by expression of their metabolic proteins (Figure 6.2N). While the developmental trajectory of metabolic clusters in the BM is unclear, it is possible that the metabolically quiescent cluster 1 (Figure 6.2F), which, although increasing its majority proportion by some 10% during the early phase of infection, was reduced by dpi 7, transits progressively towards the more metabolically active subsets, cluster 2 and 3, which may give rise to distinct MC subsets in the brain. These findings suggest that the metabolic conditioning of BM cells may prime MCs for distinct trajectories of differentiation prior to their infiltration into the inflamed brain.

6.1.3.3 MHC-II$^+$ and iNOS$^+$ MCs have distinct metabolic profiles

As MCs in WNV may adopt both NO-producing and antigen-presenting phenotypes in the brain, we next aimed to determine if these functional profiles were reflected by metabolic differences. Cluster 7 and 4 were determined to be an NO-producing and APC subset, respectively, based on their differential expression of iNOS and MHC-II (Figure 6.3A). Importantly, approximately 80% of iNOS$^+$ MCs were positive for DAF-FM (Supplementary Figure 6.3), a fluorescent probe that stains for intracellular NO, supporting a direct link between iNOS expression by these MCs and NO production. Intriguingly, compared to the NO-producing cluster 7, the APC cluster 4 expressed all metabolic proteins at lower levels

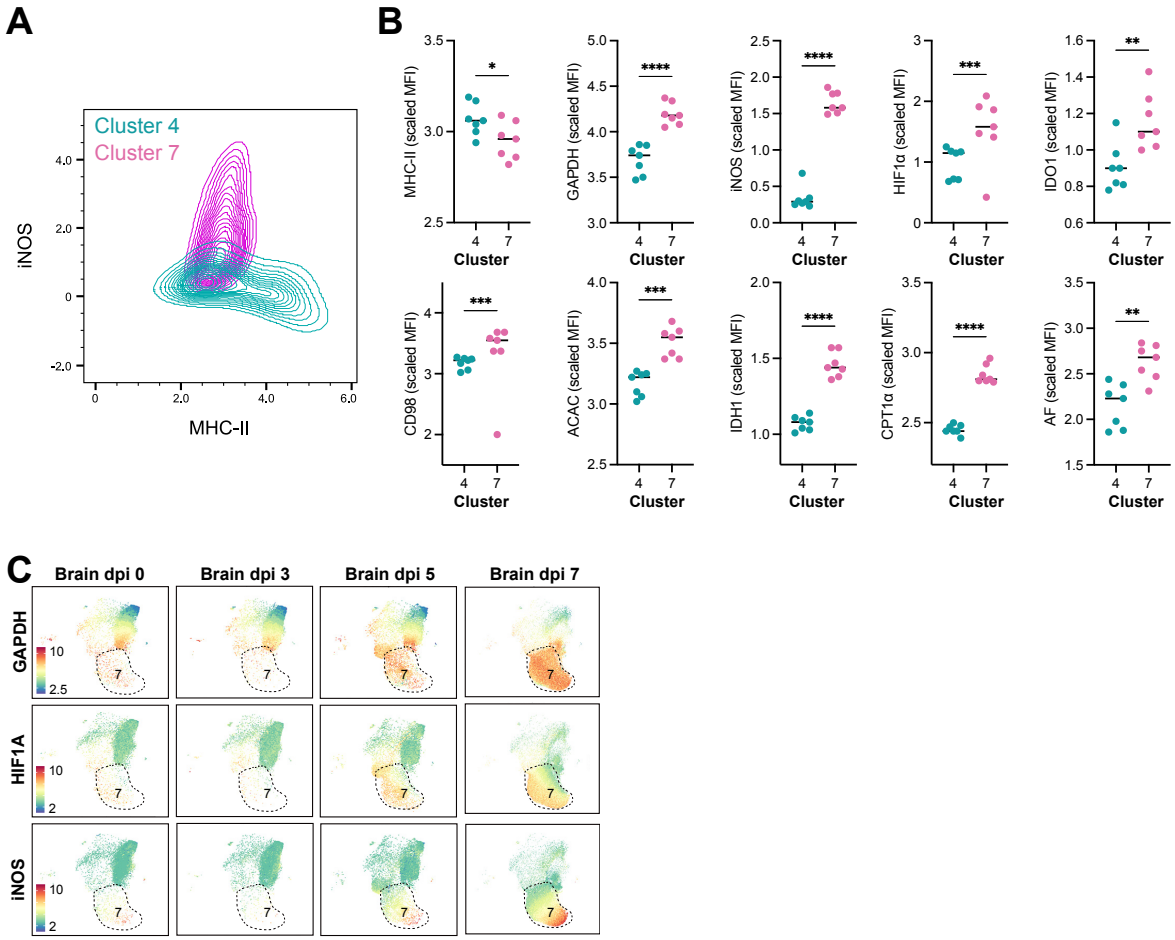
A
Cluster 4
Cluster 7
iNOS
MHC-II
B
MHC-II (scaled MFI)
GAPDH (scaled MFI)
iNOS (scaled MFI)
HIF1α (scaled MFI)
IDO1 (scaled MFI)
CD98 (scaled MFI)
ACAC (scaled MFI)
IDH1 (scaled MFI)
CPT1α (scaled MFI)
AF (scaled MFI)
Cluster
C
Brain dpi 0
Brain dpi 3
Brain dpi 5
Brain dpi 7
GAPDH
HIF1A
iNOS

Figure 6.3 MHC-II+ and iNOS+ MCs have distinct metabolic profiles in CNS viral infection.

(**A**) Contour plot depicting MHC-II and iNOS expression of metabolic cluster 4 (blue) and 7 (pink). (**B**) Arcsinh transformed MFI of selected functional and metabolic markers. (**C**) UMAP showing the expression of GAPDH, HIF1-α and iNOS in the brain in mock-infected and WNV-infected mice at 3, 5 and 7 dpi. Data are from two independent experiments with 3-4 mice per group. Statistics calculated with paired t-test. * $p<0.05$, ** $p<0.01$, *** $p<0.001$, **** $p<0.0001$. Error bars are representative of mean ± SD.

(Figure 6.3B). This observation suggests that the functional activity of cluster 7 might require synergism from multiple metabolic pathways to sustain this heightened inflammatory state, compared to that required for antigen presentation. Interestingly, these inflammatory iNOS$^+$ cells displayed an increased expression of glycolysis-related markers, such as GAPDH and HIF1-α, compared to APC MCs (Figure 6.3B and 6.3C). These markers are known to be closely linked with glycolytic activity, suggesting that an APC MC phenotype is less reliant on glycolysis than the classical M1-like phenotype associated with cluster 7. Collectively, these findings reinforce the notion that pathogenic, NO-producing MCs utilize glycolysis differently from other MC subsets, such as antigen-presenting cells, particularly in the context of virus-induced neuroinflammation.

6.1.3.4 Glycolysis inhibition is protective in WNV encephalitis

To determine whether pro-inflammatory monocyte metabolism could be therapeutically targeted in lethal infection, we next treated mice with a glycolysis inhibitor, 2-DG (Figure 6.4A), a nonmetabolizing glucose analogue and competitive inhibitor of hexokinase 1. 2-DG was administered at a dose of 2g/kg daily from 4 dpi to the disease endpoint at 7 dpi (Figure 6.4B). Remarkably, 2-DG treatment led to a discernible clinical improvement, as indicated by lower disease severity scores at 7 dpi (Figure 6.4C) and reduced weight loss (Figure 6.4D), with a modest, but significant increase in survival and mean time to death (Figure 6.4E, 6.4F). This was accompanied by significant reductions in inflammatory cytokine mRNA expression for *Tnf*, *Il6*, *Il1b*, and *Ifng*, indicating a global attenuation of neuroinflammation (Figure 6.4G). These improvements were not due to a reduction in viral load, as both 2-DG and PBS-treated mice exhibited comparable viral burdens in the brain at 7 dpi (Figure 6.4H), emphasizing that the effects of 2-DG are likely mediated through modulation of the pathological immune response within the brain.

Notably, 2-DG also reduced the overall neuroinflammatory infiltrate to approximately 35% of that seen in control-treated mice on 7 dpi (Figure 6.4I). A significant reduction in cell numbers was observed in infiltrating neutrophils, natural killer cells, CD4$^+$ and CD8$^+$ T cells, and MCs in the brain, but not microglia (Figure 6.4J). Furthermore, all these cells, including microglia, showed a decrease in GAPDH expression (Supplementary Figure 6.4). This reduction in immune cell infiltration may be due to a requirement of glycolysis for immune cell migration across endothelial barriers (Guak and Krawczyk, 2020). Alternatively, this might result from reduced MC numbers in the brain or an altered metabolic profile of microglia (Supplementary

Figure 4

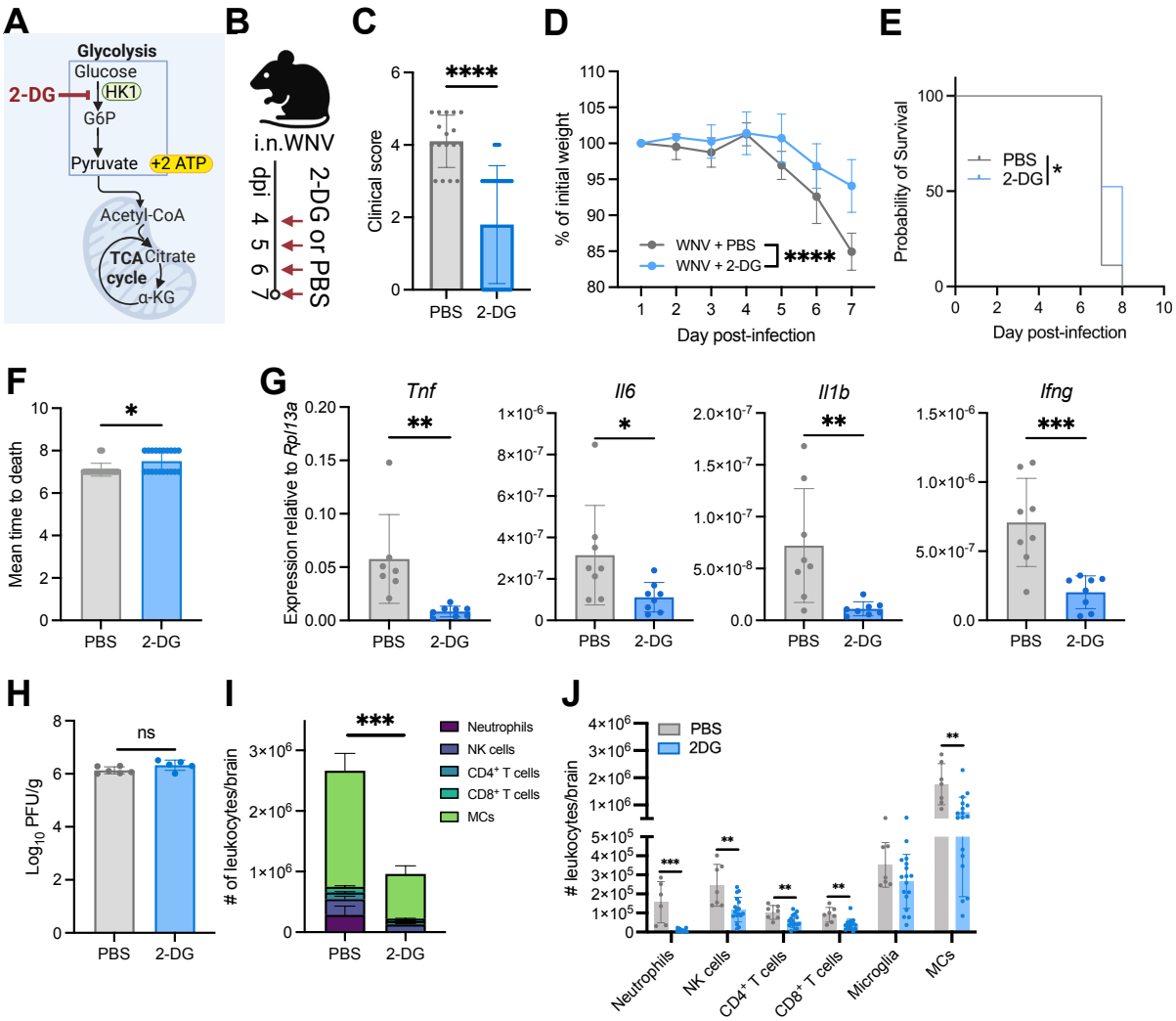
A
Glycolysis
Glucose
2-DG
HK1
G6P
Pyruvate
+2 ATP
Acetyl-CoA
TCA cycle
Citrate
α-KG
B
i.n.WNV
dpi 4 5 6 7
2-DG or PBS
C
Clinical score
****
PBS
2-DG
D
% of initial weight
WNV + PBS
WNV + 2-DG
****
Day post-infection
E
Probability of Survival
PBS
2-DG
*
Day post-infection
F
Mean time to death
*
PBS
2-DG
G
Expression relative to Rpl13a
Tnf
Il6
Il1b
Ifng
PBS
2-DG
H
Log10 PFU/g
ns
PBS
2-DG
I
# of leukocytes/brain
***
Neutrophils
NK cells
CD4+ T cells
CD8+ T cells
MCs
PBS
2-DG
J
leukocytes/brain
PBS
2DG
Neutrophils
NK cells
CD4+ T cells
CD8+ T cells
Microglia
MCs

Figure 6.4 Glycolysis inhibition is protective in WNV encephalitis.

(**A**) Schematic depicting 2-DG mechanism of action. (**B**) Schematic experimental design. WNV-infected mice were treated with 2 g/kg of 2-DG delivered i.p. daily from 4-7 dpi. (**C**) Clinical scores of 2-DG and PBS-treated mice at 7 dpi. (**D**) Weights of 2-DG and PBS-treated animals over the duration of infection shown as percentage of initial weight. (**E-F**) Survival (**E**) and mean time to death (**F**) of WNV-infected mice treated with 2-DG or PBS (vehicle control). (**G**) mRNA expression for selected pro-inflammatory cytokines in the brains of PBS- and 2-DG-treated mice at dpi 7, as determined by qPCR. Expression was normalized to the housekeeping gene *Rpl13a*. (**H**) WNV PFU in brains of 2-DG- and PBS-treated mice at 7 dpi. (**I**) Stacked bar graph showing numbers of indicated $CD45^+$ cell subsets in the brains of 2-DG- and PBS-treated mice at 7 dpi. (**J**) Numbers of infiltrating and resident immune cell populations in the brain at 7 dpi. Data in (**D**) are pooled and representative of mean ± SD. Data are from one (**E**, **F**, **G**, **H**) or two (**C**, **D**, **I**, **J**) independent experiment(s) with at least five mice per group. Statistics calculated with Mann-Whitney test (**C**, **F**, **I**, **J**), unpaired t-test (**D**, **G, H**), or Kaplan-Meier survival analysis (**E**). * $p<0.05$, ** $p<0.01$, *** $p<0.001$, **** $p<0.0001$. Error bars are representative of mean ± SD.

Figure 6.4), as both these cells contribute to the accumulation of other immune cells in the brain (Spiteri et al., 2023b, Spiteri et al., 2023a). Irrespective, these findings collectively highlight the potential of glycolysis inhibition as a therapeutic approach to attenuate immune cell infiltration during severe CNS inflammation.

6.1.3.5 Glycolysis inhibition reduces monocyte infiltration into the CNS, but does not reduce BM myelopoiesis

Glycolysis has been shown to be important for both myelopoiesis and cellular migration. We have previously shown that diminished myelopoiesis correlates with reduced brain MC numbers and better clinical outcomes in WNV infection (Spiteri et al., 2022a). Thus, to investigate whether the protective effect of 2-DG was due to a reduction in myelopoiesis and/or subsequent CNS infiltration, we first measured changes in monocyte proliferation using BrdU, which incorporates detectably into synthesising DNA (Figure 6.5A, 6.5B). Our data revealed no significant changes in BrdU incorporation following 2-DG treatment (Figure 6.5C-D), with proliferating cell proportions consistent across all monocyte differentiation phases and other myeloid cell types (Figure 6.5D, Supplementary Figure 6.5). Correspondingly, total BM monocyte counts were comparable between PBS- and 2-DG-treated mice (Figure 6.5E).

We then assessed the effect of 2-DG on cellular migration into the brain. WNV-infected mice were administered a single dose of 2-DG at 7 dpi followed by intravenous injection of the fluorescent dye, PKH26 (Figure 6.5F, 6.G). This labels blood and BM cells in the vasculature *in vivo* (Figure 6.5F, 6.5G), thereby enabling the discrete identification of cells that have infiltrated into the brain from the periphery after PKH26 injection (Spiteri et al., 2022a). Post-treatment analysis showed no significant change in total brain MC numbers, compared to PBS-treated, WNV-infected mice (Figure 6.5H). However, there was a significant decrease in the proportion of $PKH26^+$ MCs (Figure 6.5I) and a marked reduction in the infiltration rate of $PKH26^+$ MCs into the brain, but no reduction in the rate of infiltration of other dye-positive leukocytes (Figure 6.5J). This corresponded to a significant decrease in the total number of $PKH26^+$ MCs in the brain not evident in other infiltrating cells (Figure 6.5K). This indicates an acute MC-specific effect of 2-DG on MC migration into the brain. It also strongly suggests that the reduced presence of other immigrating leukocytes after longer term treatment with 2-DG from 4-7 dpi (Figure 6.4I, J) is a consequence of reduced recruitment occasioned by the accumulation of fewer MCs in the brain, rather than the dependence on glycolysis *per se* for diapedesis by non-MCs. Indeed, daily 2-DG treatment significantly reduced the expression of chemokines recruiting various immune cells to the brain, including *Ccl2*, *Ccl7*, *Ccl3*, and

Figure 5

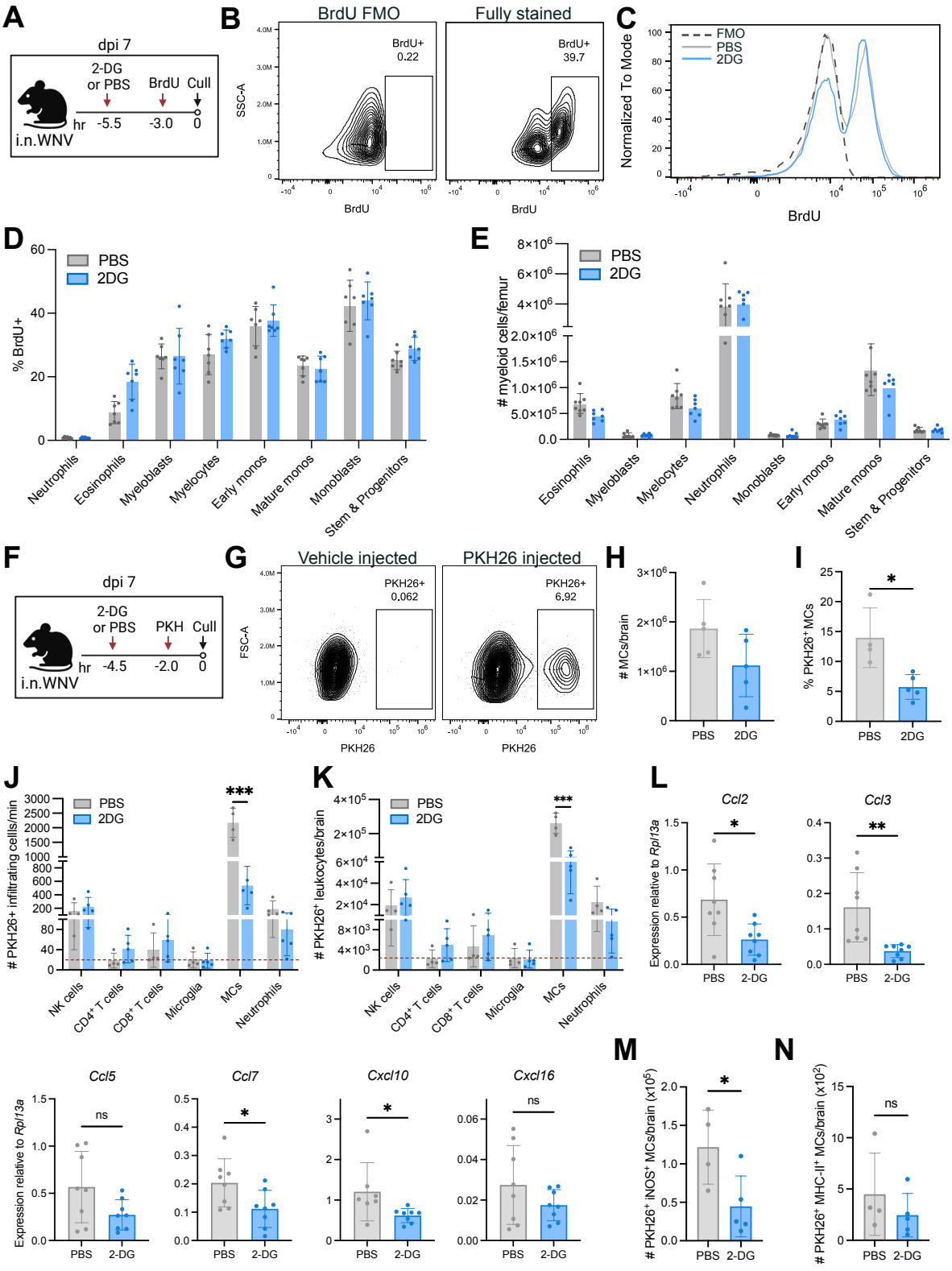
A
dpi 7
2-DG or PBS
BrdU
Cull
hr -5.5 -3.0 0
i.n.WNV
B
BrdU FMO
Fully stained
BrdU+ 0.22
BrdU+ 39.7
SSC-A
BrdU
C
FMO
PBS
2DG
Normalized To Mode
BrdU
D
PBS
2DG
% BrdU+
Neutrophils
Eosinophils
Myeloblasts
Myelocytes
Early monos
Mature monos
Monoblasts
Stem & Progenitors
E
PBS
2DG
myeloid cells/femur
Eosinophils
Myeloblasts
Myelocytes
Neutrophils
Monoblasts
Early monos
Mature monos
Stem & Progenitors
F
dpi 7
2-DG or PBS
PKH
Cull
hr -4.5 -2.0 0
i.n.WNV
G
Vehicle injected
PKH26 injected
PKH26+ 0.062
PKH26+ 6.92
FSC-A
PKH26
H
MCs/brain
PBS
2DG
I
% PKH26+ MCs
PBS
2DG
J
PBS
2DG
PKH26+ infiltrating cells/min
NK cells
CD4+ T cells
CD8+ T cells
Microglia
MCs
Neutrophils
K
PBS
2DG
PKH26+ leukocytes/brain
NK cells
CD4+ T cells
CD8+ T cells
Microglia
MCs
Neutrophils
L
Ccl2
Ccl3
Expression relative to Rpl13a
PBS
2-DG
M
PKH26+ iNOS+ MCs/brain (x10^5)
PBS 2-DG
N
PKH26+ MHC-II+ MCs/brain (x10^2)
PBS 2-DG
Ccl5
Ccl7
Cxcl10
Cxcl16
Expression relative to Rpl13a
PBS
2-DG

Figure 6.5 Glycolytic inhibition with 2-DG reduces CNS infiltration without impacting BM myelopoiesis.

(**A**) Schematic showing treatment regimen. Mice infected with WNV received 2-DG or PBS treatment once daily from 4-6 dpi and 5.5 hours prior to euthanasia at 7 dpi. BrdU was administered to both groups 2.5 hours after 2-DG treatment (3 hours before euthanasia) at 7 dpi to assess differential rates of cellular proliferation. (**B)** Contour plots showing BrdU incorporation in BM-derived monocytes compared to a FMO control. (**C**) Histogram depicting BrdU expression in mature monocytes from 2-DG-treated versus PBS-treated mice. (**D**) Proportion of BM myeloid cells incorporating BrdU. (**E)** Absolute numbers of indicated myeloid cell subsets in the femur. (**F**) Schematic showing the experimental workflow for tracking CNS infiltration. Mice were treated with 2-DG once 4.5 hours before euthanasia at 7 dpi, followed by an injection with PKH26 2.5 hours later (2 hours before euthanasia) for *in vivo* labelling of blood and BM cells. (**G**) Contour Plot showing PKH26 staining in brain MCs compared to the FMO control (*i.e.* vehicle-injected mice). (**H**) Total number of MCs present in the brain at 7 dpi. (**I**) Percentage of $PKH26^+$ MCs in the brain (*i.e.*, recently infiltrating cells). (**J, K**) Absolute numbers of indicated $CD45^+$, $PKH26^+$ leukocyte subsets infiltrating the brain per minute (**J**) or total accumulated cells in the brain (**K**). (**L**). mRNA expression for selected chemokines in the brains of PBS and 2-DG-treated mice at dpi 7, as determined by qPCR. Expression was normalized to the housekeeping gene *Rpl13a*. Mice were treated once daily as depicted in (**A**). (**M**, **N**) Absolute numbers of $PKH26^+$ $iNOS^+$ MCs (**M**), and $PKH26^+$ $MHC\text{-}II^+$ MCs (**N**) within the brain. Data are representative of one independent experiment with 4-8 mice per group. Dotted red line in J, K is indicative of threshold for background $PKH26^+$ staining as determined by positive staining of microglia. Statistics calculated by unpaired t-test (**H, I, M, N**) or multiple t-tests with two-stage step up method of Bejamini, Krieger, and Yekutieli tests for multiple comparisons (**D, E, J, K**). * $p<0.05$, *** $p<0.001$. Error bars are representative of mean ± SD.

Cxcl10 (Figure 6.5L). *Cxcl16*, produced by astrocytes and microglia, was not reduced, suggesting that 2-DG treatment does not affect chemokine production by brain-resident cells. Furthermore, 2-DG treatment did not affect the absolute numbers of effector and memory T cells, their proliferation, nor their GAPDH levels in the cervical lymph nodes draining the brain following daily 2-DG treatment from 4-7 dpi (Supplementary Figure 6.6), indicating that the reduced T cell numbers in the brain is not due to systemic effects of 2-DG on T cell expansion in the lymph nodes. Taken together, this is consistent with findings that inhibiting monocyte brain accumulation *e.g.*, via Ly6C blockade or clodronate liposome administration results in significantly reduced T cell and NK cell infiltration (Spiteri et al., 2023b, Spiteri et al., 2023a). Additionally, we found that 2-DG preferentially reduced the number of dye-positive iNOS$^+$ MCs compared to MHC-II$^+$ MCs in the brain (Figure 6.5M, 6.5N), suggesting that glycolysis inhibition may preferentially impede the differentiation of iNOS$^+$ MCs once in the brain, likely due to their particular reliance on glycolysis.

6.1.3.6 Glycolysis inhibition differentially affects NO-producing and antigen-presenting capacity of myeloid cells

We next aimed to determine whether systemic glycolysis inhibition differentially affects MC subsets. To do this, all iNOS$^+$ and MHC-II$^+$ MCs were manually gated for analysis (Figure 6.6A, 6.6E and Supplementary Figure 6.7). Metabolic profiling revealed a >80% decrease in numbers of iNOS$^+$ MCs within the inflamed brain following daily 2-DG treatment for five days (Figure 6.6B), mirroring a similar decline in the proportion of MCs expressing iNOS (Figure 6.6C). Importantly, 2-DG treatment only affected the expression of markers related to glycolysis (GAPDH) and NO production (iNOS) in MCs (Figure 6.6D), demonstrating that 2-DG treatment selectively reduced glycolysis without impacting other metabolic pathways. This was borne out by a significant increase in HIF1-α with 2-DG treatment (Figure 6.6D) and further supported by *in vitro* work suggesting that glycolysis-dependent NO production is independent of HIF1-α signalling in M1-like cells (Supplementary Figure 6.7). This pattern emphasizes the specificity of 2-DG on glycolysis, with negligible effects on other examined metabolic processes. Furthermore, clustering 2-DG-treated and PBS-treated BM and brain myeloid cells on metabolic proteins revealed no significant suppression of the HIF1-α$^+$ intermediate population (cluster 2) in the brain at dpi 7 (Supplementary Figure 6.8). This observation supports the hypothesis that this intermediate subset, in contrast to the iNOS$^+$ MC population, has a reduced reliance on glycolytic processes.

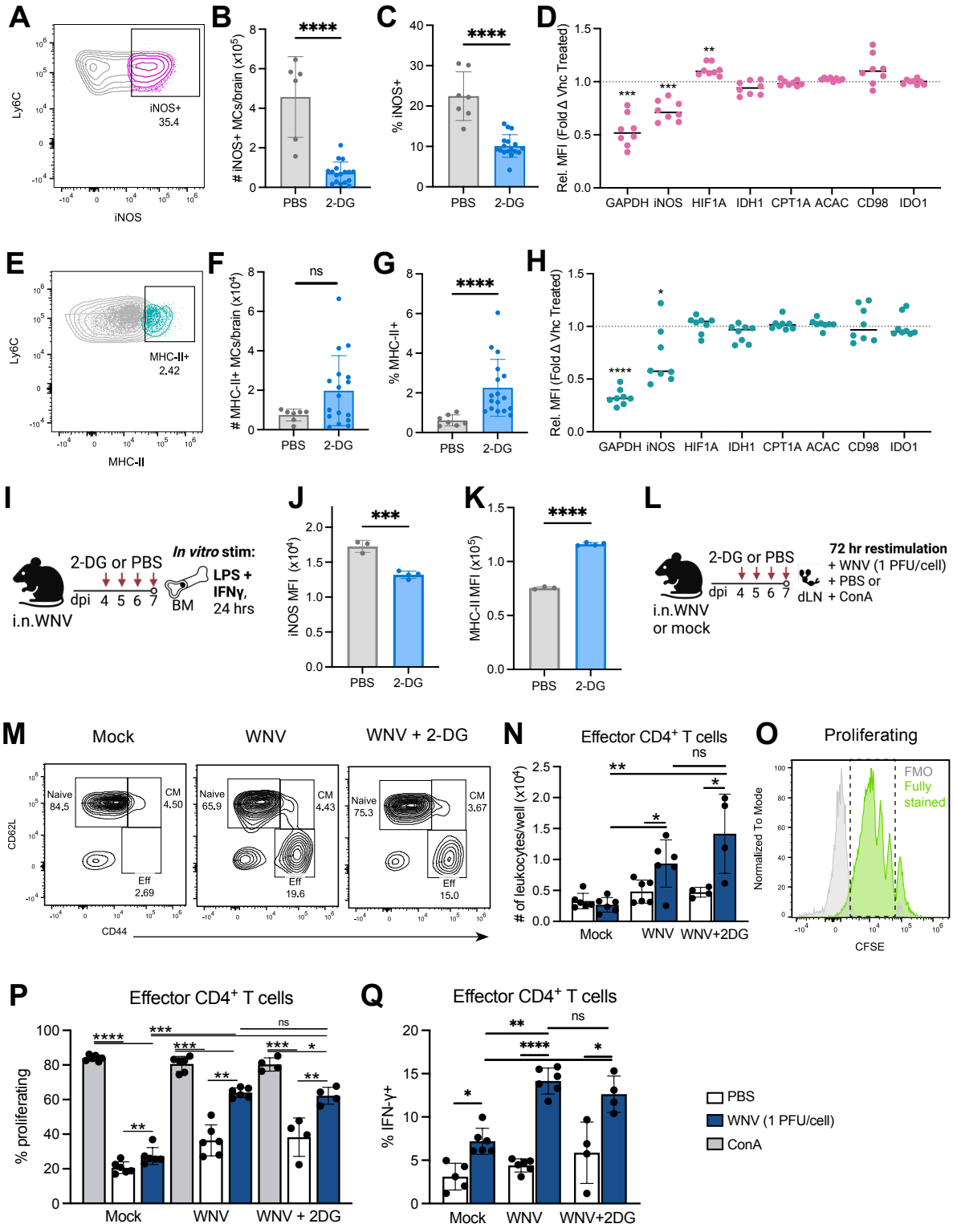
A
Ly6C
iNOS+
35.4
iNOS
B
iNOS+ MCs/brain (x10^5)
****
PBS
2-DG
C
% iNOS+
****
PBS
2-DG
D
Rel. MFI (Fold Δ Vhc Treated)
***
***
**
GAPDH iNOS HIF1A IDH1 CPT1A ACAC CD98 IDO1
E
Ly6C
MHC-II+
2.42
MHC-II
F
MHC-II+ MCs/brain (x10^4)
ns
PBS
2-DG
G
% MHC-II+
****
PBS
2-DG
H
Rel. MFI (Fold Δ Vhc Treated)
****
*
GAPDH iNOS HIF1A IDH1 CPT1A ACAC CD98 IDO1
I
2-DG or PBS
dpi 4 5 6 7
i.n.WNV
In vitro stim:
LPS + IFNγ, 24 hrs
BM
J
iNOS MFI (x10^4)
***
PBS
2-DG
K
MHC-II MFI (x10^5)
****
PBS
2-DG
L
2-DG or PBS
dpi 4 5 6 7
i.n.WNV
or mock
72 hr restimulation
+ WNV (1 PFU/cell)
+ PBS or
dLN + ConA
M
Mock
WNV
WNV + 2-DG
CD62L
CD44
Naive 84.5
CM 4.50
Eff 2.69
Naive 65.9
CM 4.43
Eff 19.6
Naive 75.3
CM 3.67
Eff 15.0
N
Effector CD4+ T cells
# of leukocytes/well (x10^4)
**
ns
*
*
Mock
WNV
WNV+2DG
O
Proliferating
Normalized To Mode
FMO
Fully stained
CFSE
P
Effector CD4+ T cells
% proliferating
****
***
***
ns
***
*
**
**
**
Mock
WNV
WNV + 2DG
Q
Effector CD4+ T cells
% IFN-γ+
**
ns
****
*
*
Mock
WNV
WNV+2DG
PBS
WNV (1 PFU/cell)
ConA

Figure 6.6 Glycolysis inhibition differentially affects iNOS+ and MHC-II+ MCs.

(A) Dot plot showing iNOS$^+$ MCs in the brain at 7 dpi. (**B, C**) Number (**B**) and percent (**C**) of iNOS$^+$ MCs in the brain at 7 dpi. (**D**) Fold-change in MFI of selected metabolic markers in 2-DG-treated mice relative to PBS-treated mice. (**E**) Dot plot showing MHC-II$^+$ MCs in the brain at 7 dpi. (**F, G**) Number (**F**) and percent **(G)** of MHC-II$^+$ MCs in the brain at 7 dpi. (**H**) Fold-change in median fluorescence intensity of selected metabolic markers in 2-DG-treated mice relative to PBS-treated mice. (**I**) Schematic outlining experimental design for BM stimulation. Whole BM cells were isolated from WNV-infected mice treated with 2-DG or PBS daily from day 4-7, and then stimulated with LPS and IFN-γ for 24 hours. (**J, K**) MFI of iNOS and MHC-II in cultured monocytes. (**L**) Schematic showing experimental design for assessment of T cell proliferation. Whole cervical draining lymph nodes (dLN) were stimulated with WNV or PBS for 1 hour, prior to being cultured with either PBS or Con A for 72 hours. (**M**) Contour plots showing gating of naïve, central memory (CM) and effector (eff) CD4$^+$ T cells based on CD62L and CD44 expression across groups stimulated with WNV. (**N**) Number of effector CD4$^+$ T cells per well of cultured lymph nodes. (**O**) Histogram depicting CFSE staining relative to fluorescence-minus-one control (FMO). The dotted box indicates proliferating cells. (**P**, **Q**) Percent of proliferating (**P**) and IFN-γ$^+$ (**Q**) effector CD4$^+$ T cells. Data are from one independent experiment with eight mice per group. Statistics calculated ordinary one-way ANOVA with Tukey's test for multiple comparisons (**D**, **H**), Mann-Whitney test (**B**, **C**, **F**, **G**, **J**, **K**), RM one-way ANOVA with Tukey's test for multiple comparisons (**P**, **N**, **Q**) and paired t-test (**N**, **Q**). * $p<0.05$, ** $p<0.01$, *** $p<0.001$, **** $p<0.0001$. Error bars are representative of mean ± SD.

Despite the substantial decrease in iNOS$^+$ MCs, the number of MHC-II$^+$ MCs present in the brain was not reduced following 2-DG treatment (Figure 6.6F). This led to a significant proportional increase of 3-4-fold in MHC-II$^+$ MCs (Figure 6.6G), emphasising the disproportionate impact of glycolysis inhibition on iNOS$^+$ cells. Interestingly, in the MHC-II$^+$ cell population, we noted a significant reduction solely in the GAPDH and iNOS expression, similar to the iNOS$^+$ cells (Figure 6.6H), indicating that pathways already reduced in this population may be inhibited still further by 2-DG in these cells.

To examine the functional implications of glycolysis inhibition in more detail, BM cells isolated from 2-DG- and PBS-treated WNV-infected mice were stimulated with classical M1 activation stimuli (IFN-γ + LPS) *in vitro* (Figure 6.6I). Monocytes from 2-DG-treated mice exhibited significantly reduced expression of iNOS relative to vehicle-treated WNV-infected mice (Figure 6.6J), suggesting that BM monocytes from 2-DG-treated mice have reduced capacity for NO production in response to inflammatory stimuli. Interestingly, although these cells had significantly reduced iNOS expression, BM monocytes from 2-DG-treated mice showed significantly increased MHC-II expression in response to inflammatory stimulation relative to control-treated mice, presumably due to IFN-γ exposure (Figure 6.6K). This further suggests that while systemic 2-DG treatment may reduce the inflammatory potential of monocytes prior to their differentiation into effector MCs, it may not affect, or may even improve their capacity for antigen presentation.

To confirm that antigen-presenting functions are not impacted by 2-DG, we isolated draining cervical lymph nodes from 4-7 dpi 2-DG- and vehicle-treated WNV-infected mice and vehicle-treated mock-infected mice at 7 dpi and stimulated them with WNV, which contains both replicating virus and free viral antigen, for 72 hours (Figure 6.6L). Effector CD4$^+$ T cell differentiation (Figure 6.6M) was significantly increased following *in vitro* viral restimulation of T cells isolated from WNV-infected mice treated with vehicle or 2-DG, compared to those from mock-infected mice (Figure 6.6N). Importantly, 2-DG-treated and vehicle-treated WNV-infected mice showed comparable numbers of effector CD4$^+$ T cells, suggesting that the capacity of antigen-presenting cells to stimulate an effector T cell response is unaffected by 2-DG treatment. Supporting this, the proportions of proliferating effector CD4$^+$ T cells (Figure 6.6O and 6.6P) and IFN-γ-producing effector T cells (Figure 6.6Q) in response to viral re-stimulation were also unaffected by 2-DG treatment. CD8$^+$ T cells remained similarly unaffected by 2-DG treatment (Supplementary Figure 6.9). Together, this demonstrates that

systemic 2-DG treatment specifically targets NO-producing MCs in cluster 7 to reduce NO, without impacting antigen-presenting function of MCs in cluster 4.

6.1.4 Discussion

This study represents the first dual approach using both scRNA-seq and spectral cytometry to inspect the metabolic profiles of MCs at a gene and protein level, uncovering for the first time the intricate metabolic diversity of these cells within the context of CNS disease. The novelty of this study lies in the observation that MCs, arising from three metabolically distinct subsets in the BM, transit to the brain and further differentiate into three distinct subsets. The first of these, a HIF1-α^{+} population, gives rise two further metabolically and functionally distinct populations, a glycolytic NO-producing population, which clearly contributes to severe neuroinflammation, and a second, non-glycolytic antigen presenting population, capable of triggering ongoing T cell responses that would facilitate viral clearance. This suggests a continuous regulatory capacity in MC metabolism that controls functional differentiation. Targeting the NO-producing population with the glycolysis inhibitor, 2-DG, specifically reduced their migration into the brain and impaired their ability to produce NO. Strikingly, this corresponded with a significant reduction in clinical and neuroinflammatory signs, highlighting the therapeutic potential of modulating immunometabolism to ameliorate disease.

Our findings indicate that MCs adopt multiple functional roles, each defined by a unique metabolic phenotype. While the NO-producing MCs described in this report exhibited a metabolic profile suggestive of the traditional M1 phenotype, this varied markedly from the conventional M1 or M2 categorization. The local tissue environment was likely a decisive factor influencing these metabolic patterns, as BM monocytes and brain MCs demonstrated distinct metabolic signatures. This observation is consonant with recent research highlighting the significance of tissue origin in shaping the metabolic characteristics of resident macrophages (Heieis et al., 2023), in which the varying nutritional and cellular contexts provided by different tissues likely drive cells towards specific metabolic pathways. Furthermore, the divergent developmental origins of microglia (arising from the yolk sac) and MCs (originating from hematopoietic stem cells in the BM) likely contributed to their metabolic differences during infection. Notably, microglia tended to maintain a more homeostatic metabolic state, while MCs infiltrating the brain shifted towards more active metabolic profiles. Overall, this distinction emphasizes the importance of both origin and environment in the metabolic identity of immune cells in the CNS during infection.

The metabolic programming of monocytes—whether established during development in the BM or upon entry into the virus-infected CNS—remains unclear. Our findings suggest metabolic cues in each organ play an important role, with trajectory analysis revealing a clear metabolic progression of monocytes migrating from the BM to the CNS. This transition is marked by a decreased expression of genes involved in ATP production, the TCA cycle, and the ETC, coupled with an increased reliance on glycolysis. While the developmental trajectory of metabolic clusters in the BM remains to be fully elucidated, our observations indicate that cluster 1, initially expanding in the early stages of infection but diminishing by dpi 7, may evolve into more metabolically active clusters 2 and 3. This initial metabolic state of BM cells could set the stage for varied differentiation pathways of MCs, effectively 'priming' them before they migrate to the inflamed brain environment. Once in the brain, BM monocytes evidently assume a HIF1-α^+ intermediate state, which may act as the branching point for divergence into iNOS$^+$ or APC MC subsets. Such a metabolic shift might be an adaptive strategy to ensure survival in the hypoxic conditions of the infected CNS (Everts et al., 2012). Indeed, the transcription factor HIF1-α, known to drive the expression of glycolytic enzymes, is crucial for myeloid cell motility during mild hypoxia such as inflammation (Cramer et al., 2003, Semba et al., 2016). Importantly, HIF1-α was significantly upregulated in glycolytic MCs in our study and maintained its expression in infiltrating MCs following 2-DG treatment, indicating its independence from glycolysis. This presumably enables immigration of APC MCs, but not iNOS$^+$ MCs. Our scRNA-seq analysis further supports this hypothesis, showing a close association between the upregulation of glycolysis and macrophage migration in *Nos2*$^+$ and *Hif1a*$^+$ MCs. Additionally, 2-DG treatment significantly reduced physical monocyte migration into the inflamed brain without impacting myelopoiesis, suggesting that glycolytic inhibition mediates its protective effect by preferentially preventing inflammatory cellular transmigration across the blood-brain barrier. The cellular specificity of this targeting may be due to the entry of these inflammatory cells at distinct anatomical locations in the CNS or their exposure to different regions of the brain that have different rates of infection and unique cytokine or chemokine profiles (Shechter et al., 2013). This link is substantiated by observations in EAE and human MS, where heightened glycolytic activity is associated with the transmigration of inflammatory macrophages into the brain (Kaushik et al., 2019). However, as 2-DG treatment reduced chemokine expression in the brain, it remains unclear whether the differential effect of 2-DG on the migration of APC and iNOS$^+$ MCs stems from inherent differences in migratory capacity or their dependence on different chemokine gradients. Moreover, determining whether the observed decrease in chemokine levels is a

consequence of the attenuated migration of MCs into the brain is challenging. This is of particular importance since MCs are essential for the synthesis of chemokines that recruit immune cells to the WNV-infected brain (Spiteri et al., 2023b).

Enhanced glycolysis observed in immune cells during WNV encephalitis and other diseases strongly suggests that targeting metabolic reprogramming within inflammatory cells could be a promising complementary approach for immune therapy. In this study, 2-DG treatment preferentially impacted pathogenic, NO-producing MCs. Furthermore, the ability of 2-DG to cross the blood-brain barrier (Zahoor et al., 2022) may contribute to ongoing targeting of these cells at the site of inflammation. This is supported by our data showing the 2-DG reduces the expression of inflammatory genes and interleukins in the CNS during WNV infection, as well as those of others (Mingo-Casas et al., 2023), suggesting a broad reduction in brain inflammation. Additionally, in EAE, 2-DG treatment skewed monocytes/macrophages towards an anti-inflammatory state in the CNS, providing protection and overall clinical improvement (Zahoor et al., 2022). Despite the evident anti-inflammatory effect of glycolysis inhibition at the sites of inflammation, we additionally observed that BM monocytes derived from 2-DG treated mice showed a decreased NO response to inflammatory stimuli outside the brain. This suggests an early modulation of their inflammatory potential, likely due to the dependence of NO synthesis on glycolysis, with the capacity to produce NO not fully restored upon their entry into the brain.

Interestingly, we show that antigen-presenting MCs have a metabolic profile distinct from those producing NO, primarily attributed to reduced glycolytic activity. MHC-II^{hi} macrophages also displayed lower reliance on glycolysis than MHC-II^{lo} macrophages (Geeraerts et al., 2021), and monocytes diminish glycolytic activity as they develop into an antigen-presenting phenotype *in vitro* (Adamik et al., 2022), suggesting a negative association between glycolysis and antigen presentation. Supporting this, elevated glucose levels have been shown to hinder antigen presentation and disrupt CD4^{+} T cell activation (Monroy-Mérida et al., 2021). Conversely, glucose limitation appears to enhance MC-mediated T cell responses, as demonstrated by the increased expression by glucose-deprived MCs of co-stimulatory molecules and interleukin-12 essential for T cell proliferation and function (Lawless et al., 2017). Thus, APC may strategically reduce glycolysis to adapt to the glucose-scarce environment generated by metabolically-active T cells, thereby prolonging the T cell response (Lawless et al., 2017). In this study, MCs may transition to an antigen-presenting role as their

glycolytic activity declines to optimize their capacity to present antigens effectively. This study did not evaluate the antigen-presenting capability of MCs from the brain due to limited cell numbers and the challenges associated with primary brain cell culture. However, APCs isolated from the draining lymph nodes of 2-DG treated mice maintained their ability to elicit an anti-viral T cell response after antigen rechallenge *ex vivo.* These findings indicate that 2-DG does not diminish the antigen presenting efficacy of APCs and does not impair the establishment of a memory T cell response.

The unaffected memory T cell response during glycolytic inhibition may be attributed to their reliance on fatty acid oxidation, a metabolic pathway essential for memory development (Gupta et al., 2019, O'Sullivan et al., 2014). Importantly, while 2-DG treatment significantly supressed glycolytic markers, it did not alter other metabolic pathways, including fatty acid oxidation. Consequently, despite a reduction in T cell numbers in the brain over three days of 2-DG treatment, T cell proliferation and memory formation evidently remained intact. Furthermore, the absence of acute inhibition of T cell immigration by 2-DG, in contrast to $iNOS^+$ MCs, strongly suggests that reduced T cell infiltration into the brain by longer term 2-DG treatment was more likely a consequence of their reduced recruitment by low MC numbers than direct migration inhibition of these cells by 2-DG. In summary, our findings suggest that glycolytic inhibition selectively hinders the infiltration of hyperinflammatory cells without affecting the functional development of a robust T cell response during WNV infection.

This research highlights that modulating the metabolic pathways active in pathogenic monocytes can mitigate disease severity by specifically tempering uncontrolled inflammation, a key contributor to disease exacerbation and progression. This nuanced approach preserves essential immune processes, including pathogen clearance and memory formation, and may be most effective when combined with anti-viral therapies. Unlike broad-acting immunosuppressants like corticosteroids, which indiscriminately suppress both detrimental and beneficial immune responses, metabolic modulation offers more targeted control of the inflammatory response. Although the effectiveness of this strategy in humans requires further study, these findings reinforce the potential of metabolic targeting to complement *e.g.,* anti-microbial treatment, as a component of combination therapy for immune regulation in diseases with severe or uncontrolled inflammation.

6.1.5 Supplementary Figures

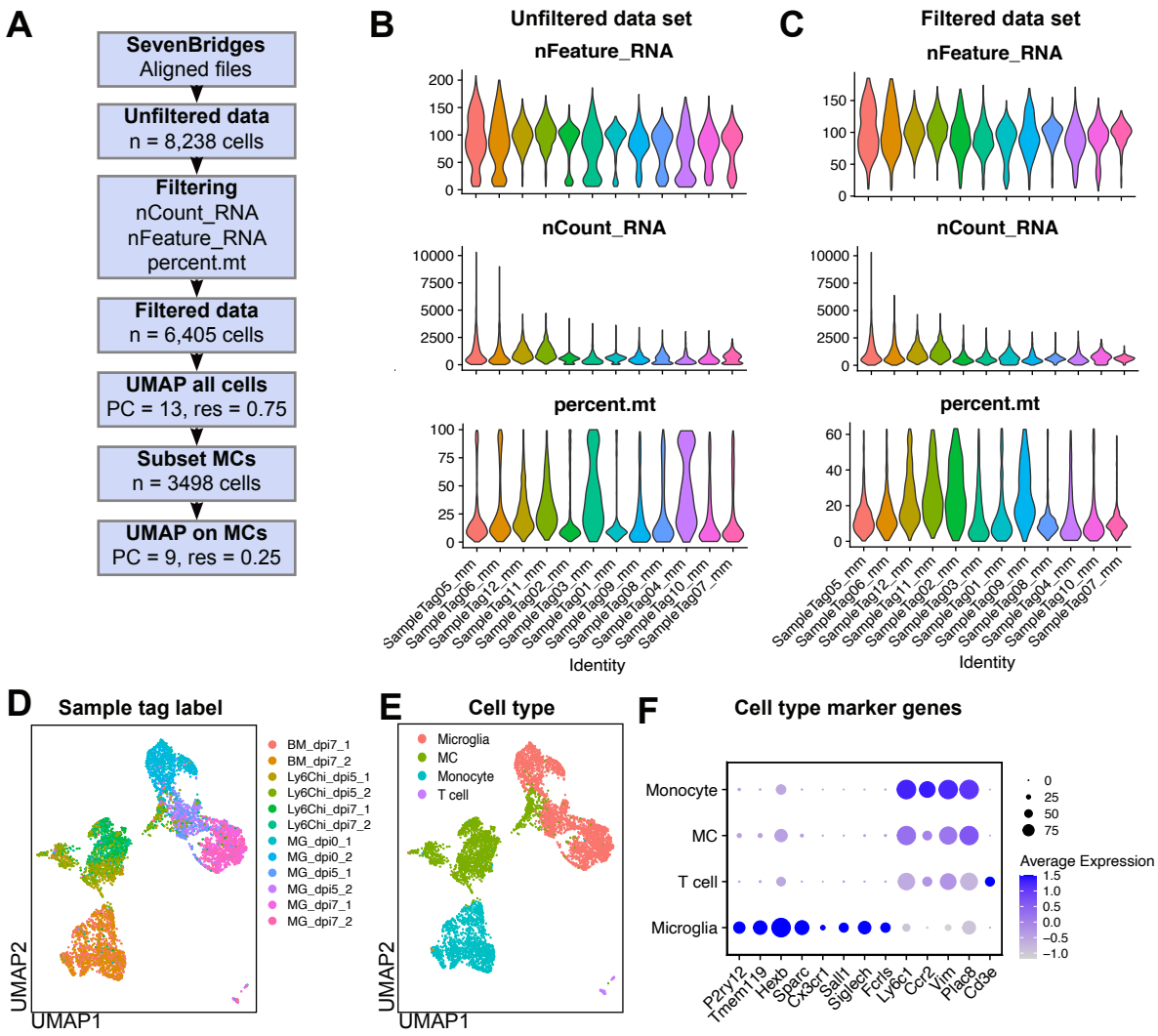
A
SevenBridges
Aligned files
Unfiltered data
n = 8,238 cells
Filtering
nCount_RNA
nFeature_RNA
percent.mt
Filtered data
n = 6,405 cells
UMAP all cells
PC = 13, res = 0.75
Subset MCs
n = 3498 cells
UMAP on MCs
PC = 9, res = 0.25
B
Unfiltered data set
nFeature_RNA
nCount_RNA
percent.mt
SampleTag05_mm
SampleTag06_mm
SampleTag12_mm
SampleTag11_mm
SampleTag02_mm
SampleTag03_mm
SampleTag01_mm
SampleTag09_mm
SampleTag08_mm
SampleTag04_mm
SampleTag10_mm
SampleTag07_mm
Identity
C
Filtered data set
nFeature_RNA
nCount_RNA
percent.mt
Identity
D
Sample tag label
BM_dpi7_1
BM_dpi7_2
Ly6Chi_dpi5_1
Ly6Chi_dpi5_2
Ly6Chi_dpi7_1
Ly6Chi_dpi7_2
MG_dpi0_1
MG_dpi0_2
MG_dpi5_1
MG_dpi5_2
MG_dpi7_1
MG_dpi7_2
UMAP2
UMAP1
E
Cell type
Microglia
MC
Monocyte
T cell
UMAP2
UMAP1
F
Cell type marker genes
Monocyte
MC
T cell
Microglia
P2ry12
Tmem119
Hexb
Sparc
Cx3cr1
Sall1
Siglech
Fcrls
Ly6c1
Ccr2
Vim
Plac8
Cd3e
Average Expression

Supplementary Figure 6.1 Quality control metrics and cell type classification for scRNA-seq data in the WNV infected brain and BM.

(**A**) Analysis workflow. (**B**) Quality control metrics, including nFeature_RNA, nCount RNA, and percent mitochondrial gene expression before and after filtering for each of the sample tags. The unfiltered data set contained 8,238 cells and the filtered data set contained 6,305 cells. (**D, E**) UMAPs showing clustering of filtered data set prior to subsetting MCs from microglia and T cells, pseudocoloured by sample name **(D)** and cell type **(E)**. (**F**) Dot plot heatmap showing the expression of select genes in identified cell types. Data are from one independent experiment with four mice per group.

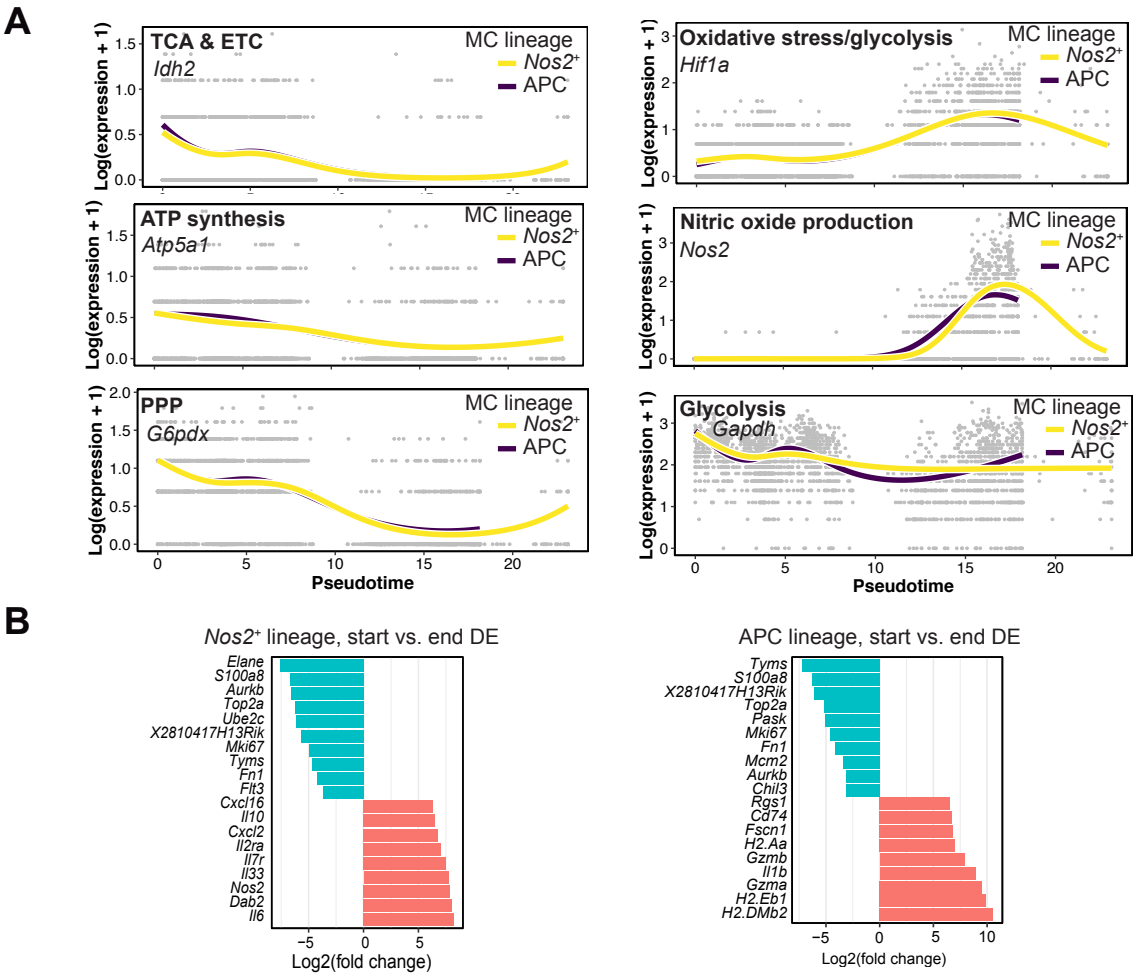
A
TCA & ETC
Idh2
Oxidative stress/glycolysis
Hif1a
ATP synthesis
Atp5a1
Nitric oxide production
Nos2
PPP
G6pdx
Glycolysis
Gapdh
MC lineage
Nos2+
APC
Log(expression + 1)
Pseudotime
B
Nos2+ lineage, start vs. end DE
Elane
S100a8
Aurkb
Top2a
Ube2c
X2810417H13Rik
Mki67
Tyms
Fn1
Flt3
Cxcl16
Il10
Cxcl2
Il2ra
Il7r
Il33
Nos2
Dab2
Il6
Log2(fold change)
APC lineage, start vs. end DE
Tyms
S100a8
X2810417H13Rik
Top2a
Pask
Mki67
Fn1
Mcm2
Aurkb
Chil3
Rgs1
Cd74
Fscn1
H2.Aa
Gzmb
Il1b
Gzma
H2.Eb1
H2.DMb2
Log2(fold change)

Supplementary Figure 6.2 Pseudotemporal ordering of Nos2+ and APC lineages with Slingshot.

(**A**) Expression of select genes in *Nos2*$^{+}$ and *APC* lineages along pseudotime. (**B**) Top differentially expressed markers between the lineage root (*Mo3*) to lineage end-point (*Nos2*$^{+}$ *MC* or *APC MC*) for each lineage. Data are represented as $\log_2$fold-change. Data are from one independent experiment with four mice per group.

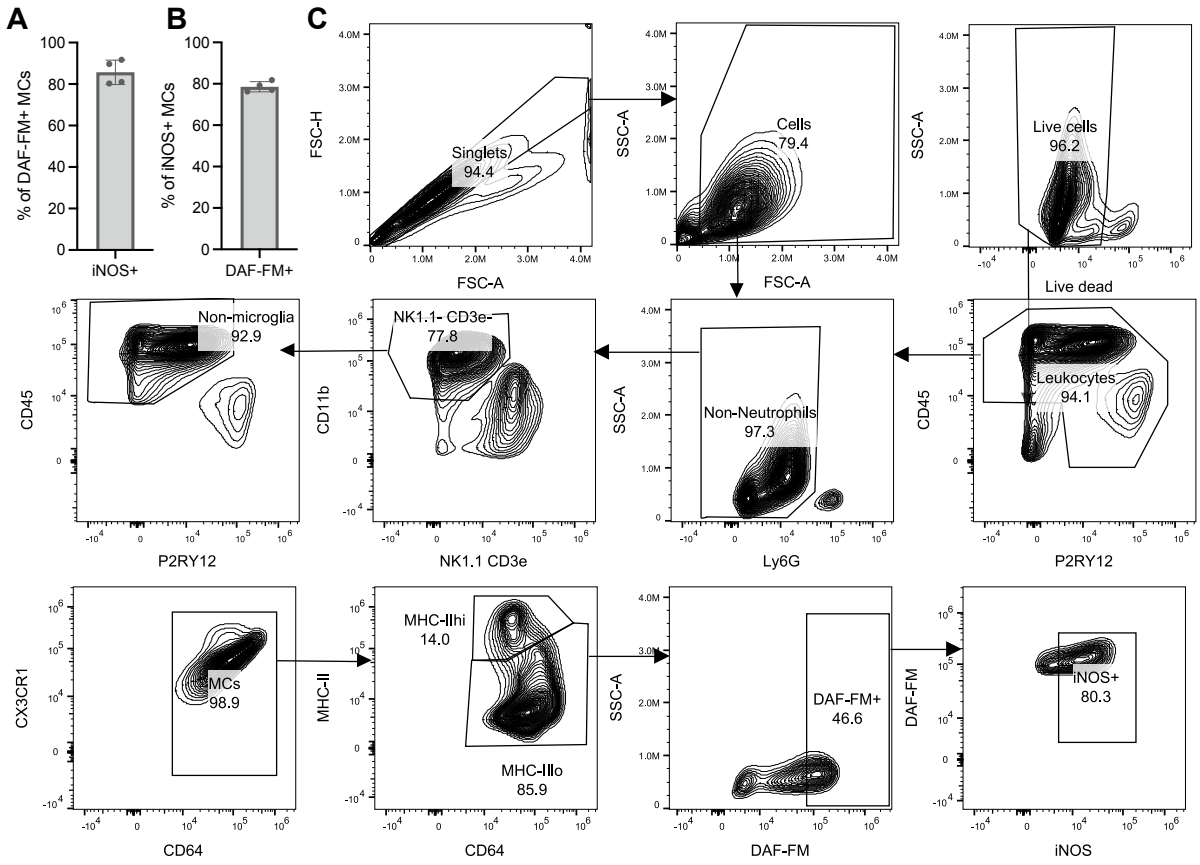
A
% of DAF-FM+ MCs
iNOS+
B
% of iNOS+ MCs
DAF-FM+
C
FSC-H
FSC-A
Singlets
94.4
SSC-A
Cells
79.4
Live cells
96.2
Live dead
Leukocytes
94.1
CD45
P2RY12
Non-microglia
92.9
CD11b
NK1.1 CD3e
NK1.1- CD3e-
77.8
SSC-A
Ly6G
Non-Neutrophils
97.3
CX3CR1
CD64
MCs
98.9
MHC-II
MHC-IIhi
14.0
MHC-IIlo
85.9
SSC-A
DAF-FM
DAF-FM+
46.6
DAF-FM
iNOS
iNOS+
80.3

Supplementary Figure 6.3 Correlation between iNOS and DAF-FM staining in brain MCs.

(**A**) Percent of $iNOS^+$ MCs in the WNV-infected brain that are positive for DAF-FM staining. (**B**) Percent of $DAF\text{-}FM^+$ MCs that are positive for iNOS staining. (**C**) Gating strategy for identifying $DAF\text{-}FM^+$, $iNOS^+$ MCs.

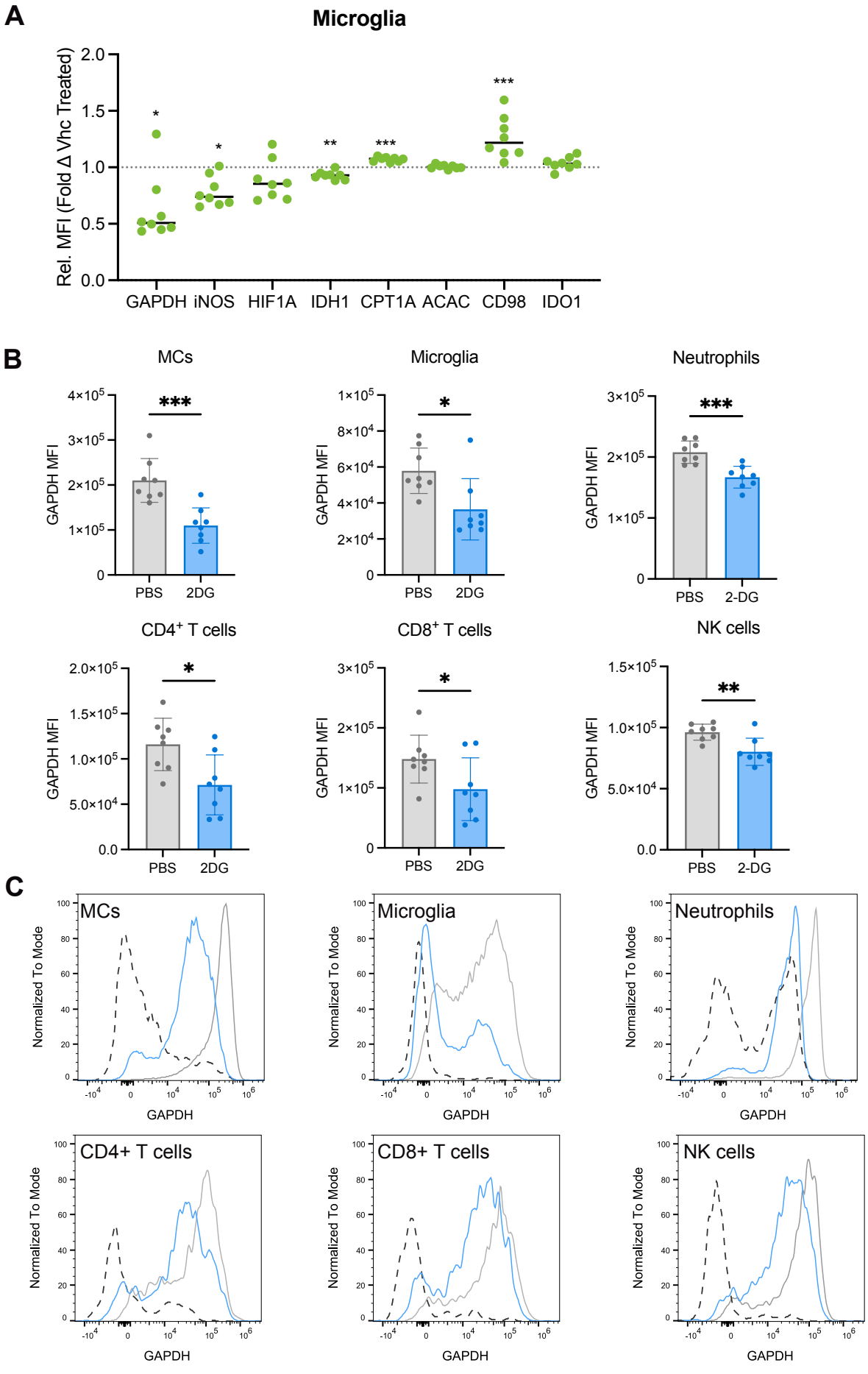
A
Microglia
Rel. MFI (Fold Δ Vhc Treated)
2.0
1.5
1.0
0.5
0.0
*
*
**
***
***
GAPDH
iNOS
HIF1A
IDH1
CPT1A
ACAC
CD98
IDO1
B
MCs
Microglia
Neutrophils
GAPDH MFI
4×10^5
3×10^5
2×10^5
1×10^5
0
***
*
***
PBS
2DG
2-DG
CD4+ T cells
CD8+ T cells
NK cells
2.0×10^5
1.5×10^5
1.0×10^5
5.0×10^4
0.0
3×10^5
1×10^5
1.5×10^5
1.0×10^5
5.0×10^4
**
C
MCs
Microglia
Neutrophils
CD4+ T cells
CD8+ T cells
NK cells
Normalized To Mode
GAPDH

Supplementary Figure 6.4 2-DG treatment uniformly downregulates glycolytic marker GAPDH across cell types.

(**A**) Fold-change in MFI of selected metabolic markers in 2-DG-treated mice relative to PBS-treated mice in microglia derived from the WNV-infected brain. (**B**) GAPDH MFI across the indicated cell types. (**C**) Histograms depicting the MFI of GAPDH in 2-DG- and PBS-treated mice at 7 dpi, relative to the FMO control. Data are from one independent experiments with eight mice per group. Statistics calculated by ordinary one-way ANOVA with Tukey's test for multiple comparisons (**A**) or an unpaired t-test (**B**). * $p<0.05$, ** $p<0.01$, ***$p<0.001$. Error bars are representative of mean ± SD.

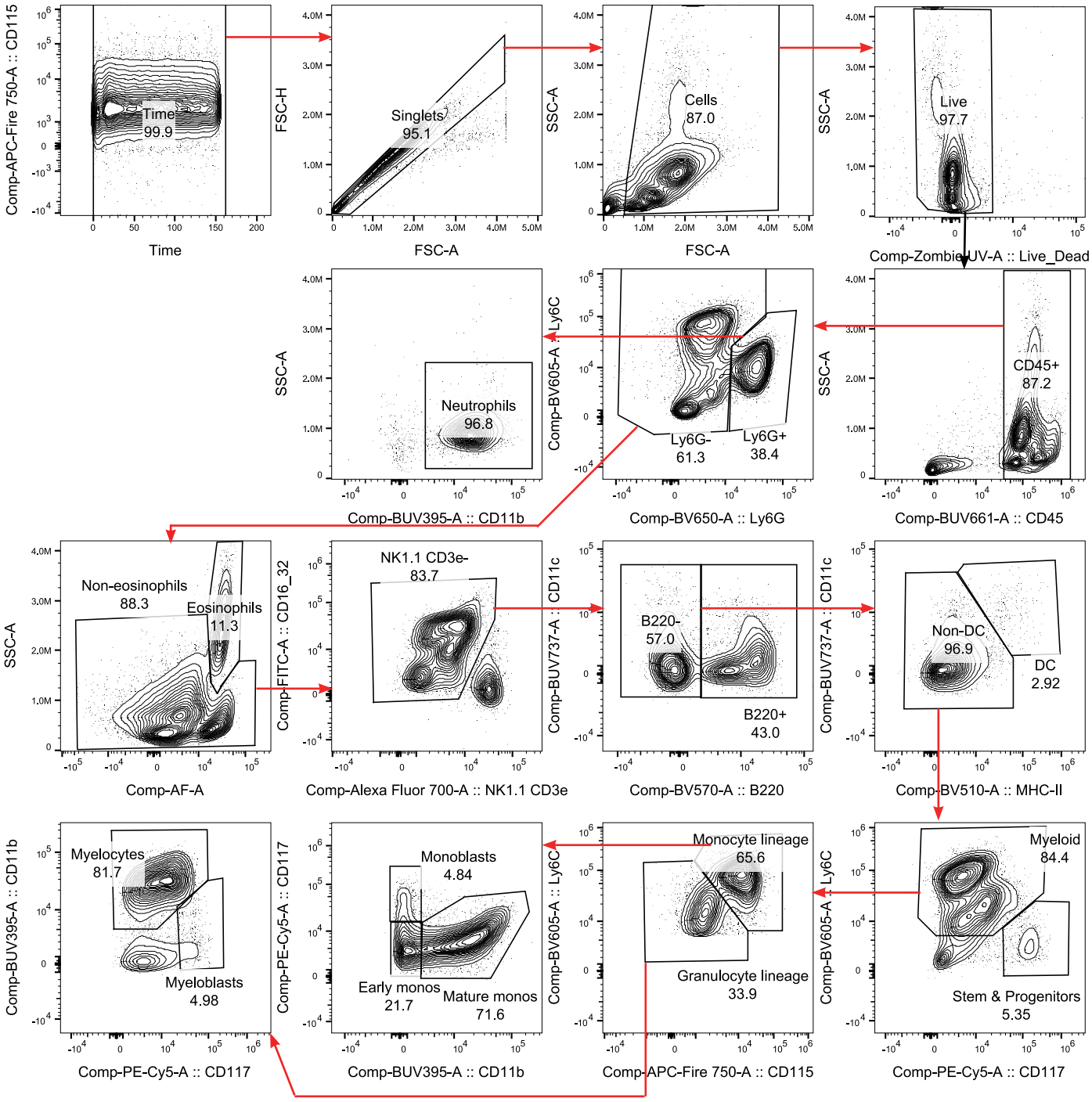
Comp-APC-Fire 750-A :: CD115
Time
Time
99.9
FSC-H
FSC-A
Singlets
95.1
SSC-A
FSC-A
Cells
87.0
SSC-A
Comp-Zombie UV-A :: Live_Dead
Live
97.7
SSC-A
Comp-BUV395-A :: CD11b
Neutrophils
96.8
Comp-BV605-A :: Ly6C
Comp-BV650-A :: Ly6G
Ly6G-
61.3
Ly6G+
38.4
SSC-A
Comp-BUV661-A :: CD45
CD45+
87.2
SSC-A
Comp-AF-A
Non-eosinophils
88.3
Eosinophils
11.3
Comp-FITC-A :: CD16_32
Comp-Alexa Fluor 700-A :: NK1.1 CD3e
NK1.1 CD3e-
83.7
Comp-BUV737-A :: CD11c
Comp-BV570-A :: B220
B220-
57.0
B220+
43.0
Comp-BUV737-A :: CD11c
Comp-BV510-A :: MHC-II
Non-DC
96.9
DC
2.92
Comp-BUV395-A :: CD11b
Comp-PE-Cy5-A :: CD117
Myelocytes
81.7
Myeloblasts
4.98
Comp-PE-Cy5-A :: CD117
Comp-BUV395-A :: CD11b
Monoblasts
4.84
Early monos
21.7
Mature monos
71.6
Comp-BV605-A :: Ly6C
Comp-APC-Fire 750-A :: CD115
Monocyte lineage
65.6
Granulocyte lineage
33.9
Comp-BV605-A :: Ly6C
Comp-PE-Cy5-A :: CD117
Myeloid
84.4
Stem & Progenitors
5.35

Supplementary Figure 6.5 Gating strategy for bone marrow myeloid populations.

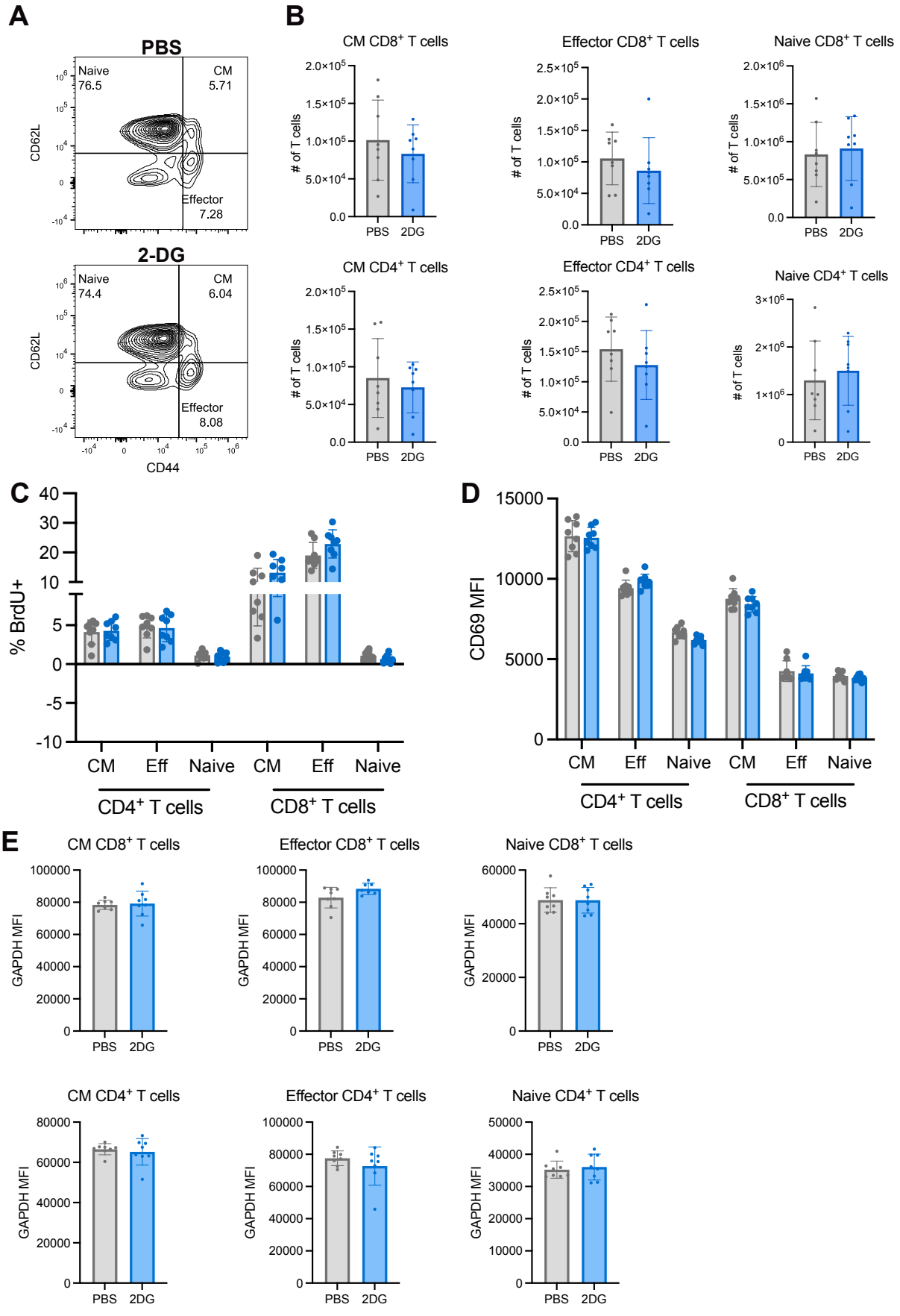
A
PBS
Naive
76.5
CM
5.71
Effector
7.28
2-DG
Naive
74.4
CM
6.04
Effector
8.08
CD62L
CD44
B
CM CD8+ T cells
Effector CD8+ T cells
Naive CD8+ T cells
CM CD4+ T cells
Effector CD4+ T cells
Naive CD4+ T cells
# of T cells
PBS
2DG
C
% BrdU+
CM
Eff
Naive
CD4+ T cells
CD8+ T cells
D
CD69 MFI
E
GAPDH MFI

Supplementary Figure 6.6 2-DG treatment from 4-7 dpi does not affect T cell proliferation in draining cervical lymph nodes.

(**A**) Contour plot showing gating of naïve, CM and effector (eff) $CD4^+$ T cells based on CD62L and CD44 expression. (**B**) Absolute cell numbers of indicated T cell populations per cervical lymph node. (**C, D**) Percentage of $BrdU^+$ T cells (**C**) and their expression of CD69 **(D)** and GAPDH (**E**) in 2-DG- and PBS-treated mice at 7 dpi. Data are from one independent experiment with eight mice per group. Statistics were calculated using an unpaired t-test (**B, E**) or multiple t-tests with two-stage step up method of Bejamini, Krieger, and Yekutieli tests for multiple comparisons (**C, D**). Error bars are representative of mean ± SD. CM, central memory; Eff, effector T cell; Treg, regulatory T cell.

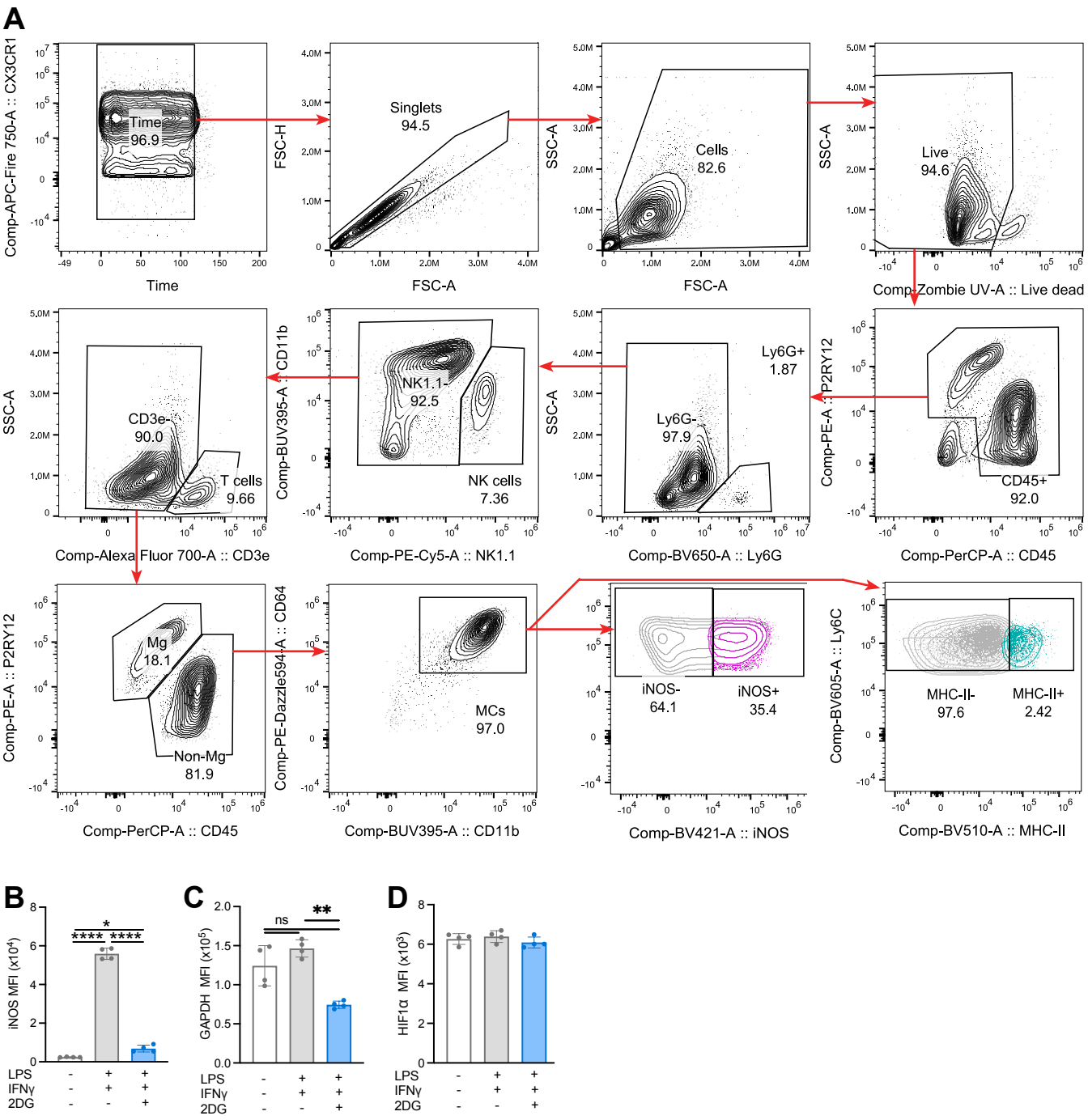
A
Comp-APC-Fire 750-A :: CX3CR1
Time
Time
96.9
FSC-H
FSC-A
Singlets
94.5
SSC-A
FSC-A
Cells
82.6
SSC-A
Comp-Zombie UV-A :: Live dead
Live
94.6
SSC-A
Comp-Alexa Fluor 700-A :: CD3e
CD3e-
90.0
T cells
9.66
Comp-BUV395-A :: CD11b
Comp-PE-Cy5-A :: NK1.1
NK1.1-
92.5
NK cells
7.36
SSC-A
Comp-BV650-A :: Ly6G
Ly6G+
1.87
Ly6G-
97.9
Comp-PE-A :: P2RY12
Comp-PerCP-A :: CD45
CD45+
92.0
Comp-PE-A :: P2RY12
Comp-PerCP-A :: CD45
Mg
18.1
Non-Mg
81.9
Comp-PE-Dazzle594-A :: CD64
Comp-BUV395-A :: CD11b
MCs
97.0
Comp-BV421-A :: iNOS
iNOS-
64.1
iNOS+
35.4
Comp-BV605-A :: Ly6C
Comp-BV510-A :: MHC-II
MHC-II-
97.6
MHC-II+
2.42
B
iNOS MFI (x10⁴)
*
**** ****
LPS
IFNγ
2DG
C
GAPDH MFI (x10⁵)
ns
**
LPS
IFNγ
2DG
D
HIF1α MFI (x10³)
LPS
IFNγ
2DG

Supplementary Figure 6.7 Gating of iNOS+ and MHC-II+ MCs in the WNV-infected brain and glycolysis-associated marker expression in ex vivo M1-stimulated monocytes.

(**A**) Gating strategy for $iNOS^+$ and $MHC\text{-}II^+$ MC populations in the brain. (**B-D**) Change in MFI of iNOS (**B**), GAPDH (**C**), and HIF1-α (**D**) in cultured BMDMs post-stimulation. Data are one independent experiment(s) with 3-4 mice per group. Statistics calculated RM one-way ANOVA with Tukey's test for multiple comparisons. * $p<0.05$, ** $p<0.01$, *** $p<0.001$, **** $p<0.0001$. Error bars are representative of mean ± SD.

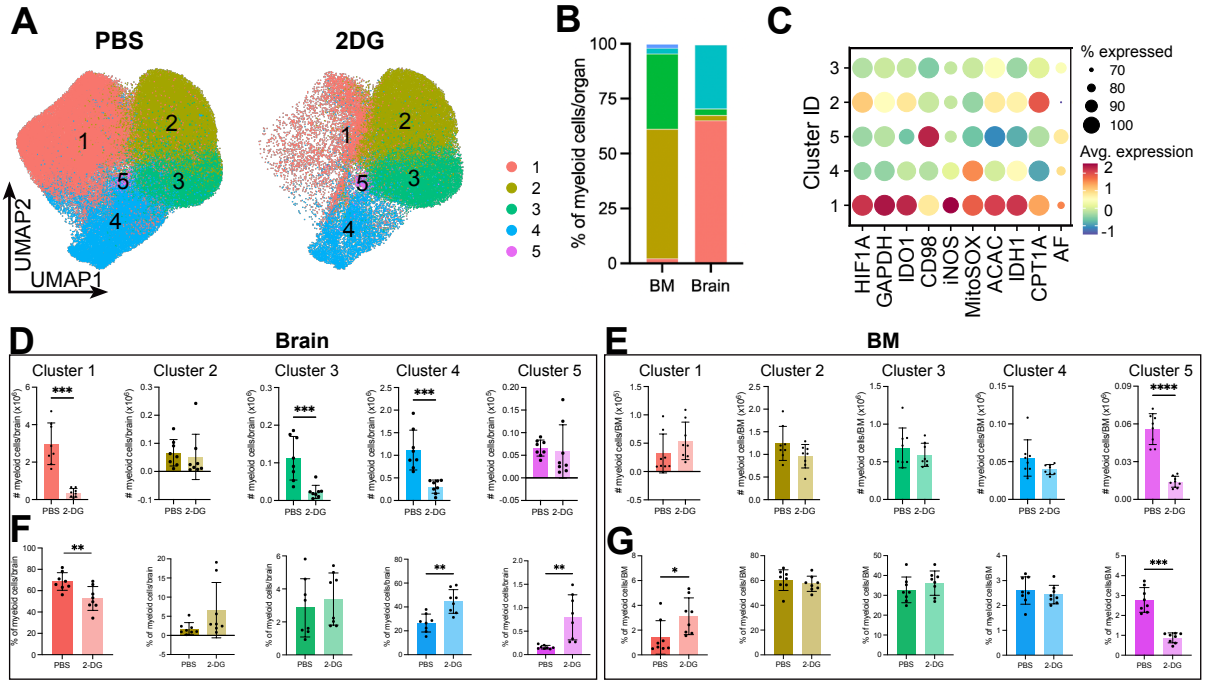
A
PBS
2DG
UMAP2
UMAP1
1
2
3
4
5
B
% of myeloid cells/organ
100
75
50
25
0
BM
Brain
C
Cluster ID
% expressed
70
80
90
100
Avg. expression
2
1
0
-1
HIF1A
GAPDH
IDO1
CD98
iNOS
MitoSOX
ACAC
IDH1
CPT1A
AF
D
Brain
Cluster 1
Cluster 2
Cluster 3
Cluster 4
Cluster 5
PBS 2-DG
E
BM
F
G

Supplementary Figure 6.8 Glycolysis inhibition suppresses pathogenic MC clusters.

(**A**) UMAPs pseudocoloured by metabolic cluster ID across PBS- and 2-DG-treated groups. UMAP represents combined myeloid cells from the BM and brain at 7 dpi. (**B**) Proportion of each metabolic cluster per organ comprising the total myeloid pool across treatment groups. (**C**) Dot plot heatmap depicting the MFI of each metabolic marker across the identified metabolic cluster at 7 dpi. Size of dot represents the percentage of cells in each cluster expressing the metabolic marker. (**D, E**) Number of myeloid cells per brain (**D**) and monocytes per femur (**E**) in each cluster in PBS- and 2-DG-treated WNV-infected mice at 7 dpi. (**F, G**) Proportion of each metabolic cluster comprising the total myeloid population in the brain (**F**) and BM (**G**) across treatment groups. Data are from one independent experiment with 7-8 mice per group. Statistics performed using unpaired t-test. * $p<0.05$, ** $p<0.01$, *** $p<0.001$, **** $p<0.0001$. Error bars are representative of mean ± SD.

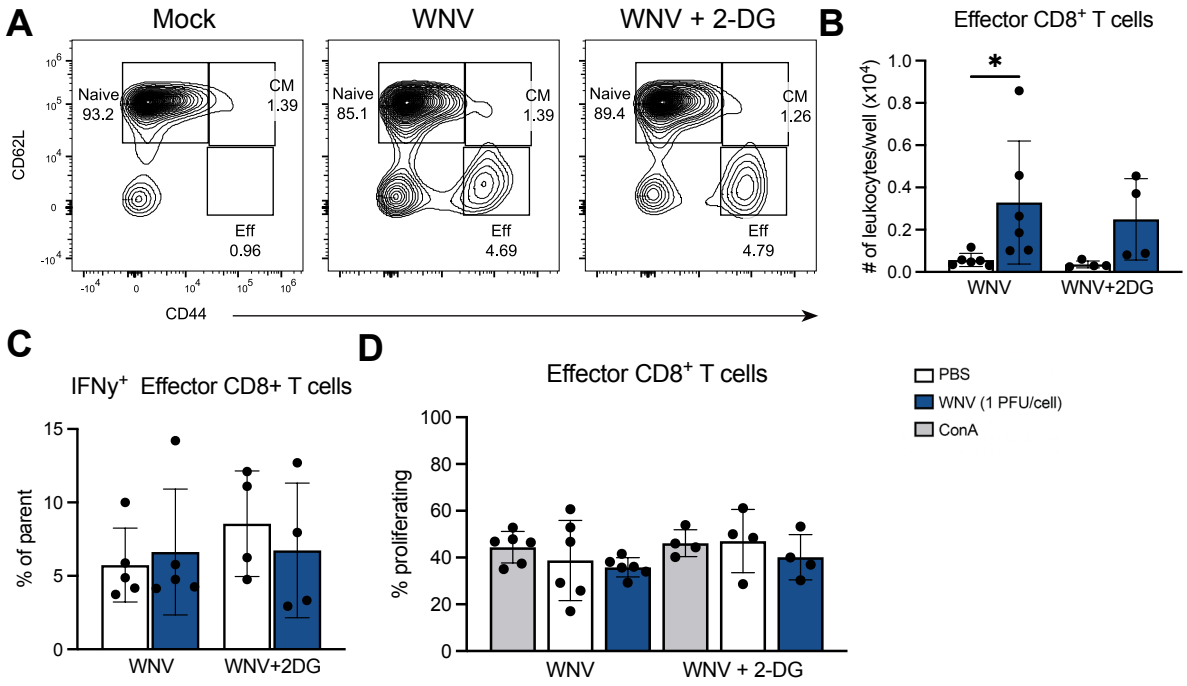
A
Mock
WNV
WNV + 2-DG
CD62L
CD44
Naive
93.2
CM
1.39
Eff
0.96
Naive
85.1
CM
1.39
Eff
4.69
Naive
89.4
CM
1.26
Eff
4.79
B
Effector CD8+ T cells
# of leukocytes/well (x10^4)
1.0
0.8
0.6
0.4
0.2
0.0
*
WNV
WNV+2DG
C
IFNy+ Effector CD8+ T cells
% of parent
15
10
5
0
WNV
WNV+2DG
D
Effector CD8+ T cells
% proliferating
100
80
60
40
20
0
WNV
WNV + 2-DG
PBS
WNV (1 PFU/cell)
ConA

Supplementary Figure 6.9 2-DG treatment does not affect CD8$^+$ T cell functionality from draining cervical lymph nodes.

Whole cervical draining lymph nodes were stimulated with WNV or PBS for 1 hour, prior to being cultured with either PBS or Con A for 72 hours, as described in Figure 6.6. (**A**) Contour plots showing gating of naïve, CM and effector (eff) CD8$^+$ T cells based on CD62L and CD44 expression across groups stimulated with WNV. (**B**) Number of effector CD8$^+$ T cells per well of cultured lymph nodes. (**C, D**) Percent of IFN-γ^+ (**C**) and proliferating (**D**) effector CD8$^+$ T cells. Data are from one independent experiment with eight mice per group. Statistics calculated by RM one-way ANOVA with Tukey's test for multiple comparisons. * $p<0.05$, ** $p<0.01$. Error bars are representative of mean ± SD.

Chapter 7: Conclusions and Future Directions

Immunometabolism is an increasingly prominent field, with the potential to reveal novel therapeutic targets and strategies by investigating the interplay between metabolic processes and immune cell functions. High-dimensional techniques like scRNA-seq and immune profiling have highlighted the functional heterogeneity of MCs. Despite these advances, it remains uncertain whether MCs adopt consistent functional states across different pathologies or what specific mechanisms drive myeloid cell heterogeneity in CNS disease. This thesis reports an investigation into how metabolic pathways shape immune responses across various pathologies, particularly focusing on MCs in CNS disease. By identifying and contrasting the metabolic profiles and functions of MCs across diseases, this work aims to enhance understanding of their functional diversity and metabolic interplay, potentially pinpointing common therapeutic targets. A novel method for assessing MC metabolism using flow cytometry was developed and validated, capitalizing on the lab's expertise in this area. This single-cell analytical approach is crucial for exploring MC heterogeneity, enabling detailed investigation at the individual cell level. By applying this method, we characterised the metabolic profiles of pathogenic, NO-producing MCs during WNV infection, leading to the development of a targeted therapeutic strategy tailored to the metabolic phenotypes and functional roles of these cells. This demonstrated the utility of this approach and the feasibility of modulating individual pathways to ameliorate immunopathology.

7.1 Single-cell methods are necessary to elucidate MC metabolism

Recent technological advances in monitoring metabolites and metabolic processes, along with innovative single-cell and genetic approaches, have given researchers an array of tools to understand and study the complexities of immunometabolism. Traditional methods for evaluating cell metabolism include extracellular flux analysis and metabolomics. Extracellular flux analysis measures real-time changes in cellular respiration and glycolysis, providing insights into the metabolic state of cells. Metabolomics, through techniques such as mass spectrometry and nuclear magnetic resonance spectroscopy, offers comprehensive profiling of metabolites within biological samples. However, these approaches have significant limitations, in particular, they provide average measurements across cell populations and lack the

resolution to capture cellular heterogeneity. Recently, however, advances in single-cell methods have revolutionized the examination of immune cell metabolism and heterogeneity. Techniques such as scRNA-seq and spectral flow cytometry allow for the analysis of metabolic states at the single cell level, uncovering diverse metabolic profiles within seemingly homogeneous cell populations. Immunometabolism profiling typically involves three stages: *discovery*, *pursuing a phenotype*, and *confirmation*. Each of these approaches were used throughout this thesis to accurately define metabolic profiles.

The *discovery* phase of immunometabolism profiling typically involves untargeted approaches. These techniques do not require prior knowledge of the metabolites present or active metabolic pathways, allowing for the identification of a wide range of metabolic processes, which is crucial for generating hypotheses and identifying potential biomarkers or metabolic pathways of interest. These include high-throughput technologies such as untargeted metabolomics, proteomics, and bulk or singe-cell sequencing. In Results Chapter II and IV, we implemented the *discovery* stage using scRNA-seq and integration across transcriptomic datasets. We elected to use this approach for several reasons: (1) it allows the simultaneous measurement of genes associated with both functional and metabolic pathways, enabling us to connect these two parameters; (2) it is a single-cell approach, enabling the examination of heterogeneity that may exist between cells, a feature not possible with other discovery based approaches; and (3) data integration across disparate experimental models and labs enabled us to identify novel cellular states that exist independently of a singular disease or experimental condition. This is crucial because it enables the identification of findings that are applicable across a broad spectrum of diseases, rather than being confined to a singular model, thereby enhancing the robustness and significance of our findings. While scRNA-seq is a powerful tool, metabolomics and proteomics offer other advantages that we did not implement in this work. Metabolomics provides a direct measurement of metabolites, which are the end products of cellular processes, thus offering a more immediate and accurate reflection of metabolic status. Proteomics allows for the quantification and characterisation of proteins involved in various metabolic pathways, which is important given the limited correlation between mRNA and their respective proteins. Both approaches can capture changes in metabolic pathways and identify post-translational modifications that are not detectable by RNA sequencing. However, these methods are limited by their inability to link metabolic changes to specific immune cell functions, a connection that is more readily enabled by scRNA-seq, thus offering a more precise understanding of how metabolic alterations influence immune responses.

The second phase involves *pursuing a phenotype*, where preliminary analyses suggest altered metabolic programs. This phase is investigated with confirmatory and more targeted analyses, such as extracellular flux analysis, targeted metabolomics, mitochondrial imaging, or flow cytometry. Pioneering work in flow and mass cytometry has led to the development of a novel approach to connect phenotype and function. This approach examines the expression of critical proteins and signalling molecules involved in various metabolic pathways to provide a surrogate measurement for pathway activity, which is combined in a panel with functional and immune cell identification markers. However, as discussed in Results Chapter II, these approaches have significant limitations in their validation of metabolic targets. We therefore aimed to create a carefully and systematically validated metabolic panel. Through targeted metabolic stimulation and inhibition experiments, we demonstrated that each of eight metabolic targets corresponded well to metabolic pathway activity, making this a novel and reliable tool to connect phenotype and function at the protein level, and enabling the advancement of *discovery*-based approaches such as scRNA-seq. This approach was developed with a range of immune cell identification and functional markers, which we subsequently applied in order to metabolically profile immune cells in the brain, BM, and draining lymph nodes during WNV infection. Although we elected to use this approach, evaluating immune cell metabolism by flow cytometry has inherent limitations. A key consideration is that flow cytometry measures protein expression as an indirect indicator of metabolic activity, which may not precisely reflect real-time pathway flux. While our validation using metabolic inhibitors and stimulants demonstrates correlation between protein levels and pathway activity, additional genetic approaches such as knockouts or siRNA could further validate antibody specificity. Nonetheless, future work could build on the method presented in this thesis by developing approaches for direct *in vivo* labelling. For instance, it may be possible to engineer reporter mice using the validated proteins for a core set of metabolic pathways, such as glycolysis (GAPDH), OXPHOS (IDH1), fatty acid oxidation (CPT1A), and fatty acid synthesis (ACAC) using four distinct fluorescent proteins with non-overlapping emission spectra, such as GFP (green fluorescent protein), RFP (red fluorescent protein), CFP (cyan fluorescent protein), and YFP (yellow fluorescent protein). This would enable real-time, *in vivo* monitoring of metabolic pathway activities within specific cell populations, allowing for the investigation of metabolic kinetics of immune cells in relation to phenotypic changes at the single-cell level – something not yet achievable with current immunometabolism approaches.

The third and final phase is the *confirmation* phase, where findings are confirmed with genetic or pharmacological approaches to further validate the phenotypic findings. This phase includes integrating metabolic data with other omics data, developing diagnostic tools, and implementing therapeutic strategies based on insights derived from the first two phases. We aimed to carry out this approach in Results Chapter IV, where we integrated a *discovery*-based approach (i.e., scRNA-seq) with the *pursuit of a phenotype* approach using a metabolism-based flow cytometry panel. This identified a specific glycolytic profile associated with pathogenic, NO-producing MCs. To confirm these findings, we further employed the *confirmation* phase via pharmacological manipulation, treating mice with the glycolysis inhibitor 2-DG, which (1) impaired the differentiation of monocytes into NO-producing cells and (2) improved disease outcomes while reducing neuroinflammation, thus supporting our findings demonstrating that glycolysis is a critical metabolic pathway primarily associated with pathogenic MCs in WNV encephalitis. However, unanswered questions remain that could be investigated with other confirmatory approaches. For instance, it would be of interest to determine whether pharmacological inhibition of HIF1α with Chrysin or monocyte-specific genetic deletion of HIF1α would impair the migration of monocytes into the WNV-infected brain, as we found that the MCs initially adopt a HIF1α^{+} profile, likely to mediate their migration into the brain, before differentiating into the terminal MC populations (i.e., antigen presenting and NO-producing MCs). This could be achieved with mice carrying the *loxP*-flanked conditional alleles of HIF1α and bred with *LysM-Cre* mice to generate myeloid-specific HIF1α deletion, as previously described (Semba et al., 2016). In addition, it would also be of interest to track the specific metabolic processes that accompany monocyte differentiation, and whether different metabolic processes are employed to skew cells towards distinct functional states. This could be investigated by stimulating myelopoiesis *in vivo*, administering specific metabolic inhibitors such as etomoxir for fatty acid oxidation inhibition and oligomycin for OXPHOS inhibition, and then examining the resulting functional subsets through metabolism-based flow cytometry following *ex vivo* stimulation with different PAMP such as LPS or CpG. These combined approaches would deepen our understanding of the metabolic mechanisms underlying myeloid cell differentiation and function in the context of WNV infection.

7.2 The M1/M2 paradigm cannot capture myeloid profiles *in vivo*

Myeloid cells exhibit remarkable plasticity. These cells are capable of rapidly changing their functional profiles through a process defined as polarisation. The M1 and M2 polarisation paradigm classifies these cells based on two functional extremes, a concept which has become dogma in both immunological and metabolic fields. This paradigm is particularly pertinent to CNS disease; various groups have categorized macrophage heterogeneity by distinguishing "classically-activated" or M1 pathological macrophages and alternatively-activated, anti-inflammatory, or "M2" reparative macrophages to elucidate disease processes (Gensel and Zhang, 2015, Tang and Le, 2016). However, these polarisation states have been primarily investigated in controlled *in vitro* settings using specific stimuli to induce function, employing bulk techniques such as metabolomics, proteomics, transcriptomics and extracellular flux assays. While these methods have been invaluable in establishing the framework for understanding macrophage metabolism, they provide average measurements across a population and thus fail to capture macrophage heterogeneity. This is particularly important as the field shifts from the M1 and M2 polarisation paradigm towards a function-based framework, recognising a spectrum of activation states in macrophages that reflects highly specialised metabolic and phenotypic changes. Moving beyond controlled *in vitro* paradigms, extensive research now demonstrates the complex factors that contribute to macrophage profiles *in vivo*. These include the *disease microenvironment*, the *ontogeny* of myeloid cells, and *temporal dynamics* (Voss et al., 2021), all of which we have addressed throughout this work.

Advances in single-cell methods have revealed that complex *disease microenvironments* drive myeloid cells to adopt highly specialised metabolic and functional profiles across CNS disease. These diverse pathogenic and protective signatures may individually drive immune-mediated pathology or promote tissue repair. However, many of these studies have focused on specific cell types, particular diseases, and/or singular experimental approaches, which has substantially hindered our ability to dissect the influence of disease environment on myeloid cell phenotype and function. To address this, we systematically integrated bulk and/or single-cell transcriptomic datasets in Results Chapter I and Results Chapter II across a wide range of murine models of neurological disease. In Results Chapter II, we found that the M1/M2 polarization signatures were inadequate for characterizing the bulk responses of myeloid cells

in CNS disease, as MCs exhibited either a combination of both M1 and M2 signatures or lacked these signatures entirely. Rather, our systematic integration approach identified the presence of a myriad of functionally and metabolically distinct myeloid subsets across CNS diseases, which included eight microglial clusters (Results Chapter I) and four to seven MC clusters (Results Chapter I and Results Chapter II). We observed the differential prevalence of each of these distinct subsets across CNS disease, which corresponded to the functional roles of these cells in each pathology. For instance, in the EAE model of MS, we observed the presence of antigen-presenting and inflammatory clusters, which may correspond to the ability of MCs to stimulate encephalitogenic T cell responses (Ko et al., 2014, Miller et al., 2007) and their contribution to inflammatory damage to myelin in EAE (Yamasaki et al., 2014). By contrast, MCs in viral encephalitis tended to adopt anti-viral, inflammatory and antigen presenting profiles, reflecting their complex roles in both contributing to viral clearance (Getts et al., 2012, Spiteri et al., 2023b) and participating in neuron damage via their production of NO (Getts et al., 2012). Importantly, in Results Chapter II, we identified that each of these functionally-distinct myeloid 'archetypes' had vastly different metabolic profiles, with the anti-viral and inflammatory NO-producing MCs being significantly more glycolytic, whereas the antigen-presenting MCs exhibited a greater reliance on the TCA cycle and the ETC. It is important to note that each of the functionally defined myeloid populations could be detected in each of the CNS diseases. Thus, rather than the pro-inflammatory (M1)/anti-inflammatory (M2) paradigm, different disease environments may stimulate the expansion of a core set of functionally defined myeloid responses, whose functions may be beneficial or detrimental, depending on the disease context.

In Results Chapter I we aimed to additionally address the influence of *ontogeny* on the functional polarisation of myeloid cells in CNS disease. In the context of the brain, microglia and MCs are ontogenetically distinct: microglia arise from yolk-sac-derived precursors seeded during embryogenesis (Kierdorf et al., 2013, Ginhoux et al., 2010), and monocytes derive from HSCs in the adult BM and are continuously generated in response to inflammatory stimuli through myelopoiesis (Geissmann et al., 2010). Our findings revealed that microglia and MCs adopted separate, highly specific responses to each setting, as we identified no commonly upregulated genes between microglia and MCs. Interestingly, MCs from different CNS diseases showed more similarities to each other than to microglia within the same disease. Microglia displayed greater functional heterogeneity, identified by more functionally distinct microglia clusters (*Mg1-8* vs *MC1-4*) and less functional overlap compared to MCs, which

commonly upregulated inflammatory processes. This enhanced heterogeneity of microglia compared to monocytes may be related to their distinct origins and lifetimes: in mice, microglia typically live for 15 months (Füger et al., 2017), whereas circulating monocytes live for 1-2 days (Yona et al., 2013), exposing microglia to a constantly changing microenvironment over their lifetime. Indeed, previous disease exposure has been shown to influence microglia function and phenotype through a process known as immune memory (Wendeln et al., 2018), in which past encounters to pathogens shape future innate responses. While the extent to which ontogeny contributes to macrophage phenotype and function remains unclear, evidence shows that even after prolonged engraftment in the brain, MCs respond differently to LPS, compared to microglia (Cronk et al., 2018) and retain an 'epigenetic legacy' of their monocytic origin (Aegerter et al., 2020, Cronk et al., 2018). Supporting this, in Results Chapter IV, we found that microglia and MCs adopted vastly distinct metabolic profiles in WNV encephalitis despite exposure to the same disease environment. Microglia exhibited a more metabolically quiescent signature, while monocytes were significantly more glycolytic. This metabolic distinction may be shared by other tissue-resident macrophages; for instance, in the lung, pro-inflammatory MCs outcompeted the resident alveolar macrophage population in Influenza A infection due to their high glycolytic and proliferative capacity, leading to long-term severe disease (Li et al., 2022a). While it is unclear whether such findings would apply the CNS, this suggests that metabolic reprograming could facilitate monocyte replenishment of the microglia population in diseases where microglial immune responses are insufficient or pathogenic compared to infiltrating monocytes. These findings emphasize the crucial role of cellular ontogeny on myeloid function and metabolic profile, a concept not encompassed by the M1/M2 framework.

In Results Chapter IV, we examined the influence of *temporal dynamics* on myeloid cell metabolism and function. Throughout the course of a disease, cellular responses, pathogens, signals, and other cues can vary significantly. Another crucial aspect of temporal dynamics is the monocyte differentiation process, typically viewed as linear in the M1/M2 paradigm. To elucidate these processes, we examined monocyte responses during WNV encephalitis, a prototypical M1-mediated disease where immunopathology results from the mass infiltration of M1-like NO-producing myeloid cells, leading to neuronal damage and mortality (Getts et al., 2008, Getts et al., 2012, Terry et al., 2015, Getts et al., 2014, Spiteri et al., 2023b). We investigated temporal dynamics over the course of disease (dpi 0, 3, 5, and 7) and traced the differentiation process of MCs from the BM to the brain. Our findings revealed a continuous metabolic evolution of MCs throughout the disease. Metabolism-based flow cytometry showed

drastic reorganisation of metabolic profiles at each time point, with the most significant changes beginning at dpi 5 and continuing to dpi 7. This process saw the emergence of various metabolically and functionally distinct subsets, including antigen-presenting and NO-producing MCs.

Interestingly, we observed a distinct differentiation program for monocytes from the BM to the brain. BM monocytes typically exhibited a metabolic profile consistent with catabolic energy-conserving processes prior to immune cell activation, characterized by higher expression of the TCA cycle and ETC (Figure 7.1). As the disease progressed, these cells transitioned into a HIF1α^+ MC subset, likely mediating their migration in a hypoxic environment of the inflamed brain, before differentiating into the distinct NO-producing and antigen-presenting subsets (Figure 7.1). Strikingly, BM monocytes from mice treated with the glycolysis inhibitor 2-DG showed a reduced capacity to differentiate into NO-producing MCs and a skewing towards an antigen-presenting phenotype. This suggests an early reprogramming in the BM strategically skews monocytes towards the necessary functional state, a process that that is strongly influenced by metabolism. Supporting this, foundational studies have shown that different PAMPs skew monocytes towards different monocyte differentiation programs: LPS challenge and subsequent TLR4 stimulation favours GMP-derived neutrophil-like monocyte production, which exhibit enhanced anti-bacterial functions, whereas the stimulation with a TLR9 PAMP, CpG, favours MDP-derived monocyte production with enhanced anti-viral capacity (Yáñez et al., 2017). Notably, this skewing may also be reflected metabolically, as different pathogens induce distinct metabolic reprogramming, generating monocytes with unique functional outputs in phagocytic capacity and cytokine production (Lachmandas et al., 2016). In addition, this process may be further influenced by differences in monocyte ontogeny. For instance, antigen-presenting (e.g., monocyte-derived DC) and iNOS$^+$ MCs have been found to originate from ontogenically distinct monocytes in the BM and are differentially induced by environmental cues (Menezes et al., 2016). Specifically, MHC-II$^+$ monocytes exposed to GM-CSF develop into antigen-presenting MCs, while MHC-II$^-$ monocytes exposed to microbial stimuli differentiate into iNOS$^+$ MCs (Menezes et al., 2016). Thus, the systemic metabolic responses to microbial antigen or cytokine environments may contribute to monocyte 'priming' in the BM that may skew their differentiation towards distinct functions tailored to support various inflammatory responses, which may be regulated by metabolic processes. This emphasizes the complex framework underlying macrophage activation, where intricate kinetic

factors influence the differentiation of monocytes into functionally distinct subsets in CNS disease.

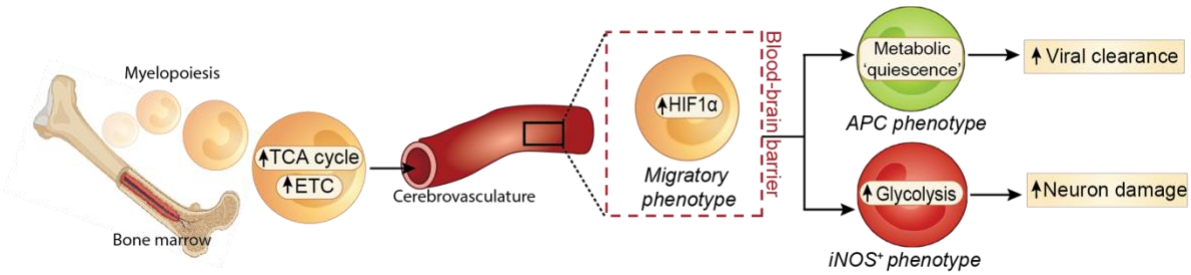

Figure 7.1 Summary of monocyte and MC metabolic profiles in WNV infection

7.3 Glycolysis delineates pathogenic, pro-inflammatory MCs

Glycolysis is a metabolic pathway that converts glucose into pyruvate, generating ATP in the process. It is typically associated with immune cell activation because it enables the rapid generation of energy required for various cell functions, such as cellular differentiation, migration, and production of inflammatory mediators (O'Neill et al., 2016). The speed required for differentiation, especially in innate immune responses, may necessitate higher glycolytic activity compared to adaptive immune processes, where differentiation occurs over several days. This metabolic pathway is espescially significant for myeloid cells, as it underpins a variety of functions, including presentation of antigen and the production of inflammatory mediators. Given that glycolysis is uniformly tied to the inflammatory functions of these cells, it is a clear therapeutic target, although it is crucial to ensure that inhibiting glycolysis does not hinder the essential immune processes needed for disease resolution. This is particularly important because various functionally distinct MCs might coeist within the same disease, each contributing differently over time to the progression and resolution of the disease.

As it is unclear to what extent glycolysis is differentially used to support various functional programs, in Results Chapter II we examined the association of glycolysis with a range of functional pathways, including phagocytosis, antigen-presentation, anti-viral response, inflammatory response, and NO production. This work was performed on a dataset integrated across various acute CNS diseases, including murine models of viral encephalitis, MS, TBI, and SCI. Although we found that glycolysis was associated with a range of MC functions, such as NO production and phagocytosis, this metabolic pathway showed no correlation with

antigen presentation. Antigen presentation had a stronger association with the TCA cycle and lipid metabolism. This suggests that the negative association between antigen presentation and glycolysis, which we observed in Results Chapter IV, is not specific to or isolated to viral encephalitis, but may be a universal feature of MC function that has not yet been uncovered. This differential reliance on glycolysis may explain previous work demonstrating that monocyte differentiation into antigen presenting cells occurs independently of glycolysis (Adamik et al., 2022), and that increased glucose uptake by monocytes impairs T cell responses (Lawless et al., 2017). The differential usage of glycolysis for these two pathways may be related to the speed necessary for these respective functions. Antigen presentation is significantly more energy-intensive, as it requires substantial energy for maturation into a DC phenotype, peptide processing, transport, and presentation, in addition to co-stimulatory interactions with T cells – a process that spans multiple days (Alloatti et al., 2016, Croft et al., 2013). Consequently, this prolonged and sustained energy demand may be better met by slower, more efficient methods of generating energy, such as OXPHOS or β-oxidation of fatty acids. These pathways provide a steady and sustained energy supply necessary for the extensive and continuous activities involved in antigen presentation. On the other hand, the production of inflammatory mediators, such as NO, occurs much more rapidly (Lewis et al., 1995). During inflammation, NO must be continuously generated as needed, requiring a constant and rapid supply of energy. Glycolysis, with its ability to quickly produce ATP, is well suited to meet the immediate and high-energy demands of NO production and other rapid inflammatory responses. This highlights a crucial aspect of cellular metabolism where different pathways may be differentially utilised based on the specific energy and temporal demands of distinct cellular functions.

In Results Chapter IV, we investigated more comprehensively the differential metabolic pathways employed by MC subsets in WNV encephalitis. We found that the antigen-presenting and NO-producing MCs had vastly different metabolic profiles that were primarily attributable to their differential use of glycolysis. Inhibiting glycolysis with 2-DG treatment preferentially impacted pathogenic, NO-producing MCs. In parallel, glycolysis inhibition broadly attenuated inflammation, reflected by the global reduction in inflammatory cytokines and chemokines, reduction in immune cell infiltration into the CNS, and overall improvement in clinical score. An important feature of this glycolysis inhibition was the preferential reduction of NO-producing MCs in the brain. This effect was found to occur independently of myelopoietic processes and resulted from two distinct mechanisms: (1) preferential impairment of the

migration of NO-producing MCs into the brain, and (2) impairment of monocyte differentiation into NO-producing MCs. Thus, glycolysis inhibition may prime the differentiation status of monocytes, skewing them into an antigen-presenting phenotype over an NO-producing phenotype. This opens up avenues for reprogramming monocytes towards distinct differentiation programs, which may beneficial or detrimental depending on the disease. In WNV encephalitis, antigen presenting MCs may be beneficial and aid in viral clearance, however, in EAE, antigen presenting cells present myelin antigen to encephalitogenic T cells, thus contributing to the autoimmune inflammatory response culminating in tissue damage and lesion formation (Spiteri et al., 2021b). Thus, the functional roles of targeting pathogenic or beneficial MCs in the context of CNS disease must be carefully considered before employing metabolic manipulation across disease scenarios.

We demonstrate that glycolysis has specific associations with the pathogenic activity of MCs in CNS disease, particularly in the context of viral encephalitis, as detailed in Results Chapter II and IV. In Results Chapter III, we also observed that the autofluorescence of immune cells, particularly myeloid cells, is attributable to the glycolytic state of these cells. Based on our findings in Chapter II and IV, this discovery opens up avenues for a simple and effective mechanism to identify pathogenic immune cells based on their autofluorescence signature. Specifically, cells with high glycolytic activity emit a strong autofluorescent signal, attributed to high NADH levels, which can be detected by flow cytometry and other fluorescence-based imaging techniques. This method allows for the rapid and non-invasive identification of pathogenic cells without the need for extensive labelling and complex assays, making it a potentially practical tool for clinical settings. Considering the prevalence of inflammation in a wide variety of infectious and non-infectious diseases, this could lead to straightforward immune monitoring based on the presence of high autofluorescence, glycolytic signatures. Indeed, in Chapter IV, we observed that the pathogenic, NO-producing MCs had a high AF signal compared to other MCs in the brain. While this was found in WNV encephalitis, we propose that such findings are likely translatable to other infectious diseases with pathogenic immune function, such as sepsis or severe COVID-19, both of which have an inflammatory monocyte-mediated component that contributes to significant tissue damage and disease exacerbation (Merad and Martin, 2020, Andonegui et al., 2018).

Several important points remain to be addressed. One consideration is the identification of metabolic inhibitors that could be used to inhibit or promote antigen presentation. Investigating

whether glycolysis stimulation or inhibition is sufficient to achieve this would be beneficial. In WNV encephalitis, we observed that treating mice with 2-DG did not improve viral clearance. This may be due to simple temporal mismatch of disease stage and intervention, but on the other hand may suggest that alternative metabolic manipulation may prove more effective. Understanding the metabolic mechanisms that drive monocyte function has significant implications, especially in diseases where myeloid cells could be reprogrammed *ex vivo* to perform more specialised functions. This approach parallels the significant metabolic component observed in immune cell metabolism and chimeric antigen receptor T or myeloid cell therapy, which is integral to their therapeutic efficacy, and could be integrated into treatments that necessitates their functional reprogramming. Additionally, given glycolysis is utilised by a wide range of other immune cells, it is crucial to ensure that broad metabolic targeting does not function like broad-acting immunosuppressants that obtund immune responses generally; however, it should be noted that therapeutic targeting of metabolic processes typically affects cells with the highest metabolic activity, which are normally inflammatory cells (Patel et al., 2019). Notwithstanding, therapeutic specificity could be improved with more targeted delivery mechanisms. For instance, drug-loaded liposomes, which are more specific to phagocytic cells, could be developed to include ligands that specifically target monocytes, thereby increasing precision in therapeutic intervention.

7.4 Conclusion

This work integrates various fields of research to comprehensively connect myeloid cell metabolism and function across CNS disease. In doing this, we have achieved the following:

1. Employed methodologies that represent a significant advance in the field of immunometabolism in the context of CNS disease. Our use of scRNA-seq in conjunction with a pioneering flow-based metabolic analytical method, provides a high-resolution view of the metabolic changes that underpin the functional diversification of MC subsets *in vivo* during infection and across CNS diseases. This nuanced understanding of metabolism-function relationships in MCs goes beyond the broad associations made in previous studies (Results Chapter I-IV).

2. Demonstrated that the M1/M2 paradigm does not accurately capture the metabolic or functional profiles of MCs across CNS disease. Indeed this work highlights their metabolic and functional heterogeneity (Results Chapter II).

3. Characterised novel conserved and disease-specific profiles of microglia and MCs spanning disparate murine models of disease, including autoimmune inflammation, ischemic injury, and neurodegeneration (Results Chapter I).

4. Validated a comprehensive metabolic panel for examining metabolism by flow cytometry at the single-cell level, facilitating in-depth exploration of cellular metabolic pathways, from glycolysis to fatty acid and amino acid metabolism. We provided explicit recommendations on experimental design and reagent concentrations and validated representative markers for each metabolic marker by metabolic inhibition and stimulation experiments (Results Chapter III).

5. Identified for the first time a unique cellular autofluorescent signature associated with glycolysis that can be detected without labelling by spectral cytometry, enabling the measurement of metabolic status without perturbation by antibody staining (Results Chapter III).

6. Delineated how both pathogenic, NO-producing MCs and protective antigen-presenting MCs differentiate from a common HIF1-α^{+} precursor, each adopting different metabolic programs, which directly correlate with their CNS functions. Specifically, we show that NO-producing MCs adopt a glycolytic and amino acid metabolic phenotype, whereas antigen-presenting MCs show a more metabolically quiescent phenotype, less reliant on glycolysis (Results Chapter IV).

7. Demonstrated a novel, continuous metabolic transition of BM monocytes that directly impacts their function on CNS infiltration, a process not previously characterized (Results Chapter IV).

8. Revealed for the first time that targeting glycolysis does not merely alter the inflammatory function of MCs, but preferentially impacts the pathogenic NO-producing subset without affecting the essential antigen-presenting capacity of the co-differentiating MC subset required for viral clearance (Results Chapter IV).

9. Showed that the therapeutic effect of glycolysis inhibition mediated protection without inhibiting myelopoiesis, but by reducing the rate of inflammatory MC infiltration into the brain and the capacity of these cells to produce damaging inflammatory mediators. Importantly, our study shows that glycolysis inhibition does not compromise the

development of an antiviral T cell response, demonstrating a critical aspect of the immune response not addressed by other works (Results Chapter IV).

Together, these findings advance our understanding of the metabolic mechanisms driving myeloid cell function in CNS disease and pave the way for developing targeted metabolic-based therapeutics that can modulate immune responses with high specificity and efficacy.

References

ABBOTT, N. J., RÖNNBÄCK, L. & HANSSON, E. 2006. Astrocyte–endothelial interactions at the blood–brain barrier. *Nature reviews neuroscience,* 7**,** 41-53.

ABEL, A. M., YANG, C., THAKAR, M. S. & MALARKANNAN, S. 2018. Natural killer cells: development, maturation, and clinical utilization. *Frontiers in immunology,* 9**,** 1869.

ADAMIK, J., MUNSON, P. V., HARTMANN, F. J., COMBES, A. J., PIERRE, P., KRUMMEL, M. F., BENDALL, S. C., ARGÜELLO, R. J. & BUTTERFIELD, L. H. 2022. Distinct metabolic states guide maturation of inflammatory and tolerogenic dendritic cells. *Nature communications,* 13**,** 5184.

AEGERTER, H., KULIKAUSKAITE, J., CROTTA, S., PATEL, H., KELLY, G., HESSEL, E. M., MACK, M., BEINKE, S. & WACK, A. 2020. Influenza-induced monocyte-derived alveolar macrophages confer prolonged antibacterial protection. *Nature immunology,* 21**,** 145-157.

AFGAN, E., BAKER, D., VAN DEN BEEK, M., BLANKENBERG, D., BOUVIER, D., CECH, M., CHILTON, J., CLEMENTS, D., CORAOR, N., EBERHARD, C., GRUNING, B., GUERLER, A., HILLMAN-JACKSON, J., VON KUSTER, G., RASCHE, E., SORANZO, N., TURAGA, N., TAYLOR, J., NEKRUTENKO, A. & GOECKS, J. 2016. The Galaxy platform for accessible, reproducible and collaborative biomedical analyses: 2016 update. *Nucleic Acids Res,* 44**,** W3-W10.

AHL, P. J., HOPKINS, R. A., XIANG, W. W., AU, B., KALIAPERUMAL, N., FAIRHURST, A.-M. & CONNOLLY, J. E. 2020. Met-Flow, a strategy for single-cell metabolic analysis highlights dynamic changes in immune subpopulations. *Communications biology,* 3**,** 1-15.

AJAMI, B., BENNETT, J. L., KRIEGER, C., MCNAGNY, K. M. & ROSSI, F. M. 2011. Infiltrating monocytes trigger EAE progression, but do not contribute to the resident microglia pool. *Nat Neurosci,* 14**,** 1142-9.

AJAMI, B., BENNETT, J. L., KRIEGER, C., TETZLAFF, W. & ROSSI, F. M. 2007. Local self-renewal can sustain CNS microglia maintenance and function throughout adult life. *Nature neuroscience,* 10**,** 1538-1543.

AJAMI, B., SAMUSIK, N., WIEGHOFER, P., HO, P. P., CROTTI, A., BJORNSON, Z., PRINZ, M., FANTL, W. J., NOLAN, G. P. & STEINMAN, L. 2018. Single-cell mass cytometry reveals distinct populations of brain myeloid cells in mouse neuroinflammation and neurodegeneration models. *Nature neuroscience,* 21**,** 541-551.

ALDER, J. K., GEORGANTAS, R. W., HILDRETH, R. L., KAPLAN, I. M., MORISOT, S., YU, X., MCDEVITT, M. & CIVIN, C. I. 2008. Kruppel-like factor 4 is essential for inflammatory monocyte differentiation in vivo. *The Journal of Immunology,* 180**,** 5645-5652.

ALEKSANDER, S. A., BALHOFF, J., CARBON, S., CHERRY, J. M., DRABKIN, H. J., EBERT, D., FEUERMANN, M., GAUDET, P. & HARRIS, N. L. 2023. The gene ontology knowledgebase in 2023. *Genetics,* 224**,** iyad031.

ALFONSO-GARCÍA, A., SMITH, T. D., DATTA, R., LUU, T. U., GRATTON, E., POTMA, E. O. & LIU, W. F. 2016. Label-free identification of macrophage phenotype by fluorescence lifetime imaging microscopy. *Journal of biomedical optics,* 21**,** 046005-046005.

ALIZADEH, A., DYCK, S. M. & KARIMI-ABDOLREZAEE, S. 2019. Traumatic spinal cord injury: an overview of pathophysiology, models and acute injury mechanisms. *Frontiers in neurology,* 10**,** 441408.

ALLOATTI, A., KOTSIAS, F., MAGALHAES, J. G. & AMIGORENA, S. 2016. Dendritic cell maturation and cross-presentation: timing matters! *Immunological reviews,* 272**,** 97-108.

ALMEIDA, L. & EVERTS, B. 2021. Fa (c) t checking: how fatty acids shape metabolism and function of macrophages and dendritic cells. *European Journal of Immunology,* 51**,** 1628-1640.

ALVAREZ, J. I., KATAYAMA, T. & PRAT, A. 2013. Glial influence on the blood brain barrier. *Glia,* 61**,** 1939-1958.

ANDERSON III, D. A., DUTERTRE, C.-A., GINHOUX, F. & MURPHY, K. M. 2021. Genetic models of human and mouse dendritic cell development and function. *Nature Reviews Immunology,* 21**,** 101-115.

ANDONEGUI, G., ZELINSKI, E. L., SCHUBERT, C. L., KNIGHT, D., CRAIG, L. A., WINSTON, B. W., SPANSWICK, S. C., PETRI, B., JENNE, C. N. & SUTHERLAND, J. C. 2018. Targeting inflammatory monocytes in sepsis-associated encephalopathy and long-term cognitive impairment. *JCI insight,* 3.

ANDREWS, S. 2010. FastQC: a quality control tool for high throughput sequence data. Babraham Bioinformatics, Babraham Institute, Cambridge, United Kingdom.

ANJUM, A., YAZID, M. D. I., FAUZI DAUD, M., IDRIS, J., NG, A. M. H., SELVI NAICKER, A., ISMAIL, O. H. R., ATHI KUMAR, R. K. & LOKANATHAN, Y. 2020. Spinal cord injury: pathophysiology, multimolecular interactions, and underlying recovery mechanisms. *International journal of molecular sciences,* 21**,** 7533.

ARGÜELLO, R. J., COMBES, A. J., CHAR, R., GIGAN, J.-P., BAAZIZ, A. I., BOUSIQUOT, E., CAMOSSETO, V., SAMAD, B., TSUI, J. & YAN, P. 2020. SCENITH: a flow cytometry-based method to functionally profile energy metabolism with single-cell resolution. *Cell metabolism,* 32**,** 1063-1075. e7.

ARMAH, H. B., WANG, G., OMALU, B. I., TESH, R. B., GYURE, K. A., CHUTE, D. J., SMITH, R. D., DULAI, P., VINTERS, H. V., KLEINSCHMIDT-DEMASTERS, B. K. & WILEY, C. A. 2007. Systemic distribution of West Nile virus infection: postmortem immunohistochemical study of six cases. *Brain Pathol,* 17**,** 354-62.

ARTYOMOV, M. N. & VAN DEN BOSSCHE, J. 2020. Immunometabolism in the single-cell era. *Cell metabolism,* 32**,** 710-725.

ASHBURNER, M., BALL, C. A., BLAKE, J. A., BOTSTEIN, D., BUTLER, H., CHERRY, J. M., DAVIS, A. P., DOLINSKI, K., DWIGHT, S. S. & EPPIG, J. T. 2000. Gene ontology: tool for the unification of biology. *Nature genetics,* 25**,** 25-29.

ASHHURST, T. M., MARSH-WAKEFIELD, F., PUTRI, G. H., SPITERI, A. G., SHINKO, D., READ, M. N., SMITH, A. L. & KING, N. J. C. 2021. Integration, exploration, and analysis of high-dimensional single-cell cytometry data using Spectre. *Cytometry A*.

ASSMANN, N., O'BRIEN, K. L., DONNELLY, R. P., DYCK, L., ZAIATZ-BITTENCOURT, V., LOFTUS, R. M., HEINRICH, P., OEFNER, P. J., LYNCH, L. & GARDINER, C. M. 2017. Srebp-controlled glucose metabolism is essential for NK cell functional responses. *Nature immunology,* 18**,** 1197-1206.

AUBIN, J. 1979. Autofluorescence of viable cultured mammalian cells. *Journal of Histochemistry & Cytochemistry,* 27**,** 36-43.

AZEVEDO, E. P., ROCHAEL, N. C., GUIMARÃES-COSTA, A. B., DE SOUZA-VIEIRA, T. S., GANILHO, J., SARAIVA, E. M., PALHANO, F. L. & FOGUEL, D. 2015. A

metabolic shift toward pentose phosphate pathway is necessary for amyloid fibril-and phorbol 12-myristate 13-acetate-induced neutrophil extracellular trap (NET) formation. *Journal of Biological Chemistry,* 290**,** 22174-22183.

BAI, F., KONG, K.-F., DAI, J., QIAN, F., ZHANG, L., BROWN, C. R., FIKRIG, E. & MONTGOMETRY, R. R. 2010. A paradoxical role for neutrophils in the pathogenesis of West Nile virus. *Journal of Infectious Diseases,* 202**,** 1804-1812.

BAI, F., THOMPSON, E. A., VIG, P. J. & LEIS, A. A. 2019. Current understanding of West Nile virus clinical manifestations, immune responses, neuroinvasion, and immunotherapeutic implications. *Pathogens,* 8**,** 193.

BAJWA, G., DEBERARDINIS, R. J., SHAO, B., HALL, B., FARRAR, J. D. & GILL, M. A. 2016. Cutting edge: critical role of glycolysis in human plasmacytoid dendritic cell antiviral responses. *The Journal of Immunology,* 196**,** 2004-2009.

BARDINA, S. V., MICHLMAYR, D., HOFFMAN, K. W., OBARA, C. J., SUM, J., CHARO, I. F., LU, W., PLETNEV, A. G. & LIM, J. K. 2015. Differential roles of chemokines CCL2 and CCL7 in monocytosis and leukocyte migration during West Nile virus infection. *The Journal of Immunology,* 195**,** 4306-4318.

BARRETT, J. P., HENRY, R. J., VILLAPOL, S., STOICA, B. A., KUMAR, A., BURNS, M. P., FADEN, A. I. & LOANE, D. J. 2017. NOX2 deficiency alters macrophage phenotype through an IL-10/STAT3 dependent mechanism: implications for traumatic brain injury. *Journal of neuroinflammation,* 14**,** 1-17.

BARRETT, T., WILHITE, S. E., LEDOUX, P., EVANGELISTA, C., KIM, I. F., TOMASHEVSKY, M., MARSHALL, K. A., PHILLIPPY, K. H., SHERMAN, P. M., HOLKO, M., YEFANOV, A., LEE, H., ZHANG, N., ROBERTSON, C. L., SEROVA, N., DAVIS, S. & SOBOLEVA, A. 2013. NCBI GEO: archive for functional genomics data sets--update. *Nucleic Acids Res,* 41**,** D991-5.

BEATTIE, L., SAWTELL, A., MANN, J., FRAME, T. C., TEAL, B., DE LABASTIDA RIVERA, F., BROWN, N., WALWYN-BROWN, K., MOORE, J. W. & MACDONALD, S. 2016. Bone marrow-derived and resident liver macrophages display unique transcriptomic signatures but similar biological functions. *Journal of hepatology,* 65**,** 758-768.

BECK, K. D., NGUYEN, H. X., GALVAN, M. D., SALAZAR, D. L., WOODRUFF, T. M. & ANDERSON, A. J. 2010. Quantitative analysis of cellular inflammation after traumatic spinal cord injury: evidence for a multiphasic inflammatory response in the acute to chronic environment. *Brain,* 133**,** 433-447.

BECKTEL, D. A., ZBESKO, J. C., FRYE, J. B., CHUNG, A. G., HAYES, M., CALDERON, K., GROVER, J. W., LI, A., GARCIA, F. G. & TAVERA-GARCIA, M. A. 2022. Repeated administration of 2-hydroxypropyl-β-cyclodextrin (HPβCD) attenuates the chronic inflammatory response to experimental stroke. *Journal of Neuroscience,* 42**,** 325-348.

BEN-NATHAN, D., HUITINGA, I., LUSTIG, S., VAN ROOIJEN, N. & KOBILER, D. 1996. West Nile virus neuroinvasion and encephalitis induced by macrophage depletion in mice. *Archives of virology,* 141**,** 459-469.

BENNETT, F. C., BENNETT, M. L., YAQOOB, F., MULINYAWE, S. B., GRANT, G. A., HAYDEN GEPHART, M., PLOWEY, E. D. & BARRES, B. A. 2018. A Combination of Ontogeny and CNS Environment Establishes Microglial Identity. *Neuron,* 98**,** 1170-1183.e8.

BENNETT, M. L., BENNETT, F. C., LIDDELOW, S. A., AJAMI, B., ZAMANIAN, J. L., FERNHOFF, N. B., MULINYAWE, S. B., BOHLEN, C. J., ADIL, A., TUCKER, A., WEISSMAN, I. L., CHANG, E. F., LI, G., GRANT, G. A., HAYDEN GEPHART,

M. G. & BARRES, B. A. 2016. New tools for studying microglia in the mouse and human CNS. *Proc Natl Acad Sci U S A,* 113**,** E1738-46.

BERGHOFF, S. A., SPIETH, L. & SAHER, G. 2022. Local cholesterol metabolism orchestrates remyelination. *Trends in Neurosciences,* 45**,** 272-283.

BERGHOFF, S. A., SPIETH, L., SUN, T., HOSANG, L., SCHLAPHOFF, L., DEPP, C., DÜKING, T., WINCHENBACH, J., NEUBER, J. & EWERS, D. 2021. Microglia facilitate repair of demyelinated lesions via post-squalene sterol synthesis. *Nature neuroscience,* 24**,** 47-60.

BEROD, L., FRIEDRICH, C., NANDAN, A., FREITAG, J., HAGEMANN, S., HARMROLFS, K., SANDOUK, A., HESSE, C., CASTRO, C. N. & BÄHRE, H. 2014. De novo fatty acid synthesis controls the fate between regulatory T and T helper 17 cells. *Nature medicine,* 20**,** 1327-1333.

BESHARA, R., SENCIO, V., SOULARD, D., BARTHÉLÉMY, A., FONTAINE, J., PINTEAU, T., DERUYTER, L., ISMAIL, M. B., PAGET, C. & SIRARD, J.-C. 2018. Alteration of Flt3-Ligand-dependent de novo generation of conventional dendritic cells during influenza infection contributes to respiratory bacterial superinfection. *PLoS Pathogens,* 14**,** e1007360.

BEUKER, C., SCHAFFLICK, D., STRECKER, J.-K., HEMING, M., LI, X., WOLBERT, J., SCHMIDT-POGODA, A., THOMAS, C., KUHLMANN, T. & ARANDA-PARDOS, I. 2022. Stroke induces disease-specific myeloid cells in the brain parenchyma and pia. *Nature communications,* 13**,** 945.

BIDAULT, G., VIRTUE, S., PETKEVICIUS, K., JOLIN, H. E., DUGOURD, A., GUÉNANTIN, A.-C., LEGGAT, J., MAHLER-ARAUJO, B., LAM, B. Y. & MA, M. K. 2021. SREBP1-induced fatty acid synthesis depletes macrophages antioxidant defences to promote their alternative activation. *Nature metabolism,* 3**,** 1150-1162.

BLAGIH, J. & JONES, R. G. 2012. Polarizing macrophages through reprogramming of glucose metabolism. *Cell metabolism,* 15**,** 793-795.

BLAKE, J. A., BALDARELLI, R., KADIN, J. A., RICHARDSON, J. E., SMITH, C. L. & BULT, C. J. 2021. Mouse Genome Database (MGD): Knowledgebase for mouse–human comparative biology. *Nucleic Acids Research,* 49**,** D981-D987.

BLANC, M., HSIEH, W. Y., ROBERTSON, K. A., KROPP, K. A., FORSTER, T., SHUI, G., LACAZE, P., WATTERSON, S., GRIFFITHS, S. J. & SPANN, N. J. 2013. The transcription factor STAT-1 couples macrophage synthesis of 25-hydroxycholesterol to the interferon antiviral response. *Immunity,* 38**,** 106-118.

BOGIE, J. F., GRAJCHEN, E., WOUTERS, E., CORRALES, A. G., DIERCKX, T., VANHERLE, S., MAILLEUX, J., GERVOIS, P., WOLFS, E. & DEHAIRS, J. 2020. Stearoyl-CoA desaturase-1 impairs the reparative properties of macrophages and microglia in the brain. *Journal of Experimental Medicine,* 217.

BOSCH, M., SÁNCHEZ-ÁLVAREZ, M., FAJARDO, A., KAPETANOVIC, R., STEINER, B., DUTRA, F., MOREIRA, L., LÓPEZ, J. A., CAMPO, R. & MARÍ, M. 2020. Mammalian lipid droplets are innate immune hubs integrating cell metabolism and host defense. *Science,* 370**,** eaay8085.

BOST, P., GILADI, A., LIU, Y., BENDJELAL, Y., XU, G., DAVID, E., BLECHER-GONEN, R., COHEN, M., MEDAGLIA, C. & LI, H. 2020. Host-viral infection maps reveal signatures of severe COVID-19 patients. *Cell,* 181**,** 1475-1488. e12.

BRAVERMAN, J. & STANLEY, S. A. 2017. Nitric oxide modulates macrophage responses to Mycobacterium tuberculosis infection through activation of HIF-1α and repression of NF-κB. *The Journal of Immunology,* 199**,** 1805-1816.

BRIEN, J. D., UHRLAUB, J. L. & NIKOLICH-ZUGICH, J. 2008. West Nile virus-specific CD4 T cells exhibit direct antiviral cytokine secretion and cytotoxicity and are sufficient for antiviral protection. *The Journal of Immunology,* 181**,** 8568-8575.

BRIONNE, A., JUANCHICH, A. & HENNEQUET-ANTIER, C. 2019. ViSEAGO: a Bioconductor package for clustering biological functions using Gene Ontology and semantic similarity. *BioData Min,* 12**,** 16.

BUCK, M. D., SOWELL, R. T., KAECH, S. M. & PEARCE, E. L. 2017. Metabolic instruction of immunity. *Cell,* 169**,** 570-586.

BURKE, S. A., WEN, L. & KING, N. J. 2004. Routes of inoculation and the immune response to a resolving genital flavivirus infection in a novel murine model. *Immunol Cell Biol,* 82**,** 174-83.

BURROWS, D. J., MCGOWN, A., JAIN, S. A., DE FELICE, M., RAMESH, T. M., SHARRACK, B. & MAJID, A. 2019. Animal models of multiple sclerosis: From rodents to zebrafish. *Mult Scler,* 25**,** 306-324.

BUTOVSKY, O., JEDRYCHOWSKI, M. P., MOORE, C. S., CIALIC, R., LANSER, A. J., GABRIELY, G., KOEGLSPERGER, T., DAKE, B., WU, P. M., DOYKAN, C. E., FANEK, Z., LIU, L., CHEN, Z., ROTHSTEIN, J. D., RANSOHOFF, R. M., GYGI, S. P., ANTEL, J. P. & WEINER, H. L. 2014. Identification of a unique TGF-β-dependent molecular and functional signature in microglia. *Nature neuroscience,* 17**,** 131-143.

BUTTGEREIT, A., LELIOS, I., YU, X., VROHLINGS, M., KRAKOSKI, N. R., GAUTIER, E. L., NISHINAKAMURA, R., BECHER, B. & GRETER, M. 2016. Sall1 is a transcriptional regulator defining microglia identity and function. *Nat Immunol,* 17**,** 1397-1406.

CABEZA-CABRERIZO, M., CARDOSO, A., MINUTTI, C. M., PEREIRA DA COSTA, M. & REIS E SOUSA, C. 2021. Dendritic cells revisited. *Annual review of immunology,* 39**,** 131-166.

CALABRESE, M., MAGLIOZZI, R., CICCARELLI, O., GEURTS, J. J., REYNOLDS, R. & MARTIN, R. 2015. Exploring the origins of grey matter damage in multiple sclerosis. *Nat Rev Neurosci,* 16**,** 147-58.

CARLSON, M. 2019. org.Mm.eg.db: Genome wide annotation for Mouse. *R package version.*

CHANCE, B. 1954. Spectrophotometry of intracellular respiratory pigments. *Science,* 120**,** 767-775.

CHANCE, B. & THORELL, B. 1959. Fluorescence measurements of mitochondrial pyridine nucleotide in aerobiosis and anaerobiosis. *Nature,* 184**,** 931-934.

CHAPMAN, N. M., BOOTHBY, M. R. & CHI, H. 2020. Metabolic coordination of T cell quiescence and activation. *Nature reviews immunology,* 20**,** 55-70.

CHEN, B. P., KUZIEL, W. A. & LANE, T. E. 2001. Lack of CCR2 results in increased mortality and impaired leukocyte activation and trafficking following infection of the central nervous system with a neurotropic coronavirus. *The Journal of Immunology,* 167**,** 4585-4592.

CHEN, H.-R., SUN, Y.-Y., CHEN, C.-W., KUO, Y.-M., KUAN, I. S., TIGER LI, Z.-R., SHORT-MILLER, J. C., SMUCKER, M. R. & KUAN, C.-Y. 2020. Fate mapping via CCR2-CreER mice reveals monocyte-to-microglia transition in development and neonatal stroke. *Science Advances,* 6**,** eabb2119.

CHENG, S.-C., QUINTIN, J., CRAMER, R. A., SHEPARDSON, K. M., SAEED, S., KUMAR, V., GIAMARELLOS-BOURBOULIS, E. J., MARTENS, J. H., RAO, N. A. & AGHAJANIREFAH, A. 2014. mTOR-and HIF-1α–mediated aerobic glycolysis as metabolic basis for trained immunity. *Science,* 345.

CHERIYAN, T., RYAN, D., WEINREB, J., CHERIYAN, J., PAUL, J., LAFAGE, V., KIRSCH, T. & ERRICO, T. 2014. Spinal cord injury models: a review. *Spinal cord,* 52**,** 588-595.

CHOUCHANI, E. T., PELL, V. R., GAUDE, E., AKSENTIJEVIĆ, D., SUNDIER, S. Y., ROBB, E. L., LOGAN, A., NADTOCHIY, S. M., ORD, E. N. & SMITH, A. C. 2014. Ischaemic accumulation of succinate controls reperfusion injury through mitochondrial ROS. *Nature,* 515**,** 431-435.

CHU, H. X., BROUGHTON, B. R., AH KIM, H., LEE, S., DRUMMOND, G. R. & SOBEY, C. G. 2015. Evidence that Ly6Chi monocytes are protective in acute ischemic stroke by promoting M2 macrophage polarization. *Stroke,* 46**,** 1929-1937.

CHUNG, A. G., FRYE, J. B., ZBESKO, J. C., CONSTANTOPOULOS, E., HAYES, M., FIGUEROA, A. G., BECKTEL, D. A., DAY, W. A., KONHILAS, J. P. & MCKAY, B. S. 2018. Liquefaction of the brain following stroke shares a similar molecular and morphological profile with atherosclerosis and mediates secondary neurodegeneration in an osteopontin-dependent mechanism. *eneuro,* 5.

CLAYTON, K., DELPECH, J. C., HERRON, S., IWAHARA, N., ERICSSON, M., SAITO, T., SAIDO, T. C., IKEZU, S. & IKEZU, T. 2021. Plaque associated microglia hyper-secrete extracellular vesicles and accelerate tau propagation in a humanized APP mouse model. *Mol Neurodegener,* 16**,** 18.

CODO, A. C., DAVANZO, G. G., DE BRITO MONTEIRO, L., DE SOUZA, G. F., MURARO, S. P., VIRGILIO-DA-SILVA, J. V., PRODONOFF, J. S., CARREGARI, V. C., DE BIAGI JUNIOR, C. A. O. & CRUNFLI, F. 2020. Elevated glucose levels favor SARS-CoV-2 infection and monocyte response through a HIF-1α/glycolysis-dependent axis. *Cell metabolism,* 32**,** 437-446. e5.

COLE, D. C., CHUNG, Y., GAGNIDZE, K., HAJDAROVIC, K. H., RAYON-ESTRADA, V., HARJANTO, D., BIGIO, B., GAL-TOTH, J., MILNER, T. A. & MCEWEN, B. S. 2017. Loss of APOBEC1 RNA-editing function in microglia exacerbates age-related CNS pathophysiology. *Proceedings of the National Academy of Sciences,* 114**,** 13272-13277.

COLLIN, M. & BIGLEY, V. 2018. Human dendritic cell subsets: an update. *Immunology,* 154**,** 3-20.

COLOMBO, A., DINKEL, L., MÜLLER, S. A., SEBASTIAN MONASOR, L., SCHIFFERER, M., CANTUTI-CASTELVETRI, L., KÖNIG, J., VIDATIC, L., BREMOVA-ERTL, T. & LIEBERMAN, A. P. 2021. Loss of NPC1 enhances phagocytic uptake and impairs lipid trafficking in microglia. *Nature communications,* 12**,** 1158.

COLONNA, M., TRINCHIERI, G. & LIU, Y.-J. 2004. Plasmacytoid dendritic cells in immunity. *Nature immunology,* 5**,** 1219-1226.

CONSTANTINESCU, C. S., FAROOQI, N., O'BRIEN, K. & GRAN, B. 2011. Experimental autoimmune encephalomyelitis (EAE) as a model for multiple sclerosis (MS). *British journal of pharmacology,* 164**,** 1079-1106.

CONWAY, J. R., LEX, A. & GEHLENBORG, N. 2017. UpSetR: an R package for the visualization of intersecting sets and their properties. *Bioinformatics*.

COONEY, S. J., BERMUDEZ-SABOGAL, S. L. & BYRNES, K. R. 2013. Cellular and temporal expression of NADPH oxidase (NOX) isotypes after brain injury. *Journal of neuroinflammation,* 10**,** 1-13.

COONEY, S. J., ZHAO, Y. & BYRNES, K. R. 2014. Characterization of the expression and inflammatory activity of NADPH oxidase after spinal cord injury. *Free radical research,* 48**,** 929-939.

CORBET, C., DRAOUI, N., POLET, F., PINTO, A., DROZAK, X., RIANT, O. & FERON, O. 2014. The SIRT1/HIF2α axis drives reductive glutamine metabolism under chronic acidosis and alters tumor response to therapy. *Cancer research,* 74**,** 5507-5519.

CORRALIZA, I. M., SOLER, G., EICHMANN, K. & MODOLELL, M. 1995. Arginase induction by suppressors of nitric oxide synthesis (IL-4, IL-10 and PGE2) in murine bone-marrow-derived macrophages. *Biochemical and biophysical research communications,* 206**,** 667-673.

COSSARIZZA, A., CHANG, H. D., RADBRUCH, A., ACS, A., ADAM, D., ADAM-KLAGES, S., AGACE, W. W., AGHAEEPOUR, N., AKDIS, M., ALLEZ, M., ALMEIDA, L. N., ALVISI, G., ANDERSON, G., ANDRÄ, I., ANNUNZIATO, F., ANSELMO, A., BACHER, P., BALDARI, C. T., BARI, S., BARNABA, V., BARROS-MARTINS, J., BATTISTINI, L., BAUER, W., BAUMGART, S., BAUMGARTH, N., BAUMJOHANN, D., BAYING, B., BEBAWY, M., BECHER, B., BEISKER, W., BENES, V., BEYAERT, R., BLANCO, A., BOARDMAN, D. A., BOGDAN, C., BORGER, J. G., BORSELLINO, G., BOULAIS, P. E., BRADFORD, J. A., BRENNER, D., BRINKMAN, R. R., BROOKS, A. E. S., BUSCH, D. H., BÜSCHER, M., BUSHNELL, T. P., CALZETTI, F., CAMERON, G., CAMMARATA, I., CAO, X., CARDELL, S. L., CASOLA, S., CASSATELLA, M. A., CAVANI, A., CELADA, A., CHATENOUD, L., CHATTOPADHYAY, P. K., CHOW, S., CHRISTAKOU, E., ČIČIN-ŠAIN, L., CLERICI, M., COLOMBO, F. S., COOK, L., COOKE, A., COOPER, A. M., CORBETT, A. J., COSMA, A., COSMI, L., COULIE, P. G., CUMANO, A., CVETKOVIC, L., DANG, V. D., DANG-HEINE, C., DAVEY, M. S., DAVIES, D., DE BIASI, S., DEL ZOTTO, G., DELA CRUZ, G. V., DELACHER, M., DELLA BELLA, S., DELLABONA, P., DENIZ, G., DESSING, M., DI SANTO, J. P., DIEFENBACH, A., DIELI, F., DOLF, A., DÖRNER, T., DRESS, R. J., DUDZIAK, D., DUSTIN, M., DUTERTRE, C. A., EBNER, F., ECKLE, S. B. G., EDINGER, M., EEDE, P., EHRHARDT, G. R. A., EICH, M., ENGEL, P., ENGELHARDT, B., ERDEI, A., et al. 2019. Guidelines for the use of flow cytometry and cell sorting in immunological studies (second edition). *Eur J Immunol,* 49**,** 1457-1973.

CRAMER, T., YAMANISHI, Y., CLAUSEN, B. E., FÖRSTER, I., PAWLINSKI, R., MACKMAN, N., HAASE, V. H., JAENISCH, R., CORR, M. & NIZET, V. 2003. HIF-1α is essential for myeloid cell-mediated inflammation. *Cell,* 112**,** 645-657.

CROCE, A. C. & BOTTIROLI, G. 2014. Autofluorescence spectroscopy and imaging: a tool for biomedical research and diagnosis. *European journal of histochemistry: EJH,* 58.

CROFT, N. P., SMITH, S. A., WONG, Y. C., TAN, C. T., DUDEK, N. L., FLESCH, I. E., LIN, L. C., TSCHARKE, D. C. & PURCELL, A. W. 2013. Kinetics of antigen expression and epitope presentation during virus infection. *PLoS pathogens,* 9**,** e1003129.

CRONK, J. C., FILIANO, A. J., LOUVEAU, A., MARIN, I., MARSH, R., JI, E., GOLDMAN, D. H., SMIRNOV, I., GERACI, N. & ACTON, S. 2018. Peripherally derived macrophages can engraft the brain independent of irradiation and maintain an identity distinct from microglia. *Journal of Experimental Medicine,* 215**,** 1627-1647.

CROXFORD, A. L., LANZINGER, M., HARTMANN, F. J., SCHREINER, B., MAIR, F., PELCZAR, P., CLAUSEN, B. E., JUNG, S., GRETER, M. & BECHER, B. 2015. The cytokine GM-CSF drives the inflammatory signature of CCR2+ monocytes and licenses autoimmunity. *Immunity,* 43**,** 502-514.

CUSICK, M. F., LIBBEY, J. E., PATEL, D. C., DOTY, D. J. & FUJINAMI, R. S. 2013. Infiltrating macrophages are key to the development of seizures following virus infection. *Journal of virology,* 87**,** 1849-1860.

DAFFIS, S., SAMUEL, M. A., KELLER, B. C., GALE JR, M. & DIAMOND, M. S. 2007. Cell-specific IRF-3 responses protect against West Nile virus infection by interferon-dependent and-independent mechanisms. *PLoS pathogens,* 3**,** e106.

DAFFIS, S., SAMUEL, M. A., SUTHAR, M. S., KELLER, B. C., GALE JR, M. & DIAMOND, M. S. 2008. Interferon regulatory factor IRF-7 induces the antiviral alpha interferon response and protects against lethal West Nile virus infection. *Journal of virology,* 82**,** 8465-8475.

DAI, X.-M., RYAN, G. R., HAPEL, A. J., DOMINGUEZ, M. G., RUSSELL, R. G., KAPP, S., SYLVESTRE, V. & STANLEY, E. R. 2002. Targeted disruption of the mouse colony-stimulating factor 1 receptor gene results in osteopetrosis, mononuclear phagocyte deficiency, increased primitive progenitor cell frequencies, and reproductive defects. *Blood, The Journal of the American Society of Hematology,* 99**,** 111-120.

DANG, E. V., MCDONALD, J. G., RUSSELL, D. W. & CYSTER, J. G. 2017. Oxysterol restraint of cholesterol synthesis prevents AIM2 inflammasome activation. *Cell,* 171**,** 1057-1071. e11.

DAS GUPTA, K., RAMNATH, D., VON PEIN, J. B., CURSON, J. E., WANG, Y., ABROL, R., KAKKANAT, A., MORADI, S. V., GUNTHER, K. S. & MURTHY, A. M. 2023. HDAC7 is an immunometabolic switch triaging danger signals for engagement of antimicrobial versus inflammatory responses in macrophages. *Proceedings of the National Academy of Sciences,* 120**,** e2212813120.

DAVIS, A. E. 2000. Mechanisms of traumatic brain injury: biomechanical, structural and cellular considerations. *Critical care nursing quarterly,* 23**,** 1-13.

DAVISON, A. M. & KING, N. J. 2011. Accelerated Dendritic Cell Differentiation from Migrating Ly6Clo Bone Marrow Monocytes in Early Dermal West Nile Virus Infection. *The Journal of Immunology,* 186**,** 2382-2396.

DE BRUIN, A. M., LIBREGTS, S. F., VALKHOF, M., BOON, L., TOUW, I. P. & NOLTE, M. A. 2012. IFNγ induces monopoiesis and inhibits neutrophil development during inflammation. *Blood, The Journal of the American Society of Hematology,* 119**,** 1543-1554.

DEL CARRATORE, F., JANKEVICS, A., EISINGA, R., HESKES, T., HONG, F. & BREITLING, R. 2017. RankProd 2.0: a refactored bioconductor package for detecting differentially expressed features in molecular profiling datasets. *Bioinformatics,* 33**,** 2774-2775.

DEL PRETE, A., ZACCAGNINO, P., DI PAOLA, M., SALTARELLA, M., CELIS, C. O., NICO, B., SANTORO, G. & LORUSSO, M. 2008. Role of mitochondria and reactive oxygen species in dendritic cell differentiation and functions. *Free Radical Biology and Medicine,* 44**,** 1443-1451.

DENDROU, C. A., FUGGER, L. & FRIESE, M. A. 2015. Immunopathology of multiple sclerosis. *Nat Rev Immunol,* 15**,** 545-58.

DEPAULA-SILVA, A. B., GORBEA, C., DOTY, D. J., LIBBEY, J. E., SANCHEZ, J. M. S., HANAK, T. J., CAZALLA, D. & FUJINAMI, R. S. 2019. Differential transcriptional profiles identify microglial- and macrophage-specific gene markers expressed during virus-induced neuroinflammation. *Journal of Neuroinflammation,* 16**,** 152.

DEPAULA-SILVA, A. B., HANAK, T. J., LIBBEY, J. E. & FUJINAMI, R. S. 2017. Theiler's murine encephalomyelitis virus infection of SJL/J and C57BL/6J mice: Models for multiple sclerosis and epilepsy. *Journal of neuroimmunology,* 308**,** 30-42.

DEVANNEY, N. A., STEWART, A. N. & GENSEL, J. C. 2020. Microglia and macrophage metabolism in CNS injury and disease: The role of immunometabolism in neurodegeneration and neurotrauma. *Experimental neurology,* 329**,** 113310.

DIAMOND, M. S., SHRESTHA, B., MEHLHOP, E., SITATI, E. & ENGLE, M. 2003. Innate and adaptive immune responses determine protection against disseminated infection by West Nile encephalitis virus. *Viral immunology,* 16**,** 259-278.

DIETSCHY, J. M. 2009. Central nervous system: cholesterol turnover, brain development and neurodegeneration.

DIJKSTRA, S., GEISERT, E. E., JR., DIJKSTRA, C. D., BAR, P. R. & JOOSTEN, E. A. 2001. CD81 and microglial activation in vitro: proliferation, phagocytosis and nitric oxide production. *J Neuroimmunol,* 114**,** 151-9.

DIJKSTRA, S., GEISERT, E. J., GISPEN, W. H., BAR, P. R. & JOOSTEN, E. A. 2000. Up-regulation of CD81 (target of the antiproliferative antibody; TAPA) by reactive microglia and astrocytes after spinal cord injury in the rat. *J Comp Neurol,* 428**,** 266-77.

DIMITRIJEVIC, O. B., STAMATOVIC, S. M., KEEP, R. F. & ANDJELKOVIC, A. V. 2007. Absence of the chemokine receptor CCR2 protects against cerebral ischemia/reperfusion injury in mice. *Stroke,* 38**,** 1345-1353.

DIVAKARUNI, A. S., HSIEH, W. Y., MINARRIETA, L., DUONG, T. N., KIM, K. K., DESOUSA, B. R., ANDREYEV, A. Y., BOWMAN, C. E., CARADONNA, K. & DRANKA, B. P. 2018. Etomoxir inhibits macrophage polarization by disrupting CoA homeostasis. *Cell metabolism,* 28**,** 490-503. e7.

DONNELLY, R. P., LOFTUS, R. M., KEATING, S. E., LIOU, K. T., BIRON, C. A., GARDINER, C. M. & FINLAY, D. K. 2014. mTORC1-dependent metabolic reprogramming is a prerequisite for NK cell effector function. *The Journal of Immunology,* 193**,** 4477-4484.

DUFORT, F. J., GUMINA, M. R., TA, N. L., TAO, Y., HEYSE, S. A., SCOTT, D. A., RICHARDSON, A. D., SEYFRIED, T. N. & CHILES, T. C. 2014. Glucose-dependent de novo lipogenesis in B lymphocytes: a requirement for atp-citrate lyase in lipopolysaccharide-induced differentiation. *Journal of Biological Chemistry,* 289**,** 7011-7024.

ECKER, C., GUO, L., VOICU, S., GIL-DE-GÓMEZ, L., MEDVEC, A., CORTINA, L., PAJDA, J., ANDOLINA, M., TORRES-CASTILLO, M. & DONATO, J. L. 2018. Differential reliance on lipid metabolism as a salvage pathway underlies functional differences of T cell subsets in poor nutrient environments. *Cell reports,* 23**,** 741-755.

ENNERFELT, H., FROST, E. L., SHAPIRO, D. A., HOLLIDAY, C., ZENGELER, K. E., VOITHOFER, G., BOLTE, A. C., LAMMERT, C. R., KULAS, J. A., ULLAND, T. K. & LUKENS, J. R. 2022. SYK coordinates neuroprotective microglial responses in neurodegenerative disease. *Cell,* 185**,** 4135-4152 e22.

ESCARTIN, C., GALEA, E., LAKATOS, A., O'CALLAGHAN, J. P., PETZOLD, G. C., SERRANO-POZO, A., STEINHÄUSER, C., VOLTERRA, A., CARMIGNOTO, G. & AGARWAL, A. 2021. Reactive astrocyte nomenclature, definitions, and future directions. *Nature neuroscience,* 24**,** 312-325.

EVERTS, B., AMIEL, E., HUANG, S. C.-C., SMITH, A. M., CHANG, C.-H., LAM, W. Y., REDMANN, V., FREITAS, T. C., BLAGIH, J. & VAN DER WINDT, G. J. 2014. TLR-driven early glycolytic reprogramming via the kinases TBK1-IKKε supports the anabolic demands of dendritic cell activation. *Nature immunology,* 15**,** 323-332.

EVERTS, B., AMIEL, E., VAN DER WINDT, G. J., FREITAS, T. C., CHOTT, R., YARASHESKI, K. E., PEARCE, E. L. & PEARCE, E. J. 2012. Commitment to glycolysis sustains survival of NO-producing inflammatory dendritic cells. *Blood, The Journal of the American Society of Hematology,* 120**,** 1422-1431.

EVRARD, M., KWOK, I. W., CHONG, S. Z., TENG, K. W., BECHT, E., CHEN, J., SIEOW, J. L., PENNY, H. L., CHING, G. C. & DEVI, S. 2018. Developmental

analysis of bone marrow neutrophils reveals populations specialized in expansion, trafficking, and effector functions. *Immunity,* 48**,** 364-379. e8.

FAAS, M., IPSEIZ, N., ACKERMANN, J., CULEMANN, S., GRÜNEBOOM, A., SCHRÖDER, F., ROTHE, T., SCHOLTYSEK, C., EBERHARDT, M. & BÖTTCHER, M. 2021. IL-33-induced metabolic reprogramming controls the differentiation of alternatively activated macrophages and the resolution of inflammation. *Immunity,* 54**,** 2531-2546. e5.

FABRE, V., BEITING, D. P., BLISS, S. K., GEBRESELASSIE, N. G., GAGLIARDO, L. F., LEE, N. A., LEE, J. J. & APPLETON, J. A. 2009. Eosinophil deficiency compromises parasite survival in chronic nematode infection. *The Journal of Immunology,* 182**,** 1577-1583.

FALLARINO, F., GROHMANN, U. & PUCCETTI, P. 2012. Indoleamine 2, 3-dioxygenase: from catalyst to signaling function. *European journal of immunology,* 42**,** 1932-1937.

FEINBERG, M. W., WARA, A. K., CAO, Z., LEBEDEVA, M. A., ROSENBAUER, F., IWASAKI, H., HIRAI, H., KATZ, J. P., HASPEL, R. L. & GRAY, S. 2007. The Kruppel-like factor KLF4 is a critical regulator of monocyte differentiation. *The EMBO journal,* 26**,** 4138-4148.

FIFE, B. T., HUFFNAGLE, G. B., KUZIEL, W. A. & KARPUS, W. J. 2000. CC chemokine receptor 2 is critical for induction of experimental autoimmune encephalomyelitis. *The Journal of experimental medicine,* 192**,** 899-906.

FRANCISCO, D. M. F., MARCHETTI, L., RODRIGUEZ-LORENZO, S., FRIAS-ANAYA, E., FIGUEIREDO, R. M., BT, R. N., WINTER, P., ROMERO, I. A., DE VRIES, H. E., ENGELHARDT, B. & BRUGGMANN, R. 2020. Advancing brain barriers RNA sequencing: guidelines from experimental design to publication. *Fluids Barriers CNS,* 17**,** 51.

FRATKIN, J. D., LEIS, A. A., STOKIC, D. S., SLAVINSKI, S. A. & GEISS, R. W. 2004. Spinal cord neuropathology in human west NileVirus infection. *Archives of pathology & laboratory medicine,* 128**,** 533-537.

FREEMERMAN, A. J., JOHNSON, A. R., SACKS, G. N., MILNER, J. J., KIRK, E. L., TROESTER, M. A., MACINTYRE, A. N., GORAKSHA-HICKS, P., RATHMELL, J. C. & MAKOWSKI, L. 2014. Metabolic reprogramming of macrophages: glucose transporter 1 (GLUT1)-mediated glucose metabolism drives a proinflammatory phenotype. *Journal of Biological Chemistry,* 289**,** 7884-7896.

FRIEDMAN, B. A., SRINIVASAN, K., AYALON, G., MEILANDT, W. J., LIN, H., HUNTLEY, M. A., CAO, Y., LEE, S. H., HADDICK, P. C. G., NGU, H., MODRUSAN, Z., LARSON, J. L., KAMINKER, J. S., VAN DER BRUG, M. P. & HANSEN, D. V. 2018. Diverse Brain Myeloid Expression Profiles Reveal Distinct Microglial Activation States and Aspects of Alzheimer's Disease Not Evident in Mouse Models. *Cell Rep,* 22**,** 832-847.

FÜGER, P., HEFENDEHL, J. K., VEERARAGHAVALU, K., WENDELN, A.-C., SCHLOSSER, C., OBERMÜLLER, U., WEGENAST-BRAUN, B. M., NEHER, J. J., MARTUS, P. & KOHSAKA, S. 2017. Microglia turnover with aging and in an Alzheimer's model via long-term in vivo single-cell imaging. *Nature neuroscience,* 20**,** 1371-1376.

FURR, S. R., CHAUHAN, V. S., STERKA JR, D., GRDZELISHVILI, V. & MARRIOTT, I. 2008. Characterization of retinoic acid–inducible gene-I expression in primary murine glia following exposure to vesicular stomatitis virus. *Journal of neurovirology,* 14**,** 503-513.

GALVÁN-PEÑA, S. & O'NEILL, L. A. 2014. Metabolic reprograming in macrophage polarization. *Frontiers in immunology,* 5**,** 109777.

GARBER, C., SOUNG, A., VOLLMER, L. L., KANMOGNE, M., LAST, A., BROWN, J. & KLEIN, R. S. 2019. T cells promote microglia-mediated synaptic elimination and cognitive dysfunction during recovery from neuropathogenic flaviviruses. *Nat Neurosci,* 22**,** 1276-1288.

GARBER, C., VASEK, M. J., VOLLMER, L. L., SUN, T., JIANG, X. & KLEIN, R. S. 2018. Astrocytes decrease adult neurogenesis during virus-induced memory dysfunction via IL-1. *Nature immunology,* 19**,** 151-161.

GEBRESELASSIE, N. G., MOORHEAD, A. R., FABRE, V., GAGLIARDO, L. F., LEE, N. A., LEE, J. J. & APPLETON, J. A. 2012. Eosinophils preserve parasitic nematode larvae by regulating local immunity. *The Journal of Immunology,* 188**,** 417-425.

GEERAERTS, X., FERNANDEZ-GARCIA, J., HARTMANN, F. J., DE GOEDE, K. E., MARTENS, L., ELKRIM, Y., DEBRAEKELEER, A., STIJLEMANS, B., VANDEKEERE, A. & RINALDI, G. 2021. Macrophages are metabolically heterogeneous within the tumor microenvironment. *Cell reports,* 37.

GEIRSDOTTIR, L., DAVID, E., KEREN-SHAUL, H., WEINER, A., BOHLEN, S. C., NEUBER, J., BALIC, A., GILADI, A., SHEBAN, F., DUTERTRE, C. A., PFEIFLE, C., PERI, F., RAFFO-ROMERO, A., VIZIOLI, J., MATIASEK, K., SCHEIWE, C., MECKEL, S., MATZ-RENSING, K., VAN DER MEER, F., THORMODSSON, F. R., STADELMANN, C., ZILKHA, N., KIMCHI, T., GINHOUX, F., ULITSKY, I., ERNY, D., AMIT, I. & PRINZ, M. 2020. Cross-Species Single-Cell Analysis Reveals Divergence of the Primate Microglia Program. *Cell,* 181**,** 746.

GEISERT, E. E., JR., WILLIAMS, R. W., GEISERT, G. R., FAN, L., ASBURY, A. M., MAECKER, H. T., DENG, J. & LEVY, S. 2002. Increased brain size and glial cell number in CD81-null mice. *J Comp Neurol,* 453**,** 22-32.

GEISSMANN, F., JUNG, S. & LITTMAN, D. R. 2003. Blood monocytes consist of two principal subsets with distinct migratory properties. *Immunity,* 19**,** 71-82.

GEISSMANN, F., MANZ, M. G., JUNG, S., SIEWEKE, M. H., MERAD, M. & LEY, K. 2010. Development of monocytes, macrophages, and dendritic cells. *Science,* 327**,** 656-61.

GENSEL, J. C. & ZHANG, B. 2015. Macrophage activation and its role in repair and pathology after spinal cord injury. *Brain research,* 1619**,** 1-11.

GETTS, D. R., MATSUMOTO, I., MÜLLER, M., GETTS, M. T., RADFORD, J., SHRESTHA, B., CAMPBELL, I. L. & KING, N. J. 2007. Role of IFN-γ in an experimental murine model of West Nile virus-induced seizures. *Journal of neurochemistry,* 103**,** 1019-1030.

GETTS, D. R., TERRY, R. L., GETTS, M. T., DEFFRASNES, C., MÜLLER, M., VAN VREDEN, C., ASHHURST, T. M., CHAMI, B., MCCARTHY, D. & WU, H. 2014. Therapeutic inflammatory monocyte modulation using immune-modifying microparticles. *Science translational medicine,* 6**,** 219ra7-219ra7.

GETTS, D. R., TERRY, R. L., GETTS, M. T., MÜLLER, M., RANA, S., DEFFRASNES, C., ASHHURST, T. M., RADFORD, J., HOFER, M. & THOMAS, S. 2012. Targeted blockade in lethal West Nile virus encephalitis indicates a crucial role for very late antigen (VLA)-4-dependent recruitment of nitric oxide-producing macrophages. *Journal of neuroinflammation,* 9**,** 246.

GETTS, D. R., TERRY, R. L., GETTS, M. T., MÜLLER, M., RANA, S., SHRESTHA, B., RADFORD, J., VAN ROOIJEN, N., CAMPBELL, I. L. & KING, N. J. C. 2008. Ly6c+ "inflammatory monocytes" are microglial precursors recruited in a pathogenic manner in West Nile virus encephalitis. *The Journal of experimental medicine,* 205**,** 2319-2337.

GIANNAKIS, N., SANSBURY, B. E., PATSALOS, A., HAYS, T. T., RILEY, C. O., HAN, X., SPITE, M. & NAGY, L. 2019. Dynamic changes to lipid mediators support transitions among macrophage subtypes during muscle regeneration. *Nature immunology,* 20**,** 626-636.

GILADI, A., WAGNER, L. K., LI, H., DÖRR, D., MEDAGLIA, C., PAUL, F., SHEMER, A., JUNG, S., YONA, S. & MACK, M. 2020. Cxcl10+ monocytes define a pathogenic subset in the central nervous system during autoimmune neuroinflammation. *Nature Immunology,* 21**,** 525-534.

GILES, D. A., DUNCKER, P. C., WILKINSON, N. M., WASHNOCK-SCHMID, J. M. & SEGAL, B. M. 2018. CNS-resident classical DCs play a critical role in CNS autoimmune disease. *J Clin Invest,* 128**,** 5322-5334.

GINHOUX, F., GRETER, M., LEBOEUF, M., NANDI, S., SEE, P., GOKHAN, S., MEHLER, M. F., CONWAY, S. J., NG, L. G. & STANLEY, E. R. 2010. Fate mapping analysis reveals that adult microglia derive from primitive macrophages. *Science,* 330**,** 841-845.

GINHOUX, F., SCHULTZE, J. L., MURRAY, P. J., OCHANDO, J. & BISWAS, S. K. 2016. New insights into the multidimensional concept of macrophage ontogeny, activation and function. *Nature immunology,* 17**,** 34-40.

GIRARD, Y. A., POPOV, V., WEN, J., HAN, V. & HIGGS, S. 2005. Ultrastructural study of West Nile virus pathogenesis in Culex pipiens quinquefasciatus (Diptera: Culicidae). *Journal of medical entomology,* 42**,** 429-444.

GLASS, W. G., LIM, J. K., CHOLERA, R., PLETNEV, A. G., GAO, J.-L. & MURPHY, P. M. 2005. Chemokine receptor CCR5 promotes leukocyte trafficking to the brain and survival in West Nile virus infection. *The Journal of experimental medicine,* 202**,** 1087-1098.

GLIEM, M., MAUSBERG, A. K., LEE, J. I., SIMIANTONAKIS, I., VAN ROOIJEN, N., HARTUNG, H. P. & JANDER, S. 2012. Macrophages prevent hemorrhagic infarct transformation in murine stroke models. *Annals of neurology,* 71**,** 743-752.

GOLDMANN, T., WIEGHOFER, P., JORDÃO, M. J. C., PRUTEK, F., HAGEMEYER, N., FRENZEL, K., AMANN, L., STASZEWSKI, O., KIERDORF, K. & KRUEGER, M. 2016. Origin, fate and dynamics of macrophages at central nervous system interfaces. *Nature immunology,* 17**,** 797.

GOMEZ PERDIGUERO, E., KLAPPROTH, K., SCHULZ, C., BUSCH, K., AZZONI, E., CROZET, L., GARNER, H., TROUILLET, C., DE BRUIJN, M. F. & GEISSMANN, F. 2015. Tissue-resident macrophages originate from yolk-sac-derived erythro-myeloid progenitors. *Nature,* 518**,** 547-551.

GONZALEZ, M. A., LU, D. R., YOUSEFI, M., KROLL, A., LO, C. H., BRISEÑO, C. G., WATSON, J. V., NOVITSKIY, S., ARIAS, V. & ZHOU, H. 2023. Phagocytosis increases an oxidative metabolic and immune suppressive signature in tumor macrophages. *Journal of Experimental Medicine,* 220**,** e20221472.

GRAJCHEN, E., WOUTERS, E., VAN DE HATERD, B., HAIDAR, M., HARDONNIÈRE, K., DIERCKX, T., VAN BROECKHOVEN, J., ERENS, C., HENDRIX, S. & KERDINE-RÖMER, S. 2020. CD36-mediated uptake of myelin debris by macrophages and microglia reduces neuroinflammation. *Journal of neuroinflammation,* 17**,** 1-14.

GRASSIVARO, F., MENON, R., ACQUAVIVA, M., OTTOBONI, L., RUFFINI, F., BERGAMASCHI, A., MUZIO, L., FARINA, C. & MARTINO, G. 2020. Convergence between microglia and peripheral macrophages phenotype during development and neuroinflammation. *Journal of Neuroscience,* 40**,** 784-795.

GRETER, M., HELFT, J., CHOW, A., HASHIMOTO, D., MORTHA, A., AGUDO-CANTERO, J., BOGUNOVIC, M., GAUTIER, E. L., MILLER, J. & LEBOEUF, M. 2012. GM-CSF controls nonlymphoid tissue dendritic cell homeostasis but is dispensable for the differentiation of inflammatory dendritic cells. *Immunity,* 36**,** 1031-1046.

GRETER, M., LELIOS, I. & CROXFORD, A. L. 2015. Microglia Versus Myeloid Cell Nomenclature during Brain Inflammation. *Front Immunol,* 6**,** 249.

GROSS, C. C., SCHULTE-MECKLENBECK, A., KLINSING, S., POSEVITZ-FEJFÁR, A., WIENDL, H. & KLOTZ, L. 2015. Dimethyl fumarate treatment alters circulating T helper cell subsets in multiple sclerosis. *Neuroimmunology & Neuroinflammation,* 3**,** e183.

GROSS, T. J., KREMENS, K., POWERS, L. S., BRINK, B., KNUTSON, T., DOMANN, F. E., PHILIBERT, R. A., MILHEM, M. M. & MONICK, M. M. 2014. Epigenetic silencing of the human NOS2 gene: rethinking the role of nitric oxide in human macrophage inflammatory responses. *The Journal of Immunology,* 192**,** 2326-2338.

GRUBMAN, A., CHOO, X. Y., CHEW, G., OUYANG, J. F., SUN, G., CROFT, N. P., ROSSELLO, F. J., SIMMONS, R., BUCKBERRY, S. & LANDIN, D. V. 2021. Transcriptional signature in microglia associated with Aβ plaque phagocytosis. *Nature communications,* 12**,** 1-22.

GUAK, H. & KRAWCZYK, C. M. 2020. Implications of cellular metabolism for immune cell migration. *Immunology,* 161**,** 200-208.

GUBSER, P. M., BANTUG, G. R., RAZIK, L., FISCHER, M., DIMELOE, S., HOENGER, G., DUROVIC, B., JAUCH, A. & HESS, C. 2013. Rapid effector function of memory CD8+ T cells requires an immediate-early glycolytic switch. *Nature immunology,* 14**,** 1064-1072.

GUILLIAMS, M., GINHOUX, F., JAKUBZICK, C., NAIK, S. H., ONAI, N., SCHRAML, B. U., SEGURA, E., TUSSIWAND, R. & YONA, S. 2014. Dendritic cells, monocytes and macrophages: a unified nomenclature based on ontogeny. *Nature Reviews Immunology,* 14**,** 571-578.

GUO, C., YE, J.-Z., SONG, M., PENG, X.-X. & LI, H. 2022. Poly I: C promotes malate to enhance innate immune response against bacterial infection. *Fish & Shellfish Immunology,* 131**,** 172-180.

GUPTA, K. D., SHAKESPEAR, M. R., CURSON, J. E., MURTHY, A. M., IYER, A., HODSON, M. P., RAMNATH, D., TILLU, V. A., VON PEIN, J. B. & REID, R. C. 2020. Class IIa histone deacetylases drive toll-like receptor-inducible glycolysis and macrophage inflammatory responses via pyruvate kinase M2. *Cell reports,* 30**,** 2712-2728. e8.

GUPTA, S. S., SHARP, R., HOFFEREK, C., KUAI, L., DORN, G. W., WANG, J. & CHEN, M. 2019. NIX-mediated mitophagy promotes effector memory formation in antigen-specific CD8+ T cells. *Cell reports,* 29**,** 1862-1877. e7.

HABARUGIRA, G., SUEN, W. W., HOBSON-PETERS, J., HALL, R. A. & BIELEFELDT-OHMANN, H. 2020. West Nile virus: an update on pathobiology, epidemiology, diagnostics, control and “one health” implications. *Pathogens,* 9**,** 589.

HALL, C. J., BOYLE, R. H., ASTIN, J. W., FLORES, M. V., OEHLERS, S. H., SANDERSON, L. E., ELLETT, F., LIESCHKE, G. J., CROSIER, K. E. & CROSIER, P. S. 2013. Immunoresponsive gene 1 augments bactericidal activity of macrophage-lineage cells by regulating β-oxidation-dependent mitochondrial ROS production. *Cell metabolism,* 18**,** 265-278.

HALL-MENDELIN, S., MCLEAN, B. J., BIELEFELDT-OHMANN, H., HOBSON-PETERS, J., HALL, R. A. & VAN DEN HURK, A. F. 2016. The insect-specific Palm

Creek virus modulates West Nile virus infection in and transmission by Australian mosquitoes. *Parasites & Vectors,* 9**,** 1-10.

HAMMOND, M. D., TAYLOR, R. A., MULLEN, M. T., AI, Y., AGUILA, H. L., MACK, M., KASNER, S. E., MCCULLOUGH, L. D. & SANSING, L. H. 2014. CCR2+ Ly6Chi inflammatory monocyte recruitment exacerbates acute disability following intracerebral hemorrhage. *Journal of Neuroscience,* 34**,** 3901-3909.

HAMMOND, T. R., DUFORT, C., DISSING-OLESEN, L., GIERA, S., YOUNG, A., WYSOKER, A., WALKER, A. J., GERGITS, F., SEGEL, M., NEMESH, J., MARSH, S. E., SAUNDERS, A., MACOSKO, E., GINHOUX, F., CHEN, J., FRANKLIN, R. J. M., PIAO, X., MCCARROLL, S. A. & STEVENS, B. 2019. Single-Cell RNA Sequencing of Microglia throughout the Mouse Lifespan and in the Injured Brain Reveals Complex Cell-State Changes. *Immunity,* 50**,** 253-271 e6.

HAO, W., CHANG, C.-P. B., TSAO, C.-C. & XU, J. 2010. Oligomycin-induced bioenergetic adaptation in cancer cells with heterogeneous bioenergetic organization. *Journal of biological chemistry,* 285**,** 12647-12654.

HAO, Y., HAO, S., ANDERSEN-NISSEN, E., MAUCK III, W. M., ZHENG, S., BUTLER, A., LEE, M. J., WILK, A. J., DARBY, C. & ZAGER, M. 2021. Integrated analysis of multimodal single-cell data. *Cell*.

HARDY, R. R., CARMACK, C. E., SHINTON, S. A., KEMP, J. D. & HAYAKAWA, K. 1991. Resolution and characterization of pro-B and pre-pro-B cell stages in normal mouse bone marrow. *The Journal of experimental medicine,* 173**,** 1213-1225.

HARTMANN, F. J., MRDJEN, D., MCCAFFREY, E., GLASS, D. R., GREENWALD, N. F., BHARADWAJ, A., KHAIR, Z., VERBERK, S. G., BARANSKI, A. & BASKAR, R. 2021. Single-cell metabolic profiling of human cytotoxic T cells. *Nature biotechnology,* 39**,** 186-197.

HE, D., MAO, Q., JIA, J., WANG, Z., LIU, T., LUO, B. & ZHANG, Z. 2022. Pentose phosphate pathway regulates tolerogenic apoptotic cell clearance and immune tolerance. *Frontiers in Immunology,* 12**,** 797091.

HE, H., MACK, J. J., GÜÇ, E., WARREN, C. M., SQUADRITO, M. L., KILARSKI, W. W., BAER, C., FRESHMAN, R. D., MCDONALD, A. I. & ZIYAD, S. 2016. Perivascular macrophages limit permeability. *Arteriosclerosis, thrombosis, and vascular biology,* 36**,** 2203-2212.

HEIEIS, G. A., PATENTE, T. A., ALMEIDA, L., VRIELING, F., TAK, T., PERONA-WRIGHT, G., MAIZELS, R. M., STIENSTRA, R. & EVERTS, B. 2023. Metabolic heterogeneity of tissue-resident macrophages in homeostasis and during helminth infection. *Nature Communications,* 14**,** 5627.

HETTINGER, J., RICHARDS, D. M., HANSSON, J., BARRA, M. M., JOSCHKO, A.-C., KRIJGSVELD, J. & FEUERER, M. 2013. Origin of monocytes and macrophages in a committed progenitor. *Nature immunology,* 14**,** 821.

HOLTMAN, I. R., RAJ, D. D., MILLER, J. A., SCHAAFSMA, W., YIN, Z., BROUWER, N., WES, P. D., MOLLER, T., ORRE, M., KAMPHUIS, W., HOL, E. M., BODDEKE, E. W. & EGGEN, B. J. 2015. Induction of a common microglia gene expression signature by aging and neurodegenerative conditions: a co-expression meta-analysis. *Acta Neuropathol Commun,* 3**,** 31.

HONG, F., BREITLING, R., MCENTEE, C. W., WITTNER, B. S., NEMHAUSER, J. L. & CHORY, J. 2006. RankProd: a bioconductor package for detecting differentially expressed genes in meta-analysis. *Bioinformatics,* 22**,** 2825-7.

HOWE, C. L., LAFRANCE-COREY, R. G., SUNDSBAK, R. S. & LAFRANCE, S. J. 2012. Inflammatory monocytes damage the hippocampus during acute picornavirus infection of the brain. *Journal of neuroinflammation,* 9**,** 50.

HOWELL, O. W., REEVES, C. A., NICHOLAS, R., CARASSITI, D., RADOTRA, B., GENTLEMAN, S. M., SERAFINI, B., ALOISI, F., RONCAROLI, F., MAGLIOZZI, R. & REYNOLDS, R. 2011. Meningeal inflammation is widespread and linked to cortical pathology in multiple sclerosis. *Brain,* 134**,** 2755-71.

HSIEH, C. L., NIEMI, E. C., WANG, S. H., LEE, C. C., BINGHAM, D., ZHANG, J., COZEN, M. L., CHARO, I., HUANG, E. J. & LIU, J. 2014. CCR2 deficiency impairs macrophage infiltration and improves cognitive function after traumatic brain injury. *Journal of neurotrauma,* 31**,** 1677-1688.

HSIEH, W.-Y., ZHOU, Q. D., YORK, A. G., WILLIAMS, K. J., SCUMPIA, P. O., KRONENBERGER, E. B., HOI, X. P., SU, B., CHI, X. & BUI, V. L. 2020. Toll-like receptors induce signal-specific reprogramming of the macrophage lipidome. *Cell metabolism,* 32**,** 128-143. e5.

HSU, P. P. & SABATINI, D. M. 2008. Cancer cell metabolism: Warburg and beyond. *Cell,* 134**,** 703-707.

HU, J., MELCHOR, G. S., LADAKIS, D., REGER, J., KIM, H. W., CHAMBERLAIN, K. A., SHULTS, N. V., OFT, H. C., SMITH, V. N. & ROSKO, L. M. 2024. Myeloid cell-associated aromatic amino acid metabolism facilitates CNS myelin regeneration. *NPJ Regenerative Medicine,* 9**,** 1.

HUANG, S. C.-C., EVERTS, B., IVANOVA, Y., O'SULLIVAN, D., NASCIMENTO, M., SMITH, A. M., BEATTY, W., LOVE-GREGORY, L., LAM, W. Y. & O'NEILL, C. M. 2014. Cell-intrinsic lysosomal lipolysis is essential for alternative activation of macrophages. *Nature immunology,* 15**,** 846-855.

HUSSMANN, K. L., SAMUEL, M. A., KIM, K. S., DIAMOND, M. S. & FREDERICKSEN, B. L. 2013. Differential replication of pathogenic and nonpathogenic strains of West Nile virus within astrocytes. *Journal of virology,* 87**,** 2814-2822.

IBRAHIM, J., NGUYEN, A. H., REHMAN, A., OCHI, A., JAMAL, M., GRAFFEO, C. S., HENNING, J. R., ZAMBIRINIS, C. P., FALLON, N. C. & BARILLA, R. 2012. Dendritic cell populations with different concentrations of lipid regulate tolerance and immunity in mouse and human liver. *Gastroenterology,* 143**,** 1061-1072.

INFANTINO, V., CONVERTINI, P., CUCCI, L., PANARO, M. A., DI NOIA, M. A., CALVELLO, R., PALMIERI, F. & IACOBAZZI, V. 2011. The mitochondrial citrate carrier: a new player in inflammation. *Biochemical Journal,* 438**,** 433-436.

INFANTINO, V., IACOBAZZI, V., MENGA, A., AVANTAGGIATI, M. L. & PALMIERI, F. 2014. A key role of the mitochondrial citrate carrier (SLC25A1) in TNFα-and IFNγ-triggered inflammation. *Biochimica et Biophysica Acta (BBA)-Gene Regulatory Mechanisms,* 1839**,** 1217-1225.

INFANTINO, V., IACOBAZZI, V., PALMIERI, F. & MENGA, A. 2013. ATP-citrate lyase is essential for macrophage inflammatory response. *Biochemical and biophysical research communications,* 440**,** 105-111.

INGERSOLL, M. A., SPANBROEK, R., LOTTAZ, C., GAUTIER, E. L., FRANKENBERGER, M., HOFFMANN, R., LANG, R., HANIFFA, M., COLLIN, M. & TACKE, F. 2010. Comparison of gene expression profiles between human and mouse monocyte subsets. *Blood, The Journal of the American Society of Hematology,* 115**,** e10-e19.

IVAN, D. C., WALTHERT, S. & LOCATELLI, G. 2021. Central nervous system barriers impact distribution and expression of iNOS and arginase-1 in infiltrating macrophages during neuroinflammation. *Frontiers in immunology,* 12.

IZIKSON, L., KLEIN, R. S., CHARO, I. F., WEINER, H. L. & LUSTER, A. D. 2000. Resistance to experimental autoimmune encephalomyelitis in mice lacking the CC chemokine receptor (CCR2). *The Journal of experimental medicine,* 192**,** 1075-1080.

JABLONSKI, K. A., AMICI, S. A., WEBB, L. M., RUIZ-ROSADO, J. D. D., POPOVICH, P. G., PARTIDA-SANCHEZ, S. & GUERAU-DE-ARELLANO, M. 2015. Novel markers to delineate murine M1 and M2 macrophages. *PloS one,* 10**,** e0145342.

JAKUBZICK, C., GAUTIER, E. L., GIBBINGS, S. L., SOJKA, D. K., SCHLITZER, A., JOHNSON, T. E., IVANOV, S., DUAN, Q., BALA, S. & CONDON, T. 2013. Minimal differentiation of classical monocytes as they survey steady-state tissues and transport antigen to lymph nodes. *Immunity,* 39**,** 599-610.

JALILI, V., AFGAN, E., GU, Q., CLEMENTS, D., BLANKENBERG, D., GOECKS, J., TAYLOR, J. & NEKRUTENKO, A. 2020. Corrigendum: The Galaxy platform for accessible, reproducible and collaborative biomedical analyses: 2020 update. *Nucleic Acids Res,* 48**,** 8205-8207.

JENSEN, H., POTEMPA, M., GOTTHARDT, D. & LANIER, L. L. 2017. Cutting edge: IL-2–induced expression of the amino acid transporters SLC1A5 and CD98 is a prerequisite for NKG2D-mediated activation of human NK cells. *The Journal of Immunology,* 199**,** 1967-1972.

JHA, A. K., HUANG, S. C.-C., SERGUSHICHEV, A., LAMPROPOULOU, V., IVANOVA, Y., LOGINICHEVA, E., CHMIELEWSKI, K., STEWART, K. M., ASHALL, J. & EVERTS, B. 2015. Network integration of parallel metabolic and transcriptional data reveals metabolic modules that regulate macrophage polarization. *Immunity,* 42**,** 419-430.

JIANG, H., SHI, H., SUN, M., WANG, Y., MENG, Q., GUO, P., CAO, Y., CHEN, J., GAO, X. & LI, E. 2016. PFKFB3-driven macrophage glycolytic metabolism is a crucial component of innate antiviral defense. *The Journal of Immunology,* 197**,** 2880-2890.

JOHNSTON, L. J., KING, N. J. & HALLIDAY, G. M. 2000. Langerhans cells migrate to local lymph nodes following cutaneous infection with an arbovirus. *Journal of Investigative Dermatology,* 114**,** 560-568.

JORDÃO, M. J. C., SANKOWSKI, R., BRENDECKE, S. M., SAGAR, LOCATELLI, G., TAI, Y.-H., TAY, T. L., SCHRAMM, E., ARMBRUSTER, S., HAGEMEYER, N., GROS, O., MAI, D., ÇIÇEK, Ö., FALK, T., KERSCHENSTEINER, M., GRÜN, D. & PRINZ, M. 2019. Single-cell profiling identifies myeloid cell subsets with distinct fates during neuroinflammation. *Science,* 363**,** eaat7554.

KAECH, S. M., WHERRY, E. J. & AHMED, R. 2002. Effector and memory T-cell differentiation: implications for vaccine development. *Nature Reviews Immunology,* 2**,** 251-262.

KARSUNKY, H., MERAD, M., COZZIO, A., WEISSMAN, I. L. & MANZ, M. G. 2003. Flt3 ligand regulates dendritic cell development from Flt3+ lymphoid and myeloid-committed progenitors to Flt3+ dendritic cells in vivo. *The Journal of experimental medicine,* 198**,** 305-313.

KATAN, M. & LUFT, A. 2018. Global Burden of Stroke. *Semin Neurol,* 38**,** 208-211.

KAUSHIK, D. K., BHATTACHARYA, A., MIRZAEI, R., RAWJI, K. S., AHN, Y., RHO, J. M. & YONG, V. W. 2019. Enhanced glycolytic metabolism supports transmigration of brain-infiltrating macrophages in multiple sclerosis. *The Journal of clinical investigation,* 129**,** 3277-3292.

KELLY, B. & O'NEILL, L. A. 2015. Metabolic reprogramming in macrophages and dendritic cells in innate immunity. *Cell research,* 25**,** 771-784.

KELLY, B., TANNAHILL, G. M., MURPHY, M. P. & O'NEILL, L. A. 2015. Metformin inhibits the production of reactive oxygen species from NADH: ubiquinone

oxidoreductase to limit induction of interleukin-1β (IL-1β) and boosts interleukin-10 (IL-10) in lipopolysaccharide (LPS)-activated macrophages. *Journal of biological chemistry,* 290**,** 20348-20359.

KEREN-SHAUL, H., SPINRAD, A., WEINER, A., MATCOVITCH-NATAN, O., DVIR-SZTERNFELD, R., ULLAND, T. K., DAVID, E., BARUCH, K., LARA-ASTAISO, D., TOTH, B., ITZKOVITZ, S., COLONNA, M., SCHWARTZ, M. & AMIT, I. 2017. A Unique Microglia Type Associated with Restricting Development of Alzheimer's Disease. *Cell,* 169**,** 1276-1290 e17.

KIELER, M., HOFMANN, M. & SCHABBAUER, G. 2021. More than just protein building blocks: How amino acids and related metabolic pathways fuel macrophage polarization. *The FEBS journal,* 288**,** 3694-3714.

KIERDORF, K., ERNY, D., GOLDMANN, T., SANDER, V., SCHULZ, C., PERDIGUERO, E. G., WIEGHOFER, P., HEINRICH, A., RIEMKE, P., HOLSCHER, C., MULLER, D. N., LUCKOW, B., BROCKER, T., DEBOWSKI, K., FRITZ, G., OPDENAKKER, G., DIEFENBACH, A., BIBER, K., HEIKENWALDER, M., GEISSMANN, F., ROSENBAUER, F. & PRINZ, M. 2013. Microglia emerge from erythromyeloid precursors via Pu.1- and Irf8-dependent pathways. *Nat Neurosci,* 16**,** 273-80.

KIGERL, K. A., GENSEL, J. C., ANKENY, D. P., ALEXANDER, J. K., DONNELLY, D. J. & POPOVICH, P. G. 2009. Identification of two distinct macrophage subsets with divergent effects causing either neurotoxicity or regeneration in the injured mouse spinal cord. *Journal of Neuroscience,* 29**,** 13435-13444.

KIGERL, K. A., MCGAUGHY, V. M. & POPOVICH, P. G. 2006. Comparative analysis of lesion development and intraspinal inflammation in four strains of mice following spinal contusion injury. *Journal of Comparative Neurology,* 494**,** 578-594.

KIM, C. C., NAKAMURA, M. C. & HSIEH, C. L. 2016. Brain trauma elicits non-canonical macrophage activation states. *Journal of neuroinflammation,* 13**,** 1-12.

KIM, D., LANGMEAD, B. & SALZBERG, S. L. 2015. HISAT: a fast spliced aligner with low memory requirements. *Nat Methods,* 12**,** 357-60.

KIM, J.-W., TCHERNYSHYOV, I., SEMENZA, G. L. & DANG, C. V. 2006. HIF-1-mediated expression of pyruvate dehydrogenase kinase: a metabolic switch required for cellular adaptation to hypoxia. *Cell metabolism,* 3**,** 177-185.

KING, I. L., DICKENDESHER, T. L. & SEGAL, B. M. 2009. Circulating Ly-6C+ myeloid precursors migrate to the CNS and play a pathogenic role during autoimmune demyelinating disease. *Blood, The Journal of the American Society of Hematology,* 113**,** 3190-3197.

KING, N. J., GETTS, D. R., GETTS, M. T., RANA, S., SHRESTHA, B. & KESSON, A. M. 2007. Immunopathology of flavivirus infections. *Immunol Cell Biol,* 85**,** 33-42.

KING, N. J. C., VAN VREDEN, C., TERRY, R. L., GETTS, D. R., YEUNG, A. W. S., TEAGUE-GETTS, M., DAVISON, A. M., DEFFRASNES, C. & MUNOZ-ERAZO, L. 2011. *The Immunopathogenesis of Neurotropic Flavivirus Infection,* Prague, InTech.

KIPP, M., NYAMOYA, S., HOCHSTRASSER, T. & AMOR, S. 2017. Multiple sclerosis animal models: a clinical and histopathological perspective. *Brain Pathol,* 27**,** 123-137.

KIRITSY, M. C., MCCANN, K., MOTT, D., HOLLAND, S. M., BEHAR, S. M., SASSETTI, C. M. & OLIVE, A. J. 2021. Mitochondrial respiration contributes to the interferon gamma response in antigen-presenting cells. *Elife,* 10**,** e65109.

KLEIN, R. S., GARBER, C., FUNK, K. E., SALIMI, H., SOUNG, A., KANMOGNE, M., MANIVASAGAM, S., AGNER, S. & CAIN, M. 2019. Neuroinflammation During RNA Viral Infections. *Annu Rev Immunol,* 37**,** 73-95.

KLEIN, R. S., LIN, E., ZHANG, B., LUSTER, A. D., TOLLETT, J., SAMUEL, M. A., ENGLE, M. & DIAMOND, M. S. 2005. Neuronal CXCL10 directs CD8+ T-cell recruitment and control of West Nile virus encephalitis. *Journal of virology,* 79**,** 11457-11466.

KO, H.-J., BRADY, J. L., RYG-CORNEJO, V., HANSEN, D. S., VREMEC, D., SHORTMAN, K., ZHAN, Y. & LEW, A. M. 2014. GM-CSF–responsive monocyte-derived dendritic cells are pivotal in Th17 pathogenesis. *The Journal of Immunology,* 192**,** 2202-2209.

KOLDE, R. 2012. Pheatmap: pretty heatmaps. *R package version,* 1.

KOMUCZKI, J., TUZLAK, S., FRIEBEL, E., HARTWIG, T., SPATH, S., ROSENSTIEL, P., WAISMAN, A., OPITZ, L., OUKKA, M. & SCHREINER, B. 2019. Fate-mapping of GM-CSF expression identifies a discrete subset of inflammation-driving T helper cells regulated by cytokines IL-23 and IL-1β. *Immunity,* 50**,** 1289-1304. e6.

KOPF, H., DE LA ROSA, G. M., HOWARD, O. Z. & CHEN, X. 2007. Rapamycin inhibits differentiation of Th17 cells and promotes generation of FoxP3+ T regulatory cells. *International immunopharmacology,* 7**,** 1819-1824.

KOPPER, T. J. & GENSEL, J. C. 2018. Myelin as an inflammatory mediator: Myelin interactions with complement, macrophages, and microglia in spinal cord injury. *Journal of neuroscience research,* 96**,** 969-977.

KRASEMANN, S., MADORE, C., CIALIC, R., BAUFELD, C., CALCAGNO, N., EL FATIMY, R., BECKERS, L., O'LOUGHLIN, E., XU, Y., FANEK, Z., GRECO, D. J., SMITH, S. T., TWEET, G., HUMULOCK, Z., ZRZAVY, T., CONDE-SANROMAN, P., GACIAS, M., WENG, Z., CHEN, H., TJON, E., MAZAHERI, F., HARTMANN, K., MADI, A., ULRICH, J. D., GLATZEL, M., WORTHMANN, A., HEEREN, J., BUDNIK, B., LEMERE, C., IKEZU, T., HEPPNER, F. L., LITVAK, V., HOLTZMAN, D. M., LASSMANN, H., WEINER, H. L., OCHANDO, J., HAASS, C. & BUTOVSKY, O. 2017. The TREM2-APOE Pathway Drives the Transcriptional Phenotype of Dysfunctional Microglia in Neurodegenerative Diseases. *Immunity,* 47**,** 566-581 e9.

KRAWCZYK, C. M., HOLOWKA, T., SUN, J., BLAGIH, J., AMIEL, E., DEBERARDINIS, R. J., CROSS, J. R., JUNG, E., THOMPSON, C. B. & JONES, R. G. 2010. Toll-like receptor–induced changes in glycolytic metabolism regulate dendritic cell activation. *Blood, The Journal of the American Society of Hematology,* 115**,** 4742-4749.

KRONENBERG, G., UHLEMANN, R., RICHTER, N., KLEMPIN, F., WEGNER, S., STAERCK, L., WOLF, S., UCKERT, W., KETTENMANN, H. & ENDRES, M. 2018. Distinguishing features of microglia-and monocyte-derived macrophages after stroke. *Acta neuropathologica,* 135**,** 551-568.

KUHLMANN, T., LUDWIN, S., PRAT, A., ANTEL, J., BRUCK, W. & LASSMANN, H. 2017. An updated histological classification system for multiple sclerosis lesions. *Acta Neuropathol,* 133**,** 13-24.

KUHN, S., GRITTI, L., CROOKS, D. & DOMBROWSKI, Y. 2019. Oligodendrocytes in development, myelin generation and beyond. *Cells,* 8**,** 1424.

KUMAR, M., VERMA, S. & NERURKAR, V. R. 2010. Pro-inflammatory cytokines derived from West Nile virus (WNV)-infected SK-N-SH cells mediate neuroinflammatory markers and neuronal death. *Journal of neuroinflammation,* 7**,** 1-14.

KURISU, K., ZHENG, Z., KIM, J. Y., SHI, J., KANOKE, A., LIU, J., HSIEH, C. L. & YENARI, M. A. 2019. Triggering receptor expressed on myeloid cells-2 expression in the brain is required for maximal phagocytic activity and improved neurological outcomes following experimental stroke. *Journal of Cerebral Blood Flow & Metabolism,* 39**,** 1906-1918.

KUROTAKI, D., OSATO, N., NISHIYAMA, A., YAMAMOTO, M., BAN, T., SATO, H., NAKABAYASHI, J., UMEHARA, M., MIYAKE, N. & MATSUMOTO, N. 2013. Essential role of the IRF8-KLF4 transcription factor cascade in murine monocyte differentiation. *Blood, The Journal of the American Society of Hematology,* 121**,** 1839-1849.

KWIDZINSKI, E. & BECHMANN, I. 2007. IDO expression in the brain: a double-edged sword. *Journal of Molecular Medicine,* 85**,** 1351-1359.

LABRECQUE, N. & CERMAKIAN, N. 2015. Circadian Clocks in the Immune System. *J Biol Rhythms,* 30**,** 277-90.

LACHMANDAS, E., BOUTENS, L., RATTER, J. M., HIJMANS, A., HOOIVELD, G. J., JOOSTEN, L. A., RODENBURG, R. J., FRANSEN, J. A., HOUTKOOPER, R. H. & VAN CREVEL, R. 2016. Microbial stimulation of different Toll-like receptor signalling pathways induces diverse metabolic programmes in human monocytes. *Nature microbiology,* 2**,** 1-10.

LAMPROPOULOU, V., SERGUSHICHEV, A., BAMBOUSKOVA, M., NAIR, S., VINCENT, E. E., LOGINICHEVA, E., CERVANTES-BARRAGAN, L., MA, X., HUANG, S. C.-C. & GRISS, T. 2016. Itaconate links inhibition of succinate dehydrogenase with macrophage metabolic remodeling and regulation of inflammation. *Cell metabolism,* 24**,** 158-166.

LANIER, L. L. 2005. NK cell recognition. *Annu. Rev. Immunol.,* 23**,** 225-274.

LANTERI, M. C., O'BRIEN, K. M., PURTHA, W. E., CAMERON, M. J., LUND, J. M., OWEN, R. E., HEITMAN, J. W., CUSTER, B., HIRSCHKORN, D. F. & TOBLER, L. H. 2009. Tregs control the development of symptomatic West Nile virus infection in humans and mice. *The Journal of clinical investigation,* 119**,** 3266-3277.

LAURO, C., CHECE, G., MONACO, L., ANTONANGELI, F., PERUZZI, G., RINALDO, S., PAONE, A., CUTRUZZOLÀ, F. & LIMATOLA, C. 2019. Fractalkine modulates microglia metabolism in brain ischemia. *Frontiers in cellular neuroscience,* 13**,** 414.

LAUTERBACH, M. A., HANKE, J. E., SEREFIDOU, M., MANGAN, M. S., KOLBE, C.-C., HESS, T., ROTHE, M., KAISER, R., HOSS, F. & GEHLEN, J. 2019. Toll-like receptor signaling rewires macrophage metabolism and promotes histone acetylation via ATP-citrate lyase. *Immunity,* 51**,** 997-1011. e7.

LAWLESS, S. J., KEDIA-MEHTA, N., WALLS, J. F., MCGARRIGLE, R., CONVERY, O., SINCLAIR, L. V., NAVARRO, M. N., MURRAY, J. & FINLAY, D. K. 2017. Glucose represses dendritic cell-induced T cell responses. *Nature communications,* 8**,** 15620.

LEBIEN, T. W. & TEDDER, T. F. 2008. B lymphocytes: how they develop and function. *Blood, The Journal of the American Society of Hematology,* 112**,** 1570-1580.

LEE, H.-G., WHEELER, M. A. & QUINTANA, F. J. 2022. Function and therapeutic value of astrocytes in neurological diseases. *Nature reviews Drug discovery,* 21**,** 339-358.

LEE, J.-H., PHELAN, P., SHIN, M., OH, B.-C., HAN, X., IM, S.-S. & OSBORNE, T. F. 2018. SREBP-1a–stimulated lipid synthesis is required for macrophage phagocytosis downstream of TLR4-directed mTORC1. *Proceedings of the National Academy of Sciences,* 115**,** E12228-E12234.

LEUSCHNER, F., RAUCH, P. J., UENO, T., GORBATOV, R., MARINELLI, B., LEE, W. W., DUTTA, P., WEI, Y., ROBBINS, C. & IWAMOTO, Y. 2012. Rapid monocyte

kinetics in acute myocardial infarction are sustained by extramedullary monocytopoiesis. *Journal of Experimental Medicine,* 209**,** 123-137.

LEVINE, L. S., HIAM-GALVEZ, K. J., MARQUEZ, D. M., TENVOOREN, I., MADDEN, M. Z., CONTRERAS, D. C., DAHUNSI, D. O., IRISH, J. M., OLUWOLE, O. O. & RATHMELL, J. C. 2021. Single-cell analysis by mass cytometry reveals metabolic states of early-activated CD8+ T cells during the primary immune response. *Immunity,* 54**,** 829-844. e5.

LEWIS, N. D., HILL, J. D., JUCHEM, K. W., STEFANOPOULOS, D. E. & MODIS, L. K. 2014. RNA sequencing of microglia and monocyte-derived macrophages from mice with experimental autoimmune encephalomyelitis illustrates a changing phenotype with disease course. *J Neuroimmunol,* 277**,** 26-38.

LEWIS, R. S., TAMIR, S., TANNENBAUM, S. R. & DEEN, W. M. 1995. Kinetic analysis of the fate of nitric oxide synthesized by macrophages in vitro. *Journal of Biological Chemistry,* 270**,** 29350-29355.

LI, F., PIATTINI, F., POHLMEIER, L., FENG, Q., REHRAUER, H. & KOPF, M. 2022a. Monocyte-derived alveolar macrophages autonomously determine severe outcome of respiratory viral infection. *Science Immunology,* 7**,** eabj5761.

LI, M., SANTPERE, G., IMAMURA KAWASAWA, Y., EVGRAFOV, O. V., GULDEN, F. O., POCHAREDDY, S., SUNKIN, S. M., LI, Z., SHIN, Y., ZHU, Y., SOUSA, A. M. M., WERLING, D. M., KITCHEN, R. R., KANG, H. J., PLETIKOS, M., CHOI, J., MUCHNIK, S., XU, X., WANG, D., LORENTE-GALDOS, B., LIU, S., GIUSTI-RODRIGUEZ, P., WON, H., DE LEEUW, C. A., PARDINAS, A. F., BRAINSPAN, C., PSYCH, E. C., PSYCH, E. D. S., HU, M., JIN, F., LI, Y., OWEN, M. J., O'DONOVAN, M. C., WALTERS, J. T. R., POSTHUMA, D., REIMERS, M. A., LEVITT, P., WEINBERGER, D. R., HYDE, T. M., KLEINMAN, J. E., GESCHWIND, D. H., HAWRYLYCZ, M. J., STATE, M. W., SANDERS, S. J., SULLIVAN, P. F., GERSTEIN, M. B., LEIN, E. S., KNOWLES, J. A. & SESTAN, N. 2018a. Integrative functional genomic analysis of human brain development and neuropsychiatric risks. *Science,* 362.

LI, S., YU, J., HUBER, A., KRYCZEK, I., WANG, Z., JIANG, L., LI, X., DU, W., LI, G. & WEI, S. 2022b. Metabolism drives macrophage heterogeneity in the tumor microenvironment. *Cell reports,* 39.

LI, T., LI, X., ATTRI, K. S., LIU, C., LI, L., HERRING, L. E., ASARA, J. M., LEI, Y. L., SINGH, P. K. & GAO, C. 2018b. O-GlcNAc transferase links glucose metabolism to MAVS-mediated antiviral innate immunity. *Cell host & microbe,* 24**,** 791-803. e6.

LI, Y., LU, B., SHENG, L., ZHU, Z., SUN, H., ZHOU, Y., YANG, Y., XUE, D., CHEN, W. & TIAN, X. 2018c. Hexokinase 2-dependent hyperglycolysis driving microglial activation contributes to ischemic brain injury. *Journal of neurochemistry,* 144**,** 186-200.

LIAO, N.-S., BIX, M., ZIJLSTRA, M., JAENISCH, R. & RAULET, D. 1991. MHC class I deficiency: susceptibility to natural killer (NK) cells and impaired NK activity. *Science,* 253**,** 199-202.

LIAO, Y., SMYTH, G. K. & SHI, W. 2014. featureCounts: an efficient general purpose program for assigning sequence reads to genomic features. *Bioinformatics,* 30**,** 923-30.

LIM, H. Y., LIM, S. Y., TAN, C. K., THIAM, C. H., GOH, C. C., CARBAJO, D., CHEW, S. H. S., SEE, P., CHAKAROV, S. & WANG, X. N. 2018. Hyaluronan receptor LYVE-1-expressing macrophages maintain arterial tone through hyaluronan-mediated regulation of smooth muscle cell collagen. *Immunity,* 49**,** 326-341. e7.

LIM, J. K., OBARA, C. J., RIVOLLIER, A., PLETNEV, A. G., KELSALL, B. L. & MURPHY, P. M. 2011a. Chemokine receptor Ccr2 is critical for monocyte accumulation and survival in West Nile virus encephalitis. *The Journal of Immunology,* 186**,** 471-478.

LIM, P.-Y., BEHR, M. J., CHADWICK, C. M., SHI, P.-Y. & BERNARD, K. A. 2011b. Keratinocytes are cell targets of West Nile virus in vivo. *Journal of virology,* 85**,** 5197-5201.

LIN, N. & SIMON, M. C. 2016. Hypoxia-inducible factors: key regulators of myeloid cells during inflammation. *The Journal of clinical investigation,* 126**,** 3661-3671.

LINDSEY, N. P., STAPLES, J. E., LEHMAN, J. A. & FISCHER, M. 2010. Surveillance for human west nile virus disease—United states, 1999–2008. *MMWR Surveill Summ,* 59**,** 1-17.

LIU, C., WU, C., YANG, Q., GAO, J., LI, L., YANG, D. & LUO, L. 2016. Macrophages mediate the repair of brain vascular rupture through direct physical adhesion and mechanical traction. *Immunity,* 44**,** 1162-1176.

LIU, D., CHANG, C., LU, N., WANG, X., LU, Q., REN, X., REN, P., ZHAO, D., WANG, L. & ZHU, Y. 2017a. Comprehensive proteomics analysis reveals metabolic reprogramming of tumor-associated macrophages stimulated by the tumor microenvironment. *Journal of Proteome Research,* 16**,** 288-297.

LIU, J., GAO, C., SODICOFF, J., KOZAREVA, V., MACOSKO, E. Z. & WELCH, J. D. 2020. Jointly defining cell types from multiple single-cell datasets using LIGER. *Nature Protocols,* 15**,** 3632-3662.

LIU, P.-S., CHEN, Y.-T., LI, X., HSUEH, P.-C., TZENG, S.-F., CHEN, H., SHI, P.-Z., XIE, X., PARIK, S. & PLANQUE, M. 2023. CD40 signal rewires fatty acid and glutamine metabolism for stimulating macrophage anti-tumorigenic functions. *Nature immunology,* 24**,** 452-462.

LIU, P.-S., WANG, H., LI, X., CHAO, T., TEAV, T., CHRISTEN, S., DI CONZA, G., CHENG, W.-C., CHOU, C.-H. & VAVAKOVA, M. 2017b. α-ketoglutarate orchestrates macrophage activation through metabolic and epigenetic reprogramming. *Nature immunology,* 18**,** 985-994.

LOCATELLI, G., THEODOROU, D., KENDIRLI, A., JORDAO, M. J. C., STASZEWSKI, O., PHULPHAGAR, K., CANTUTI-CASTELVETRI, L., DAGKALIS, A., BESSIS, A. & SIMONS, M. 2018. Mononuclear phagocytes locally specify and adapt their phenotype in a multiple sclerosis model. *Nature neuroscience,* 21**,** 1196-1208.

LOVE, M. I., HUBER, W. & ANDERS, S. 2014. Moderated estimation of fold change and dispersion for RNA-seq data with DESeq2. *Genome Biol,* 15**,** 550.

LUCCHINETTI, C., BRUCK, W., PARISI, J., SCHEITHAUER, B., RODRIGUEZ, M. & LASSMANN, H. 2000. Heterogeneity of multiple sclerosis lesions: implications for the pathogenesis of demyelination. *Ann Neurol,* 47**,** 707-17.

MA, J., LIU, R., PENG, H., ZHOU, J. & LI, H. 2010. CD81 inhibits the proliferation of astrocytes by inducing G(0)/G (1) arrest in vitro. *J Huazhong Univ Sci Technolog Med Sci,* 30**,** 201-5.

MAAS, A. I., STOCCHETTI, N. & BULLOCK, R. 2008. Moderate and severe traumatic brain injury in adults. *The Lancet Neurology,* 7**,** 728-741.

MACDONALD, K., ROWE, V., BOFINGER, H. M., THOMAS, R., SASMONO, T., HUME, D. A. & HILL, G. R. 2005. The colony-stimulating factor 1 receptor is expressed on dendritic cells during differentiation and regulates their expansion. *The Journal of Immunology,* 175**,** 1399-1405.

MACDONALD, K. P., MUNSTER, D. J., CLARK, G. J., DZIONEK, A., SCHMITZ, J. & HART, D. N. 2002. Characterization of human blood dendritic cell subsets. *Blood, The Journal of the American Society of Hematology,* 100**,** 4512-4520.

MACDONALD, K. P., PALMER, J. S., CRONAU, S., SEPPANEN, E., OLVER, S., RAFFELT, N. C., KUNS, R., PETTIT, A. R., CLOUSTON, A. & WAINWRIGHT, B. 2010. An antibody against the colony-stimulating factor 1 receptor depletes the resident subset of monocytes and tissue-and tumor-associated macrophages but does not inhibit inflammation. *Blood, The Journal of the American Society of Hematology,* 116**,** 3955-3963.

MACMICKING, J., XIE, Q.-W. & NATHAN, C. 1997. Nitric oxide and macrophage function. *Annual review of immunology,* 15**,** 323-350.

MACRAE, I. 2011. Preclinical stroke research–advantages and disadvantages of the most common rodent models of focal ischaemia. *British journal of pharmacology,* 164**,** 1062-1078.

MADDEN, K. 2003. West Nile virus infection and its neurological manifestations. *Clin Med Res,* 1**,** 145-50.

MAECKER, H. T., TODD, S. C. & LEVY, S. 1997. The tetraspanin superfamily: molecular facilitators. *FASEB J,* 11**,** 428-42.

MAH, A. Y., RASHIDI, A., KEPPEL, M. P., SAUCIER, N., MOORE, E. K., ALINGER, J. B., TRIPATHY, S. K., AGARWAL, S. K., JENG, E. K. & WONG, H. C. 2017. Glycolytic requirement for NK cell cytotoxicity and cytomegalovirus control. *JCI insight,* 2.

MARIK, C., FELTS, P. A., BAUER, J., LASSMANN, H. & SMITH, K. J. 2007. Lesion genesis in a subset of patients with multiple sclerosis: a role for innate immunity? *Brain,* 130**,** 2800-2815.

MARIONI, R. E., HARRIS, S. E., ZHANG, Q., MCRAE, A. F., HAGENAARS, S. P., HILL, W. D., DAVIES, G., RITCHIE, C. W., GALE, C. R., STARR, J. M., GOATE, A. M., PORTEOUS, D. J., YANG, J., EVANS, K. L., DEARY, I. J., WRAY, N. R. & VISSCHER, P. M. 2018. GWAS on family history of Alzheimer's disease. *Transl Psychiatry,* 8**,** 99.

MARTIN, D. B. & VAGELOS, P. R. 1962. The mechanism of tricarboxylic acid cycle regulation of fatty acid synthesis. *Journal of Biological Chemistry,* 237**,** 1787-1792.

MARTIN, M. 2011. Cutadapt removes adapter sequences from high-throughput sequencing reads. *EMBnet. journal,* 17**,** 10-12.

MASS, E., BALLESTEROS, I., FARLIK, M., HALBRITTER, F., GÜNTHER, P., CROZET, L., JACOME-GALARZA, C. E., HÄNDLER, K., KLUGHAMMER, J. & KOBAYASHI, Y. 2016. Specification of tissue-resident macrophages during organogenesis. *Science,* 353**,** aaf4238.

MASUDA, T., AMANN, L., SANKOWSKI, R., STASZEWSKI, O., LENZ, M., P, D. E., SNAIDERO, N., COSTA JORDAO, M. J., BOTTCHER, C., KIERDORF, K., JUNG, S., PRILLER, J., MISGELD, T., VLACHOS, A., MEYER-LUEHMANN, M., KNOBELOCH, K. P. & PRINZ, M. 2020. Novel Hexb-based tools for studying microglia in the CNS. *Nat Immunol,* 21**,** 802-815.

MASUDA, T., SANKOWSKI, R., STASZEWSKI, O., BOTTCHER, C., AMANN, L., SAGAR, SCHEIWE, C., NESSLER, S., KUNZ, P., VAN LOO, G., COENEN, V. A., REINACHER, P. C., MICHEL, A., SURE, U., GOLD, R., GRUN, D., PRILLER, J., STADELMANN, C. & PRINZ, M. 2019. Spatial and temporal heterogeneity of mouse and human microglia at single-cell resolution. *Nature,* 566**,** 388-392.

MATHYS, H., DAVILA-VELDERRAIN, J., PENG, Z., GAO, F., MOHAMMADI, S., YOUNG, J. Z., MENON, M., HE, L., ABDURROB, F., JIANG, X., MARTORELL,

A. J., RANSOHOFF, R. M., HAFLER, B. P., BENNETT, D. A., KELLIS, M. & TSAI, L. H. 2019. Single-cell transcriptomic analysis of Alzheimer's disease. *Nature,* 570**,** 332-337.

MCKERCHER, S. R., TORBETT, B. E., ANDERSON, K. L., HENKEL, G. W., VESTAL, D. J., BARIBAULT, H., KLEMSZ, M., FEENEY, A. J., WU, G. E. & PAIGE, C. J. 1996. Targeted disruption of the PU. 1 gene results in multiple hematopoietic abnormalities. *The EMBO journal,* 15**,** 5647-5658.

MCQUADE, A. & BLURTON-JONES, M. 2019. Microglia in Alzheimer's Disease: Exploring How Genetics and Phenotype Influence Risk. *J Mol Biol,* 431**,** 1805-1817.

MEGHRAOUI-KHEDDAR, A., BARTHELEMY, S., BOISSONNAS, A. & COMBADIÈRE, C. 2020. Revising CX3CR1 expression on murine classical and non-classical monocytes. *Frontiers in immunology,* 11**,** 1117.

MENDIOLA, A. S., RYU, J. K., BARDEHLE, S., MEYER-FRANKE, A., ANG, K. K., WILSON, C., BAETEN, K. M., HANSPERS, K., MERLINI, M., THOMAS, S., PETERSEN, M. A., WILLIAMS, A., THOMAS, R., RAFALSKI, V. A., MEZA-ACEVEDO, R., TOGNATTA, R., YAN, Z., PFAFF, S. J., MACHADO, M. R., BEDARD, C., RIOS CORONADO, P. E., JIANG, X., WANG, J., PLEISS, M. A., GREEN, A. J., ZAMVIL, S. S., PICO, A. R., BRUNEAU, B. G., ARKIN, M. R. & AKASSOGLOU, K. 2020. Transcriptional profiling and therapeutic targeting of oxidative stress in neuroinflammation. *Nat Immunol,* 21**,** 513-524.

MENEZES, S., MELANDRI, D., ANSELMI, G., PERCHET, T., LOSCHKO, J., DUBROT, J., PATEL, R., GAUTIER, E. L., HUGUES, S. & LONGHI, M. P. 2016. The heterogeneity of Ly6Chi monocytes controls their differentiation into iNOS+ macrophages or monocyte-derived dendritic cells. *Immunity,* 45**,** 1205-1218.

MERAD, M. & MARTIN, J. C. 2020. Pathological inflammation in patients with COVID-19: a key role for monocytes and macrophages. *Nature reviews immunology,* 20**,** 355-362.

MERLIN, J., IVANOV, S., DUMONT, A., SERGUSHICHEV, A., GALL, J., STUNAULT, M., AYRAULT, M., VAILLANT, N., CASTIGLIONE, A. & SWAIN, A. 2021. Non-canonical glutamine transamination sustains efferocytosis by coupling redox buffering to oxidative phosphorylation. *Nature metabolism,* 3**,** 1313-1326.

METALLO, C. M., GAMEIRO, P. A., BELL, E. L., MATTAINI, K. R., YANG, J., HILLER, K., JEWELL, C. M., JOHNSON, Z. R., IRVINE, D. J. & GUARENTE, L. 2012. Reductive glutamine metabolism by IDH1 mediates lipogenesis under hypoxia. *Nature,* 481**,** 380-384.

MICHALEK, R. D., GERRIETS, V. A., JACOBS, S. R., MACINTYRE, A. N., MACIVER, N. J., MASON, E. F., SULLIVAN, S. A., NICHOLS, A. G. & RATHMELL, J. C. 2011. Cutting edge: distinct glycolytic and lipid oxidative metabolic programs are essential for effector and regulatory CD4+ T cell subsets. *The Journal of immunology,* 186**,** 3299-3303.

MICHELUCCI, A., CORDES, T., GHELFI, J., PAILOT, A., REILING, N., GOLDMANN, O., BINZ, T., WEGNER, A., TALLAM, A. & RAUSELL, A. 2013. Immune-responsive gene 1 protein links metabolism to immunity by catalyzing itaconic acid production. *Proceedings of the National Academy of Sciences,* 110**,** 7820-7825.

MILACIC, M., BEAVERS, D., CONLEY, P., GONG, C., GILLESPIE, M., GRISS, J., HAW, R., JASSAL, B., MATTHEWS, L. & MAY, B. 2024. The reactome pathway knowledgebase 2024. *Nucleic acids research,* 52**,** D672-D678.

MILDNER, A., MACK, M., SCHMIDT, H., BRÜCK, W., DJUKIC, M., ZABEL, M. D., HILLE, A., PRILLER, J. & PRINZ, M. 2009. CCR2+Ly-6Chi monocytes are crucial

for the effector phase of autoimmunity in the central nervous system. *Brain,* 132**,** 2487-2500.

MILDNER, A., SCHMIDT, H., NITSCHE, M., MERKLER, D., HANISCH, U.-K., MACK, M., HEIKENWALDER, M., BRÜCK, W., PRILLER, J. & PRINZ, M. 2007. Microglia in the adult brain arise from Ly-6ChiCCR2+ monocytes only under defined host conditions. *Nature Neuroscience,* 10**,** 1544-1553.

MILDNER, A., SCHÖNHEIT, J., GILADI, A., DAVID, E., LARA-ASTIASO, D., LORENZO-VIVAS, E., PAUL, F., CHAPPELL-MAOR, L., PRILLER, J. & LEUTZ, A. 2017. Genomic characterization of murine monocytes reveals C/EBPβ transcription factor dependence of Ly6C− cells. *Immunity,* 46**,** 849-862. e7.

MILICH, L. M., CHOI, J. S., RYAN, C., CERQUEIRA, S. R., BENAVIDES, S., YAHN, S. L., TSOULFAS, P. & LEE, J. K. 2021. Single-cell analysis of the cellular heterogeneity and interactions in the injured mouse spinal cord. *J Exp Med,* 218.

MILICH, L. M., RYAN, C. B. & LEE, J. K. 2019. The origin, fate, and contribution of macrophages to spinal cord injury pathology. *Acta neuropathologica,* 137**,** 785-797.

MILLER, A., NAGY, C., KNAPP, B., LAENGLE, J., PONWEISER, E., GROEGER, M., STARKL, P., BERGMANN, M., WAGNER, O. & HASCHEMI, A. 2017. Exploring metabolic configurations of single cells within complex tissue microenvironments. *Cell Metabolism,* 26**,** 788-800. e6.

MILLER, S. D., MCMAHON, E. J., SCHREINER, B. & BAILEY, S. L. 2007. Antigen presentation in the CNS by myeloid dendritic cells drives progression of relapsing experimental autoimmune encephalomyelitis. *Annals of the New York Academy of Sciences,* 1103**,** 179-191.

MILLS, C. D., KINCAID, K., ALT, J. M., HEILMAN, M. J. & HILL, A. M. 2000. M-1/M-2 macrophages and the Th1/Th2 paradigm. *The Journal of immunology,* 164**,** 6166-6173.

MILLS, E. L., KELLY, B., LOGAN, A., COSTA, A. S., VARMA, M., BRYANT, C. E., TOURLOMOUSIS, P., DÄBRITZ, J. H. M., GOTTLIEB, E. & LATORRE, I. 2016. Succinate dehydrogenase supports metabolic repurposing of mitochondria to drive inflammatory macrophages. *Cell,* 167**,** 457-470. e13.

MINGO-CASAS, P., BLÁZQUEZ, A.-B., GÓMEZ DE CEDRÓN, M., SAN-FÉLIX, A., MOLINA, S., ESCRIBANO-ROMERO, E., CALVO-PINILLA, E., JIMÉNEZ DE OYA, N., RAMÍREZ DE MOLINA, A. & SAIZ, J.-C. 2023. Glycolytic shift during West Nile virus infection provides new therapeutic opportunities. *Journal of Neuroinflammation,* 20**,** 217.

MONROY-MÉRIDA, G., GUZMÁN-BELTRÁN, S., HERNÁNDEZ, F., SANTOS-MENDOZA, T. & BOBADILLA, K. 2021. High glucose concentrations impair the processing and presentation of Mycobacterium tuberculosis antigens in vitro. *Biomolecules,* 11**,** 1763.

MOON, J.-S., NAKAHIRA, K., CHUNG, K.-P., DENICOLA, G. M., KOO, M. J., PABÓN, M. A., ROONEY, K. T., YOON, J.-H., RYTER, S. W. & STOUT-DELGADO, H. 2016. NOX4-dependent fatty acid oxidation promotes NLRP3 inflammasome activation in macrophages. *Nature medicine,* 22**,** 1002-1012.

MORDICA, W. J., WOODS, K. M., CLEM, R. J., PASSARELLI, A. L. & CHAPES, S. K. 2009. Macrophage cell lines use CD81 in cell growth regulation. *In Vitro Cell Dev Biol Anim,* 45**,** 213-25.

MORIOKA, S., PERRY, J. S., RAYMOND, M. H., MEDINA, C. B., ZHU, Y., ZHAO, L., SERBULEA, V., ONENGUT-GUMUSCU, S., LEITINGER, N. & KUCENAS, S. 2018. Efferocytosis induces a novel SLC program to promote glucose uptake and lactate release. *Nature,* 563**,** 714-718.

MORRISON, T., WATTS, E. R., SADIKU, P. & WALMSLEY, S. R. 2023. The emerging role for metabolism in fueling neutrophilic inflammation. *Immunological reviews,* 314**,** 427-441.

MOSSADEGH-KELLER, N., SARRAZIN, S., KANDALLA, P. K., ESPINOSA, L., STANLEY, E. R., NUTT, S. L., MOORE, J. & SIEWEKE, M. H. 2013. M-CSF instructs myeloid lineage fate in single haematopoietic stem cells. *Nature,* 497**,** 239-243.

MOSTASHARI, F., BUNNING, M. L., KITSUTANI, P. T., SINGER, D. A., NASH, D., COOPER, M. J., KATZ, N., LILJEBJELKE, K. A., BIGGERSTAFF, B. J. & FINE, A. D. 2001. Epidemic West Nile encephalitis, New York, 1999: results of a household-based seroepidemiological survey. *The lancet,* 358**,** 261-264.

MULLARKY, E. & CANTLEY, L. C. 2015. Diverting glycolysis to combat oxidative stress. *Innovative medicine: basic research and development***,** 3-23.

MUNDT, S., MRDJEN, D., UTZ, S. G., GRETER, M., SCHREINER, B. & BECHER, B. 2019. Conventional DCs sample and present myelin antigens in the healthy CNS and allow parenchymal T cell entry to initiate neuroinflammation. *Sci Immunol,* 4.

MUÑOZ, J., RUIZ, S., SORIGUER, R., ALCAIDE, M., VIANA, D. S., ROIZ, D., VAZQUEZ, A. & FIGUEROLA, J. 2012. Feeding patterns of potential West Nile virus vectors in south-west Spain. *PloS one,* 7**,** e39549.

MURAOKA, S., JEDRYCHOWSKI, M. P., IWAHARA, N., ABDULLAH, M., ONOS, K. D., KEEZER, K. J., HU, J., IKEZU, S., HOWELL, G. R., GYGI, S. P. & IKEZU, T. 2021. Enrichment of Neurodegenerative Microglia Signature in Brain-Derived Extracellular Vesicles Isolated from Alzheimer's Disease Mouse Models. *J Proteome Res,* 20**,** 1733-1743.

MURRAY, P. J., ALLEN, J. E., BISWAS, S. K., FISHER, E. A., GILROY, D. W., GOERDT, S., GORDON, S., HAMILTON, J. A., IVASHKIV, L. B. & LAWRENCE, T. 2014. Macrophage activation and polarization: nomenclature and experimental guidelines. *Immunity,* 41**,** 14-20.

NAGHAVI, M., ABAJOBIR, A. A., ABBAFATI, C., ABBAS, K. M., ABD-ALLAH, F., ABERA, S. F., ABOYANS, V., ADETOKUNBOH, O., AFSHIN, A. & AGRAWAL, A. 2017. Global, regional, and national age-sex specific mortality for 264 causes of death, 1980–2016: a systematic analysis for the Global Burden of Disease Study 2016. *The Lancet,* 390**,** 1151-1210.

NAKAYA, M., XIAO, Y., ZHOU, X., CHANG, J.-H., CHANG, M., CHENG, X., BLONSKA, M., LIN, X. & SUN, S.-C. 2014. Inflammatory T cell responses rely on amino acid transporter ASCT2 facilitation of glutamine uptake and mTORC1 kinase activation. *Immunity,* 40**,** 692-705.

NATHAN, C. F., MURRAY, H. W., WIEBE, M. E. & RUBIN, B. Y. 1983. Identification of interferon-gamma as the lymphokine that activates human macrophage oxidative metabolism and antimicrobial activity. *The Journal of experimental medicine,* 158**,** 670-689.

NI, D., TAN, J., NIEWOLD, P., SPITERI, A. G., PINGET, G. V., KING, N. J. C. & MACIA, L. 2022. Impact of dietary fiber on West Nile Virus infection. *Frontiers in Immunology,* 13**,** 784486.

NIJLAND, P. G., MICHAILIDOU, I., WITTE, M. E., MIZEE, M. R., VAN DER POL, S. M., VAN HET HOF, B., REIJERKERK, A., PELLERIN, L., VAN DER VALK, P. & DE VRIES, H. E. 2014. Cellular distribution of glucose and monocarboxylate transporters in human brain white matter and multiple sclerosis lesions. *Glia,* 62**,** 1125-1141.

NIKIĆ, I., MERKLER, D., SORBARA, C., BRINKOETTER, M., KREUTZFELDT, M., BAREYRE, F. M., BRÜCK, W., BISHOP, D., MISGELD, T. & KERSCHENSTEINER, M. 2011. A reversible form of axon damage in experimental autoimmune encephalomyelitis and multiple sclerosis. *Nature medicine,* 17**,** 495-499.

NOELIA, A., BENSINGER, S. J., HONG, C., BECEIRO, S., BRADLEY, M. N., ZELCER, N., DENIZ, J., RAMIREZ, C., DÍAZ, M. & GALLARDO, G. 2009. Apoptotic cells promote their own clearance and immune tolerance through activation of the nuclear receptor LXR. *Immunity,* 31**,** 245-258.

O'NEILL, L. A., KISHTON, R. J. & RATHMELL, J. 2016. A guide to immunometabolism for immunologists. *Nature Reviews Immunology,* 16**,** 553-565.

O'NEILL, L. A. & PEARCE, E. J. 2016. Immunometabolism governs dendritic cell and macrophage function. *Journal of Experimental Medicine,* 213**,** 15-23.

O'SULLIVAN, D., VAN DER WINDT, G. J., HUANG, S. C.-C., CURTIS, J. D., CHANG, C.-H., BUCK, M. D., QIU, J., SMITH, A. M., LAM, W. Y. & DIPLATO, L. M. 2014. Memory CD8+ T cells use cell-intrinsic lipolysis to support the metabolic programming necessary for development. *Immunity,* 41**,** 75-88.

OLAH, M., MENON, V., HABIB, N., TAGA, M. F., MA, Y., YUNG, C. J., CIMPEAN, M., KHAIRALLAH, A., CORONAS-SAMANO, G., SANKOWSKI, R., GRUN, D., KROSHILINA, A. A., DIONNE, D., SARKIS, R. A., COSGROVE, G. R., HELGAGER, J., GOLDEN, J. A., PENNELL, P. B., PRINZ, M., VONSATTEL, J. P. G., TEICH, A. F., SCHNEIDER, J. A., BENNETT, D. A., REGEV, A., ELYAMAN, W., BRADSHAW, E. M. & DE JAGER, P. L. 2020. Single cell RNA sequencing of human microglia uncovers a subset associated with Alzheimer's disease. *Nat Commun,* 11**,** 6129.

OMALU, B. I., SHAKIR, A. A., WANG, G., LIPKIN, W. I. & WILEY, C. A. 2003. Fatal fulminant pan-meningo-polioencephalitis due to West Nile virus. *Brain pathology,* 13**,** 465-472.

ORECCHIONI, M., GHOSHEH, Y., PRAMOD, A. B. & LEY, K. 2019. Macrophage polarization: different gene signatures in M1 (LPS+) vs. classically and M2 (LPS–) vs. alternatively activated macrophages. *Frontiers in immunology,* 10**,** 1084.

OSUNA-RAMOS, J. F., REYES-RUIZ, J. M. & DEL ANGEL, R. M. 2018. The role of host cholesterol during flavivirus infection. *Frontiers in cellular and infection microbiology,* 8**,** 388.

PALFRAMAN, R. T., JUNG, S., CHENG, G., WENINGER, W., LUO, Y., DORF, M., LITTMAN, D. R., ROLLINS, B. J., ZWEERINK, H. & ROT, A. 2001. Inflammatory chemokine transport and presentation in HEV: a remote control mechanism for monocyte recruitment to lymph nodes in inflamed tissues. *The Journal of experimental medicine,* 194**,** 1361-1374.

PALMIERI, E. M., GONZALEZ-COTTO, M., BASELER, W. A., DAVIES, L. C., GHESQUIÈRE, B., MAIO, N., RICE, C. M., ROUAULT, T. A., CASSEL, T. & HIGASHI, R. M. 2020. Nitric oxide orchestrates metabolic rewiring in M1 macrophages by targeting aconitase 2 and pyruvate dehydrogenase. *Nature communications,* 11**,** 1-17.

PALMIERI, E. M., SPERA, I., MENGA, A., INFANTINO, V., PORCELLI, V., IACOBAZZI, V., PIERRI, C. L., HOOPER, D. C., PALMIERI, F. & CASTEGNA, A. 2015. Acetylation of human mitochondrial citrate carrier modulates mitochondrial citrate/malate exchange activity to sustain NADPH production during macrophage activation. *Biochimica et Biophysica Acta (BBA)-Bioenergetics,* 1847**,** 729-738.

PALSSON-MCDERMOTT, E. M., CURTIS, A. M., GOEL, G., LAUTERBACH, M. A., SHEEDY, F. J., GLEESON, L. E., VAN DEN BOSCH, M. W., QUINN, S. R.,

DOMINGO-FERNANDEZ, R. & JOHNSTON, D. G. 2015. Pyruvate kinase M2 regulates Hif-1α activity and IL-1β induction and is a critical determinant of the warburg effect in LPS-activated macrophages. *Cell metabolism,* 21**,** 65-80.

PANTEL, A., TEIXEIRA, A., HADDAD, E., WOOD, E. G., STEINMAN, R. M. & LONGHI, M. P. 2014. Direct type I IFN but not MDA5/TLR3 activation of dendritic cells is required for maturation and metabolic shift to glycolysis after poly IC stimulation. *PLoS biology,* 12**,** e1001759.

PAOLICELLI, R. C., BERGAMINI, G. & RAJENDRAN, L. 2019. Cell-to-cell Communication by Extracellular Vesicles: Focus on Microglia. *Neuroscience,* 405**,** 148-157.

PAPANDREOU, I., CAIRNS, R. A., FONTANA, L., LIM, A. L. & DENKO, N. C. 2006. HIF-1 mediates adaptation to hypoxia by actively downregulating mitochondrial oxygen consumption. *Cell metabolism,* 3**,** 187-197.

PARK, D., HAN, C. Z., ELLIOTT, M. R., KINCHEN, J. M., TRAMPONT, P. C., DAS, S., COLLINS, S., LYSIAK, J. J., HOEHN, K. L. & RAVICHANDRAN, K. S. 2011. Continued clearance of apoptotic cells critically depends on the phagocyte Ucp2 protein. *Nature,* 477**,** 220-224.

PASSLICK, B., FLIEGER, D. & ZIEGLER-HEITBROCK, H. 1989. Identification and characterization of a novel monocyte subpopulation in human peripheral blood.

PATEL, C. H., LEONE, R. D., HORTON, M. R. & POWELL, J. D. 2019. Targeting metabolism to regulate immune responses in autoimmunity and cancer. *Nature Reviews Drug Discovery,* 18**,** 669-688.

PAVILLON, N., HOBRO, A. J., AKIRA, S. & SMITH, N. I. 2018. Noninvasive detection of macrophage activation with single-cell resolution through machine learning. *Proceedings of the National Academy of Sciences,* 115**,** E2676-E2685.

PAVLOU, S., WANG, L., XU, H. & CHEN, M. 2017. Higher phagocytic activity of thioglycollate-elicited peritoneal macrophages is related to metabolic status of the cells. *Journal of inflammation,* 14**,** 1-6.

PEDERSEN, C. B., DAM, S. H., BARNKOB, M. B., LEIPOLD, M. D., PURROY, N., RASSENTI, L. Z., KIPPS, T. J., NGUYEN, J., LEDERER, J. A. & GOHIL, S. H. 2022. cyCombine allows for robust integration of single-cell cytometry datasets within and across technologies. *Nature communications,* 13**,** 1698.

PENG, T., DU, S.-Y., SON, M. & DIAMOND, B. 2021. HIF-1α is a negative regulator of interferon regulatory factors: Implications for interferon production by hypoxic monocytes. *Proceedings of the National Academy of Sciences,* 118**,** e2106017118.

PENKERT, H., BERTRAND, A., TIWARI, V., BREIMANN, S., MÜLLER, S. A., JORDAN, P. M., GERL, M. J., KLOSE, C., CANTUTI-CASTELVETRI, L. & BOSCH-QUERALT, M. 2021. Proteomic and lipidomic profiling of demyelinating lesions identifies fatty acids as modulators in lesion recovery. *Cell Reports,* 37.

PERRONE, L. A., BELSER, J. A., WADFORD, D. A., KATZ, J. M. & TUMPEY, T. M. 2013. Inducible nitric oxide contributes to viral pathogenesis following highly pathogenic influenza virus infection in mice. *The Journal of infectious diseases,* 207**,** 1576-1584.

PERUZZOTTI-JAMETTI, L., BERNSTOCK, J. D., VICARIO, N., COSTA, A. S., KWOK, C. K., LEONARDI, T., BOOTY, L. M., BICCI, I., BALZAROTTI, B. & VOLPE, G. 2018. Macrophage-derived extracellular succinate licenses neural stem cells to suppress chronic neuroinflammation. *Cell stem cell,* 22**,** 355-368. e13.

PETERSEN, L., CARSON, P., BIGGERSTAFF, B., CUSTER, B., BORCHARDT, S. & BUSCH, M. 2013a. Estimated cumulative incidence of West Nile virus infection in US adults, 1999–2010. *Epidemiology & Infection,* 141**,** 591-595.

PETERSEN, L. R., BRAULT, A. C. & NASCI, R. S. 2013b. West Nile virus: review of the literature. *Jama,* 310**,** 308-315.

PHAN, T. G., GRAY, E. E. & CYSTER, J. G. 2009. The microanatomy of B cell activation. *Current opinion in immunology,* 21**,** 258-265.

PHARES, T. W., KEAN, R. B., MIKHEEVA, T. & HOOPER, D. C. 2006. Regional differences in blood-brain barrier permeability changes and inflammation in the apathogenic clearance of virus from the central nervous system. *The Journal of Immunology,* 176**,** 7666-7675.

PIEPER, K., GRIMBACHER, B. & EIBEL, H. 2013. B-cell biology and development. *Journal of Allergy and Clinical Immunology,* 131**,** 959-971.

PILLAY, J., DEN BRABER, I., VRISEKOOP, N., KWAST, L. M., DE BOER, R. J., BORGHANS, J. A., TESSELAAR, K. & KOENDERMAN, L. 2010. In vivo labeling with 2H2O reveals a human neutrophil lifespan of 5.4 days. *Blood, The Journal of the American Society of Hematology,* 116**,** 625-627.

POLIANI, P. L., WANG, Y., FONTANA, E., ROBINETTE, M. L., YAMANISHI, Y., GILFILLAN, S. & COLONNA, M. 2015. TREM2 sustains microglial expansion during aging and response to demyelination. *J Clin Invest,* 125**,** 2161-70.

POPESCU, B. F. & LUCCHINETTI, C. F. 2012. Meningeal and cortical grey matter pathology in multiple sclerosis. *BMC Neurol,* 12**,** 11.

PSACHOULIA, K., CHAMBERLAIN, K. A., HEO, D., DAVIS, S. E., PASKUS, J. D., NANESCU, S. E., DUPREE, J. L., WYNN, T. A. & HUANG, J. K. 2016. IL4I1 augments CNS remyelination and axonal protection by modulating T cell driven inflammation. *Brain,* 139**,** 3121-3136.

QUALLS, J. E., SUBRAMANIAN, C., RAFI, W., SMITH, A. M., BALOUZIAN, L., DEFREITAS, A. A., SHIREY, K. A., REUTTERER, B., KERNBAUER, E. & STOCKINGER, S. 2012. Sustained generation of nitric oxide and control of mycobacterial infection requires argininosuccinate synthase 1. *Cell host & microbe,* 12**,** 313-323.

RAE, C. & GRAHAM, A. 2008. Fatty acid synthase inhibitor, C75, blocks resistin-induced increases in lipid accumulation by human macrophages. *Diabetes, Obesity and Metabolism,* 10**,** 1271-1274.

RAPPUOLI, R., PIZZA, M., DEL GIUDICE, G. & DE GREGORIO, E. 2014. Vaccines, new opportunities for a new society. *Proceedings of the National Academy of Sciences,* 111**,** 12288-12293.

RAUD, B., ROY, D. G., DIVAKARUNI, A. S., TARASENKO, T. N., FRANKE, R., MA, E. H., SAMBORSKA, B., HSIEH, W. Y., WONG, A. H. & STÜVE, P. 2018. Etomoxir actions on regulatory and memory T cells are independent of Cpt1a-mediated fatty acid oxidation. *Cell metabolism,* 28**,** 504-515. e7.

RAVISHANKAR, B., LIU, H., SHINDE, R., CHANDLER, P., BABAN, B., TANAKA, M., MUNN, D. H., MELLOR, A. L., KARLSSON, M. C. & MCGAHA, T. L. 2012. Tolerance to apoptotic cells is regulated by indoleamine 2, 3-dioxygenase. *Proceedings of the National Academy of Sciences,* 109**,** 3909-3914.

RAVISHANKAR, B., LIU, H., SHINDE, R., CHAUDHARY, K., XIAO, W., BRADLEY, J., KORITZINSKY, M., MADAIO, M. P. & MCGAHA, T. L. 2015. The amino acid sensor GCN2 inhibits inflammatory responses to apoptotic cells promoting tolerance and suppressing systemic autoimmunity. *Proceedings of the National Academy of Sciences,* 112**,** 10774-10779.

REBOLDI, A., DANG, E. V., MCDONALD, J. G., LIANG, G., RUSSELL, D. W. & CYSTER, J. G. 2014. 25-Hydroxycholesterol suppresses interleukin-1–driven inflammation downstream of type I interferon. *Science,* 345**,** 679-684.

RÉU, P., KHOSRAVI, A., BERNARD, S., MOLD, J. E., SALEHPOUR, M., ALKASS, K., PERL, S., TISDALE, J., POSSNERT, G. & DRUID, H. 2017. The lifespan and turnover of microglia in the human brain. *Cell reports,* 20**,** 779-784.

RITZEL, R. M., PATEL, A. R., GRENIER, J. M., CRAPSER, J., VERMA, R., JELLISON, E. R. & MCCULLOUGH, L. D. 2015. Functional differences between microglia and monocytes after ischemic stroke. *J Neuroinflammation,* 12**,** 106.

RIUS, J., GUMA, M., SCHACHTRUP, C., AKASSOGLOU, K., ZINKERNAGEL, A. S., NIZET, V., JOHNSON, R. S., HADDAD, G. G. & KARIN, M. 2008. NF-κB links innate immunity to the hypoxic response through transcriptional regulation of HIF-1α. *Nature,* 453**,** 807-811.

RODRIGUEZ, P. C., ZEA, A. H., CULOTTA, K. S., ZABALETA, J., OCHOA, J. B. & OCHOA, A. C. 2002. Regulation of t cell receptor cd3ζ chain expression byl-arginine. *Journal of Biological Chemistry,* 277**,** 21123-21129.

RODRÍGUEZ-PRADOS, J.-C., TRAVÉS, P. G., CUENCA, J., RICO, D., ARAGONÉS, J., MARTIN-SANZ, P., CASCANTE, M. & BOSCÁ, L. 2010. Substrate fate in activated macrophages: a comparison between innate, classic, and alternative activation. *The Journal of Immunology,* 185**,** 605-614.

ROE, K., ORILLO, B. & VERMA, S. 2014. West Nile virus-induced cell adhesion molecules on human brain microvascular endothelial cells regulate leukocyte adhesion and modulate permeability of the in vitro blood-brain barrier model. *PLoS One,* 9**,** e102598.

ROHL, C., LUCIUS, R. & SIEVERS, J. 2007. The effect of activated microglia on astrogliosis parameters in astrocyte cultures. *Brain Res,* 1129**,** 43-52.

ROSA NETO, J. C., CALDER, P. C., CURI, R., NEWSHOLME, P., SETHI, J. K. & SILVEIRA, L. S. 2021. The immunometabolic roles of various fatty acids in macrophages and lymphocytes. *International Journal of Molecular Sciences,* 22**,** 8460.

ROSAS-BALLINA, M., GUAN, X. L., SCHMIDT, A. & BUMANN, D. 2020. Classical activation of macrophages leads to lipid droplet formation without de novo fatty acid synthesis. *Frontiers in immunology,* 11**,** 506452.

ROSENBERG, H. F., DYER, K. D. & FOSTER, P. S. 2013. Eosinophils: changing perspectives in health and disease. *Nature Reviews Immunology,* 13**,** 9-22.

ROTH, P., BARTOCCI, A. & STANLEY, E. R. 1997. Lipopolysaccharide induces synthesis of mouse colony-stimulating factor-1 in vivo. *Journal of immunology (Baltimore, Md.: 1950),* 158**,** 3874-3880.

RUBIC, T., LAMETSCHWANDTNER, G., JOST, S., HINTEREGGER, S., KUND, J., CARBALLIDO-PERRIG, N., SCHWÄRZLER, C., JUNT, T., VOSHOL, H. & MEINGASSNER, J. G. 2008. Triggering the succinate receptor GPR91 on dendritic cells enhances immunity. *Nature immunology,* 9**,** 1261-1269.

RYAN, C. B., CHOI, J. S., AL-ALI, H. & LEE, J. K. 2022. Myelin and non-myelin debris contribute to foamy macrophage formation after spinal cord injury. *Neurobiology of disease,* 163**,** 105608.

SAFAIYAN, S., KANNAIYAN, N., SNAIDERO, N., BRIOSCHI, S., BIBER, K., YONA, S., EDINGER, A. L., JUNG, S., ROSSNER, M. J. & SIMONS, M. 2016. Age-related myelin degradation burdens the clearance function of microglia during aging. *Nature neuroscience,* 19**,** 995-998.

SAIZ, J. C., MARTIN-ACEBES, M. A., BLAZQUEZ, A. B., ESCRIBANO-ROMERO, E., PODEROSO, T. & JIMENEZ DE OYA, N. 2021. Pathogenicity and virulence of West Nile virus revisited eight decades after its first isolation. *Virulence,* 12**,** 1145-1173.

SAMAAN, Z., MCDERMID VAZ, S., BAWOR, M., POTTER, T. H., ESKANDARIAN, S. & LOEB, M. 2016. Neuropsychological Impact of West Nile Virus Infection: An Extensive Neuropsychiatric Assessment of 49 Cases in Canada. *PLoS One,* 11**,** e0158364.

SAMPSON, B. A., AMBROSI, C., CHARLOT, A., REIBER, K., VERESS, J. F. & ARMBRUSTMACHER, V. 2000. The pathology of human West Nile Virus infection. *Hum Pathol,* 31**,** 527-31.

SAMUEL, M. A. & DIAMOND, M. S. 2006. Pathogenesis of West Nile Virus infection: a balance between virulence, innate and adaptive immunity, and viral evasion. *Journal of virology,* 80**,** 9349-9360.

SAMUEL, M. A., MORREY, J. D. & DIAMOND, M. S. 2007a. Caspase 3-dependent cell death of neurons contributes to the pathogenesis of West Nile virus encephalitis. *Journal of virology,* 81**,** 2614-2623.

SAMUEL, M. A., WANG, H., SIDDHARTHAN, V., MORREY, J. D. & DIAMOND, M. S. 2007b. Axonal transport mediates West Nile virus entry into the central nervous system and induces acute flaccid paralysis. *Proceedings of the National Academy of Sciences,* 104**,** 17140-17145.

SANIN, D. E., GE, Y., MARINKOVIC, E., KABAT, A. M., CASTOLDI, A., CAPUTA, G., GRZES, K. M., CURTIS, J. D., THOMPSON, E. A., WILLENBORG, S., DICHTL, S., REINHARDT, S., DAHL, A., PEARCE, E. L., EMING, S. A., GERBAULET, A., ROERS, A., MURRAY, P. J. & PEARCE, E. J. 2022. A common framework of monocyte-derived macrophage activation. *Sci Immunol,* 7**,** eabl7482.

SANMARCO, L. M., RONE, J. M., POLONIO, C. M., FERNANDEZ LAHORE, G., GIOVANNONI, F., FERRARA, K., GUTIERREZ-VAZQUEZ, C., LI, N., SOKOLOVSKA, A. & PLASENCIA, A. 2023. Lactate limits CNS autoimmunity by stabilizing HIF-1α in dendritic cells. *Nature,* 620**,** 881-889.

SAVARIN, C., DUTTA, R. & BERGMANN, C. C. 2018. Distinct gene profiles of bone marrow-derived macrophages and microglia during neurotropic coronavirus-induced demyelination. *Frontiers in immunology,* 9**,** 1325.

SCHAEFER, P. M., KALININA, S., RUECK, A., VON ARNIM, C. A. & VON EINEM, B. 2019. NADH autofluorescence—a marker on its way to boost bioenergetic research. *Cytometry Part A,* 95**,** 34-46.

SCHAIRER, D. O., CHOUAKE, J. S., NOSANCHUK, J. D. & FRIEDMAN, A. J. 2012. The potential of nitric oxide releasing therapies as antimicrobial agents. *Virulence,* 3**,** 271-279.

SCHILPEROORT, M., NGAI, D., KATERELOS, M., POWER, D. A. & TABAS, I. 2023. PFKFB2-mediated glycolysis promotes lactate-driven continual efferocytosis by macrophages. *Nature Metabolism,* 5**,** 431-444.

SCHIRMER, L., ALBERT, M., BUSS, A., SCHULZ-SCHAEFFER, W. J., ANTEL, J. P., BRÜCK, W. & STADELMANN, C. 2009. Substantial early, but nonprogressive neuronal loss in multiple sclerosis (MS) spinal cord. *Annals of Neurology: Official Journal of the American Neurological Association and the Child Neurology Society,* 66**,** 698-704.

SCHLACHETZKI, J. C. M., PROTS, I., TAO, J., CHUN, H. B., SAIJO, K., GOSSELIN, D., WINNER, B., GLASS, C. K. & WINKLER, J. 2018. A monocyte gene expression signature in the early clinical course of Parkinson's disease. *Sci Rep,* 8**,** 10757.

SCHLITZER, A., SIVAKAMASUNDARI, V., CHEN, J., SUMATOH, H. R. B., SCHREUDER, J., LUM, J., MALLERET, B., ZHANG, S., LARBI, A. & ZOLEZZI, F. 2015. Identification of cDC1-and cDC2-committed DC progenitors reveals early

lineage priming at the common DC progenitor stage in the bone marrow. *Nature immunology,* 16**,** 718-728.

SCHNEIDER, B. S. & HIGGS, S. 2008. The enhancement of arbovirus transmission and disease by mosquito saliva is associated with modulation of the host immune response. *Transactions of the Royal Society of Tropical Medicine and Hygiene,* 102**,** 400-408.

SCHNEIDER, B. S., SOONG, L., COFFEY, L. L., STEVENSON, H. L., MCGEE, C. E. & HIGGS, S. 2010. Aedes aegypti saliva alters leukocyte recruitment and cytokine signaling by antigen-presenting cells during West Nile virus infection. *PloS one,* 5**,** e11704.

SCHNEIDER, B. S., SOONG, L., GIRARD, Y. A., CAMPBELL, G., MASON, P. & HIGGS, S. 2006. Potentiation of West Nile encephalitis by mosquito feeding. *Viral immunology,* 19**,** 74-82.

SCHUMANN, J. 2016. It is all about fluidity: Fatty acids and macrophage phagocytosis. *European journal of pharmacology,* 785**,** 18-23.

SCHWANHÄUSSER, B., BUSSE, D., LI, N., DITTMAR, G., SCHUCHHARDT, J., WOLF, J., CHEN, W. & SELBACH, M. 2011. Global quantification of mammalian gene expression control. *Nature,* 473**,** 337-342.

SEIM, G. L., BRITT, E. C., JOHN, S. V., YEO, F. J., JOHNSON, A. R., EISENSTEIN, R. S., PAGLIARINI, D. J. & FAN, J. 2019. Two-stage metabolic remodelling in macrophages in response to lipopolysaccharide and interferon-γ stimulation. *Nature metabolism,* 1**,** 731-742.

SEMBA, H., TAKEDA, N., ISAGAWA, T., SUGIURA, Y., HONDA, K., WAKE, M., MIYAZAWA, H., YAMAGUCHI, Y., MIURA, M. & JENKINS, D. M. 2016. HIF-1α-PDK1 axis-induced active glycolysis plays an essential role in macrophage migratory capacity. *Nature communications,* 7**,** 11635.

SHECHTER, R., MILLER, O., YOVEL, G., ROSENZWEIG, N., LONDON, A., RUCKH, J., KIM, K.-W., KLEIN, E., KALCHENKO, V. & BENDEL, P. 2013. Recruitment of beneficial M2 macrophages to injured spinal cord is orchestrated by remote brain choroid plexus. *Immunity,* 38**,** 555-569.

SHEN, L., HU, P., ZHANG, Y., JI, Z., SHAN, X., NI, L., NING, N., WANG, J., TIAN, H. & SHUI, G. 2021. Serine metabolism antagonizes antiviral innate immunity by preventing ATP6V0d2-mediated YAP lysosomal degradation. *Cell Metabolism,* 33**,** 971-987. e6.

SHENG, X., ZHAO, J., LI, M., XU, Y., ZHOU, Y., XU, J., HE, R., LU, H., WU, T. & DUAN, C. 2021. Bone marrow mesenchymal stem cell-derived exosomes accelerate functional recovery after spinal cord injury by promoting the phagocytosis of macrophages to clean myelin debris. *Frontiers in Cell and Developmental Biology,* 9**,** 772205.

SHI, L. Z., WANG, R., HUANG, G., VOGEL, P., NEALE, G., GREEN, D. R. & CHI, H. 2011. HIF1α–dependent glycolytic pathway orchestrates a metabolic checkpoint for the differentiation of TH17 and Treg cells. *Journal of experimental medicine,* 208**,** 1367-1376.

SHRESTHA, B. & DIAMOND, M. S. 2004. Role of CD8+ T cells in control of West Nile virus infection. *Journal of virology,* 78**,** 8312-8321.

SHRESTHA, B. & DIAMOND, M. S. 2007. Fas ligand interactions contribute to CD8+ T-cell-mediated control of West Nile virus infection in the central nervous system. *Journal of virology,* 81**,** 11749-11757.

SHRESTHA, B., PINTO, A. K., GREEN, S., BOSCH, I. & DIAMOND, M. S. 2012. CD8+ T cells use TRAIL to restrict West Nile virus pathogenesis by controlling infection in neurons. *Journal of virology,* 86**,** 8937-8948.

SHRESTHA, B., SAMUEL, M. A. & DIAMOND, M. S. 2006. CD8+ T cells require perforin to clear West Nile virus from infected neurons. *Journal of virology,* 80**,** 119-129.

SITATI, E. M. & DIAMOND, M. S. 2006. CD4+ T-cell responses are required for clearance of West Nile virus from the central nervous system. *Journal of virology,* 80**,** 12060-12069.

SOBUE, A., KOMINE, O., HARA, Y., ENDO, F., MIZOGUCHI, H., WATANABE, S., MURAYAMA, S., SAITO, T., SAIDO, T. C., SAHARA, N., HIGUCHI, M., OGI, T. & YAMANAKA, K. 2021. Microglial gene signature reveals loss of homeostatic microglia associated with neurodegeneration of Alzheimer's disease. *Acta Neuropathol Commun,* 9**,** 1.

SOMEBANG, K., RUDOLPH, J., IMHOF, I., LI, L., NIEMI, E. C., SHIGENAGA, J., TRAN, H., GILL, T. M., LO, I., ZABEL, B. A., SCHMAJUK, G., WIPKE, B. T., GYONEVA, S., JANDRESKI, L., CRAFT, M., BENEDETTO, G., PLOWEY, E. D., CHARO, I., CAMPBELL, J., YE, C. J., PANTER, S. S., NAKAMURA, M. C., ECKALBAR, W. & HSIEH, C. L. 2021. CCR2 deficiency alters activation of microglia subsets in traumatic brain injury. *Cell Rep,* 36**,** 109727.

SOMMER, C. J. 2017. Ischemic stroke: experimental models and reality. *Acta neuropathologica,* 133**,** 245-261.

SORIANO-BAGUET, L. & BRENNER, D. 2023. Metabolism and epigenetics at the heart of T cell function. *Trends in immunology,* 44**,** 231-244.

SOUSA, C., GOLEBIEWSKA, A., POOVATHINGAL, S. K., KAOMA, T., PIRES-AFONSO, Y., MARTINA, S., COOWAR, D., AZUAJE, F., SKUPIN, A., BALLING, R., BIBER, K., NICLOU, S. P. & MICHELUCCI, A. 2018. Single-cell transcriptomics reveals distinct inflammation-induced microglia signatures. *EMBO Rep,* 19.

SPATH, S., KOMUCZKI, J., HERMANN, M., PELCZAR, P., MAIR, F., SCHREINER, B. & BECHER, B. 2017. Dysregulation of the cytokine GM-CSF induces spontaneous phagocyte invasion and immunopathology in the central nervous system. *Immunity,* 46**,** 245-260.

SPITERI, A. G. & KING, N. J. 2023. Putting PLX5622 into perspective: microglia in central nervous system viral infection. *Neural Regeneration Research,* 18**,** 1269-1270.

SPITERI, A. G., NI, D., LING, Z. L., MACIA, L., CAMPBELL, I. L., HOFER, M. J. & KING, N. J. C. 2022a. PLX5622 Reduces Disease Severity in Lethal CNS Infection by Off-Target Inhibition of Peripheral Inflammatory Monocyte Production. *Frontiers in immunology,* 13**,** 851556-851556.

SPITERI, A. G., TERRY, R. L., WISHART, C. L., ASHHURST, T. M., CAMPBELL, I. L., HOFER, M. J. & KING, N. J. C. 2021a. High-parameter Cytometry Unmasks Microglial Cell Spatio-temporal Response Kinetics in Severe Neuroinflammatory Disease.

SPITERI, A. G., VAN VREDEN, C., ASHHURST, T. M., NIEWOLD, P. & KING, N. J. C. 2023a. Clodronate is not protective in lethal viral encephalitis despite substantially reducing inflammatory monocyte infiltration in the CNS. *Front Immunol,* 14**,** 1203561.

SPITERI, A. G., WISHART, C. L. & KING, N. J. C. 2020. Immovable object meets unstoppable force? Dialogue between resident and peripheral myeloid cells in the inflamed brain. *Frontiers in Immunology,* 11**,** 3164.

SPITERI, A. G., WISHART, C. L., NI, D., VIENGKHOU, B., MACIA, L., HOFER, M. J. & KING, N. J. 2023b. Temporal tracking of microglial and monocyte single-cell transcriptomics in lethal flavivirus infection. *Acta Neuropathologica Communications,* 11**,** 60.

SPITERI, A. G., WISHART, C. L., PAMPHLETT, R., LOCATELLI, G. & KING, N. J. 2021b. Microglia and monocytes in inflammatory CNS disease: integrating phenotype and function. *Acta neuropathologica***,** 1-46.

SPITERI, A. G., WISHART, C. L., PAMPHLETT, R., LOCATELLI, G. & KING, N. J. C. 2022b. Microglia and monocytes in inflammatory CNS disease: integrating phenotype and function. *Acta Neuropathol,* 143**,** 179-224.

SPITERI, A. G., WISHART, C. L., PINGET, G. V., PUROHIT, S. K., MACIA, L., KING, N. J. & NIEWOLD, P. 2024. NK cell profiling in West Nile virus encephalitis reveals potential metabolic basis for functional inhibition. *Immunology and Cell Biology*.

SRINIVASAN, K., FRIEDMAN, B. A., ETXEBERRIA, A., HUNTLEY, M. A., VAN DER BRUG, M. P., FOREMAN, O., PAW, J. S., MODRUSAN, Z., BEACH, T. G., SERRANO, G. E. & HANSEN, D. V. 2020. Alzheimer's Patient Microglia Exhibit Enhanced Aging and Unique Transcriptional Activation. *Cell Rep,* 31**,** 107843.

STEIN, M., KESHAV, S., HARRIS, N. & GORDON, S. 1992. Interleukin 4 potently enhances murine macrophage mannose receptor activity: a marker of alternative immunologic macrophage activation. *The Journal of experimental medicine,* 176**,** 287-292.

STEWART, C. R., STUART, L. M., WILKINSON, K., VAN GILS, J. M., DENG, J., HALLE, A., RAYNER, K. J., BOYER, L., ZHONG, R. & FRAZIER, W. A. 2010. CD36 ligands promote sterile inflammation through assembly of a Toll-like receptor 4 and 6 heterodimer. *Nature immunology,* 11**,** 155-161.

STIENSTRA, R., NETEA-MAIER, R. T., RIKSEN, N. P., JOOSTEN, L. A. & NETEA, M. G. 2017. Specific and complex reprogramming of cellular metabolism in myeloid cells during innate immune responses. *Cell metabolism,* 26**,** 142-156.

STONEDAHL, S., CLARKE, P. & TYLER, K. L. 2020. The role of microglia during West Nile virus infection of the central nervous system. *Vaccines,* 8**,** 485.

STREET, K., RISSO, D., FLETCHER, R. B., DAS, D., NGAI, J., YOSEF, N., PURDOM, E. & DUDOIT, S. 2018. Slingshot: cell lineage and pseudotime inference for single-cell transcriptomics. *BMC genomics,* 19**,** 1-16.

STYER, L. M., LIM, P.-Y., LOUIE, K. L., ALBRIGHT, R. G., KRAMER, L. D. & BERNARD, K. A. 2011. Mosquito saliva causes enhancement of West Nile virus infection in mice. *Journal of virology,* 85**,** 1517-1527.

SUMBAYEV, V. V., NICHOLAS, S. A., STREATFIELD, C. L. & GIBBS, B. F. 2009. Involvement of hypoxia-inducible factor-1 HiF (1α) in IgE-mediated primary human basophil responses. *European journal of immunology,* 39**,** 3511-3519.

SUTHAR, M. S., DIAMOND, M. S. & GALE JR, M. 2013. West Nile virus infection and immunity. *Nature Reviews Microbiology,* 11**,** 115-128.

SUTHAR, M. S., MA, D. Y., THOMAS, S., LUND, J. M., ZHANG, N., DAFFIS, S., RUDENSKY, A. Y., BEVAN, M. J., CLARK, E. A. & KAJA, M.-K. 2010. IPS-1 is essential for the control of West Nile virus infection and immunity. *PLoS pathogens,* 6**,** e1000757.

SWAIN, A., BAMBOUSKOVA, M., KIM, H., ANDHEY, P. S., DUNCAN, D., AUCLAIR, K., CHUBUKOV, V., SIMONS, D. M., RODDY, T. P. & STEWART, K. M. 2020. Comparative evaluation of itaconate and its derivatives reveals divergent inflammasome and type I interferon regulation in macrophages. *Nature metabolism,* 2**,** 594-602.

SWANN, J. W., OLSON, O. C. & PASSEGUÉ, E. 2024. Made to order: emergency myelopoiesis and demand-adapted innate immune cell production. *Nature Reviews Immunology***,** 1-18.

SZEPESI, Z., MANOUCHEHRIAN, O., BACHILLER, S. & DEIERBORG, T. 2018. Bidirectional microglia–neuron communication in health and disease. *Frontiers in cellular neuroscience,* 12**,** 323.

SZRETTER, K. J., DANIELS, B. P., CHO, H., GAINEY, M. D., YOKOYAMA, W. M., GALE JR, M., VIRGIN, H. W., KLEIN, R. S., SEN, G. C. & DIAMOND, M. S. 2012. 2′-O methylation of the viral mRNA cap by West Nile virus evades ifit1-dependent and-independent mechanisms of host restriction in vivo. *PLoS pathogens,* 8**,** e1002698.

SZULCZEWSKI, J. M., INMAN, D. R., ENTENBERG, D., PONIK, S. M., AGUIRRE-GHISO, J., CASTRACANE, J., CONDEELIS, J., ELICEIRI, K. W. & KEELY, P. J. 2016. In vivo visualization of stromal macrophages via label-free FLIM-based metabolite imaging. *Scientific reports,* 6**,** 25086.

TAN, J., NI, D., RIBEIRO, R. V., PINGET, G. V. & MACIA, L. 2021a. How Changes in the Nutritional Landscape Shape Gut Immunometabolism. *Nutrients,* 13.

TAN, J., NI, D., WALI, J. A., COX, D. A., PINGET, G. V., TAITZ, J., DAIEN, C. I., SENIOR, A., READ, M. N., SIMPSON, S. J., KING, N. J. C. & MACIA, L. 2021b. Dietary carbohydrate, particularly glucose, drives B cell lymphopoiesis and function. *iScience,* 24**,** 102835.

TAN, Z., XIE, N., BANERJEE, S., CUI, H., FU, M., THANNICKAL, V. J. & LIU, G. 2015. The monocarboxylate transporter 4 is required for glycolytic reprogramming and inflammatory response in macrophages. *Journal of Biological Chemistry,* 290**,** 46-55.

TANABE, S., SAITOH, S., MIYAJIMA, H., ITOKAZU, T. & YAMASHITA, T. 2019. Microglia suppress the secondary progression of autoimmune encephalomyelitis. *Glia,* 67**,** 1694-1704.

TANG, Y. & LE, W. 2016. Differential roles of M1 and M2 microglia in neurodegenerative diseases. *Molecular neurobiology,* 53**,** 1181-1194.

TANNAHILL, G., CURTIS, A., ADAMIK, J., PALSSON-MCDERMOTT, E., MCGETTRICK, A., GOEL, G., FREZZA, C., BERNARD, N., KELLY, B. & FOLEY, N. 2013. Succinate is an inflammatory signal that induces IL-1β through HIF-1α. *Nature,* 496**,** 238-242.

TAY, T. L., MAI, D., DAUTZENBERG, J., FERNÁNDEZ-KLETT, F., LIN, G., SAGAR, N., DATTA, M., DROUGARD, A., STEMPFL, T. & ARDURA-FABREGAT, A. 2017. A new fate mapping system reveals context-dependent random or clonal expansion of microglia. *Nature neuroscience,* 20**,** 793-803.

TAY, T. L., SAGAR, DAUTZENBERG, J., GRUN, D. & PRINZ, M. 2018. Unique microglia recovery population revealed by single-cell RNAseq following neurodegeneration. *Acta Neuropathol Commun,* 6**,** 87.

TAYLOR, C. T. & COLGAN, S. P. 2017. Regulation of immunity and inflammation by hypoxia in immunological niches. *Nature Reviews Immunology,* 17**,** 774-785.

TAYLOR, C. T. & SCHOLZ, C. C. 2022. The effect of HIF on metabolism and immunity. *Nature Reviews Nephrology,* 18**,** 573-587.

TERRY, R. L., DEFFRASNES, C., GETTS, D. R., MINTEN, C., VAN VREDEN, C., ASHHURST, T. M., GETTS, M. T., XIE, R. D. V., CAMPBELL, I. L. & KING, N. J. 2015. Defective inflammatory monocyte development in IRF8-deficient mice abrogates migration to the West Nile virus-infected brain. *Journal of innate immunity,* 7**,** 102-112.

TERRY, R. L., GETTS, D. R., DEFFRASNES, C., VAN VREDEN, C., CAMPBELL, I. L. & KING, N. J. 2012. Inflammatory monocytes and the pathogenesis of viral encephalitis. *J Neuroinflammation,* 9**,** 270.

THOMAS, A. C. & MATTILA, J. T. 2014. "Of mice and men": arginine metabolism in macrophages. *Frontiers in immunology,* 5**,** 112253.

THOMAS, S. R., MOHR, D. & STOCKER, R. 1994. Nitric oxide inhibits indoleamine 2, 3-dioxygenase activity in interferon-gamma primed mononuclear phagocytes. *Journal of Biological Chemistry,* 269**,** 14457-14464.

THOMAS, S. R. & STOCKER, R. 1999. Redox reactions related to indoleamine 2, 3-dioxygenase and tryptophan metabolism along the kynurenine pathway. *Redox Report,* 4**,** 199-220.

TIROSH, I., IZAR, B., PRAKADAN, S. M., WADSWORTH, M. H., TREACY, D., TROMBETTA, J. J., ROTEM, A., RODMAN, C., LIAN, C. & MURPHY, G. 2016. Dissecting the multicellular ecosystem of metastatic melanoma by single-cell RNA-seq. *Science,* 352**,** 189-196.

TOWN, T., JENG, D., ALEXOPOULOU, L., TAN, J. & FLAVELL, R. A. 2006. Microglia recognize double-stranded RNA via TLR3. *The Journal of Immunology,* 176**,** 3804-3812.

TROMPETTE, A., GOLLWITZER, E. S., PATTARONI, C., LOPEZ-MEJIA, I. C., RIVA, E., PERNOT, J., UBAGS, N., FAJAS, L., NICOD, L. P. & MARSLAND, B. J. 2018. Dietary fiber confers protection against flu by shaping Ly6c− patrolling monocyte hematopoiesis and CD8+ T cell metabolism. *Immunity,* 48**,** 992-1005. e8.

TSAI, T.-L., ZHOU, T.-A., HSIEH, Y.-T., WANG, J.-C., CHENG, H.-K., HUANG, C.-H., TSAI, P.-Y., FAN, H.-H., FENG, H.-K. & HUANG, Y.-C. 2022. Multiomics reveal the central role of pentose phosphate pathway in resident thymic macrophages to cope with efferocytosis-associated stress. *Cell Reports,* 40.

UNIPROT, C. 2021. UniProt: the universal protein knowledgebase in 2021. *Nucleic Acids Res,* 49**,** D480-D489.

VAN BROECKHOVEN, J., SOMMER, D., DOOLEY, D., HENDRIX, S. & FRANSSEN, A. J. 2021. Macrophage phagocytosis after spinal cord injury: when friends become foes. *Brain,* 144**,** 2933-2945.

VAN DEN BOSSCHE, J., BAARDMAN, J., OTTO, N. A., VAN DER VELDEN, S., NEELE, A. E., VAN DEN BERG, S. M., LUQUE-MARTIN, R., CHEN, H.-J., BOSHUIZEN, M. C. & AHMED, M. 2016. Mitochondrial dysfunction prevents repolarization of inflammatory macrophages. *Cell reports,* 17**,** 684-696.

VAN DEN BOSSCHE, J., O'NEILL, L. A. & MENON, D. 2017. Macrophage immunometabolism: where are we (going)? *Trends in immunology,* 38**,** 395-406.

VAN DER WINDT, G. J., EVERTS, B., CHANG, C.-H., CURTIS, J. D., FREITAS, T. C., AMIEL, E., PEARCE, E. J. & PEARCE, E. L. 2012. Mitochondrial respiratory capacity is a critical regulator of CD8+ T cell memory development. *Immunity,* 36**,** 68-78.

VAN DER WINDT, G. J., O'SULLIVAN, D., EVERTS, B., HUANG, S. C.-C., BUCK, M. D., CURTIS, J. D., CHANG, C.-H., SMITH, A. M., AI, T. & FAUBERT, B. 2013. CD8 memory T cells have a bioenergetic advantage that underlies their rapid recall ability. *Proceedings of the National Academy of Sciences,* 110**,** 14336-14341.

VAN FURTH, R., COHN, Z., HIRSCH, J., HUMPHREY, J., SPECTOR, W. & LANGEVOORT, H. 1972. Mononuclear phagocytic system: new classification of macrophages, monocytes and of their cell line. *Bulletin of the World Health Organization,* 47**,** 651-658.

VAN HOVE, H., MARTENS, L., SCHEYLTJENS, I., DE VLAMINCK, K., ANTUNES, A. R. P., DE PRIJCK, S., VANDAMME, N., DE SCHEPPER, S., VAN ISTERDAEL, G. & SCOTT, C. L. 2019. A single-cell atlas of mouse brain macrophages reveals unique transcriptional identities shaped by ontogeny and tissue environment. *Nature neuroscience,* 22**,** 1021-1035.

VAN MARLE, G., ANTONY, J., OSTERMANN, H., DUNHAM, C., HUNT, T., HALLIDAY, W., MAINGAT, F., URBANOWSKI, M. D., HOBMAN, T. & PEELING, J. 2007. West Nile virus-induced neuroinflammation: glial infection and capsid protein-mediated neurovirulence. *Journal of virology,* 81**,** 10933-10949.

VAN ROOIJEN, N. 1989. The liposome-mediated macrophage 'suicide' technique. *J Immunol Methods,* 124**,** 1-6.

VAN ROOIJEN, N. & SANDERS, A. 1994. Liposome mediated depletion of macrophages: mechanism of action, preparation of liposomes and applications. *J Immunol Methods,* 174**,** 83-93.

VAN ROOIJEN, N. & VAN NIEUWMEGEN, R. 1984. Elimination of phagocytic cells in the spleen after intravenous injection of liposome-encapsulated dichloromethylene diphosphonate. An enzyme-histochemical study. *Cell Tissue Res,* 238**,** 355-8.

VAN WAGENINGEN, T. A., VLAAR, E., KOOIJ, G., JONGENELEN, C. A. M., GEURTS, J. J. G. & VAN DAM, A. M. 2019. Regulation of microglial TMEM119 and P2RY12 immunoreactivity in multiple sclerosis white and grey matter lesions is dependent on their inflammatory environment. *Acta Neuropathol Commun,* 7**,** 206.

VANKRIEKELSVENNE, E., CHRZANOWSKI, U., MANZHULA, K., GREINER, T., WREE, A., HAWLITSCHKA, A., LLOVERA, G., ZHAN, J., JOOST, S., SCHMITZ, C., PONSAERTS, P., AMOR, S., NUTMA, E., KIPP, M. & KADDATZ, H. 2022. Transmembrane protein 119 is neither a specific nor a reliable marker for microglia. *Glia,* 70**,** 1170-1190.

VANROSSUM, G. & DEBOER, J. 1991. Interactively testing remote servers using the Python programming language. *CWI quarterly,* 4**,** 283-304.

VARGA, T., MOUNIER, R., HORVATH, A., CUVELLIER, S., DUMONT, F., POLISKA, S., ARDJOUNE, H., JUBAN, G., NAGY, L. & CHAZAUD, B. 2016. Highly dynamic transcriptional signature of distinct macrophage subsets during sterile inflammation, resolution, and tissue repair. *The Journal of Immunology,* 196**,** 4771-4782.

VERA ALVAREZ, R., PONGOR, L. S., MARINO-RAMIREZ, L. & LANDSMAN, D. 2019. TPMCalculator: one-step software to quantify mRNA abundance of genomic features. *Bioinformatics,* 35**,** 1960-1962.

VERBERK, S. G., DE GOEDE, K. E., GORKI, F. S., VAN DIERENDONCK, X. A., ARGÜELLO, R. J. & VAN DEN BOSSCHE, J. 2022. An integrated toolbox to profile macrophage immunometabolism. *Cell reports methods,* 2**,** 100192.

VERMA, S., LO, Y., CHAPAGAIN, M., LUM, S., KUMAR, M., GURJAV, U., LUO, H., NAKATSUKA, A. & NERURKAR, V. R. 2009. West Nile virus infection modulates human brain microvascular endothelial cells tight junction proteins and cell adhesion molecules: Transmigration across the in vitro blood-brain barrier. *Virology,* 385**,** 425-433.

VIJAYAN, V., PRADHAN, P., BRAUD, L., FUCHS, H. R., GUELER, F., MOTTERLINI, R., FORESTI, R. & IMMENSCHUH, S. 2019. Human and murine macrophages exhibit differential metabolic responses to lipopolysaccharide-A divergent role for glycolysis. *Redox biology,* 22**,** 101147.

VIOLA, A., MUNARI, F., SÁNCHEZ-RODRÍGUEZ, R., SCOLARO, T. & CASTEGNA, A. 2019. The metabolic signature of macrophage responses. *Frontiers in immunology,* 10**,** 1462.

VIVIER, E., RAULET, D. H., MORETTA, A., CALIGIURI, M. A., ZITVOGEL, L., LANIER, L. L., YOKOYAMA, W. M. & UGOLINI, S. 2011. Innate or adaptive immunity? The example of natural killer cells. *science,* 331**,** 44-49.

VOET, S., PRINZ, M. & VAN LOO, G. 2019. Microglia in Central Nervous System Inflammation and Multiple Sclerosis Pathology. *Trends Mol Med,* 25**,** 112-123.

VOLTERRA, A. & MELDOLESI, J. 2005. Astrocytes, from brain glue to communication elements: the revolution continues. *Nature Reviews Neuroscience,* 6**,** 626-640.

VORA, N. M., HOLMAN, R. C., MEHAL, J. M., STEINER, C. A., BLANTON, J. & SEJVAR, J. 2014. Burden of encephalitis-associated hospitalizations in the United States, 1998-2010. *Neurology,* 82**,** 443-51.

VOS, T., ABAJOBIR, A. A., ABATE, K. H., ABBAFATI, C., ABBAS, K. M., ABD-ALLAH, F., ABDULKADER, R. S., ABDULLE, A. M., ABEBO, T. A. & ABERA, S. F. 2017. Global, regional, and national incidence, prevalence, and years lived with disability for 328 diseases and injuries for 195 countries, 1990–2016: a systematic analysis for the Global Burden of Disease Study 2016. *The Lancet,* 390**,** 1211-1259.

VOSS, K., HONG, H. S., BADER, J. E., SUGIURA, A., LYSSIOTIS, C. A. & RATHMELL, J. C. 2021. A guide to interrogating immunometabolism. *Nature Reviews Immunology,* 21**,** 637-652.

WALSH, A. J., MUELLER, K. P., TWEED, K., JONES, I., WALSH, C. M., PISCOPO, N. J., NIEMI, N. M., PAGLIARINI, D. J., SAHA, K. & SKALA, M. C. 2021. Classification of T-cell activation via autofluorescence lifetime imaging. *Nature biomedical engineering,* 5**,** 77-88.

WALTL, I., KÄUFER, C., BRÖER, S., CHHATBAR, C., GHITA, L., GERHAUSER, I., ANJUM, M., KALINKE, U. & LÖSCHER, W. 2018. Macrophage depletion by liposome-encapsulated clodronate suppresses seizures but not hippocampal damage after acute viral encephalitis. *Neurobiology of disease,* 110**,** 192-205.

WANG, A., HUEN, S. C., LUAN, H. H., YU, S., ZHANG, C., GALLEZOT, J.-D., BOOTH, C. J. & MEDZHITOV, R. 2016. Opposing effects of fasting metabolism on tissue tolerance in bacterial and viral inflammation. *Cell,* 166**,** 1512-1525. e12.

WANG, F., ZHANG, S., VUCKOVIC, I., JEON, R., LERMAN, A., FOLMES, C. D., DZEJA, P. P. & HERRMANN, J. 2018. Glycolytic stimulation is not a requirement for M2 macrophage differentiation. *Cell metabolism,* 28**,** 463-475. e4.

WANG, M., ZHAO, Y. & ZHANG, B. 2015. Efficient Test and Visualization of Multi-Set Intersections. *Sci Rep,* 5**,** 16923.

WANG, R., DILLON, C. P., SHI, L. Z., MILASTA, S., CARTER, R., FINKELSTEIN, D., MCCORMICK, L. L., FITZGERALD, P., CHI, H. & MUNGER, J. 2011. The transcription factor Myc controls metabolic reprogramming upon T lymphocyte activation. *Immunity,* 35**,** 871-882.

WANG, T., LIU, H., LIAN, G., ZHANG, S.-Y., WANG, X. & JIANG, C. 2017. HIF1α-induced glycolysis metabolism is essential to the activation of inflammatory macrophages. *Mediators of inflammation,* 2017.

WANG, T., TOWN, T., ALEXOPOULOU, L., ANDERSON, J. F., FIKRIG, E. & FLAVELL, R. A. 2004. Toll-like receptor 3 mediates West Nile virus entry into the brain causing lethal encephalitis. *Nature medicine,* 10**,** 1366-1373.

WANG, X.-F., WANG, H.-S., WANG, H., ZHANG, F., WANG, K.-F., GUO, Q., ZHANG, G., CAI, S.-H. & DU, J. 2014. The role of indoleamine 2, 3-dioxygenase (IDO) in

immune tolerance: focus on macrophage polarization of THP-1 cells. *Cellular immunology,* 289**,** 42-48.

WANG, Y., LOBIGS, M., LEE, E. & MÜLLBACHER, A. 2003. CD8+ T Cells Mediate Recovery andImmunopathology in West Nile VirusEncephalitis. *Journal of virology,* 77**,** 13323-13334.

WANG, Y.-T., TRZECIAK, A. J., ROJAS, W. S., SAAVEDRA, P., CHEN, Y.-T., CHIRAYIL, R., ETCHEGARAY, J. I., LUCAS, C. D., PULESTON, D. J. & KESHARI, K. R. 2023. Metabolic adaptation supports enhanced macrophage efferocytosis in limited-oxygen environments. *Cell metabolism,* 35**,** 316-331. e6.

WARBURG, O., WIND, F. & NEGELEIN, E. 1927. The metabolism of tumors in the body. *The Journal of general physiology,* 8**,** 519.

WARDLAW, A., BRIGHTLING, C., GREEN, R., WOLTMANN, G. & PAVORD, I. 2000. Eosinophils in asthma and other allergic diseases. *British medical bulletin,* 56**,** 985-1003.

WATERS, L. R., AHSAN, F. M., WOLF, D. M., SHIRIHAI, O. & TEITELL, M. A. 2018. Initial B cell activation induces metabolic reprogramming and mitochondrial remodeling. *IScience,* 5**,** 99-109.

WATTANANIT, S., TORNERO, D., GRAUBARDT, N., MEMANISHVILI, T., MONNI, E., TATARISHVILI, J., MISKINYTE, G., GE, R., AHLENIUS, H. & LINDVALL, O. 2016. Monocyte-derived macrophages contribute to spontaneous long-term functional recovery after stroke in mice. *Journal of Neuroscience,* 36**,** 4182-4195.

WEATHERHEAD, J. E., MILLER, V. E., GARCIA, M. N., HASBUN, R., SALAZAR, L., DIMACHKIE, M. M. & MURRAY, K. O. 2015. Long-term neurological outcomes in West Nile virus-infected patients: an observational study. *Am J Trop Med Hyg,* 92**,** 1006-1012.

WEBER, M. S., PROD'HOMME, T., YOUSSEF, S., DUNN, S. E., RUNDLE, C. D., LEE, L., PATARROYO, J. C., STÜVE, O., SOBEL, R. A. & STEINMAN, L. 2007. Type II monocytes modulate T cell–mediated central nervous system autoimmune disease. *Nature medicine,* 13**,** 935-943.

WEI, X., SONG, H., YIN, L., RIZZO, M. G., SIDHU, R., COVEY, D. F., ORY, D. S. & SEMENKOVICH, C. F. 2016. Fatty acid synthesis configures the plasma membrane for inflammation in diabetes. *Nature,* 539**,** 294-298.

WEINREB, C., RODRIGUEZ-FRATICELLI, A., CAMARGO, F. D. & KLEIN, A. M. 2020. Lineage tracing on transcriptional landscapes links state to fate during differentiation. *Science,* 367**,** eaaw3381.

WELCH, J. D., KOZAREVA, V., FERREIRA, A., VANDERBURG, C., MARTIN, C. & MACOSKO, E. Z. 2019. Single-cell multi-omic integration compares and contrasts features of brain cell identity. *Cell,* 177**,** 1873-1887. e17.

WEN, H., GRIS, D., LEI, Y., JHA, S., ZHANG, L., HUANG, M. T.-H., BRICKEY, W. J. & TING, J. P. 2011. Fatty acid–induced NLRP3-ASC inflammasome activation interferes with insulin signaling. *Nature immunology,* 12**,** 408-415.

WENDELN, A.-C., DEGENHARDT, K., KAURANI, L., GERTIG, M., ULAS, T., JAIN, G., WAGNER, J., HÄSLER, L. M., WILD, K. & SKODRAS, A. 2018. Innate immune memory in the brain shapes neurological disease hallmarks. *Nature,* 556**,** 332-338.

WERNER, Y., MASS, E., ASHOK KUMAR, P., ULAS, T., HANDLER, K., HORNE, A., KLEE, K., LUPP, A., SCHUTZ, D., SAABER, F., REDECKER, C., SCHULTZE, J. L., GEISSMANN, F. & STUMM, R. 2020. Cxcr4 distinguishes HSC-derived monocytes from microglia and reveals monocyte immune responses to experimental stroke. *Nat Neurosci,* 23**,** 351-362.

WICKHAM, H. 2006. An introduction to ggplot: An implementation of the grammar of graphics in R. *Statistics*.
WICKHAM, H. & WICKHAM, M. H. 2007. The ggplot package. Google Scholar.
WIMMER, I., SCHARLER, C., ZRZAVY, T., KADOWAKI, T., MODLAGL, V., ROJC, K., TROSCHER, A. R., KITIC, M., UEDA, S., BRADL, M. & LASSMANN, H. 2019. Microglia pre-activation and neurodegeneration precipitate neuroinflammation without exacerbating tissue injury in experimental autoimmune encephalomyelitis. *Acta Neuropathol Commun,* 7**,** 14.
WISE, D. R., WARD, P. S., SHAY, J. E., CROSS, J. R., GRUBER, J. J., SACHDEVA, U. M., PLATT, J. M., DEMATTEO, R. G., SIMON, M. C. & THOMPSON, C. B. 2011. Hypoxia promotes isocitrate dehydrogenase-dependent carboxylation of α-ketoglutarate to citrate to support cell growth and viability. *Proceedings of the National Academy of Sciences,* 108**,** 19611-19616.
WISHART, C. L., SPITERI, A.G., LOCATELLI, G. & KING, N.J.C. 2022. Connecting Transcriptomes Across Neuroinflammatory Disease Reveals Conserved and Unique Microglial and Monocyte Response Programs. *Available at SSRN: https://ssrn.com/abstract=3970230 or http://dx.doi.org/10.2139/ssrn.3970230*.
WOLF, N. K., KISSIOV, D. U. & RAULET, D. H. 2023. Roles of natural killer cells in immunity to cancer, and applications to immunotherapy. *Nature Reviews Immunology,* 23**,** 90-105.
WOO, M.-S., YANG, J., BELTRAN, C. & CHO, S. 2016. Cell surface CD36 protein in monocyte/macrophage contributes to phagocytosis during the resolution phase of ischemic stroke in mice. *Journal of Biological Chemistry,* 291**,** 23654-23661.
WOUTERS, E., GRAJCHEN, E., JORISSEN, W., DIERCKX, T., WETZELS, S., LOIX, M., TULLENERS, M. P., STAELS, B., STINISSEN, P. & HAIDAR, M. 2020. Altered PPARγ expression promotes myelin-induced foam cell formation in macrophages in multiple sclerosis. *International Journal of Molecular Sciences,* 21**,** 9329.
XIAO, J., LI, W., ZHENG, X., QI, L., WANG, H., ZHANG, C., WAN, X., ZHENG, Y., ZHONG, R. & ZHOU, X. 2020. Targeting 7-dehydrocholesterol reductase integrates cholesterol metabolism and IRF3 activation to eliminate infection. *Immunity,* 52**,** 109-122. e6.
XIONG, Y., MAHMOOD, A. & CHOPP, M. 2013. Animal models of traumatic brain injury. *Nature Reviews Neuroscience,* 14**,** 128-142.
XU, Z., SHI, L., WANG, Y., ZHANG, J., HUANG, L., ZHANG, C., LIU, S., ZHAO, P., LIU, H. & ZHU, L. 2020. Pathological findings of COVID-19 associated with acute respiratory distress syndrome. *The Lancet respiratory medicine,* 8**,** 420-422.
XUE, J., SCHMIDT, S. V., SANDER, J., DRAFFEHN, A., KREBS, W., QUESTER, I., DE NARDO, D., GOHEL, T. D., EMDE, M. & SCHMIDLEITHNER, L. 2014. Transcriptome-based network analysis reveals a spectrum model of human macrophage activation. *Immunity,* 40**,** 274-288.
YALCIN, A., TELANG, S., CLEM, B. & CHESNEY, J. 2009. Regulation of glucose metabolism by 6-phosphofructo-2-kinase/fructose-2, 6-bisphosphatases in cancer. *Experimental and molecular pathology,* 86**,** 174-179.
YAMASAKI, R., LU, H., BUTOVSKY, O., OHNO, N., RIETSCH, A. M., CIALIC, R., WU, P. M., DOYKAN, C. E., LIN, J., COTLEUR, A. C., KIDD, G., ZORLU, M. M., SUN, N., HU, W., LIU, L., LEE, J. C., TAYLOR, S. E., UEHLEIN, L., DIXON, D., GU, J., FLORUTA, C. M., ZHU, M., CHARO, I. F., WEINER, H. L. & RANSOHOFF, R. M. 2014. Differential roles of microglia and monocytes in the inflamed central nervous system. *J Exp Med,* 211**,** 1533-49.

YÁÑEZ, A., COETZEE, S. G., OLSSON, A., MUENCH, D. E., BERMAN, B. P., HAZELETT, D. J., SALOMONIS, N., GRIMES, H. L. & GOODRIDGE, H. S. 2017. Granulocyte-monocyte progenitors and monocyte-dendritic cell progenitors independently produce functionally distinct monocytes. *Immunity,* 47**,** 890-902. e4.

YANG, H. S., ONOS, K. D., CHOI, K., KEEZER, K. J., SKELLY, D. A., CARTER, G. W. & HOWELL, G. R. 2021. Natural genetic variation determines microglia heterogeneity in wild-derived mouse models of Alzheimer's disease. *Cell Rep,* 34**,** 108739.

YAO, C.-H., LIU, G.-Y., WANG, R., MOON, S. H., GROSS, R. W. & PATTI, G. J. 2018. Identifying off-target effects of etomoxir reveals that carnitine palmitoyltransferase I is essential for cancer cell proliferation independent of β-oxidation. *PLoS biology,* 16**,** e2003782.

YEUDALL, S., UPCHURCH, C. M., SEEGREN, P. V., PAVELEC, C. M., GREULICH, J., LEMKE, M. C., HARRIS, T. E., DESAI, B. N., HOEHN, K. L. & LEITINGER, N. 2022. Macrophage acetyl-CoA carboxylase regulates acute inflammation through control of glucose and lipid metabolism. *Science Advances,* 8**,** eabq1984.

YIN, X., CHEN, S. & EISENBARTH, S. C. 2021. Dendritic cell regulation of T helper cells. *Annual review of immunology,* 39**,** 759-790.

YONA, S., KIM, K.-W., WOLF, Y., MILDNER, A., VAROL, D., BREKER, M., STRAUSS-AYALI, D., VIUKOV, S., GUILLIAMS, M. & MISHARIN, A. 2013. Fate mapping reveals origins and dynamics of monocytes and tissue macrophages under homeostasis. *Immunity,* 38**,** 79-91.

YONG, H. Y. F., RAWJI, K. S., GHORBANI, S., XUE, M. & YONG, V. W. 2019. The benefits of neuroinflammation for the repair of the injured central nervous system. *Cell Mol Immunol,* 16**,** 540-546.

YOO, H. C., PARK, S. J., NAM, M., KANG, J., KIM, K., YEO, J. H., KIM, J.-K., HEO, Y., LEE, H. S. & LEE, M. Y. 2020. A variant of SLC1A5 is a mitochondrial glutamine transporter for metabolic reprogramming in cancer cells. *Cell metabolism,* 31**,** 267-283. e12.

YORK, A. G., WILLIAMS, K. J., ARGUS, J. P., ZHOU, Q. D., BRAR, G., VERGNES, L., GRAY, E. E., ZHEN, A., WU, N. C. & YAMADA, D. H. 2015. Limiting cholesterol biosynthetic flux spontaneously engages type I IFN signaling. *Cell,* 163**,** 1716-1729.

YUAN, Y., YAN, Z., MIAO, J., CAI, R., ZHANG, M., WANG, Y., WANG, L., DANG, W., WANG, D. & XIANG, D. 2019. Autofluorescence of NADH is a new biomarker for sorting and characterizing cancer stem cells in human glioma. *Stem Cell Research & Therapy,* 10**,** 1-13.

YURDAGUL, A., SUBRAMANIAN, M., WANG, X., CROWN, S. B., ILKAYEVA, O. R., DARVILLE, L., KOLLURU, G. K., RYMOND, C. C., GERLACH, B. D. & ZHENG, Z. 2020. Macrophage metabolism of apoptotic cell-derived arginine promotes continual efferocytosis and resolution of injury. *Cell metabolism,* 31**,** 518-533. e10.

ZACCAGNINO, P., SALTARELLA, M., MAIORANO, S., GABALLO, A., SANTORO, G., NICO, B., LORUSSO, M. & DEL PRETE, A. 2012. An active mitochondrial biogenesis occurs during dendritic cell differentiation. *The international journal of biochemistry & cell biology,* 44**,** 1962-1969.

ZAHOOR, I., SUHAIL, H., DATTA, I., AHMED, M. E., POISSON, L. M., WATERS, J., RASHID, F., BIN, R., SINGH, J. & CERGHET, M. 2022. Blood-based untargeted metabolomics in relapsing-remitting multiple sclerosis revealed the testable therapeutic target. *Proceedings of the National Academy of Sciences,* 119**,** e2123265119.

ZASŁONA, Z. & O'NEILL, L. A. 2020. Cytokine-like roles for metabolites in immunity. *Molecular cell,* 78**,** 814-823.

ZEIGER, S. L., MUSIEK, E. S., ZANONI, G., VIDARI, G., MORROW, J. D., MILNE, G. J. & MCLAUGHLIN, B. 2009. Neurotoxic lipid peroxidation species formed by ischemic stroke increase injury. *Free Radical Biology and Medicine,* 47**,** 1422-1431.

ZHANG, B., BAILEY, W. M., MCVICAR, A. L. & GENSEL, J. C. 2016. Age increases reactive oxygen species production in macrophages and potentiates oxidative damage after spinal cord injury. *Neurobiology of aging,* 47**,** 157-167.

ZHANG, B., BAILEY, W. M., MCVICAR, A. L., STEWART, A. N., VELDHORST, A. K. & GENSEL, J. C. 2019a. Reducing age-dependent monocyte-derived macrophage activation contributes to the therapeutic efficacy of NADPH oxidase inhibition in spinal cord injury. *Brain, behavior, and immunity,* 76**,** 139-150.

ZHANG, B., CHAN, Y. K., LU, B., DIAMOND, M. S. & KLEIN, R. S. 2008. CXCR3 mediates region-specific antiviral T cell trafficking within the central nervous system during West Nile virus encephalitis. *The Journal of Immunology,* 180**,** 2641-2649.

ZHANG, B., PATEL, J., CROYLE, M., DIAMOND, M. S. & KLEIN, R. S. 2010. TNF-α-dependent regulation of CXCR3 expression modulates neuronal survival during West Nile virus encephalitis. *Journal of neuroimmunology,* 224**,** 28-38.

ZHANG, D., TANG, Z., HUANG, H., ZHOU, G., CUI, C., WENG, Y., LIU, W., KIM, S., LEE, S. & PEREZ-NEUT, M. 2019b. Metabolic regulation of gene expression by histone lactylation. *Nature,* 574**,** 575-580.

ZHANG, N. & BEVAN, M. J. 2011. CD8+ T cells: foot soldiers of the immune system. *Immunity,* 35**,** 161-168.

ZHANG, Q., ZHU, C., LI, X., SHI, Y. & ZHANG, Z. 2021. CCR2 downregulation attenuates spinal cord injury by suppressing inflammatory monocytes. *Synapse,* 75**,** e22191.

ZHANG, Q.-G., LAIRD, M. D., HAN, D., NGUYEN, K., SCOTT, E., DONG, Y., DHANDAPANI, K. M. & BRANN, D. W. 2012. Critical role of NADPH oxidase in neuronal oxidative damage and microglia activation following traumatic brain injury. *PloS one,* 7**,** e34504.

ZHANG, S., WEINBERG, S., DEBERGE, M., GAINULLINA, A., SCHIPMA, M., KINCHEN, J. M., BEN-SAHRA, I., GIUS, D. R., YVAN-CHARVET, L. & CHANDEL, N. S. 2019c. Efferocytosis fuels requirements of fatty acid oxidation and the electron transport chain to polarize macrophages for tissue repair. *Cell metabolism,* 29**,** 443-456. e5.

ZHANG, Y., CHEN, K., SLOAN, S. A., BENNETT, M. L., SCHOLZE, A. R., O'KEEFFE, S., PHATNANI, H. P., GUARNIERI, P., CANEDA, C., RUDERISCH, N., DENG, S., LIDDELOW, S. A., ZHANG, C., DANEMAN, R., MANIATIS, T., BARRES, B. A. & WU, J. Q. 2014. An RNA-sequencing transcriptome and splicing database of glia, neurons, and vascular cells of the cerebral cortex. *J Neurosci,* 34**,** 11929-47.

ZHU, B., BANDO, Y., XIAO, S., YANG, K., ANDERSON, A. C., KUCHROO, V. K. & KHOURY, S. J. 2007. CD11b+Ly-6C(hi) suppressive monocytes in experimental autoimmune encephalomyelitis. *J Immunol,* 179**,** 5228-37.

ZHU, J. & PAUL, W. E. 2008. CD4 T cells: fates, functions, and faults. *Blood, The Journal of the American Society of Hematology,* 112**,** 1557-1569.

ZHU, L., SHE, Z.-G., CHENG, X., QIN, J.-J., ZHANG, X.-J., CAI, J., LEI, F., WANG, H., XIE, J. & WANG, W. 2020. Association of blood glucose control and outcomes in patients with COVID-19 and pre-existing type 2 diabetes. *Cell metabolism,* 31**,** 1068-1077. e3.

ZHU, Y., DUN, H., YE, L., TERADA, Y., SHRIVER, L. P., PATTI, G. J., KREISEL, D., GELMAN, A. E. & WONG, B. W. 2022. Targeting fatty acid β-oxidation impairs monocyte differentiation and prolongs heart allograft survival. *JCI insight,* 7.

ZHU, Y., LYAPICHEV, K., LEE, D., MOTTI, D., FERRARO, N., ZHANG, Y., YAHN, S., SODERBLOM, C., ZHA, J. & BETHEA, J. 2017. Macrophage transcriptional profile identifies lipid catabolic pathways that can be therapeutically targeted after spinal cord injury. *Journal of Neuroscience,* 37**,** 2362-2376.

ZHU, Y., SODERBLOM, C., KRISHNAN, V., ASHBAUGH, J., BETHEA, J. & LEE, J. 2015. Hematogenous macrophage depletion reduces the fibrotic scar and increases axonal growth after spinal cord injury. *Neurobiology of disease,* 74**,** 114-125.

ZOU, S., FOSTER, G. A., DODD, R. Y., PETERSEN, L. R. & STRAMER, S. L. 2010. West Nile fever characteristics among viremic persons identified through blood donor screening. *The Journal of infectious diseases,* 202**,** 1354-1361.